

Engineering an oxygen-tolerant hydrogen metabolism in cyanobacteria

Dissertation

in fulfillment of the requirements for the degree “Dr. rer. nat.”
of the Faculty of Natural Sciences I - Biosciences -
at Martin-Luther-University Halle-Wittenberg,

submitted by

M. Sc. Sara Lupacchini

Date of defence: 30.11.2023

Reviewers: Prof. Dr. Bruno Bühler, Prof. Dr. Kirstin
Gutekunst, Prof. Dr. R. Gary Sawers

Acknowledgements

My gratitude goes first of all to my doctoral father Prof. Bruno Bühler and my supervisor Dr. Jörg Toepel. Thanks to drive my scientific and personal development and push me to confront with my weaknesses. I am deeply grateful to have had you as mentors by my side through this journey. Also, thank you for valuing time spent outside the workplace, I will take precious memories with me. I want to thank Prof. Andreas Schmid for the valuable scientific inputs and formative discussion. Thank you for always having an open ear for me, regardless of the topic.

I thank Prof. Lorenz Adrian, Prof. Oliver Lenz, and Dr. Lars Lauterbach for generous support and discussion and by providing access to their lab equipment. Thank to Dr. Stephan Klähn for the important contributions to this work. I express my gratitude to Prof. Kristin Gutekunst and Prof. Gary Sewers for their willingness to review my thesis.

A special thanks goes to Ron, who trained me on the molecular biology and (sand) fields. I was helped daily by Anja, Daniel, Kristin, Jochen Pål, Peter, Ron and Sebastian, thanks for always being kind to me and answering my (too) many questions. I want to thank the students Florian, Jan Hendrik and Max, who contributed to this thesis with valuable experimental work and ideas. I want to thank the Applied Biocatalysis group for the complicity that was created group meeting after group meeting and for all the long evenings that followed. In particular I would like to thanks Adrian and about our American experience, it is enough to say: we had a good one! A special thanks goes to Fabian, Mahir, Paul and Samuel. You have been the best travelling buddies I could ever wish for. I'm really fortunate to have had the chance to work in such a joyful, inspiring environment, which was made possible by all my former SOMA/UMB colleagues: Amadeus, Amelie, Bin, Caro (Bertelmann and Ruhl), Christian, Daniel, Diletta, Franz, Hanna, Hans, Inge, Katharina, Katja, Kristin, Jacky, Jens, Jianqi, Jochen, Johannes, Juliane, Laura, Laurine, Lisa, Magda, Martin, Maria, Merle, Minmin, Nina, Pål, Paul, Peter, Rohan, Sebastian, Selina, Sonja, Stephan, Tim and Vu.

Grazie a Miriam e Sara per aver ricreato qui quella famiglia italiana di cui avevo bisogno.

Voglio ringraziare tutta la mia famiglia, che mi ha sostenuto e fatto sentire protetta anche da lontano. Francesco, non potro mai ringraziarti abbastanza per essere sempre al mio fianco, senza mai chiedere niente in cambio, per non aver mai mollato anche di fronte alla me più difficile. Tu sei la mia arma segreta, la mia certezza piu solida.

“Noi siamo quel che facciamo. Le intenzioni, specialmente se buone, e i rimorsi, specialmente se giusti, ognuno, dentro di sè, può giocarseli come vuole, fino alla disintegrazione, alla follia. Ma un fatto è un fatto: non ha contraddizioni, non ha ambiguità, non contiene il diverso e il contrario.”

Leonardo Sciascia, *Candido ovvero un sogno fatto in Sicilia*, (1977).

Funding and support

This project (Nr. 100361842) was financed from funds of the European Regional Development Fund (EFRE) and co-financed by means of taxation based on the budget adopted by the representatives of the Landtag of Saxony. We further acknowledge the use of the facilities of the Center for Biocatalysis (MiKat-No. 100196171) at the Helmholtz Centre for Environmental Research, which was also supported by EFRE and by the representatives of the Landtag of Saxony. Protein mass spectrometry was done at the Center for Chemical Microscopy (ProVIS) at the Helmholtz Center for Environmental Research.

Table of contents

Acknowledgements	i
Funding and support	iii
Table of contents	iv
Summary	v
Zusammenfassung	vii
List of abbreviations	ix
Chapter 1 General Introduction	1
Chapter 2 Materials & Methods	22
Chapter 3 Rewiring cyanobacterial photosynthesis by the implementation of an oxygen-tolerant hydrogenase.....	39
Chapter 4 The activity of an O ₂ -tolerant hydrogenase recombinantly expressed in <i>Synechocystis</i> sp. PCC 6803 is controlled by fine-tuned gene expression in combination with sink and source availability.	55
Chapter 5 Co-expression of auxiliary and structural <i>Cupriavidus necator</i> genes enhances and stabilizes O ₂ -tolerant hydrogenase activity in <i>Synechocystis</i>	71
Chapter 6 Toward a synthetic hydrogen sensor in cyanobacteria: Functional production of an oxygen-tolerant regulatory hydrogenase in <i>Synechocystis</i> sp. PCC 6803	84
Chapter 7 General Discussion.....	86
Chapter 8 Conclusions & Outlook	95
References	97
Appendix	122
Curriculum Vitae	156
Declaration of authorship	158

Summary

Cyanobacteria can be employed as carbon-neutral factories capturing electrons directly from light-driven water oxidation for highly valuable chemicals and biofuels production, which makes them attractive from both an environmental and economic perspective.

Gas-processing biocatalysts such as [NiFe] hydrogenases in cyanobacteria are gaining attention because of their ability to utilize or produce H₂ and perform redox reactions with minimal overpotential. Molecular hydrogen (H₂) constitutes a high-energy and clean fuel, producing only water upon its use. However, cyanobacterial hydrogenases are notoriously O₂-sensitive, which impairs their application in the frame of oxygenic metabolism, e.g. for photo-H₂ production. A specific group of bidirectional [NiFe] hydrogenases is, however, known to be O₂-tolerant with the potential to be applied under aerobic conditions and to establish an O₂-tolerant H₂ metabolism for either photo-H₂ production or to support electron demanding processes (e.g. biocatalytic oxyfunctionalizations). Hydrogenases are complex metalloenzymes relying on a multi-step maturation process, which often limits their heterologous expression. O₂-tolerant hydrogenase production in phototrophs has not been achieved yet, and was a main goal of this PhD thesis together with the characterization and optimization of resulting strains.

The third chapter describes the functional expression of genes encoding the O₂-tolerant hydrogenase of *Cupriavidus necator* (*CnSH*) in the cyanobacterial model strain *Synechocystis* sp. PCC 6803 (*Synechocystis*). This was accomplished by introducing only the structural *hox* genes from *C. necator*. Intriguingly, the maturation apparatus of *Synechocystis* is able to assemble functional *CnSH* under aerobic conditions. *CnSH*-containing *Synechocystis* showed H₂ oxidation activity during oxygenic photosynthesis up to ambient O₂ concentrations. Further, *CnSH* enabled lithoautotrophic growth of *Synechocystis* in light with H₂ as sole electron donor. Thereby, *CnSH* was shown to integrate into the phototrophic redox metabolism and interact with the photosynthetic electron transport chain. As expected, photo-H₂ production via *CnSH* was hampered by its strict dependency on NAD(H), which is not a primary electron carrier in photosynthetically active cells. *Synechocystis* with *CnSH* only produced H₂ upon glucose supplementation. Moreover, specific *CnSH* activities determined in *Synechocystis* cell extracts (0.018 U mg_{Prot}⁻¹) were low compared to activities reported for heterotrophic hosts (*P. putida*: 0.16 U mg_{Prot}⁻¹; *E. coli* 1.2 U mg_{Prot}⁻¹). Such poor expression and the fast decay of *CnSH* activity in *Synechocystis* was then tackled by the development of an advanced modular cloning system (based on CyanoGate), which enabled the screening of regulatory genetic elements. Thereby, higher levels of functional *CnSH* and specific H₂ oxidation activity were reached in *Synechocystis* as described in the fourth chapter.

Physiological investigations revealed that *CnSH* activity during phototrophic growth is ruled by source (H_2) and sink (CO_2) availability. Also upon avoidance of such limitations, an increase in *CnSH* levels did not always translate in an activity gain, indicating a shortage in the *CnSH* maturation process. By means of the CyanoGate cloning tool, new *Synechocystis* strains were generated co-expressing *CnSH* operon together with maturation genes of *C. necator* as described in chapter five. Our data demonstrated that a fine balance between maturase abundance and *CnSH* gene expression is crucial to maximize functional *CnSH* levels in *Synechocystis*. The combination of improved and balanced expression enabled an up to 7-fold increase in *CnSH* activity in *Synechocystis* ($0.12 \text{ U mg}_{\text{Prot}}^{-1}$). Under appropriate reaction conditions, this also stabilized *CnSH* activities during oxygenic photosynthesis ($30 \text{ U g}_{\text{CDW}}^{-1}$ over 8 h). The sixth additional chapter describes the regulatory hydrogenase (RH) from *C. necator* produced in *Synechocystis*, underling different requirements to achieve active recombinant hydrogenases in the same host. In conclusion, the research in this thesis led to efficient O_2 -tolerant hydrogenase expression in cyanobacteria and provides insights into its operation and integration in oxygenic metabolism. This paves the way for (1) H_2 -supported O_2 -dependent biotransformations in phototrophs and (2) photo- H_2 production. The latter will require enzyme engineering to enable the direct utilization of electrons derived from photosynthetic water oxidation. In the context of photo-biotechnology, our study constitutes a blueprint, how to systematically approach recombinant protein production in cyanobacteria.

Zusammenfassung

Cyanobakterien können als kohlenstoffneutrale Zell-Fabriken eingesetzt werden, die Elektronen direkt aus der lichtgetriebenen Wasseroxidation für die Herstellung hochwertiger Chemikalien und Biokraftstoffe nutzen, was sie sowohl aus ökologischer als auch aus wirtschaftlicher Sicht attraktiv macht. Biokatalysatoren wie [NiFe]-Hydrogenasen in Cyanobakterien gewinnen zunehmend an Aufmerksamkeit, da sie H_2 nutzen oder produzieren und Redoxreaktionen mit minimalem Überpotenzial durchführen können. Molekularer Wasserstoff (H_2) ist ein energiereicher und sauberer Brennstoff, der bei seiner Verwendung nur Wasser produziert. Cyanobakterielle Hydrogenasen sind jedoch O_2 -sensitiv, was ihre Anwendung im Rahmen der erwartbaren Sauerstoffstoffproduktion durch die Photosynthese, z.B. für die Photo- H_2 -Produktion, beeinträchtigt. Es ist jedoch bekannt, dass eine bestimmte Gruppe bidirektionaler [NiFe]-Hydrogenasen O_2 -tolerant ist und das Potenzial hat, unter aeroben Bedingungen eingesetzt zu werden. Damit wird es möglich einen O_2 -toleranten H_2 -Metabolismus entweder für die Photo- H_2 -Produktion oder die Unterstützung von elektronenfordernden Prozessen (z.B. biokatalytische Oxyfunktionalisierungen) zu etablieren. Hydrogenasen sind komplexe Metalloenzyme, die einen komplexen Reifungsprozess benötigen, der ihre heterologe Expression oft einschränkt. Die funktionale Produktion von O_2 -toleranten Hydrogenasen in Cyanobakterien wurde bisher nicht erreicht und war zusammen mit der Charakterisierung und Optimierung der resultierenden Stämme ein Hauptziel dieser Dissertation. In einem ersten Schritt wurde die funktionelle Expression der O_2 -toleranten Hydrogenase von *Cupriavidus necator* (*CnSH*) im cyanobakteriellen Modellstamm *Synechocystis* sp. PCC 6803 (*Synechocystis*) erreicht, indem nur die strukturellen Hox-Gene von *C. necator* eingeführt wurden. Interessanterweise sind die Maturationsproteine von *Synechocystis* in der Lage, die *CnSH* unter aeroben Bedingungen funktional zusammensetzen. Die *CnSH* in *Synechocystis* zeigt H_2 -Oxidationsaktivität, gleichzeitig zur oxygenen Photosynthese, bis hin zu O_2 -Konzentrationen von 20%. Darüber hinaus ermöglichte *CnSH* das lithoautotrophe Wachstum von *Synechocystis* im Licht mit H_2 als alleinigen Elektronendonator. Ich konnte zeigen, dass *CnSH* Elektronen in den phototrophen Redoxstoffwechsel einspeist und mit der photosynthetischen Elektronentransportkette wechselwirkt. Erwartungsgemäß konnte nur eine geringe Photo- H_2 -Produktion durch die *CnSH* nachgewiesen werden, bedingt durch die strikte Abhängigkeit von NAD(H), welches nicht der primäre Elektronträger in photosynthetisch aktiven Zellen ist. *Synechocystis* mit *CnSH* produzierte H_2 nur nach Glukosezugabe.

Die spezifischen *CnSH*-Aktivitäten, die in *Synechocystis*-Zellextrakten ($0,018 \text{ U mg}^{-1} \text{ totprot}$) bestimmt wurden, waren im Vergleich zu den Aktivitäten, die für heterotrophe Wirte berichtet wurden (*P. putida*: $0,16 \text{ U mg}^{-1} \text{ totprot}$; *E. coli* $1,2 \text{ U mg}^{-1} \text{ totprot}$), gering. Die Expression wurde dann durch die Entwicklung eines fortschrittlichen modularen Klonierungssystems (basierend auf CyanoGate) verbessert, dieses erlaubte zudem ein Screening regulatorischer genetischer Elemente. Dadurch wurden höhere funktionelle *CnSH*- und spezifische H_2 -Oxidationsaktivitäten in *Synechocystis* erreicht, wie im vierten Kapitel beschrieben. Physiologische Untersuchungen zeigten, dass die *CnSH*-Aktivität während des phototrophen Wachstums von der Verfügbarkeit von H_2 und CO_2 bestimmt wird. Auch bei optimaler Versorgung führte ein Anstieg des *CnSH*-Spiegels nicht immer zu einem Aktivitätsgewinn, was auf eine Einschränkung des *CnSH*-Reifungsprozesses hindeutet. Mit Hilfe des CyanoGate Klonierungssystems wurden neue *Synechocystis*-Stämme generiert, die das *CnSH*-Operon zusammen mit Reifungsgenen von *C. necator* koexprimieren, wie in Kapitel fünf beschrieben. Unsere Daten zeigten, dass ein feines Gleichgewicht zwischen Maturase-Abundanz und *CnSH*-Genexpression entscheidend ist, um die funktionellen *CnSH* Mengen in *Synechocystis* zu maximieren. Die Kombination aus verbesserter und ausgewogener Expression ermöglichte eine bis zu 7-fache Erhöhung der *CnSH*-Aktivität in *Synechocystis* ($0,12 \text{ U mg}^{-1} \text{ totprot}$). Unter geeigneten Reaktionsbedingungen stabilisierte dies auch die *CnSH*-Aktivitäten während der oxygenen Photosynthese (30 U gCDW^{-1} über 8 h). Das sechste zusätzliche Kapitel beschreibt Produktion der regulatorische Hydrogenase (RH) von *C. necator*, in *Synechocystis*. Diese Hydrogenase ist funktional unterschiedlich zu den anderen Hydrogenasen und bedingte eine spezielle Herangehensweise um aktive rekombinante Hydrogenasen im selben Wirt zu erreichen. Zusammenfassend, diese Arbeit führte zu einer effizienten O_2 -toleranten Hydrogenase-Expression in Cyanobakterien und lieferte neue Einblicke in deren Funktionsweise und Integration in die Elektronentransportkette der Photosynthese. Dies ebnet den Weg für (1) H_2 -gestützte O_2 -abhängige Biotransformationen in phototrophen Organismen und (2) Photo- H_2 -Produktion. Letztere erfordert Enzymengineering, um direkt Elektronen zu nutzen, die aus der photosynthetischen Wasseroxidation stammen. Im Kontext der Photobiotechnologie stellt unsere Studie eine Blaupause dar, wie rekombinante Proteinproduktion in Cyanobakterien systematisch durchgeführt werden kann.

List of abbreviations

%	Percent
°C	Degree celsius
aa	amino acid
ATP	Adenosine triphosphate
BG11	Standard medium for cyanobacteria
bp	base pair
BPV	Biophotovoltaics
C	Carbon
CBB cycle	Calvin-Benson-Bassham cycle
CCM	Carbon concentration mechanism
CDW	Cell dry weight
CET	Cyclic electron flux
Chl <i>a</i>	Chlorophyll <i>a</i>
CN	Cyanides
<i>Cn_hox</i>	<i>C. necator hox</i> operon
<i>Cn_hyp</i>	<i>C. necator hyp</i> operon
CoA	Coenzyme A
Cyt	Cytochrome
DBMIB	2,5-dibrom-6-isopropyl-3-methyl-1,4-benzochinone
DCMU	3-(3,4-dichlorophenyl)-1,1-dimethylurea
ddH ₂ O	double-distilled H ₂ O (purified water)
DMSO	Dimethyl sulfoxide
DNA	Deoxyribonucleic acid
dNTP	Desoxynucleotidtriphosphat
DSP	Downstream processing
DTT	Dithiothreitol
e-	electron
<i>E. coli</i>	<i>Escherichia coli</i>
EMP	Embden-Meyerhof-Parnas
<i>et al.</i>	<i>Et alii, et aliae, et alia</i>
ETC	Electron transport chain
Fdx/Fd	Ferredoxin
FeFe	iron-iron
FeS	iron-sulfur
Flv	Flavodiiron proteins
FMN	Flavin mononucleotide
FNR	Ferredoxin: NADP oxidoreductase
GABA	γ-Aminobutyric acid
GC	Gas chromatography
Glc	Glucose
Gya	Billion years ago
h	hour
H ₂ ase	Hydrogenase
HR	Homologous region
HRP-conjugated	Horseradish peroxidase
IPTG	Isopropyl-β-D-t-hiogalactopyranoside
KPi	Potassium phosphate

LB	Lysogeny broth
LET	Linear electron flux
LUCA	Last universal common ancestors
NAD(P/H)	Nicotinamide adenine dinucleotide (phosphate) (red/ox)
NBT	Nitro blue Tetrazolium Chloride
NDH-1	NADH dehydrogenase-like complex type-1
NiFe	Nickel-iron
nLC-MS/MS	Nanoscale liquid chromatography- tandem mass spectrometry
OD750	Optical density at 750 nm
OEC	Oxygen evolving reaction center
OPP	Oxidative pentose phosphate pathway
PAL	Present atmospheric level
PAR	Photosynthetically active radiation
PBS	Phycobilisomes
pGGC	Plasmid golden gate cloning
PHB	Polyhydroxybutyrate
PMSF	Phenylmethylsulfonyl fluoride
P _{nrsB}	<i>nrsB</i> promoter
PntAB	Pyridine nucleotide transhydrogenase
P _{psbA2}	<i>psbA2A</i> promoter
P _{rhaBAD}	<i>rhaBAD</i> promoter
PSI	Photosystem I
PSII	Photosystem II
R	Resistance
RBS	Ribosomal binding site
RC	Reaction center
rgLy	reductive glycine pathway
RNA	Ribonucleic acid
rpm	revolutions per minute
RT	Room temperature
rTCA	reductive tri-carboxylic acid
SDS-PAGE	Sodium dodecyl sulphate-polyacrylamide gel electrophoresis
sp.	species
Ta	Annealing temperature
TBS	Tris-buffered saline
TpsbC	<i>psbC</i> terminator
Trx	Thioredoxin
U	Unit [1 μ mole product per min]
UV-Vis	Ultraviolet- Visible
v/v	volume/volume
w/v	weight/ volume
WL	Wood-Ljungdahl
WT	Wild-type
Xgal	5-bromo-4-chloro-3-indolyl- β -D-galactopyranoside

Abbreviations are introduced in the text when used the first time within a chapter.

Chapter 1

General Introduction

This research work lays the foundation on combining the metabolic features of two autotrophic species: *Cupriavidus necator* (Betaproteobacteria), a chemo-litho-autotrophic organism and *Synechocystis* sp. PCC 6803 (Cyanobacteria), an oxygenic photoautotrophic microbe. As a result of this study, we learned that our findings can be explained by their linked autotrophy evolution and specifically hydrogen metabolism. The first part of the introductory chapter focuses on the co-evolution and diversification of autotrophic lifestyles and the specific traits of the two model species. The second part describes the biotechnological applications of hydrogenases (from here H₂ases), including strains, enzymes, and approaches.

By definition, chemolitho- and photo-autotrophic bacteria share the ability to fix inorganic carbon, in this case from carbon dioxide (CO₂), into biomass (autotrophic = self-nourishing), but they differ on the energy exploited. Chemolithotrophic species derive energy from chemical reactions based also on inorganic substrates such as hydrogen (H₂), hydrogen sulfide (H₂S), ammonia (NH₃), ferrous iron (Fe²⁺), and other reduced compounds (lithotrophic). A peculiar type of chemolithotrophy is present in “knallgas” bacteria, which can oxidize H₂ to produce water (H₂+1/2O₂ → H₂O). The best studied hydrogenotrophic species is *Cupriavidus necator* (from here *C. necator*), which is able to mediate H₂ driven oxygen (O₂) reduction through O₂-tolerant H₂ases [1]. Oxygenic phototrophic bacteria, such as cyanobacteria, draw energy from sunlight and derive reduction equivalents necessary to reduce CO₂ from H₂O, which is oxidized to O₂ [2].

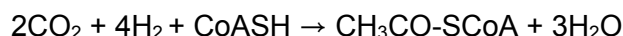
1.1. Autotrophy evolution and diversification

1.1.1. CO₂ fixing bacteria

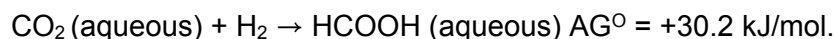
“Carbon fixation is the metabolic anchor embedding life within geochemistry” [3].

All living matter on Earth depends on CO₂ introduction into the biological carbon cycle. In accordance with the vision of an anaerobic hot primordial world, chemo-litho-autotrophic thermophilic anaerobes were most likely the last universal common ancestors (LUCA) performing H₂-dependent CO₂ fixation [4]. It is well accepted that the first three CO₂ fixation pathways possessed by LUCA are the Wood-Ljungdahl (WL) pathway, which together with an incomplete reductive tri-carboxylic acid (rTCA) cycle, formed the reductive acetyl-CoA pathway. The third one, newly described, is the reductive glycine pathway (rgLy) that leads to glycine and serine synthesis directly from CO₂. Because the reductive acetyl-CoA pathway operates near thermodynamic equilibrium, it can be reversed to complete oxidation of acetyl-CoA rather than its flux into the TCA cycle [5]. The primordial evolution of the reductive acetyl-CoA pathway is supported by several evidences: 1) further evolved anabolic pathways originate from five

universal precursors: acetyl-CoA, pyruvate, oxaloacetate, succinyl-CoA, and 2-oxoglutarate, all derived from reductive acetyl-CoA pathways [3]. 2) The WL pathway is the only carbon fixation route able to provide energy conservation via ATP, and 3) it is widespread in a variety of bacteria and archaea, including acetogens and methanogens, sulfate reducers, and possibly anaerobic ammonium oxidizers. This autotrophic pathway includes the direct C1 reduction via the tetrahydrofolate (THF) metabolism in eubacteria (some archaea use tetrahydromethanopterin, H₄MPT, as THF analog) to a level of a methyl group (CH₃), followed by a second CO₂ molecule reduced to carbon monoxide and condensed with the CH₃ and coenzyme A (CoA), yielding acetyl CoA. The overall reaction is the following:



Acetyl-coA is an energy-rich thioester, functioning as origin of all C3-C6 bodies. Therefore, it is considered the central building block of carbon metabolism [6]. In earlier time, H₂ was excluded as first source of electrons, because H₂ oxidation coupled to CO₂ reduction is thermodynamically unfavorable under standard conditions considering the partial redox potential [7]:



However, the hypothesis of abiotic CO₂ reduction by H₂ is plausible due to the alkaline hydrothermal vents existing on the early earth, naturally abundant of H₂ (mM range) and metal sulfides (NiS and FeS) as catalyst [8]. Biological CO₂ fixation in the WL pathway is mediated by reduced ferredoxin (Fd^{2-red}). Each reduction step in the carboxylation reaction, including the formate dehydrogenase (E°': -420 mV) in eubacteria and the formyl methanofuran dehydrogenase (E°': -500 mV) in the methanogenic counterpart, has a more negative standard potential than H₂ (E°': -414 mv). Therefore, H₂-based ferredoxin reduction is endergonic and needs to be coupled to an energy-yielding process to overcome the energy barrier of this reaction. In principle, ancient members of H₂ases, metalloenzymes containing iron sulfur (FeS) clusters for electron transfer, could ensure H₂-mediated ferredoxin reduction mainly via two mechanisms: via electron bifurcation or via chemiosmotic coupling [6]. Electron bifurcating H₂ase can couple the endergonic reduction of low potential, high energy substrate (e.g. ferredoxin) with the exergonic reduction of high potential, low energy substrate (e.g. NAD(P)), without the expenditure of ATP. H₂-driven reduction of ferredoxin is catalyzed by two different electron-bifurcating H₂ases. In methanogens without cytochromes (e.g. *C. kluyvery*), a cytoplasmic [NiFe]-H₂ase (MvhADG) is associated with a heterosulfide reductase (HdrABC), which couples the oxidation of H₂ to the reduction of the cytoplasmic heterodisulfide. The second group is represented by [FeFe]-HydABC and the related [NiFe]-HydABC_{SL}, which are found in anaerobic bacteria. They reversibly oxidize

H₂ and couple the endergonic generation of Fd^{2_{-red}} from H₂ to the exergonic electron flow from H₂ to NAD [9][10]. Alternatively, H₂-mediated ferredoxin reduction is linked to the consumption of a membrane ion gradient by an energy-converting [NiFe] H₂ases (Ech). They constitute a phylogenetically distinct class of membrane-bound H₂ases and are widespread in methanogenic archaea and eubacteria (e.g. firmicutes and deltaproteobacteria) [11].

The WL pathway, the reductive tri-carboxylic acid (TCA) cycle, and the reductive glycine pathway were lately accompanied by the evolution of 4 additional autotrophic pathways: the dicarboxylate/4-hydroxybutyrate cycle, the 3-hydroxypropionate/4-hydroxybutyrate cycle, the 3-hydroxypropionate bicycle, and the Calvin-Benson-Bassham (CBB) cycle. Among them, the CBB is currently the predominant CO₂-fixing mechanism among the extant living organisms [12]. The initial reaction is the carboxylation and cleavage of ribulose-1,5-bisphosphate (RuBP) into two molecules of 3-phospho-glycerate (3PG) and is catalyzed by the ribulose-1,5-bisphosphate carboxylase/oxygenase (Rubisco). This key enzyme is the most abundant one in life on earth and is found in all three domains of life: bacteria, archaea, and eukaryotes. The first type of rubisco dates back to over 2.9 billion years ago, before the great oxygenation event, having evolved in a non-autotrophic context from an enolase in the methionine salvage pathway [13][14]. This enzyme diversified in several forms, of which I, II, and III are characterized by a CO₂ fixing ability, while form IV (Rubisco-like proteins (RLPs)) retains the earlier methionine salvage role [15]. The leading and modern-day form I operates in proteobacteria, cyanobacteria, diatoms, algae, and plants, which connects the evolution of the protein with the development of the world's dominant photoautotrophic organisms [16]. Its ancestors were found in chemo-litho-autotrophs and most likely the rubisco operon was shared via multiple events of horizontal gene transfer within proteobacteria, between proteobacteria and cyanobacteria and between proteobacteria and plastids [17].

1.1.2. From chemo-litho-autotrophs to oxygenic photo-autotrophs - via H₂ metabolism

Geological and phylogenetic records show that anoxygenic ancestors of the modern oxygenic photosynthetic prokaryotes (cyanobacteria) performed CO₂ fixation using H₂ as a reductant [18]. It is argued that H₂ was the first electron source because sedimentary rock formations in Australia [19][20] and Africa (3.3-3.5 millennia ago), where the first cyano-like organisms were found, did not contain traces of oxidized iron and sulfur compounds, ruling out iron (II) and sulfide as candidates [21]. Thereby, chemo-litho-autotrophic H₂ consumers might have profited from energy-converting membrane-bound [NiFe] H₂ases, which catalyze the reversible reduction of ferredoxin with H₂, driven by an electrochemical ion gradient across the membrane. In the heterotrophic archaeon *Pyrococcus furiosus*, the reverse counterpart can be found, a membrane-

bound H₂ase fueled by sugar-derived electrons to produce H₂, also coupled with a chemiosmotic activity. The transmembrane electrochemical ion gradient is then exploited for energy conservation by generating ATP [22]. Therefore, the presence of a bidirectional H₂ase catalyzing, on the one hand, H₂ evolution from Fd^{2⁻red} to drive vectorial proton transport (for ATP generation) and, on the other hand, H₂ consumption to reduce Fd, could provide both ATP and Fd^{2⁻red} for CO₂ fixation. A different version of a membrane-bound H₂ uptake [NiFe] H₂ase is present in *C. necator*, which catalyzes H₂ oxidation with O₂ as terminal electron acceptor (*Knallgas* reaction). This enzyme is a component of the respiratory chain, feeding H₂-derived electrons to the quinone pool via a membrane-integral cytochrome *b* subunit. The electron transport results in the generation of a proton-motive force exploited for ATP synthesis [23][24].

It is currently a well-accepted hypothesis that the first photoautotrophic organism evolved a primitive light cycle as a supplemental source of energy – to become less dependent from H₂-based carbon fixation and ATP generation. The continuous drop in atmospheric H₂ concentration during the Archaean period probably pushed the evolution of the minimal photosynthetic machinery. Reaction center-1 (RCI) developed by multiple duplication events from a simpler chlorophyll-binding membrane protein [25]. As the emergence of Chlorophyll (Chl) is a key event in the evolution of photosynthetic activity, tracking the appearance of Chl and its precursors also can provide insight into the physiological transition from chemolithoautotrophy to photoautotrophy (**Table 1.1**). Because all forms of anoxygenic photosynthesis involve(d) electron transport chains featuring cytochromes, quinones and electron acceptors (e.g., Fe³⁺, S⁰), cells that evolved such photosynthesis implemented RCI in the respiratory chain (RCI, membrane-bound H₂ase, quinones, cytochromes) to establish the first H₂-based anoxygenic photosynthesis [26].

Table 1.1. Following the evolution of chlorophyll precursors to date back cyanobacterial ancestors.
Table adapted from [26].

Relative age	Tetrapyrrole	Physiology	Modern group	Electron sources
Modern (~3 Gya ago [27])	Chlorophyll	Phototrophy (RCI-II)	Cyanobacteria	H ₂ S, H ₂ O
Advanced	Chlorophyll	Phototrophy (RCI)	Cyanobacteria, chlorobia	H ₂ S
Intermediate-2	Porphyrins	Mixotrophy	None	H ₂ S
Intermediate-1	Heme	Anaerobic respiration	Sulfur reducers, autotrophic, ε-proteobacteria	Organics, H ₂
Primordial (~3.5 Gya ago [28])	Cobalamin	Chemolithoautotrophy	Acetogens, metanogens	H ₂

Enhanced growth and carbohydrate synthesis with light-access as energy source, boosted as well carbohydrate degradation during night. Consequently, carbohydrates took over hydrogen as primary electron donors during anoxygenic respiration. Mainly sugar oxidation derived-NADPH or $\text{Fd}^{2-}_{\text{red}}$ were recycled via NADH dehydrogenase-like complex type-1 (NDH-1 complex) compared to H_2 -derived electrons. Therefore, it is plausible that as H_2 became a secondary electron donor, the hydrogenase part lost its permanent attachment to NDH-1 complex [29]. It is now well established that NDH-1 evolved from the group 4 membrane-bound [NiFe] H_2 ases [30]. The initial benefit of photosynthesis was to provide access to additional/ alternative reductants other than less-available H_2 , such as H_2S and Fe^{2+} . However, those electron donors have a lower midpoint potential than H_2 (H_2/H^+ : -414 mV; $\text{H}_2\text{S}/\text{SO}_4^{2-}$: -220 mV; $\text{Fe}^{2+}/\text{Fe}^{3+}$: 760 mV) meaning less energy to be harvested to produce ATP. The need to reinforce proton translocation and ATP synthesis might have been fulfilled by the evolution of a high-potential RCII via gene duplication [25][31]. As soon as the activity of the two RCs became connected via quinone pools as electron mediators, RCII exploited soluble reductants such as Fe^{2+} or Mn^{2+} to provide electrons to the faster oxidant RCI. RCII driven Mn^{2+} oxidation may have represented the first evolutionary intermediate of the current tetra-manganese calcium cluster (Mn_4Ca) [32]. This complex elevates the electrochemical potential of the reaction center and together with the acquisition of Chl a, as strong photo-oxidant, it became the oxygen evolving reaction center (OEC), able to oxidize a weak reducing substrate like water. The complexity and fundamental importance of the four-electron reaction explains, why this catalytic core remained highly conserved among photosynthetic organisms [27]. Finally, the evolution of O_2 enabled the last step, the establishment of aerobic respiration via the integration of terminal oxidases (Cyd, Ctal, Ctall) into the thylakoid membrane, which were acquired via horizontal gene transfer. These enzymes fulfilled important roles still conserved in cyanobacteria, such as ATP production during night, detoxification of the cell from O_2 and drainage of the over reduction of the electron transport chain during shifts in light intensity [33]. This latter function is shared with the bidirectional [NiFe] H_2 ase, which developed mainly as an electron valve for the cell. In fact, photo- H_2 production during the first seconds of (sudden) light exposure serves as a temporary repository for surplus electrons, which can reenter via the reverse reaction and the NDH-1 complex in the electron transport chain (ETC). Eventually, the complete asset of the ETC (PSII to PSI, quinone pool, Cyt, NDH-1, terminal oxidases) resemble the current version in cyanobacterial thylakoids [29]. Aerobic sugar metabolism including respiration leads to 18 times higher energy yield (ATP) than anaerobic sugar-based metabolism and therefore boosted the evolution of complex, multicellular, eukaryotic organisms [27]. The rise of oxygenic photoautotrophs caused a dramatic change in the atmospheric gas composition from a C_1 -rich O_2 -

free atmosphere ($\text{CO}_2 > 300$ of present atmospheric level (PAL); $\text{O}_2 < 10^{-5}$ PAL) to a C_i -depleted and O_2 -rich environment (CO_2 : ~ 1 to 10 PAL; O_2 : 10^{-1} -1 PAL) at the end of the Proterozoic era [34][35]. This transition resulted in a strong selective pressure on key enzymes of autotrophic metabolism. The most significant example is that of Rubisco, a not bona fide carboxylase, which can react with O_2 . Cyanobacteria preserved the carboxylase activity of Rubisco by evolving the carbon concentrating mechanism, in combination with compartmentalization (carboxysomes) and the salvage pathway called photorespiration [16][36].

1.1.3. Regulation of CO_2 metabolism in chemolitho- and photo-autotrophs

Nowadays, the study of CBB cycle regulation in photoautotrophic and chemolithoautotrophic bacteria gains ecological and biotechnological relevance, because of the potential of these organisms for climate change mitigation and sustainable biomanufacturing [37][38]. In this chapter comparing autotrophic CO_2 metabolisms, I mostly refer to *C. necator* and *Synechocystis* sp. PCC 6803 (from here on *Synechocystis*) as model chemolitho- and photo-autotrophic (cyanobacterial) organisms, respectively. The CBB cycle has a complex, multi-level regulation to cope with short- and long-term adaptation to different trophic and environmental conditions. In addition, it coordinates with metabolisms related to inorganic energy resources, supporting the autotrophic life style, such as light and molecular H_2 [12]. The CBB cycle also has to be coordinated with the central carbon metabolism as it overlaps with the pentose phosphate pathway, glycolysis, and sugar metabolism (carbohydrate storage enzymes). In chemolithoautotrophs, the expression of CBB enzymes depends on the substrate applied and therefore on the trophic condition. During lithoautotrophic and formatotrophic growth (formate oxidation via formate dehydrogenase generates NADH and CO_2), CBB enzymes are strongly expressed [39]. During heterotrophic growth on organic substrates, *C. necator* prefers organic acids over sugars as carbon and energy source. Among the sugars, fructose is the preferred glycolytic substrate, but it also can aerobically metabolize glucose and glycerol [40]. Interestingly, CBB cycle enzymes are present during such heterotrophic growth. The point behind this is that heterotrophic metabolism of substrates with higher degree of reduction than biomass is used to provide additional energy to (re-)fix CO_2 and convey a growth benefit. When *C. necator* grows on glucose and fructose, part of the CO_2 is re-assimilated to support storage in terms of polyhydroxybutyrate (PHB) accumulation. The synthesis of autotrophic enzymes, even when not required by *C. necator*, indicates its high metabolic flexibility and readiness for lithoautotrophic growth when H_2 or formate become available, thereby increasing fitness in fluctuating environments [39]. Interestingly, the type of carbon metabolism regulation in cyanobacteria shows a correlation with genome size: e.g., *Synechococcus* PCC 7942, with an approximately 40% smaller genome than *Synechocystis*,

relies on transcriptional level regulation, whereas *Synechocystis* can benefit from a number of isoenzymes with different kinetic properties to respond via biochemical regulation of fluxes [41]. During photoautotrophic growth, glycogen synthesis supported by the CBB cycle and its degradation via the oxidative pentose phosphate pathway (OPP) occur simultaneously. This seemingly wasteful metabolism however allows fast adaptation to light-to-dark transition and stabilizes cellular metabolism and redox state [41][42]. During photomixotrophy, when glucose and CO₂ are assimilated simultaneously, the Embden-Meyerhof-Parnas (EMP) pathway is enhanced, leading to increased NADH formation. Consequently, transhydrogenases (PntAB) are needed to equilibrate NAD(P)H pools. Then, the CBB cycle can work as energy valve to release high redox pressure and enable cofactor re-oxidation. The presence of multiple branches in TCA cycle (such as glyoxylate shunt, GABA shunt, glyoxylate shunt, OgdA/SsaD bypass and malic shunt) confers metabolic plasticity for rapid acclimation during different trophic conditions and nutrient availability. E.g. during photomixotrophic growth the malic shunt provides an alternative route for pyruvate biosynthesis, since pyruvate kinase is allosterically inhibited by ATP during photosynthetic growth [43][44]. Overall the long-term regulation in both autotrophs primarily occurs at the transcriptional level. In contrast, fast adaptation to environmental changes relies on metabolite-protein interaction regulation [45][46]. In oxygenic photoautotrophs the light-dependent redox state is the prominent regulatory signal, which is translated by thioredoxin (Trx)-based regulation [47]. Interestingly, the only essential Trx found in *Synechocystis* was Thioredoxin A (TrxA), which is equally effective under photoautotrophic and heterotrophic conditions. Compared to eukaryotic Trx-based regulation acting on CCB cycle, TrxA in *Synechocystis* interacts with the carbon-concentrating mechanism, which is a main regulator/controller of CO₂ assimilation in cyanobacteria [48].

1.2. Cyanobacteria

Two groups of oxygenic photoautotrophic bacteria are distinguished, differing in photosynthetic pigment content: cyanobacteria, which contain Chl a and phycobilins, and prochlorophytes, which contain the chlorophylls a and b [49]. Cyanobacteria, as prokaryotes, largely lack cell compartmentalization, but evolved a highly structured membrane system called thylakoids [50]. These photosynthetic lamellae harbor photosystems associated with special light harvesting complexes, the so-called phycobilisomes (PBS), which work as antenna complexes absorbing in a characteristic spectrum of light. Contrary to the long-held belief that photosynthetic active radiation (PAR) falls only in the range of visible light ($\lambda = 400\text{--}700\text{ nm}$) for oxygenic photosynthesis in cyanobacteria, algae and plants, it was later discovered the ability of some marine cyanobacteria to use far-red light (above 700 nm). The synthesis of additional Chl types (such as

d and f) and long-wavelength absorbing PBS account for this [51]. In addition, specialized compartments are present in the cytosol, such as carboxysomes (seat of carbon fixation) and storage bodies accumulating glycogen, cyanophycin etc. [52]. Due to the cell-wall structure they are classified as gram-negative bacteria [53][54]. Cyanobacteria present a variety of morphologies such as unicellular, colonial, or filamentous, of which the latter ones can feature 3 different cell types: vegetative, climate resistant akinetes, and heterocysts. All heterocyst- and some non-heterocyst-forming species are able to fix atmospheric nitrogen [55]. In these so called diazotrophic bacteria, N_2 reduction to NH_3 comes along with the production of molecular H_2 . N_2 -fixing strains possess, besides a nitrogenase, a [NiFe] uptake H_2 ase (HupSL), which catalyzes H_2 oxidation to recycle energy. The second type of H_2 ase found in many diazotrophic and also non-diazotrophic bacteria is a bidirectional [NiFe] H_2 ase [56]. Cyanobacteria are massively present in seawater and fresh water and contribute one fourth of the inorganic carbon fixation on earth [57]. Consequently, they have a crucial impact on the world climate, CO_2 content of the ocean, and related parameters such as pH, which determine the presence of other organisms [50]. Eventually, they are the blue print of all oxygenic phototrophs, as an endosymbiotic event between a cyanobacterium and a non-phototrophic host is believed to have led to chloroplasts and, consequently, the first eukaryotic phototroph [58].

1.2.1 *Synechocystis* sp. PCC 6803

The freshwater unicellular cyanobacterium *Synechocystis* sp. PCC 6803 was the first cyanobacterium, which was fully sequenced, i.e., in 1996 by a Japanese working group, with a genome size of 3,573,470 base pairs (bp) coding for 3168 potential protein-encoding genes [59]. In addition to chromosomal DNA, *Synechocystis* contains four large plasmids, encoding for 3168 potential proteins, and three small plasmids recently adapted for genetic engineering purposes [60]. The early characterization of *Synechocystis* genome sequences gave this strain a head start to become the model organism for photobiotechnological applications. Indeed, most of the protocols and genetic toolboxes for constructing mutants are established for *Synechocystis*. Additionally, there are activities towards a strain bank with single knockouts of most genes of *Synechocystis* (CyanoSource) and a CRISPRi library to identify specific phenotypes [52][61]. Despite these steps, a lot research is still required. E.g., only ~30% of the coding sequences have an assigned function, which is less than half compared to *E. coli* [52]. *Synechocystis* offers different traits, which can be exploited, such as optimal growth over a wide temperature range (22-43°C) and the tolerance of high pH values (~ 11), which can help to avoid contaminations. Additionally, it can adapt to a broad span of salt concentrations, making both fresh and salt water suitable for cultivation [62]. For a cyanobacterium, *Synechocystis* shows a rapid growth with a

doubling time of ~4.3 h under carbon saturated conditions (continuous gas bubbling, 1-5% CO₂). Recently discovered faster growing *Synechococcus elongatus* strains, such as UTEX 2973 with a minimal doubling time of 1.5 h, may, however, represent interesting novel platform strains for biotechnological applications [37].

1.2.2 Photo-biotechnological application of cyanobacteria

In the last 120 years, the global CO₂ emissions from fossil resource use for energy and industrial purposes raised from 2 to over 36 billion tons per year (<https://www.iea.org/data-and-statistics/charts/global-co2-emissions-from-energy-combustion-and-industrial-processes-1900-2022>, IEA), accompanied with a steady increase of earth temperature and, consequently, catastrophic weather phenomena. Thus, efforts in both, the reduction of CO₂ emissions and carbon capture technologies, are a must to stop these drastic developments [63]. Cyanobacteria are the carbon capture machinery par excellence, since they recycle ~20% of global CO₂. With only solar energy and water required to fix CO₂, they are a promising candidate for biotechnological developments [64]. The CO₂ fixation efficiency of cyanobacteria is 10–50% greater than that of plants and similar to that of eukaryotic microalgae, profiting from a lower degree of structural complexity, which also helps to make genetic modifications faster and more efficient. As a clear advantage over heterotrophic microbes such as *E. coli* and *S. cerevisiae*, cyanobacteria use inorganic carbon and feature a minimal nutrient requirement [65]. On the other side, heterotrophic strains outcompete cyanobacterial ones in terms of achieved production rates, yields, and titers. The major limiting factor is the rather dilute character of the energy source sunlight, which necessitates its efficient conversion to chemical energy [37]. The maximum theoretical efficiency of the photosynthetic light reaction is 17%, while the final efficiency including the dark reaction of CO₂ fixation, biomass synthesis, and maintenance often is less than 1%. Indeed, branching off electrons from the light reaction (PSII and PSI) will retain a high quantum efficiency for product formation in a range between 10-14%, 10-20-fold higher than for carbon-based products [66]. Thus, such direct use of the light reaction, e.g., for H₂ production via biophotolysis or biophotovoltaics (BPV) approaches, is of high interest with high optimization potential regarding the ETC step, at which electrons are withdrawn [67].

1.2.3 White H₂

H₂ gas is a promising energy carrier, which can be produced in a carbon neutral way and features a 3 times higher energy density than gasoline (lower heating value of 120.1 MJ/kg) and a superior efficiency in fuel cells than hydrocarbons (about 35-50%) [68]. Currently, various technologies are being developed for H₂ production. They are classified on a color code level based on the energy

source utilized and CO₂ emissions. Even though the green H₂ concept based on renewable energy sources (hydro, solar and wind) to power water electrolysis reached acceptable efficiencies, these technologies are penalized by high costs, especially when it comes to minerals and metals [69]. One of the most appealing processes to produce H₂ in the future is to engineer natural photosynthesis. The so called white H₂ is achievable via two approaches using whole-cell biocatalysis: biophotolysis and BPV [67]. Biophotolysis implies the direct coupling of oxygenic photosynthesis to H₂ formation via H₂ases. The net reaction is based on water-splitting using sunlight energy with H₂ and O₂ as products [70]. In BPV, the microbial electrolysis cell concept is applied to phototrophs. Thereby, the anode is connected to the photosynthetic electron transport chain, with the transferred electrons driving proton reduction at the cathode side. Biophotolysis and BPV have the advantage to withdraw electrons directly from the light reaction, whereas other biological approaches such as fermentative H₂ production depend on carbon metabolism and respective energy loss. BPV and biophotolysis are constrained by various biology-related factors, e.g., the efficiency of electron transfer to the anode in the case of BPV. The following part illustrates the major limitations of biophotolysis, specifically biocatalyst-related ones. One above all is the O₂-sensitivity of cyanobacterial [NiFe] H₂ases, documented by the activity drop after transition from dark to light at the onset of the photosynthesis. Secondly, the electron transfer efficiency between photosynthetic ETC and H₂ases constitutes a bottleneck, also involving competition for reduction equivalents with downstream assimilatory pathway [71][68]. Although H₂ production via the *Synechocystis* H₂ase (*SynH₂ase*) is energetically feasible, since it relies on reduced ferredoxin/ flavodoxin as electron carrier (F_{d_{red/ox}}: -430 mV; H₂/H⁺: -413 mV) [72], the challenge is to divert electrons from cellular metabolism to biologically futile H₂ production. A direct competitor for photosynthetic electrons is the CBB cycle fueled with electrons via Ferredoxin-NADP⁺-Oxidoreductase (FNR), which prevails over the H₂ase due to its abundance, higher affinity for ferredoxin, and eventually direct connection to PSI [73][71]. Recent advances in addressing these issues include fusion of the [NiFe] H₂ase module from *Synechocystis* with PSI, which enabled photo-H₂ production *in vivo* under anaerobic conditions for a longer period of time. The increased electron transfer efficiency from the ETC reduced the competition with anabolic pathways [74]. Additionally, in cyanobacteria, enhanced photo-H₂ production was demonstrated by inhibiting nitrate assimilation and the terminal oxidase, which represent additional competitive electron sinks [75]. A third metabolic constraint to biophotolysis is the increase in the ATP/NADPH ratio, once H₂ase consumes most of the electrons from photosynthesis, ATP accumulation will eventually stop the electron transport. Therefore, future efforts need to focus on the partial uncoupling between water-derived electron supply and ATP synthesis [76]. Together with solving

these obstacles, reaction engineering and downstream processing (DSP) need to be implemented to enable efficient product recovery and overcome O₂ accumulation, which in combination with H₂ forms a dangerous oxy-hydrogen gas [67].

1.3 Hydrogenases

One of the most ancient microbial metabolic reaction is the interconversion of molecular H₂, protons, and electrons ($2\text{H}^+ + 2\text{e}^- \leftrightarrow \text{H}_2$) catalyzed by H₂ases. The vast majority of H₂ases are metalloenzymes with two types of metal complexes: 1) the iron- sulfur clusters, [2Fe2S], [3Fe4S], and [4Fe4S], able to shuttle electrons between the catalytic center binding H₂ and the H₂ase redox partner and 2) a metal duo located in the reaction center which defines the enzyme class, [NiFe]- or [Fe]-H₂ase [77]. A different type are the metal-free H₂ases found in some methanogens functioning as H₂-forming methylene-tetra-hydro-methanopterin dehydrogenase (Hmd) that does not contain FeS cluster and Ni [78]. These three H₂ase groups are phylogenetically distinct based on sequence and structure evidence and also differentially distributed among domains and kingdoms. While [FeFe] H₂ases are found in anaerobic bacteria and anaerobic or phototrophic eukaryotes, they are not present in cyanobacteria and archaea. On the other hand, [NiFe] H₂ases are absent in the eukarya domain [79]. Despite the independent evolutionary origins and different taxonomic distribution, [NiFe] and [FeFe] H₂ases evolved the same solution to catalyze H₂ activation, employing carbon monoxide (CO) and cyanides (CN) groups linked to a Fe atom in the catalytic site. This represents a clear case of convergent evolution [80]. H₂ases recycle the over-reduced pool of electron carriers (e.g., during anaerobic metabolism), “storing” electrons in the form of H₂, or fuel the cellular anabolism with H₂-derived electrons. Generally, [FeFe] H₂ases are rather involved in proton reduction, while [NiFe] H₂ases are biased towards H₂ oxidation, although this depends on the metabolic context [81]. One common feature of most H₂ases is their inactivation by O₂, but the oxidized catalytic site of [NiFe] H₂ases can be reactivated upon reduction and removal of O₂. In contrast, the oxidative inactivation of [FeFe] H₂ases is irreversible, as O₂ binding leads to protein destruction. There are, however, O₂-tolerant and O₂-insensitive [NiFe] H₂ases, which feature unaltered activity at ambient O₂ concentration or a catalytic site completely impermeable to O₂, respectively (details in Chapter 1.5.3) [82][83].

1.3.1 [NiFe] H₂ases

The minimal core enzyme of [NiFe] H₂ases consists of an α - β heterodimer. The large α subunit (~60 kDa) hosts the bimetallic [NiFe] active site coordinated with 4 conserved cysteine residues. The catalytic site also comprises 3 non-protein ligands, 1 CO and 2 CN⁻, bound to the Fe atom [84]. The small β subunit (~30 kDa) harbors up to 3 [FeS] clusters. [NiFe] H₂ases are

predominantly involved in energy yielding processes and H₂-related gene regulation. Some microorganisms possess multiple H₂ases and display a high metabolic flexibility [85] [86]. [NiFe] H₂ases are encoded by multicistronic operons including structural genes and usually genes encoding accessory proteins. Strictly associated to H₂ase production are a set of pleiotropic *hyp* genes encoding for a [NiFe] H₂ase maturation machinery. Based on the phylogenetic analysis of genes encoding the small and large subunits, [NiFe] H₂ases are divided in 5 groups, with a physiology-related definition (**Table 1.2**) [80].

Table 1.2. [NiFe] H₂ase groups. Table adapted from [77], [85], [80]. In bold the 3d group to which the bidirectional H₂ases from *Synechocystis* and *C. necator* belong.

Group	Function	Domain/phyla
1	Membrane-bound uptake H ₂ ase	Archea, Proteobacteria
2	2a Cyanobacterial uptake H ₂ ase	Cyanobacteria
	2b H ₂ -sensing H ₂ ase	Proteobacteria
3	3a F ₄₂₀ - reducing H ₂ ase	Archea
	3b Bifunctional (NADP) H ₂ ase	
	3c Methyl viologen-reducing H ₂ ase	
	3d Bidirectional NAD(P)-linked H₂ase	Proteobacteria, Cyanobacteria
4	Membrane-bound H ₂ -evolving H ₂ ase	Archea, Proteobacteria
5	High-affinity H ₂ ase	Actinobacteria, Proteobacteria, Acidobacteria, Chloroflexi

1.3.2. Group 3D H₂ases: two key examples from *C. necator* and *Synechocystis*

The essential dimeric H₂ase structure in this group associates with other subunits able to bind soluble cofactors such as, NAD/ NADP, cofactor 420, flavodoxin, and ferredoxin and works reversibly. The NAD(P)-dependent bidirectional [NiFe] H₂ases feature 3 main redox active cofactors: [NiFe], FeS, and one or two flavin mononucleotide (FMN) molecules [79]. The group 3D H₂ases mainly occur in cyanobacteria and proteobacteria. Two of the best studied examples are the *Synechocystis* H₂ase (*SynH₂ase*) and the soluble *C. necator* H₂ase (*CnSH*). They share the heterotetrameric core structure HoxHYUF, composed of 2 dimeric moieties. HoxHY represents the H₂ase module (harboring the [NiFe] active site) and HoxUF the NAD(P)H:acceptor oxidoreductase (diaphorase) module [86]. The HoxUF complex is homologous to Complex I subunits of the electron transport chain [87]. *CnSH* includes a distinct accessory homodimeric

subunit, HoxI₂, loosely attached to the diaphorase HoxUF module and with putative NADPH-sensing function [88]. An additional HoxE subunit is commonly found in the diaphorase module of O₂-sensitive H₂ases like cyanobacterial ones, probably involved in membrane attachment and coenzyme interaction [89][90]. The HoxEFU diaphorase module of *Synechocystis* can interact with many redox partners such as NAD(P)(H), ferredoxin, and flavodoxin, although ferredoxin and flavodoxin are believed to be preferred [72], while HoxFU of *CnSH* is strictly NADH-dependent. *SynH₂ase* acts as an electron valve, producing H₂ to release redox poise of the cells under anaerobic fermentative growth and at the onset of photosynthesis (for ~30 s) [91][92]. It works as an electrons sink also under mixotrophic and nitrate-limiting conditions since it was found to be essential for *Synechocystis* survival [72]. The produced H₂ can later be consumed again to harvest its chemical energy to fuel the PQ pool. Its bidirectional activity stops as soon as the catalytic site is exposed to O₂, when a Ni-Fe bridging hydroxyl group evolves, which prevents H₂ activation. Under reducing conditions, reactivation quickly happens upon O₂ removal (in less than 90 s) [91]. Among group 3D, the first isolated and genetically characterized H₂ase was the hexameric, soluble O₂-tolerant NAD-dependent H₂ase from *C. necator* (HoxFUYHI₂) [93][94]. Within the core structure, the electron transfer between HoxF and HoxH is mediated by a series of four FeS clusters and two FMN molecules [95]. In the diaphorase module, FMN-b is accommodated in the NADH-binding pocket, acting as a connector between NADH, carrying two electrons, and the iron-sulfur clusters (three [4Fe4S], one [2Fe2S]), which can only transfer one electron at the time [96][97]. The small H₂ase subunit HoxY harbors a proximal iron sulfur cluster (presumably a [4Fe4S]) and a second FMN molecule (FMN-a) exclusively present in *CnSH* and described as loosely bound, but easily reconstitutable by external addition (**Fig. 1.1**).

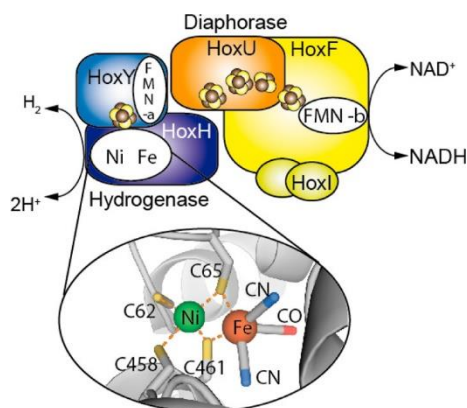


Figure 1.1 Schematic overview of the structure of the soluble *C. necator* H₂ase. The hydrogenase and diaphorase modules are shown separately including their cofactors. Due to the lack of a *CnSH* crystal structure, the zoom in circle of the Ni-Fe active site originates from the homology model based on the *D. vulgaris* H₂ase structure. Figure from [99].

The FMN-a close to the catalytic site provides 2 electrons for complete O₂ reduction to water (see chapter 1.3.3 for details). An FMN-a depleted version was shown to be unable to catalyze H₂-driven NADH formation [98]. During lithoautotrophic growth on H₂, CO₂, and O₂, *CnSH* plays a key role in the energy metabolism, supplying H₂-originated electrons as NADH to fix CO₂ via the CBB cycle. In addition, NADH can be re-oxidized by Complex I channeling electrons into the respiratory chain to generate ATP via the proton gradient [40]. As already described, *C. necator* is a facultative hydrogenotroph with the ability to metabolized various organic substrate. Due to the scarcity of molecular H₂, it was not surprising to discover H₂ase expression to be regulated by the trophic state. *CnSH* was found highly active during lithoautotrophic and formatotrophic conditions, but also during heterotrophic growth on poor substrates and H₂, while lower activities were detected upon growth on preferred substrates such as organic acids and fructose [100]. On the basis of what is discussed regarding the regulation of the CBB cycle, substrates supporting high H₂ase activity are those with lower reduction degree than biomass, thus requiring additional reduction equivalents to (re-)fix CO₂. The *CnSH* can work in both directions depending on H₂, NAD⁺, and NADH concentrations, as the thermodynamic potentials of the two half-reaction catalyzed by the H₂ase (2H⁺/H₂: -413 mV) and diaphorase subunits (NAD⁺/NADH: -320 mV) are close [101]. Over-potential driving NAD⁺ reduction occurs under aerobic conditions when the NAD/NADH pool is largely oxidized. The reverse reaction only occurs transiently during the shift from aerobic to anaerobic conditions [23]. A high NADH/NAD ratio (e.g., 100:1 for a decrease of redox potential to -379 mV) and low H₂ concentrations are needed to drive NADH-mediated proton reduction. In this context, *CnSH* acts as energy valve oxidizing the over-reduced NADH pool. Similarly to the *SynH₂ase*, it transiently stores an electron surplus as H₂. The catalytic bias of *CnSH* is towards H₂ oxidation activity (342 s⁻¹), rather than H₂ production (0.11 s⁻⁹) [93][99][83].

1.3.3 O₂-tolerant H₂ases

The β-proteobacterium *C. necator* hosts 4 different [NiFe] H₂ases, two O₂-tolerant ones being membrane-bound (MBH) and soluble (*CnSH*) and two O₂-insensitive H₂ases one of regulatory type (RH) and one Actinobacterial (AH) [83].

Thanks to a special redox cofactor setup, O₂-tolerant enzymes are able to deliver 4 electrons/protons and completely reduce O₂ in the active site to harmless water. In contrast to O₂-sensitive [NiFe] H₂ases, *CnSH* and MBH do not exhibit the two common oxidized states of the catalytic site, Ni_U-A and Ni_r-B, indicative for the presence of an O₂ species bound to [NiFe] center [102]. EPR studies [103], mutation studies [104], and the resolved crystal structure of *C. necator* MBH [105] revealed a novel [4Fe3S] cluster species in close proximity to the active site with the crucial role to assist the reductive removal of O₂ [106]. The O₂ tolerance mechanism of *CnSH* differs from

that of MBH for 2 reasons. Firstly, the reduced cytoplasmatic environment ensures a redox potential that well matches the midpoint potential of internal redox cofactors and favors the reduced resting state Ni_a-C. This asset allows reversible electron flow from either H₂ or NADH to the catalytic center (bidirectional activity), which is fundamental for efficient O₂ detoxification. Indeed, a bridging hydride in the catalytic site is ready to deliver 2 electrons in case of O₂ attack (Fig. 1.2).

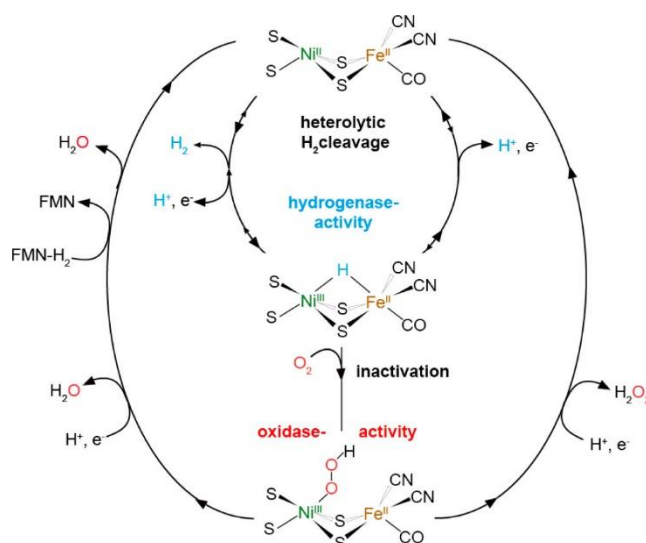


Figure 1.2: O₂-tolerance mechanism of CnSH [99]. H₂ and NADH mediated-O₂ reduction at the catalytic site leads to the formation of H₂O₂ (right reaction) or H₂O (left reaction).

Upon hydroperoxo formation, a protonation is sufficient to release H₂O₂ [99]. Secondly, there is no indication for a [4Fe3S] cluster proximal to the catalytic center of CnSH, as it is the case for MBH [107], but the unique FMN-a cofactor is responsible to deliver two further hydrides to the hydroperoxo ligand to reduce it to water. Overall, the presence of FMN-a positively correlates with full reduction of O₂ into two water molecules. Thus, the O₂-tolerance of CnSH relies on the formation of H₂O₂ and, especially, harmless water and no more toxic radical species [99][108]. Due to their oxidase activity, O₂-tolerant H₂ases exhibit unaltered bidirectional activity at atmospheric levels of O₂ when compared to anaerobic conditions, and only 20% lower activity in an atmosphere saturated with 60% O₂. However, when O₂ saturation is twice the ambient level, 3% of the electrons derived from H₂ flow into O₂ reduction, while the reverse reaction fueled by NADH leads to 1.6 higher O₂ reduction compared to H₂ production, as O₂ outcompetes protons at the [NiFe] active site [109][99].

In contrast, O₂ insensitive H₂ases are non-reactive towards O₂, meaning that even in the presence of O₂, the bridging position between [NiFe] remains vacant without forming an OH-complex. This is the case for RH and AH of *C. necator*, which are insensitive to O₂ species and CO [110][111].

RH is a member of the group 2b sensing H₂ases with no role in H₂ metabolism, but governing the expression of SH and MBH via a signal-transmission circuit [112]. For regulatory H₂ases, complete insensitivity to O₂ is essential for their H₂-sensing role in aerobic environments, so that they can forward the signal of H₂ availability without delay. Interestingly, their O₂ protection mechanism is based on two uncommon bulky amino acids (isoleucine and phenylalanine) at the active site gate, which reduce the gas channel size and thus prevent O₂ entrance [113].

1.3.4 Maturation of [NiFe] H₂ases

[NiFe] H₂ases are encoded by multicistronic operons that encompass structural and auxiliary genes. Specifically, a minimal set of six pleiotropic genes (*hyp* genes) are required for the maturation of the [NiFe] core structure in the premature H₂ase large subunit [114][115]. In *C. necator*, the operons encoding for structural and auxiliary genes are located on the megaplasmid PHG1. The seven *hyp* genes (*hypA1B1CDEX*), responsible for MBH, SH, as well as RH maturation, are placed within the MBH operon, while AH-specific maturases encoding genes are arranged in the AH operon. The *CnSH* operon (*hoxFUYHWIA2B2F2*) comprises, beside five SH-related ORFs, also the gene for the H₂ase-specific endopeptidase *hoxW* and duplicates of three *hyp* genes (*hypA2B2F2*). This subset alone is not sufficient for *CnSH* maturation. HypC1, D1, and E1 were shown to be necessary to fully assemble the active site, whereas only one copy of each *hypF*, *hypA*, and *hypB* suffices for this purpose [116]. In *Synechocystis*, the structural genes are clustered in the same operon (*hoxEFUWH*), while, exceptionally, all *hyp* genes, namely *hypABCDEF*, are scattered throughout the genome [117]. *Synechocystis* contains 2 homologues of the *hypAB* genes, but only the *hypA1B1* copy is necessary for the production of an active H₂ase. Although the *SynH₂ase* is active only under anaerobic condition, both *hox* and *hyp* operons are constitutively expressed [118]. The minimal set of *hypABCDEF* gene products are dedicated to the synthesis and assembly of the Fe(CN⁻)₂CO cluster and the nickel ion within HoxH apoprotein in few sequential steps. The current model of the maturation is based on studies firstly performed on the H₂ase 3 from *E. coli* and consists of few main stages: the biosynthesis of the CN⁻, CO, and the {Fe(CO)(CN⁻)} complex, nickel incorporation, and a proteolytic step (**Fig. 1.3A**). HypF thereby catalyzes the synthesis of CN⁻ from carbamoylphosphate, whereas HypE functions as carrier delivering the CN⁻ ligand to the Fe center coordinated by a HypCD protein complex (**Fig. 1.3B**). CO biosynthesis has been elucidated to occur from the Ci pool in aerobic H₂-oxidising bacteria including *C. necator*, *Rhizobium leguminosarum*, and *Aquifex aeolicus*. These strains carry a *hypX* gene encoding an enzyme responsible for the release of CO from N¹⁰-formyltetrahydrofolate via a thioformate intermediate (**Fig. 1.3C**) [119][120]. However, it is still not clear, how the delivery of CO to the Fe happens. The *Synechocystis* genome does not contain a

hypX homologue, and CO biogenesis and incorporation are still not unraveled. Only after {Fe(CO)(CN)} delivery to premature HoxH, Ni insertion occurs via the metallochaperons HypAB (Fig. 1.3) [121] [124]. Eventually, a specific endopeptidase named HoxW catalyzed the C-terminal cleavage of HoxH, triggering the final conformation change to the active form [123].

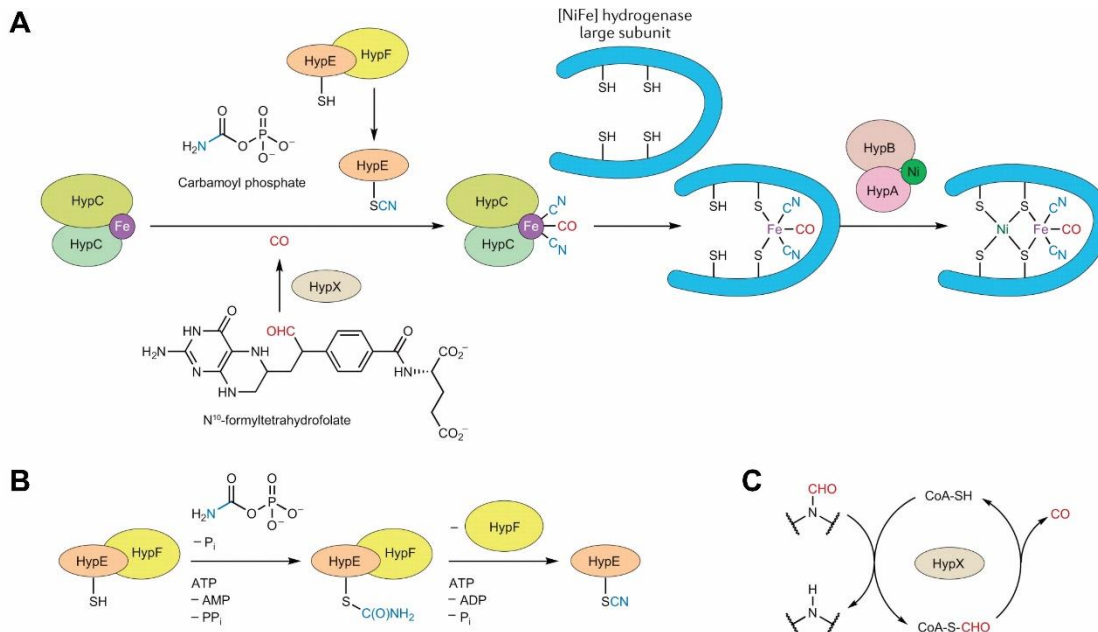


Figure 1.3. General [NiFe] H₂ase maturation process proposed for *CnSH*. (A) the current model includes three main steps catalyzed by the Hyp proteins: ligands biosynthesis, {Fe(CO)(CN)} complex formation and insertion in HoxH, and nickel delivery. The final proteolytic cleavage is not represented in the figure. (B) CN⁻ and (C) CO ligands biosynthesis from organic source. HypX activity is specific for aerobic H₂-oxidising bacteria as *C. necator*. Modified picture from Britt *et al.*, 2020 [122].

1.3.5 Recombinant expression of [NiFe] H₂ases

Due to the high complexity and specificity of the maturation system for the respective H₂ase, the functional heterologous expression of [NiFe] H₂ases has been reported mainly in closely related hosts or in hosts with high homology level of *hox* and *hyp* sequences. However, to reach recombinant enzyme activity comparable to the native host, it is usually required to co-express the specific maturation proteins. It is of biotechnological interest to optimize the heterologous biosynthesis of [NiFe] H₂ases, hence ensuring highly active H₂ases in heterotrophic or phototrophic host organisms [124]. In this regard, Wells *et al.* aimed to improve H₂ production in *E. coli* via recombinant expression of the *SynH₂ase* (HoxEFUYH) together with its maturation factors HypABFCDE and HoxW. They reported full H₂ase activity only when all seven maturases were co-expressed. Every single deletion affected the *SynH₂ase* activity to different extents. However, only *hypA* and *hoxW* turned out to be essential [125]. Various successful attempts also targeted the recombinant expression of the O₂-tolerant *CnSH* in heterotrophic organisms and

recently in a phototrophic organism [126] [127][128][129] [130]. Interestingly, they do not converge on whether or not it was necessary to co-express the specific *C. necator* maturation apparatus to achieve a functional recombinant enzyme. Despite the need for further research, key differences among these studies include the genetic background of the host strains, growth conditions applied, the fine tuning between exogenous H₂ase and auxiliary proteins synthesis, and the research goals. Overall, when the partial or entire set of *C. necator hyp* genes was co-expressed, resulting protein yields and activities were the highest. It is noteworthy to mention the results from Schiffel and co-workers, who showed CnSH yields and activity in *E. coli* comparable to the native host, by generating an advanced cloning system and co-expressing the entire maturation apparatus of *C. necator* [128].

1.3.6 Biotechnological application of CnSH

CnSH offers undeniable advantages for biotechnology. Together with the O₂ tolerance, its bidirectional activity and cytoplasmatic localization allow a broad range of industrial applications. Various attempts aiming at CnSH application in heterotrophic hosts are summarized in the following.

1.3.6.1. H₂ oxidation

The biased CnSH activity towards H₂ oxidation is attractive for fuel cell- and redox biocatalysis applications. High-yield production of recombinant O₂ tolerant [NiFe] H₂ases has been achieved in *C. necator* and *E. coli*, being attractive for application in a H₂-driven fuel cell [131] and for redox cofactor regeneration [132]. Cofactor-dependent oxidoreductases, e.g., dehydrogenases and oxygenases, perform industrially relevant biotransformations, which rely on continuous NAD(P)H supply. The stoichiometric addition of these cofactors is expensive and economically unfeasible, while the commonly employed NAD(P)H-recycling systems, e.g., formate and glucose dehydrogenases involve side product formation and often suffer from low catalytic and resource use efficiencies. The O₂-tolerance of NAD⁺ reducing H₂ases is a necessity for a combination with oxygenase catalysis. H₂ is a cheap substrate and, via H₂ase catalysis, provides reduction equivalents without side product formation and with high efficiency [133]. Many examples are present for *in vitro* cofactor regeneration with CnSH, such as the combination of diaphorase NAD⁺ reductase with different H₂ase modules coated on graphite particles [134]. H₂-driven whole-cell biotransformation involving CnSH-based cofactor regeneration offers an appealing alternative to *in vitro* systems, as it does not require protein purification but can profit from higher enzyme stability in the cellular context and continuous enzyme regeneration. In the last decades, *C. necator* was engineered for the biosynthesis of high value chemicals and biofuels under

lithoautrophic conditions [135][136]. The first successful heterologous *CnSH* expression in a non- H_2 oxidizing host has been reported to enable H_2 -driven biotransformation of n-octane to 1-octanol in *P. putida* catalyzed by a P450 monooxygenase [137].

1.3.6.2. H_2 production

Recombinant expression of a NADH-dependent H_2 ase in *E. coli* is attractive as it allows fermentative H_2 production by supporting the cell in NADH re-oxidation during fermentative growth without competing for energy designated to cellular metabolism. Due to its NADH dependency, various attempts aimed to improve fermentative H_2 production in *E. coli* via the recombinant expression of *CnSH*. A remarkable achievement *in vivo* has been reported by Ghosh and coworkers with *CnSH* able to produce 2 mols H_2 per glucose, which is close to the theoretical maximum [129]. Regarding the strategy employed, it is important to mention that the study used the native *CnSH* genomic sequence and co-expression of a subset of *CnHyp* proteins (HypA2B2F2). Some years later, Lamont and Sargent also reported the functional integration of recombinant *CnSH* in *E. coli* metabolism. The approach differed mainly by the use of codon-optimized structural genes and by completely relying on the Hyp proteins from *E. coli* for *CnSH* maturation. The H_2 production achieved was, however, significantly lower, which may be explained by inefficient expression and/or maturation of *CnSH*. [126]. Similarly, Teramoto *et al.*, recombinantly expressed *CnSH* in a different *E. coli* strain (W3110) using the minimal set of structural genes and *hoxW*. However, the recombinant *E. coli* strain produced less H_2 than the native one, and the activity of *CnSH* was repressed when highly expressed. All together, these results might indicate the need for a fine balance of synthesis and maturation of exogenous protein [127].

1.4 Scope of the thesis

The biotechnological application of cyanobacteria for the production of high value chemicals and biofuels is attractive from an environmental perspective, as they can be considered carbon-neutral “machines”. In comparison to more complex eukaryotic photoautotrophs, they profit from a higher CO_2 fixation efficiency and a simpler cellular organization, also simplifying genetic manipulation. However, the commercial employment of cyanobacteria as cell factories still suffers from high costs and low biomass- and product titers. One can however distinguish between electron- and carbon-based products. Whereas the latter refers to CO_2 -based product formation, the former only depends on the light reaction and directly exploits light-driven water oxidation to fuel biosynthesis with “sustainable and cheap” electrons [37][138]. This application area includes biophotolysis and light-driven O_2 -dependent and electron-demanding biocatalysis as prominent

examples. H₂ases thereby either function as product forming enzyme or can provide surplus electrons in addition to those from the light reaction. The O₂-sensitivity of cyanobacterial bidirectional H₂ases, e.g., from *Synechocystis*, limits their feasibility for such applications. Thus, this study aimed at establishing an O₂-tolerant H₂ase and H₂ metabolism in *Synechocystis* by substituting the native H₂ase with the soluble bidirectional O₂-tolerant [NiFe] H₂ase from *C. necator* (*CnSH*). **Chapter 3** describes the efforts towards the construction of the first cyanobacterial strain containing a functional O₂-tolerant H₂ase and its characterization regarding H₂ oxidation activity during oxygenic photosynthesis and the limited conditions which allow H₂ production with the *CnSH* in *Synechocystis*. In heterologous systems, H₂ase abundance and/or maturation may well limit the enzyme activity. Based on the findings of chapter 3, we aimed to increase proteins level by establishing a controlled and stable recombinant expression of *C. necator hox* operon in *Synechocystis*. **Chapter 4** enlightens the application of an advance modular cloning system to efficiently choose and screen genetic elements for the optimal construction of the *CnSH* expression system. Besides protein production, we investigated which factors (e.g. substrate and sink availability) influence the H₂ase activity *in vivo*. **Chapter 5** aimed to optimize *CnSH* post-translational process, by co-expressing its associated maturation factors (*CnHyp* proteins). For this purpose, we designed different expression systems to modulate the synthesis of the entire *hyp* operon along with the production of the structural proteins. Finally, the **Chapter 6** provides, via the characterization of a recombinant *Synechocystis* strain expressing the regulatory H₂ase (RH) of *C. necator*, an interesting comparison between the two recombinant *Synechocystis* strains expressing the SH and RH from *C. necator*.

Chapter 2

Materials & Methods

2.1. *Synechocystis* strains

Table 2.1 Strains used and generated in this work.

Strain	Characteristics	Ref.
<i>E. coli</i> DH5 α	F ⁻ F80lacZDM15 Δ (lacZYA-argF) U169 recA1 endA1 hsdR17 (rK ⁻ , mK ⁺) phoA supE 44 λ B- thi ⁻¹ gyrA96 relA1	[139]
<i>S. cerevisiae</i> BJ 5464	MATalpha ura3-52 trp1 leu2-delta1 his3- Δ 200 pep4::HIS3 prb1-delta1.6R can1 GAL	ATCC
<i>Syn</i> _WT	<i>Synechocystis</i> sp. PCC 6803 wild type. Geographical origin: California, USA. Received from Pasteur Culture Collection of Cyanobacteria (PCC, Paris, France)	[140]
<i>Syn</i> _ Δ hox	<i>Synechocystis</i> sp. PCC 6803 strain in which the native <i>hox</i> operon was replaced by kan ^R Antibiotic cassette. Integration of chl ^R antibiotic cassette between <i>slr1597</i> and <i>sll1514</i>	[74]
<i>Syn</i> _CnSH ⁺	<i>hox</i> operon of <i>C. necator</i> was fused to the <i>psbA2</i> promoter; cassette was integrated into the original locus of the native <i>hox</i> genes from the WT (Δ hox::PpsbA2hoxFUyHW(PCC6803))	This study
<i>Syn</i> _P _{nrsB} CnSHg	<i>hox</i> operon as constructed in pGGC 212 was integrated into the original locus of the native <i>hox</i> genes from the WT (Δ hox::PpsbA2hoxFUyHWI(PCC6803))	This study
<i>Syn</i> _P _{nrsB} CnSHp	The replicative plasmid containing the <i>hox</i> operon, pGGC 209 was introduced in <i>Syn</i> _ Δ hox.	This study
+pP _{nrsB} CnHyp	<i>Syn</i> _P _{nrsB} CnSHg transformed with pGGC 271 pSEVA plasmid, harboring <i>Cn_hyp</i> synthetic operon fused to the <i>nrsB</i> promoter.	This study
+pP _{rhaBAD} CnHyp	<i>Syn</i> _P _{nrsB} CnSHg transformed with pGGC 272 pSEVA plasmid harboring <i>Cn_hyp</i> synthetic operon fused to the <i>rhaBAD</i> promoter	This study
+pP _{psbA2} CnHyp	<i>Syn</i> _P _{nrsB} CnSHg transformed with pGGC 273 pSEVA plasmid harboring <i>Cn_hyp</i> synthetic operon fused to the <i>psbA2</i> promoter	This study
+pP _{nrsB} CnHypX	<i>Syn</i> _P _{nrsB} CnSHg transformed with pGGC 243 pSEVA plasmid harboring the native sequence of <i>Cn_hypX</i> gene, fused to the <i>nrsB</i> promoter.	This study
+pP _{rhaBAD} CnHypX	<i>Syn</i> _P _{nrsB} CnSHg transformed with pGGC 244 pSEVA plasmid harboring the native sequence of <i>Cn_hypX</i> gene, fused to the <i>rhaBAD</i> promoter.	This study

2.2. Plasmids & Oligonucleotides

The list of plasmids and primers used and generated in this study are listed in **Table S2.1** and **Table S2.2** respectively.

2.3. Chemicals

Unless otherwise stated, all chemicals used in this work were mainly obtained from Advansta (Bering Dr, CA, USA) AppliChem (Darmstadt, Germany), Becton Dickinson and Company (East Rutherford, NJ, USA) Bio-Rad (Hercules, CA, USA), Chemsolute (Renningen, Germany), Macherey & Nagel (Düren, Germany), Merck (Darmstadt, Germany), New England Bio Labs (NEB), NIPPON Genetics EUROPE (Düren, Germany), Promega (Madison, WI, USA), Roth (Darmstadt, Germany), Sigma-Aldrich (St. Louis, MO, USA), Thermo Fisher Scientific (Waltham, MA, USA).

2.4. Software and Database

Chromeleon 7, CorelDRAW 2018, Geneious 10.2., Origin 2018, Microsoft Excel 2013, Microsoft PowerPoint 2013, Proteome Discoverer 2.4, Universal Protein Resource (UniProt) [141], Basic Local Alignment Search Tool (BLAST) [142], National Center of Biotechnology Information (NCBI).

2.5. Microbiological methods

2.5.1. *Synechocystis* growth conditions

All cyanobacterial strains were grown photoautotrophically in yBG11 medium buffered with 10 mM HEPES at pH 7.2 [143]. Cultures were incubated in growth chambers (Minitron LED Option HT) at 30°C under continuous illumination with 25-100 $\mu\text{mol photons m}^{-2} \text{s}^{-1}$. If not stated differently, cells were grown in baffled Erlenmeyer flasks under continuous shaking at 150 rpm (amplitude 2.5 cm) and depending on the experiment, in presence of either ambient CO₂ (air) or conditions with enriched CO₂ (2%), (v/v). Humidity was kept constant at 75%. Plate cultivation was conducted on BG11 [54] solidified with 1.5% (w/v) Bactoagar, supplemented with 3 g l⁻¹ Na₂S₂O₃ and incubated in growth chambers at 30°C, with 25-50 $\mu\text{mol photons m}^{-2} \text{s}^{-1}$, ambient CO₂, 75% humidity. For recombinant *Synechocystis* strains, the respective antibiotics were added at final concentrations of 40, 50 or 20 $\mu\text{g ml}^{-1}$ for kanamycin, spectinomycin or chloramphenicol, respectively. Optionally, nickel sulfate and ferric ammonium citrate were supplemented for induction in support of CnSH maturation [144]. While the concentration of ferric ammonium citrate was the same for all the experimental conditions tested (17 μM) [145], the nickel sulfate, as promoter inducer in certain case, was added 24 h prior harvesting the cells and the final

concentration varied between 1 and 10 μM . When specified, 48 h prior the assay L-rhamnose with a final concentration of 0.1 mM or 2 mM was added to the cultures to induce gene expression.

2.5.2. *E. coli* and *S. cerevisiae* growth conditions

For molecular cloning *E. coli* DH5 α and *S. cerevisiae* BJ 5464 were used. *S. cerevisiae* BJ 5464 was grown in YPAD medium at 30°C. Selection was performed on drop-out agar without uracil at 30°C for 3-4 days [146]. *E. coli* strain DH5 α was used for cloning procedures/ plasmids propagation and grown in liquid Luria-Bertani (LB) medium shaking at 180–200 rpm or solid (1.5% agar) at 37°C [147]. For selection of specific plasmids, the medium was supplemented with 100 $\mu\text{g ml}^{-1}$ ampicillin, 35 $\mu\text{g ml}^{-1}$ chloramphenicol, 50 $\mu\text{g ml}^{-1}$ kanamycin, and 40 $\mu\text{g ml}^{-1}$ streptomycin. 1 mM IPTG, 40 mg ml^{-1} Xgal were added to LB agar plates when necessary to select for positive clones through blue-white screening [148].

2.6. Molecular biology techniques

2.6.1. Polymerase chain reaction (PCR)

DNA fragments from gDNA, extracted plasmid and cells in single-colony were amplified by PCR method [149]. The proofreading *Phusion* polymerase (*Phusion*[™] High-Fidelity DNA Polymerase, Thermo) was chosen with gDNA or purified plasmid as template with the reaction set up and cycling program described in **Table S2.3**. PCR products for subsequent cloning applications were run on gel electrophoresis for DNA separation [150] or directly purified from the reaction mix with NucleoSpin® Gel and PCR Clean-up Kit (Macherey & Nagel). Single colony PCR was performed for *Synechocystis* cells to verify the presence of the heterologous DNA material upon transformation. Cells from a single colony on BG11 agar plate were picked and resuspended in 30 μl of deionized water (ddH_2O) for a quick step of cells disruption. The cells suspension was transferred in a tube filled with 0.09 – 0.15 mm glass beads (1/4 of the volume), vortexed for 1 min and subsequently incubated at 95°C for 5 min and centrifuged at 11,000 g for 1 min to remove beads and cells debris. 3 μl supernatant was used then as template in a 10 μl reaction using GoTaq mix (GoTaq® DNA Polymerase, Promega). The cycling program was adapted as followed: initial denaturation 1 min at 98°C, 1 min/kb annealing time.

2.6.2. Cloning methods

2.6.2.1. Cloning strategy for *Syn_CnSH*⁺ construction

To introduce the soluble hydrogenase of *C. necator* (*CnSH*) in *Synechocystis*, the respective operon comprising *hoxF*, *hoxU*, *hoxY*, *hoxH* and *hoxW* derived from plasmid pGE3382, was transcriptionally fused to the *psbA2* promoter (the construct is given in **Fig. 3.1A**) using the

genome integration vector pMQ80. It should be noted that we excluded the *hox1* gene, located downstream of *hoxW* in the native *hox* operon, from our strain design. Instead, a spectinomycin resistance cassette derived from pHP45Ω was placed downstream of *hoxW*. The designed construct was flanked by 500 bp stretches representing the regions up- and downstream of the *hox*-operon in *Synechocystis*. The primers included 30 to 60 bp homologous overhangs to be recombined with the linearized vector or with other amplified DNA fragments. The construct was assembled *in vivo* using *S. cerevisiae* BJ 5464. *S. cerevisiae* BJ 5464 was transformed by the high-efficient LiAc/SS carrier DNA/PEG method [146]. Recovery of plasmids from *S. cerevisiae* was done using the yeast DNA extraction Kit (Thermo Scientific) according to the manufacturer's instructions. For propagation and screening purposes, the isolated plasmid DNA was used for transformation of *E. coli* cells.

2.6.2.2. Cloning system based on CyanoGate: general description

Shuttle vectors were built as part of a modular cloning strategy based on the established Golden Gate cloning system [151] [152]. The presented system is comparable to the previously published CyanoGate [153]. The advantage of a modular cloning system is the possibility to easily create a library of different genetic elements and assemble them in the desired way. The usage of type IIS restriction enzymes, like *Bpil* and *Bsal*, allows the simultaneous assembly of multiple DNA fragments in correct orientations. Compared to the CyanoGate system, in this work the order of restriction enzymes was switched and combined with different restriction site overhangs. A schematic view of the procedure from the amplification of each basal genetic element until the level 2 assembly is represented in **Fig. 2.1**.

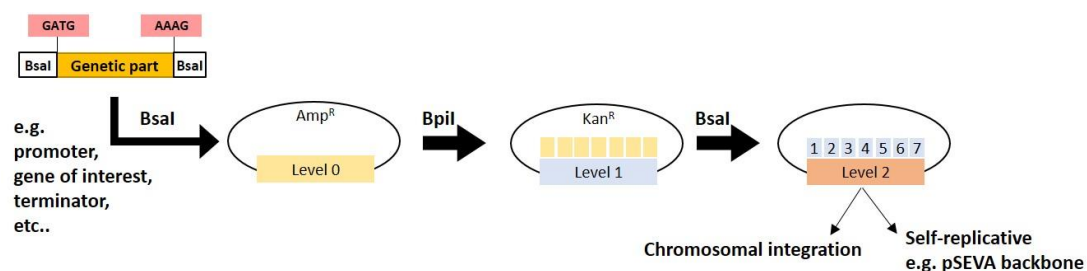


Figure 2.1. Overview of the modular cloning system (MoClo) combined with Golden Gate cloning.

The following figures (**Fig. 2.2-4**) describe in detailed each cloning step and, as an example, the genetic elements used to generate *C. necator* *hox* operon are represented (Chapter 4). However this cloning procedure was used to assemble *C. necator* *hyp* operon as well (Chapter 5).

As in the CyanoGate system, the genetic elements of interest initially were cloned in the so-called level 0 entry vectors through *Bsal* restriction site overlaps (**Fig.2.2**).

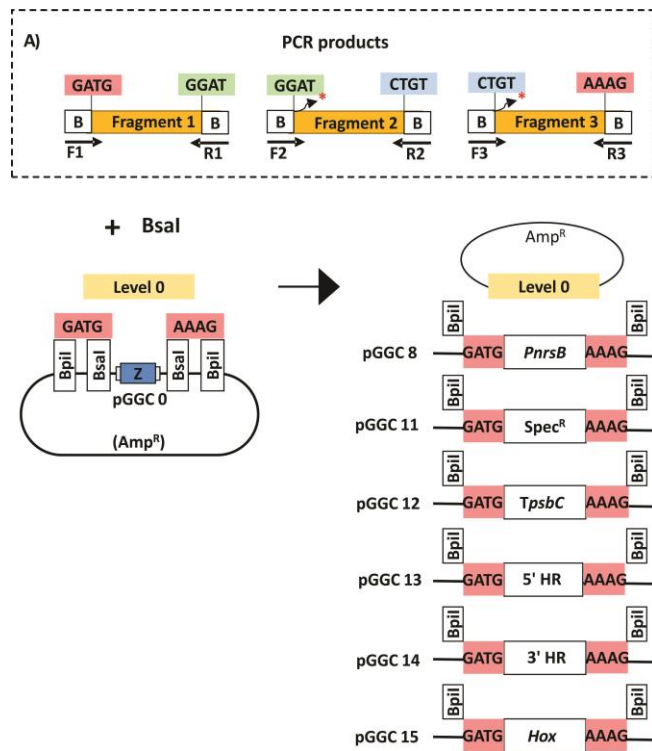


Figure 2.2. PCR products cloned in the level 0 vector. At first, each genetic element of interest was amplified either from *Synechocystis* genomic DNA or from existing vectors with primers flanked by a *Bsal* recognition site (B) containing 4 bp overhangs (GATG; AAAG) in order to fit into level 0 vectors. If necessary, internal *Bpil*/*Bsal* restriction sites were removed using specific overlapping primers containing a single silent nucleotide mismatch in the *Bsal*/*Bpil* recognition site (asterisk in **panel A**). Where necessary, the same procedure was applied to remove internal *Bpil*/*Bsal* restriction sites in the vector backbones, which are then defined as domesticated. pGGC: plasmid Golden Gate cloning; z: *lac z* gene; *PnrsB*: *nrsb* promoter; *Spec^R*: spectinomycin resistance; *TpsbC*: *psbC* terminator; 5'HR: 5'homologous region; 3'HR: 3'homologous region; *Hox*: *C. necator hox* genes cluster.

In the second step, each genetic element was cloned into level 1 “positioning level” vectors by using the second type II restriction enzyme *Bpil*. Level 1 vectors were designed to contain *Bsal* restriction site up- and downstream of *Bpil* restriction site. We generated in total level 1 vectors for 7 positions. Each positioning vector creates specific overhangs after *Bsal* digestion that matches only with the overhangs from the follow up position vector (**Fig. 2.3**).

In the last step, up to 7 genetic elements from the level 1 vectors were assembled into a final level 2 expression vector. When less than seven genetic elements were combined in level 2 vectors, we used end-linkers to fill the remaining positions (**Fig.2.4**).

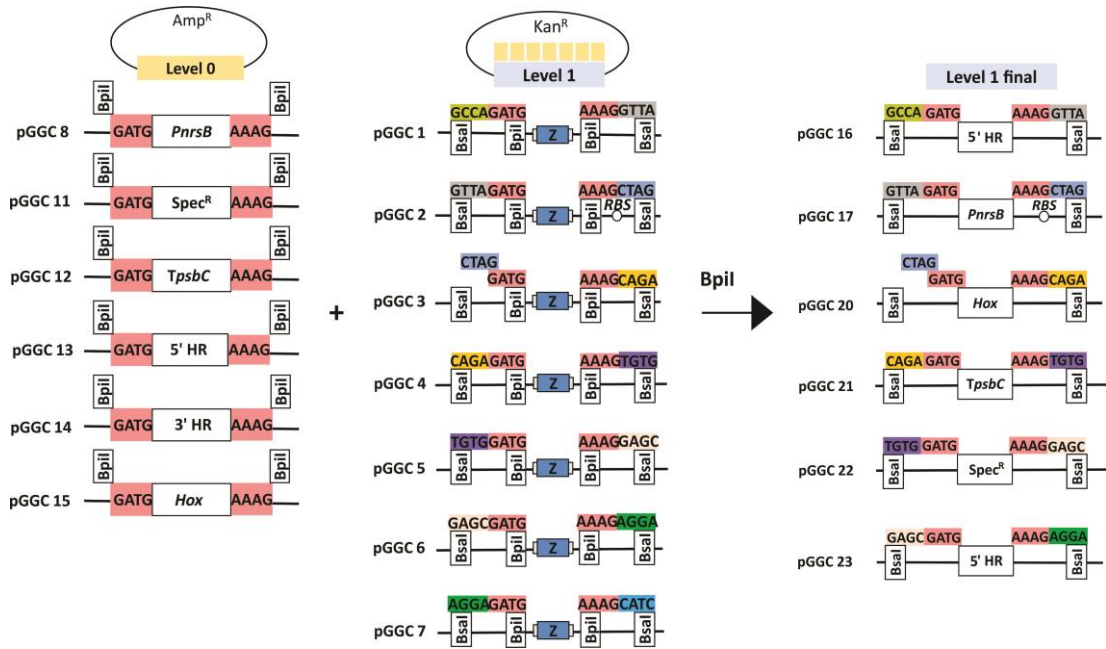


Figure 2.3. Cloning step from level 0 to level 1 positioning vectors via *Bpil*.

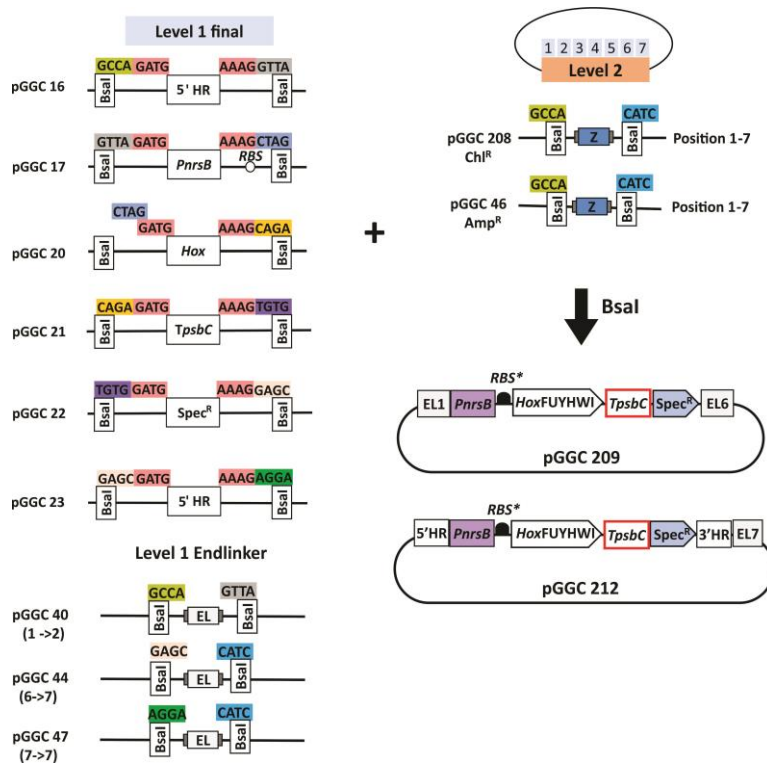


Figure 2.4. From level 1 to level 2 vectors in a single digestion-ligation step. 7 genetic elements were combined in an oriented manner based on specific pairs overhang.

Afterwards, the resulting level 2 vectors were introduced into *Synechosystis* strain. The Modular cloning system preparation is summarised as follows:

Level 0 generation: the domesticated pUC18 vector was amplified without *lacZ* cassette (encodes β -galactosidase), using primers flanked by *MluI* and *NcoI* recognition sites and including the recognition sequences for *Bpil* and *BsaI* in inverse orientation relative to each other that produce the identical sticky end overhangs GATG and AAAG after cutting. The *lacZ* cassette was amplified individually with primers flanked also by *MluI* and *NcoI*. Both purified fragments, the pUC18 backbone and *lacZ* fragment, were digested with *MluI* and *NcoI* and ligated to generate the empty level 0 vector with *lacZ* cassette flanked up- and downstream with *Bpil-BsaI* restriction sites.

Level 1 generation: the pUK21 backbone was modified as described for level 0 vectors with the difference that the *lacZ* expression cassette was flanked up- and downstream with *BsaI-Bpil* restriction sites. *Bpil* restriction results in the overhangs GATG and AAAG, which are matching with the overhangs carried by the genetic elements in level 0 vectors. The introduced *BsaI* restriction sites generate new unique overhangs for each of the seven level 1 position plasmids we generated. The level 1 position 2 vector was additionally modified by inserting the RBS sequence between the *Bpil* and *BsaI* restriction site upstream of the *lacZ* expression cassette.

For level 1 end-linker generation, the pUK21 vector was amplified with primers flanked by *Bpil* restriction sites. The forward primer also carried the end-linker sequence flanked with *BsaI* restriction sites. The purified PCR product was digested with *Bpil* and ligated to the final end-linker vectors. We generated various level 1 end-linker, to cover positions from 1 to 7 in final level 2 vectors. Furthermore, we designed two types of level 2 vectors for the generation of replicative and genome integration vectors. As replicative vector, pSEVA 351[154] carrying the RSF1010 origin of replication, was modified as described for level 0 generation. In the vector backbone downstream of the T1 regulatory element, the T0 regulatory terminator element was replaced by the *lacZ* expression cassette flanked by two *BsaI* restriction sites that produce the overhangs GCCA and CATC to assemble up to seven level 1 vectors. As genome integration vector, the domesticated pBluescript II SK(+) backbone was modified by implementing a *lacZ* expression cassette as done before for the replicative vector.

2.6.2.3. Golden gate assembly of shuttle vectors

Golden Gate assembly reactions were performed with the restriction enzymes *BsaI*-HF®v2 (New England Biolabs) or *Bpil* FD (Thermo Fisher Scientific) and T4 DNA Ligase HC (Promega). The modular assembly protocols for level 0, 1, 2 generation is summarized in **Table 2.1**.

Table 2.1 Protocol for plasmid generation

Component	Level 0	Level 1	Level 2
DNA	PCR product (40 fmol)	Level 0 vector (40 fmol)	Level 1 vectors (pos. 1 to 7) (40 fmol)
Vector DNA	Level 0 vector (40 fmol)	Level 1 vector (40 fmol)	Level 2 vector (80 fmol)
NEB T4 DNA ligase Buffer (10x)	1x	1x	1x
Enzyme	<i>Bsal</i> -HFv2 (10U)	<i>Bpi</i> I FD (0.5µl)	<i>Bsal</i> -HFv2 (20U)
T4 DNA Ligase	6U	6U	6U
Nuclease free water	Up to 20 µl		

Incubate the reactions at:	
Level 0/1	Level 2
37°C for 2 h 50°C for 5 min 80°C for 5 min	37°C for 2 min 16°C for 5 min 50°C for 5 min 80°C for 5 min
} X5	
4°C hold	

2.6.3. Plasmid propagation in *E. coli* electrocompetent cells

2 µl of each ligation reaction mixture were mixed with an aliquot of ~60 µl of *E. coli* DH5α electrocompetent cells [155], transferred into ice-cold electroporation cuvette (2 mm) and transformed by conducting 2.5 kV, 25 µF, 200 Ω for approximately 5 ms (Eppendorf Eporator®, Hamburg, Germany). The cells were resuspended in 1 ml of LB medium and incubated for 45 min, 37°C, and 350 rpm. Afterwards, cells were plated on LB-Agar plates supplemented with the antibiotic necessary for selection and incubated overnight at 37°C. Successful transformation of plasmids generated via CyanoGate was verified via blue-white screening of positive clones [156]. In this case agar plates were supplemented with 1 mM IPTG, 40 mg ml⁻¹ Xgal. Clones were picked from the LB plates and grown overnight at 37°C and in 4 ml LB medium containing the requested antibiotics. Plasmid DNA was isolated using the whole culture and the *NucleoSpin Miniprep Kit* (Macherey & Nagel) according to the manufacturer's instructions.

2.6.4. Transformation of *Synechocystis* cells

2.6.4.1. Genes delivery into the chromosome: natural transformation

The resulting constructs were introduced into a *Synechocystis* mutant, in which the native *hox* genes were deleted and which was further modified by introducing a chloramphenicol resistance cassette (chl^R) into the intergenic region between *slr1597* and *sl1514* to facilitate future modifications [74] (in the manuscript referred to as *Syn_Δhox*). Thereby, the constructed operon coding for *CnSH* was prone to replace the kanamycin cassette originating from the *hox* gene deletion. Natural transformation of *Synechocystis* was done according to standard protocols.

Briefly, 300 μ l of cell culture (OD_{750} ~0.4) were incubated with 6 ng plasmid-DNA in the dark at 30°C for 6 h with a short hand shaking every 2 h. The suspension was plated on a nitrocellulose membrane, placed on BG11 agar plates and incubated at 25 μ mol photons $m^{-2} s^{-1}$ overnight. The membrane was moved to a fresh agar plate containing the selective antibiotics at 40% of the normal operating concentrations (see above). Cells were grown for 4 weeks at 50 μ mol photons $m^{-2} s^{-1}$, ambient CO_2 and 30°C. Afterwards, single green colonies were picked and plated on new agar containing increased antibiotics concentrations. This step was consecutively repeated to achieve segregated transformants and the correct genomic integration of heterologous DNA was finally verified by colony PCR.

2.6.4.2. Electroporation

Electro-competent *Syn_Δhox* cells were transformed with modified pSEVA351 (RSF1010) replicative vectors, according to a standard protocol [157]. In brief, electro-competent cells were generated by cultivation in yBG11 medium as detailed below at ambient CO_2 (air). Cultures with a volume of 30 ml were inoculated to an OD_{750} of 0.05-0.07 and harvested in the logarithmic growth phase (OD_{750} ca. 0.5-1) by centrifugation (10 min, 4°C, 3,900 g). Cell pellets were washed 3 times in 10 ml ice cold HEPES (1 mM, pH 7.5) and re-suspended in 1 ml of the same buffer giving an OD_{750} of ~30. For electroporation, 80 μ l of electro-competent cells in HEPES were transferred into ice-cold electroporation cuvette (2 mm), mixed with 500 ng of purified plasmid, and transformed (2500 V, 5 ms). Then, cells were resuspended in 1 ml fresh yBG11 medium, plated on BG11 agar plates supplemented with the lowest concentration of selecting antibiotic (spec^R 20 μ g ml^{-1}), and incubated at 25 μ mol photons $m^{-2} s^{-1}$, ambient CO_2 , 30°C until colonies appeared. Afterwards, single colonies were picked and transferred onto fresh agar plates containing increased antibiotic concentrations and incubated at 50 μ mol photons $m^{-2} s^{-1}$, ambient CO_2 , 30°C. Plasmid presence was verified by colony PCR as previously described.

2.6.5. Genomic DNA extraction from *Synechocystis*

Synechocystis cells were grown phototrophically at standard conditions (final cells concentration: $1 \cdot 10^7$ - $1 \cdot 10^8$). 10-35 ml of cell cultures were centrifuged (5 min, 10,000 g, 4°C). All steps were carried out on ice. Chromosomal DNA was isolated using DNA Isolation kit (Bacterial DNA-Mini-Kit, peqGOLD, Avantor, USA) according to the manufacturer's instructions. In brief, the cells pellet was washed with 1x 400 μ l of TE buffer and resuspended in 1 ml of Lysis Buffer T. $\frac{1}{4}$ of a new tube was filled with glass beads mixture of three different sizes: 0.09 – 0.15 mm, 0.17 – 0.18 mm and 0.5 mm (Sartorius™) and the cell suspension on top. Cells disruption was performed by using Precellys® Evolution Super Homogenizer equipped with Cryolys® cooling system (10,000 g, 4°C,

3x30 s, 30 s break) and afterwards the cell suspension was centrifuged 10 min, 10,000 rpm, 4°C. The supernatant was transferred into a new reaction tube, mixed with 30 µl of proteinase K and 20 µL RNAase-A and incubated for 10 min 70°C, 350 rpm. 200 µl of DNA binding buffer was added before loading the column and centrifuging for 1 min, 11,000 g. The flow through was discarded and the column washed 2x with Washing Buffer (1min, 11,000 g). An additional centrifuge step was run to dry the column, 2 min at the same speed. Finally, to elute the chromosomal DNA from the column, the Elution Buffer was added before final centrifugation step (1 min, 11,000 g).

2.6.6. Sequencing

The Sanger sequencing [158] of generated PCR products, purified plasmids and *Synechocystis* strains genomic DNA was carried out by the company *GENEWIZ (South Plainfield, NJ, US)* following the company instruction.

2.6.7. RNA extraction

35 ml of *Synechocystis* cultures (with an OD₇₅₀ of 0.8–1.0) were rapidly harvested by vacuum filtration on hydrophilic polyethersulfone filters (Supor® 800 Membrane Disc Filters, 0.8 µm - 47 mm). The filters covered with cells were immediately dissolved in PGTX solution, then frozen in liquid nitrogen and stored at -80°C until use. Total RNA was extracted as described [159].

2.6.8. Northern blot analysis

For Northern blot analysis, 3 µg of total RNA were incubated in sample loading buffer (R1386-5VL, Sigma-Aldrich) at 65°C for 5 min. Denatured RNA was separated on MEN-buffered 1.5% [w/v] agarose gels containing 6% (v/v) formaldehyde. The separated RNA was transferred to Hybond-N⁺ nylon membranes (GE Healthcare) by capillary blotting and cross-linked by UV-illumination (125 mJ). The membranes were hybridized with single-stranded, [α -³²P]UTP-incorporated RNA probes complementary to the target RNA. Hybridization and ³²P detection was performed as described previously [160]. Probe generation and labeling was performed utilizing the MAXIscript™ T7 kit (ThermoFisher) according to the manufacturer's protocol. The primer pairs used to generate DNA templates for *in vitro* transcription are shown in **Table S2.2**. The probe templates were amplified from the plasmid pAGS9 (*hoxF*) or genomic DNA of *Synechocystis* (5S rRNA, loading control).

2.6.9. qRT-PCR

For the isolation of RNA, *Syn_P_{nrsB}CnSHg*, +*pP_{nrsB}CnHyp*, +*pP_{rhaBAD}CnHyp* and +*pP_{psbA2}CnHyp* strains were grown until reaching an OD₇₅₀ ~ 0.8. Each strain culture was supplemented with 10

μM NiSO_4 , which induces *Cn_hox* expression in all strains, but also *Cn_hyp* operon in $+pP_{nrsB}CnHyp$. Instead $+pP_{rhaBAD}CnHyp$ strain culture was treated with final concentrations of 0.1 μM or 2 mM L-rhamnose. Immediately afterwards (time 0 h) and after 24 h nickel and rhamnose addition, cells were harvested by centrifugation (5,000 g, 10 min, 4°C). RNA isolation was performed as described previously. Then 550 ng RNA of each sample was subjected to RNase-free DNase I digestion (Thermo Scientific) and the following cDNA synthesis was performed using the High-Capacity cDNA Reverse Transcription kit (Thermo Scientific) as given in the manufacturer's instructions. The amplified cDNA was diluted 1:10 before using it with Power SYBR Green Master mix (Thermo Scientific) to perform the Quantitative real-time polymerase chain reaction (qRT-PCR), according to the manufacturer's instructions. Samples were run on a StepOnePlus™ Real-Time PCR System (Thermo Scientific). Sequences of primer pairs for amplification of specific regions within either the reference gene *mnpB* (RS 297/298) or *hypA* (RS 295/296) and *hypX* (RS 308/309) are given in **Table S2.2**. The relative abundance was calculated and normalized to the housekeeping reference gene *mnpB* [161] ($\Delta\Delta\text{Ct}$ method) [162]. For comparative analysis, the relative transcript levels of the genes in the induced strains were normalized to that in the non-induced control strains.

2.7. Cell disruption and protein identification

2.7.1. *Synechocystis* cell disruption

Cells cultures (OD_{750} 2-4) were harvested and resuspended in 50 mM KP_i buffer (pH 7.0), supplemented with 5% (w/v) glycerol and 1 mM PMSF [144]. All steps were carried out on ice. Cells were mixed with a glass beads mixture of three different sizes: 0.09 – 0.15 mm, 0.17 – 0.18 mm and 0.5 mm (Sartorius™) and disrupted by using Precellys® Evolution Super Homogenizer equipped with Cryolys® cooling system (6800 g, 4°C, 3x30 s). After centrifugation (5 min, 4°C, 10,000 g) to separate the beads, the liquid phase was transferred into a new tube and centrifuged for 45 min at 17000 g and 4°C. The total protein concentration of the cell extract was quantified using the Bradford method [163].

2.7.2. Mass spectrometric identification of protein

To identify subunits of the heterologously produced *CnSH*, gel slices with the stained H_2ase were further processed: disulfide bridges were reduced with dithiothreitol, resulting sulfhydryl groups were acetamidylated with iodoacetamide, proteins were digested with trypsin and the resulting peptides were eluted from the gel pieces as described before [164]. Peptides were desalted with ZipTip- $\mu\text{C}18$ material (Merck Millipore) and analyzed by nano-liquid chromatography tandem mass spectrometry (nLC-MS/MS) using an Orbitrap Fusion Tribrid mass spectrometer (Thermo

Scientific) concatenated to a nanoLC system (Dionex Ultimate 3000RSLC; Thermo Scientific) via a TriVersa NanoMate ion source (Advion) operated in positive mode. A maximum number of 4×10^5 ions were injected and measured in the Orbitrap at 120,000 resolution. Precursor ions were selected for fragmentation using an inclusion list generated from the amino acid sequences of the cloned *hox*-genes with a very narrow precursor mass tolerance of 0.8 ppm but not using dynamic exclusion of precursors after their first detection. Fragments were generated with higher collision energy fragmentation (30% intensity \pm 3% with stepped gradient) and measured in the Orbitrap at 60000 resolution and an AGC target of 5×10^4 ions. Subunits were identified with Proteome Discoverer (version 2.4, Thermo Fisher Scientific) using SequestHT as a search engine and the UniProt protein database of *Synechocystis* sp. PCC 6803 and the sequences of *C. necator* Hox proteins as a database with the following settings: cleavage with trypsin allowing up to two miscleavages; precursor mass tolerance 10 ppm, fragment tolerance 0.1 Da; oxidation of methionine residues and carbamidomethylation on cysteine residues were included as variable and fixed modification, respectively; the false discovery rate of identified peptide sequences was kept below <1% using the Target Decoy PSM Evaluator [164].

2.7.3. SDS-polyacrylamide gel electrophoresis and Western Blot

For Western Blot analysis, soluble fraction corresponding to 20-30 μg total protein was mixed with the same volume of 2x SDS loading dye buffer (121.14 g l^{-1} Tris HCl, 40 g l^{-1} SDS, 30.8 g l^{-1} DTT, 0.5 g l^{-1} Bromphenol blue, 200 g l^{-1} Glycerol) and heated at 99°C for 10 min for complete protein denaturation. Proteins were separated by electrophoresis [165] on polyacrylamide gradient gels (4–15% Mini-PROTEAN TGX Precast Gels, Bio-Rad, USA), using a SDS running buffer (3.03 g l^{-1} Tris, 1 g l^{-1} SDS, 18.77 g l^{-1} Glycine, pH 8.3), for about 80 min at 120 V. The Protein Ladder SM26616 (Thermo Fisher, USA) was loaded next to protein samples. For blotting, standard procedures were followed [166]. Specifically, 6 x Whatman filter papers, 1 x 0.45 μm pore size nitrocellulose membrane (GVS), and the SDS gel were stacked and equilibrated for 5 min in the blotting buffer (3 g l^{-1} Tris, 14.4 g l^{-1} Glycine, 200 ml l^{-1} MeOH) before blotting for 30 min (0.8 mA/cm^2 , Biometra). The blotted membrane was then blocked in TTBS buffer (0.05 M Tris, 0.15 M NaCl, pH 7.4, 0.05% (v/v) Tween 20) containing 5% (wt/v) BSA on a rocking table for 1 h. Then, the antibody against HoxH (0.35 g/l, Eurogentec, Belgium) was added with a dilution of 1:20.000 and the membrane was hybridized overnight at 4°C. Afterwards, the membrane was carefully washed with TTBS and incubated for 1 h in TTBS + 3% (w/v) BSA with Goat anti-Rabbit IgG HRP-conjugated (10 $\mu\text{g ml}^{-1}$), titered 1:500 (Invitrogen, USA). Finally, after washing 5x with TTBS, the membrane was supplied with substrate solution WesternBright ECL (Advansta, USA) and

subjected to chemiluminescence detection using a Fusion FX7 EDGE V0.7 imaging system (VILBER, Germany) following the manufacturer's instructions. As loading control, 10 µg of total soluble protein were treated as previously described for Western Blot analysis and run on SDS-PAGE according to Laemmli [165]. The SDS gel was stained with Coomassie Brilliant Blue R-2500 staining solution (5 g l⁻¹ methanol 50% (v/v), acetic acid 10% (v/v), water 40% (v/v)) for 20 min, followed by 20 min of incubation with a destaining solution (10% (v/v), acetic acid 5% (v/v), water 85% (v/v)) in order to visualize proteins.

2.8. Hydrogenase activity assay

2.8.1. *In vitro* H₂-oxidation activity

2.8.1.1. H₂-dependent reduction of a colorimetric dye

The soluble protein fractions were diluted in loading dye solution (50 mM K_{Pi} (pH 7.0), 5% glycerol, 0.25% bromophenolblue) and separated on non-denaturing polyacrylamide gradient gels (4–15 % Mini-PROTEAN TGX Precast Gels, Bio-Rad) at 4°C. The gel was then incubated for 30 min at 30°C in an airtight 120 ml bottle containing 100 ml H₂-saturated 50 mM Tris/HCl buffer, pH 8.0. Then, 800 µM NAD⁺ and 60 µM NBT was added and the bottle was incubated in the dark for 30 min at 30°C to visualize the location of the active H₂ase complex in the gel [144]. H₂ase activity reduces NAD⁺ to NADH, which transfers electrons to NBT. Reduction of the latter oxidant colorimetric dye results in a dark blue precipitation in the gel.

2.8.1.2. H₂-dependent reduction of NAD⁺

The soluble protein fraction of *Synechocystis* strain was utilized to determine the H₂ase activity via H₂-dependent NAD⁺ reduction. The activity buffer (50 mM Tris/HCl, pH 8.0) was bubbled with H₂ in a gas-washing bottle kept in a water bath at 30°C for 30 min prior to the assays. H₂-saturated buffer (1.9 ml) was injected into a 3 ml quartz glass cuvette through a rubber septum and supplemented with 1 mM NAD⁺ and 1 µM FMN. 1 mM DTT was left out when the experimental set up was optimized (from Chapter 4), since had no beneficial effect on CnSH activity in soluble cell extracts [144]. The cuvette was flushed again with H₂ for some minutes. Afterwards, the reaction was started by adding 10-20 µl of soluble protein fraction. NADH formation was measured at 30°C recording absorption at 365 nm with a UV-Vis spectrophotometer (Varian Cary® 50). The SH activity was calculated as U per g total protein with an extinction coefficient $\epsilon_{\text{NADH}(365)}$ of 3.3 mM⁻¹ cm⁻¹. The same assay was used to test the O₂ tolerance the CnSH from *Syn_CnSH*⁺ utilizing a buffer saturated with specific gas mixtures of H₂, O₂ and N₂ in sealed 3 ml cuvettes (**Fig. S3.1, Table S3.1**) [144]. Optimized experimental procedure as explanation to the higher detection of *Syn_CnSH*⁺ activity in Chapter 4 compared to Chapter 3, refers mainly to the

use of soluble cell extracts obtained from fresh growing cultures instead of frozen cell pellet stored at -20°C.

2.8.2. *In vivo* H₂ oxidation activity

2.8.2.1. H₂ consumption measured via Gas chromatography (GC)

Synechocystis cultures were grown photoautotrophically with 2% CO₂ as described above until an OD₇₅₀ of 2.5-5. H₂ consumption was performed either using directly the cell suspension or as lately optimized diluting the cultures with fresh yBG11 medium to an equal OD₇₅₀ 3. Samples (5 ml) of each strain were transferred into 10 ml or 20 ml glass vials (10/20 ml Crimp Top HS Vial, Thermo Scientific™) closed with gas-tight caps (ND20 magnetic crimp cap, Aluminum, 10mm center hole, septa molded butyl, 3.0 mm, 55° shore A (Th. Geyer, Renningen Germany). The headspace of the sealed vials was flushed for 1 min with 100% N₂, followed by 10 s flushing with a gas mixture of 10% H₂ and 90% N₂ or directly 1 min using a gas flow mixing station (PCU-10 Display and Control Device, Vögtlin) with different gas mixtures, including H₂, CO₂, N₂ and O₂, depending on the experimental set up. The closed vials were incubated at 30°C, 50 μmol photons m⁻² s⁻¹ and 150 rpm. During the incubation time, H₂ concentrations were measured over a time of 6, 8, 12, 24, or 48 h depending on the condition applied. When needed, 20 μM of 3-(3,4-dichlorophenyl)-1,1-dimethylurea (DCMU) or 20 μM of DBMIB (2,5-dibrom-6-isopropyl-3-methyl-1,4-benzochinone) were added directly into the glass vials. Gas analysis was conducted on a TRACE 1310 gas chromatograph (Thermo Scientific) equipped with a TracePLOT TG-BOND Sieve 5A column (length: 30 m; inside diameter: 0.32 mm; film thickness: 0.30 μm, Thermo Scientific). Other settings: Thermal Conductivity Detector (TCD): 100°C and Oven: 50°C. A sample volume of 100 μl was injected using the TriPlusRSH automated injection. The carrier gas (argon) flow rate was set to 2 ml min⁻¹. The total run time was 2.4 min. H₂ and O₂ were quantified using calibration curves of both gases, determined with defined gas mixtures (Air Products, PA, USA). The H₂ase specific activity was calculated in U (1 U corresponds to consumption of 1 μmol H₂ min⁻¹) per g of cell dry weight (CDW). Therefore, 1 ml of cell suspension was adjusted to a cell dry weight (CDW) of 1 g_{CDW} l⁻¹ using a correlation factor of 0.225 g_{CDW} l⁻¹ for OD₇₅₀ = 1 as determined previously [167].

2.8.3. *In vivo* H₂ production

2.8.3.1. H₂ production measured via Gas chromatography (GC)

For fermentative H₂ production, aliquots (5 ml) of *Synechocystis* cultures with an OD₇₅₀ of 3-5 were supplemented with a final concentration of 10 mM glucose and prior the incubation in 10 ml sealed glass vials. The headspace of all vials was flushed for 1 min with N₂ to create anoxic

conditions and vials were incubated at 30°C, 150 rpm under dark conditions. Two different conditions were tested to measure H₂ production under illumination. 1) Cell cultures were cultivated up to an OD₇₅₀ of 2.5, centrifuged (4000 g, 5 min and RT) and resuspended in 0.1 M KP_i buffer (pH 7.2), with 10 mM glucose to a final OD₇₅₀ of 5. 2) Cell cultures were kept in the cultivation medium (yBG11) and supplemented with 10 mM glucose and 20 μM DBMIB. Afterwards, aliquots (5mL) of cell cultures were transferred in 10mL vials and the headspace was flushed for 1 min with N₂ to create anoxic conditions and the vials were incubated at 30°C, 50 μmol photons m⁻² s⁻¹ and 150 rpm. Gas composition was determined regularly via GC over the time range specified in every results section. H₂ and O₂ were quantified using calibration curves of both gases, determined with defined gas mixtures (Air Products, PA, USA). The H₂ase specific activity was calculated in U (1 U corresponds to consumption of 1 μmol H₂ min⁻¹) per g of cell dry weight (CDW). Therefore, 1 ml of cell suspension was adjusted to a cell dry weight (CDW) of 1 g_{CDW} l⁻¹ using a correlation factor of 0.225 g_{CDW} l⁻¹ for OD₇₅₀ = 1 as determined previously [167].

2.8.3.2. Clark electrode

H₂ase activity in *Synechocystis* cells was measured with a Clark-type-electrode (*DW 1 Liquid Clark Electrode; Hansatech Inst., Norfolk, UK*) by using methyl viologen and sodium dithionite as artificial electron donors, under anaerobic conditions as described [75][168]. Before performing the measurements the electrode was prepared, tested for H₂ sensitivity and calibrated by following the manufactures instructions. Cell cultures were grown photoautotrophically to an OD₇₅₀ of 3, aliquots were mixed with 5 mM methylviologen and 10 mM sodium dithionite to directly record the H₂ase activity *in vivo*.

2.9. Physiological characterization: growth analysis with H₂ as electron source

Synechocystis cultures were grown photoautotrophically with 2% CO₂ as described above until an OD₇₅₀ of 5-7 was reached. The cells were harvested by centrifugation (4000 g, 5 min and 4°C) and resuspended in *CnSH* medium to a final OD of ~2.5. Five ml of each culture were transferred into 10 ml glass vials and incubated at 30°C, 150 rpm in a cultivation chamber for seven days, under dark or light conditions, with/without DCMU and in the presence of defined gas mixtures using a flow mixing station (PCU-10 Display and control device, Vögtlin). Every 24 h H₂ and O₂ concentrations in the headspace of the vials were monitored via GC as described above. Vials were purged with an initial gas mixture every 24 h and gas composition was confirmed by GC after flushing. At day 1 (prior incubation) and after 7 days of cultivation, cultures were subjected to OD₇₅₀, cells number, cell diameter (Multi-sizer™ 3 COULTER COUNTER®), CDW and pH determination measurement. For CDW determination, 5 ml cell culture were centrifuged (6000 g,

5 min, RT), washed with deionized water, centrifuged again and dried in glass tubes kept at 80°C (Thermo Scientific, Heratherm) until their weight remained constant.

Chapter 3

Rewiring cyanobacterial photosynthesis by the implementation of an oxygen-tolerant hydrogenase

Sara Lupacchini, Jens Appel, Ron Stauder, Paul Bolay, Stephan Klähn, Elisabeth Lettau, Lorenz Adrian, Lars Lauterbach, Bruno Bühler, Andreas Schmid, Jörg Toepel

Author Contributions:

Sara Lupacchini, Ron Stauder, Paul Bolay and Elisabeth Lettau carried out the experiments and analyses. Jörg Toepel designed the study, drafted the manuscript, and all authors contributed to writing the final version of the paper. All authors gave final approval for publication

Published in:

Metabolic Engineering, **2021**, 68, 199–209. Doi: <https://doi.org/10.1016/j.ymben.2021.10.006>

The Supplementary Material can be found in the Appendix Section 3.

Abstract

Molecular hydrogen (H₂) is considered as an ideal energy carrier to replace fossil fuels in future. Biotechnological H₂ production driven by oxygenic photosynthesis appears highly promising, as biocatalyst and H₂ syntheses rely only on light, water and CO₂ and not on rare metals. This biological process requires the coupling the photosynthetic water oxidizing apparatus to a H₂-producing hydrogenase. However, this strategy is impeded by the simultaneous release of oxygen (O₂) which is a strong inhibitor of most hydrogenases. Here, we addressed this challenge, i.e. the introduction of an O₂-tolerant hydrogenase into phototrophic bacteria, namely the cyanobacterial model strain *Synechocystis* sp. PCC 6803. To this end, the gene cluster encoding the soluble, O₂ tolerant and NAD(H)-dependent hydrogenase from *Cupriavidus necator* (*CnSH*) were functionally transferred to a *Synechocystis* sp. PCC 6803 featuring a knockout of the native O₂ sensitive hydrogenase. Intriguingly, photosynthetically active cells produced active O₂ tolerant *CnSH* and activity was detected *in vitro* and *in vivo*. Further, *CnSH* was shown to enable the constructed strain *Syn_CnSH*⁺ to utilize H₂ as sole electron source to fix CO₂. *Syn_CnSH*⁺ also was able to produce H₂ under dark fermentative conditions as well as in presence of light, under conditions fostering intracellular NADH excess. These findings highlight a high level of interconnection between *CnSH* and cyanobacterial redox metabolism. This study lays a foundation for further engineering, e.g. of electron transfer to *CnSH* via NADPH or ferredoxin, to finally enable photosynthesis driven H₂ production.

3.1. Introduction

H₂ has a gravimetric energy content three times higher than mineral oil as well as a better energy conversion efficiency to electricity [169]. Moreover, the use of H₂, e.g. for electricity generation, avoids greenhouse gas emissions as long as its production is based on renewable (energy) sources. Accordingly, H₂ is widely recognized as clean fuel and could be the basis for a sustainable, i.e. CO₂-neutral (bio)economy. In general, H₂ can be produced from fossil carbon as well as directly from water by utilizing various technologies. Biotechnological solutions generally gathered attention in recent years. H₂ production via oxygenic photosynthesis, the natural light-driven water splitting process in plants, algae as well as cyanobacteria, would be an ideal approach circumventing detours via electricity or energy-rich carbon compounds [170][83]. Whereas the theoretical maximum solar to hydrogen energy conversion efficiency (STH) of photoautotrophic microorganisms is estimated to be around 10-15% and may be increased to 20-30% by withdrawing electrons directly at PSII, photovoltaic/electrolysis approaches can achieve 20-24% [171]. Although the biological approach cannot be considered superior in energy conversion efficiency, it clearly is in terms of resource demands, as catalysts rely on fixed CO₂ as major resource and do not demand large amounts of (rare) metals, as it is the case for photovoltaics and electrolysis. Having said that, some green algae and cyanobacteria are considered excellent microbial hosts for the generation H₂ and other biofuels [172][173]. Hydrogenases catalyzing the reduction of protons to H₂ are regarded as the most promising enzymes to channel electrons derived from photosynthetic water splitting to H₂ formation [174]. However, water oxidation concomitantly leads to the formation of O₂, which strongly inhibits the active site of most hydrogenases [72]. [FeFe] and [NiFe] hydrogenases constitute the most prominent H₂-forming hydrogenases [174][175]. [FeFe] hydrogenases are characterized by a high turnover number, but are highly sensitive to irreversible inactivation by O₂ [173][81]. In contrast, [NiFe] hydrogenases show lower turnover numbers, but are considered as O₂-stable as they feature a reversible inactivation by O₂. Remarkably, some [NiFe] hydrogenases are truly O₂-tolerant as they stay active even in the presence of O₂, rendering those ideal candidates for a sustained H₂ production using oxygenic phototrophs [176][106][170]. Several approaches focused on prolonging the activity of intrinsic O₂-sensitive hydrogenases [177][171] or aimed at engineering intrinsic hydrogenases towards O₂ tolerance [178][179]. Especially the cyanobacterial model strain *Synechocystis* sp. PCC 6803 (hereafter *Synechocystis*) harboring a bidirectional [NiFe] hydrogenase was applied to demonstrate photosynthetic H₂ production. The H₂ production capacity of this O₂ sensitive enzyme was demonstrated in heterotrophic hosts such as *Escherichia coli* or *Enterobacter aerogenes* under anaerobic conditions [180][125]. Another

approach was the tethering of hydrogenases directly to ferredoxin or photosystem I [74][181][182][183][184]. Nevertheless, in all these approaches, O₂ sensitivity of hydrogenases remained the major drawback. The ‘Knallgas’ bacterium *C. necator*, a H₂ metabolizing chemolithotrophic bacterium, harbors the best-described O₂-tolerant hydrogenases. Its soluble, O₂ tolerant and NAD(H)-dependent hydrogenase (*CnSH*) natively utilizes H₂ as electron donor for NAD⁺ reduction and thereby supplies reduction equivalents for CO₂ fixation and respiration [93]. During shifts from aerobic to anaerobic conditions, the enzyme was also found to catalyze NADH mediated H₂ formation [23]. *CnSH* is heterohexameric composed of a hydrogenase module (HoxHY), a diaphorase module (HoxFU) and two copies of the nonessential HoxI protein [88]. Its active site harbors one atom of iron and nickel each, which are connected by two bridging cysteines and two terminal cysteines at the nickel. The iron atom has three ligands that are untypical for biological systems, namely two cyanides-and one carbonyl [102]. The [NiFe] active site is connected to the NAD(H)-binding site by one [2Fe2S] and four [4Fe4S] clusters as well as two flavin mononucleotide (FMN) molecules. The biosynthesis of the active site requires a sophisticated maturation machinery encoded by the so-called *hyp* genes [114]. Finally, HoxH undergoes C-terminal processing catalyzed by the enzyme-specific endopeptidase HoxW [123]. The O₂ tolerance of the *CnSH* is explained by its capability to “detoxify” O₂ to harmless H₂O and also H₂O₂ by reverse electron transfer from the proximal flavin mononucleotide (FMN) cofactor and further [FeS] clusters [99]. *C. necator* hydrogenase genes have been recombinantly expressed in heterotrophic hosts, as reviewed by [176]. The multicomponent nature of *CnSH* and its complex active site maturation make its heterologous production a challenge [137][128]. When *CnSH* was overexpressed in *E. coli*, it showed only residual activity in the absence of its native maturation proteins. Further, the membrane-bound hydrogenase has been assembled *in vitro* with photosystem I (PSI) of *Synechocystis* [185]. Functional production of an O₂ tolerant *C. necator* hydrogenase in phototrophs and its *in vivo* coupling to the photosynthetic apparatus however remained elusive. The present study tackles this challenge and demonstrates the functional implementation of *CnSH* in *Synechocystis* and its coupling to the cyanobacterial metabolism, including stable activity. This approach combined with electron transfer engineering, e.g., electron transfer to *CnSH* from ferredoxin, NADPH or PS I directly as shown for a native *Synechocystis* hydrogenase [74], augurs well for efficient photosynthesis-driven H₂ production.

3.2. Results

3.2.1. Functional expression of the *CnSH* gene cluster in a model cyanobacterium

To implement a functional O₂-tolerant hydrogenase in *Synechocystis*, the *hox* operon from *C. necator* encoding the four essential *CnSH* subunits was introduced via homologous recombination into the chromosome of a *Synechocystis* strain with a deletion of the native hydrogenase genes (*Syn_Δhox*, [74]). An overview of the genetic setup is given in **Fig. 3.1A**. It involves transcription control of the pentacistronic *hox* operon via the light inducible *psbA2* promoter, which is highly active in photosynthetically active cells [186]. To avoid interference with the host metabolism, the *hoxI* gene was not transferred. *HoxI* is not essential for hydrogenase activity and has a potential regulatory function [88]. The obtained recombinant strain *Syn_CnSH*⁺ was analyzed by PCR confirming correct gene integration into the chromosome as well as complete segregation, i.e. the absence of any residual alleles from the wild type (*Syn_WT*) or the maternal *Syn_Δhox* strain (**Fig. 3.1B**). *CnSH* gene transcription was verified by Northern blot using a *hoxF*-specific probe (**Fig. 3.1C**). Specific transcripts were detected in *Syn_CnSH*⁺, which were absent in *Syn_WT* and in *Syn_Δhox*. This confirmed functionality of the artificial promoter::gene fusion and hence, successful *CnSH* gene transcription in *Synechocystis*. To test for functional *CnSH* assembly, proteins were extracted from the aerobically cultivated photosynthetically active cells and in-gel activity staining was conducted (**Fig. 3.1D**). Whereas *CnSH* activity was not detected for the protein extracts from *Syn_WT* and *Syn_Δhox*, a strong signal was detected derived from the *Syn_CnSH*⁺ protein extract. This ultimately proved functional *CnSH* production and assembly. To examine the presence of all four *CnSH* subunits, the corresponding band was excised and analyzed by mass spectrometry. Indeed, all subunits (*HoxH*, *HoxF*, *HoxU*, and *HoxY*) of the hydrogenase complex were unambiguously identified (**Fig. 3.1E**). Subsequently, specific *CnSH* activity and O₂ tolerance were evaluated *in vitro* by measuring H₂-driven NAD⁺ reduction in soluble cell extracts. In *CnSH* crude extracts a maximum *CnSH* activity of about 18 ± 1.4 U g⁻¹ of total protein was measured in H₂-saturated buffer. This indicates a lower *CnSH* expression level in *Syn_CnSH*⁺ compared to its native host, as a higher activity was reported for *C. necator* crude extracts (800 U g⁻¹ of total protein) [93]. As expected, neither *Syn_WT* nor *Syn_Δhox* extracts showed hydrogenase activity (**Fig. 3.1F**). Remarkably, activity of *CnSH* extracted from *Synechocystis* cells was not impeded by the presence of O₂ as similar specific activities were obtained under aerobic (20% O₂, 80% H₂) and anaerobic (20% N₂, 80% H₂) conditions (**Fig. 3.1F**); for the complete dataset see Appendix, (**Fig. S3.1** and **Table S3.1**). This confirmed O₂ tolerance of the *CnSH* synthesized and matured in cyanobacterial cells and hence paves the way for continuous *CnSH* activity in photosynthetically active cells.

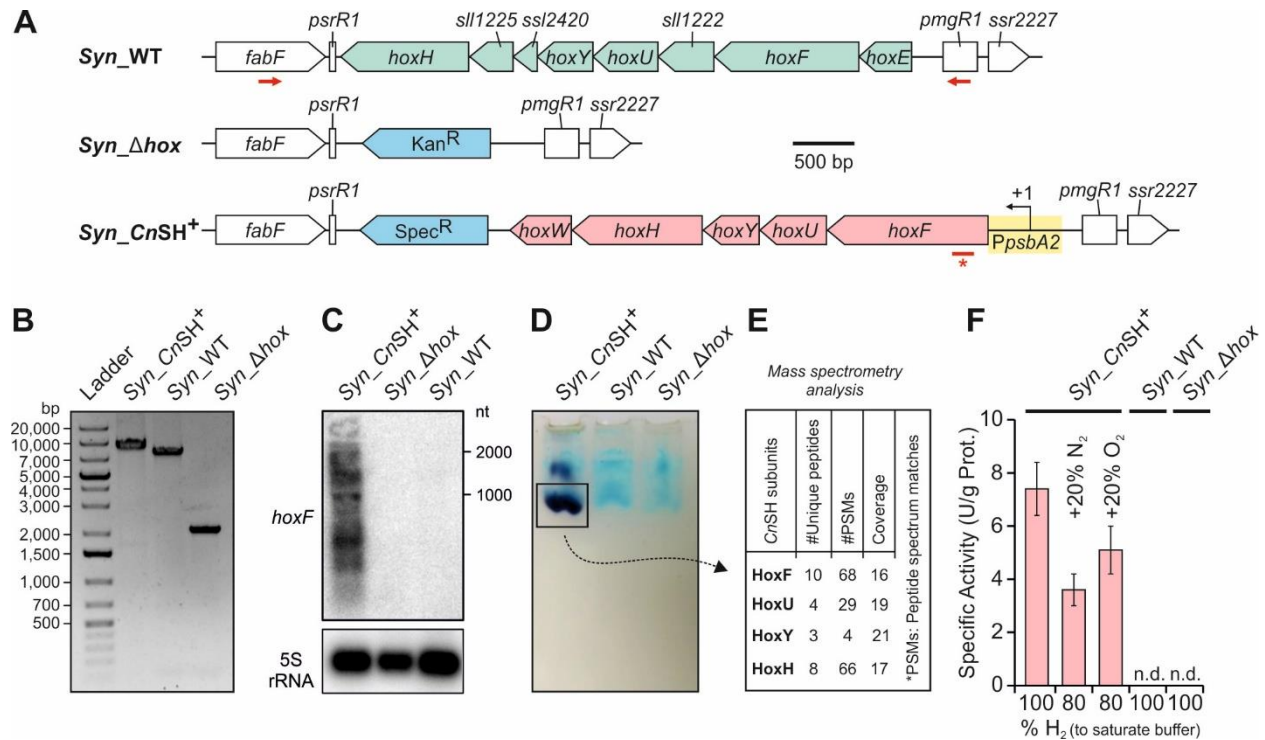


Figure 3.1. Implementation of a functional O₂-tolerant hydrogenase in the cyanobacterium *Synechocystis*. (A) Genetic setup of the used and/or generated strains. Red arrows and the asterisk indicate the binding sites of primers and the probe used to verify the correct gene arrangement and its transcription, respectively. (B) Colony-PCR obtained by using the primers indicated in panel A and cell material from the given strains. (C) Northern blot verifying the presence of the *CnSH* *hox* transcript. A nylon membrane harboring separated and crosslinked RNA from the given strains was hybridized with a ³²P-labeled, single-stranded RNA probe targeting *hoxF* mRNA. 5S rRNA is shown as loading control. (D) In-gel activity staining verifying *CnSH* activity. For this, cells were grown photoautotrophically under aerobic conditions, soluble proteins isolated, and 500 μg of soluble proteins were separated by native PAGE. Activity staining involved the coupling of hydrogenase mediated NADH formation to NADH-mediated reduction of NBT resulting in prominent dark-colored bands. The smaller dark band detected for *Syn_CnSH⁺* likely represents the homodimeric form of *CnSH*. Light blue colored bands are attributed to protein staining by the loading buffer, not to enzyme activity. (E) Mass spectrometry analysis of the dark blue stained band (boxed) resulted in the detection of multiple unique peptides and peptide-spectrum matches (PSMs) for all essential *CnSH* subunits. (F) Specific *CnSH* activity in crude extracts of photosynthetically grown cells measured in buffer saturated either with 100% H₂ or gas mixtures composed of 80% H₂ and 20% of N₂ or O₂.

3.2.2. Cyanobacterial cells show hydrogenase activity during oxygenic photosynthesis

Based on the promising data obtained *in vitro*, hydrogenase activity and O₂ tolerance were investigated *in vivo* by monitoring H₂ consumption of *Syn_CnSH⁺*, *Syn_WT*, and *Syn_Δhox* cultures. For this purpose, cells were maintained in yBG11 medium in sealed glass vials under continuous illumination. Cell suspensions were incubated with a defined headspace gas mixture containing 10% H₂ and 90% N₂. Indeed, strain *Syn_CnSH⁺* entirely consumed the provided H₂

within a few hours (**Fig. 3.2A**). During the first 4 h of light incubation *Syn_CnSH*⁺ showed a specific H₂ uptake rate of up to 15 U g_{CDW}⁻¹ (CDW: cell dry weight), which significantly dropped afterwards. Nevertheless, H₂ consumption persisted even in presence of up to 12.5% O₂ again confirmed O₂ tolerance of the *CnSH* assembled by *Synechocystis*. To verify that our observations were clearly linked to specific *CnSH* activity *in vivo*, we tested the negative control strains *Syn_WT* and *Syn_Δhox* under the same conditions. In photosynthetically active cells (proven by O₂ accumulation similar to the *Syn_CnSH*⁺ strain), only a slight decrease in H₂ concentrations could be detected within 24 h, which is in clear contrast to the complete H₂ consumption of *Syn_CnSH*⁺ in the same time range (**Fig. 3.2B**). As shown via an abiotic control (yBG11), this slight decrease in H₂ concentration was due to slow H₂ diffusion through the vial caps and not to hydrogenase activity. In subsequent experiments the gas phase was adapted e.g. to avoid H₂ limitation or inhibition of photosynthesis caused by low CO₂ availability. In particular, the H₂ concentration was increased to 20% and 10% CO₂ was provided. H₂ was consumed in a similar way as observed with less H₂ and without CO₂, but was not depleted. Simultaneously, the O₂ concentration rose above 25% within 12 h (**Fig. 3.2C**, **Fig. S3.2**). In this regard, it is important to note that the measured O₂ and H₂ concentrations differ from the applied gas mixture, due to the inability to measure CO₂ via GC. The decreasing H₂ consumption rate may be due to inhibition of *CnSH* by O₂ or to a sink limitation, i.e. a limitation in the final electron acceptor, triggered by CO₂ depletion in the presence of vigorous electron supply via photosynthetic water oxidation. To elucidate this further, the electron flow from PSII was blocked by the addition of 3-(3,4-dichlorophenyl)-1,1-dimethylurea (DCMU) under otherwise identical conditions. DCMU treated cells consumed H₂ with an elevated consumption rate of around 20 U g_{CDW}⁻¹, which persisted until H₂ levels approached depletion (**Fig. 3.2D**). These results indicate efficient H₂ consumption by *CnSH* *in vivo*, which, in the presence of photosynthetic water oxidation, appears to be limited by sink availability or inhibited by O₂ accumulation, which is not expected for *CnSH* up to an O₂ concentration of 80% [99]. To evaluate a possible inhibition by O₂ initial H₂ oxidation activities of *Syn_CnSH*⁺ (20% H₂ starting concentration) were measured at different initial O₂ (5, 10, and 20%) and accordingly reduced N₂ concentrations. No significant effect of the O₂ concentration on the H₂ consumption rate was found during 2 h of incubation (**Table S3.2**), indicating a high O₂ tolerance of *CnSH* *in vivo*. The decreasing activity observed in **Fig 3.2C** thus can be attributed to an increasing sink limitation as major cause. Additionally, specific methylviologen-mediated H₂ formation activities were determined for *Syn_CnSH*⁺ and *Syn_WT* by means of a Clark-type-electrode under anaerobic condition (**Table S3.3**), indicating that they contained a similar active hydrogenase level.

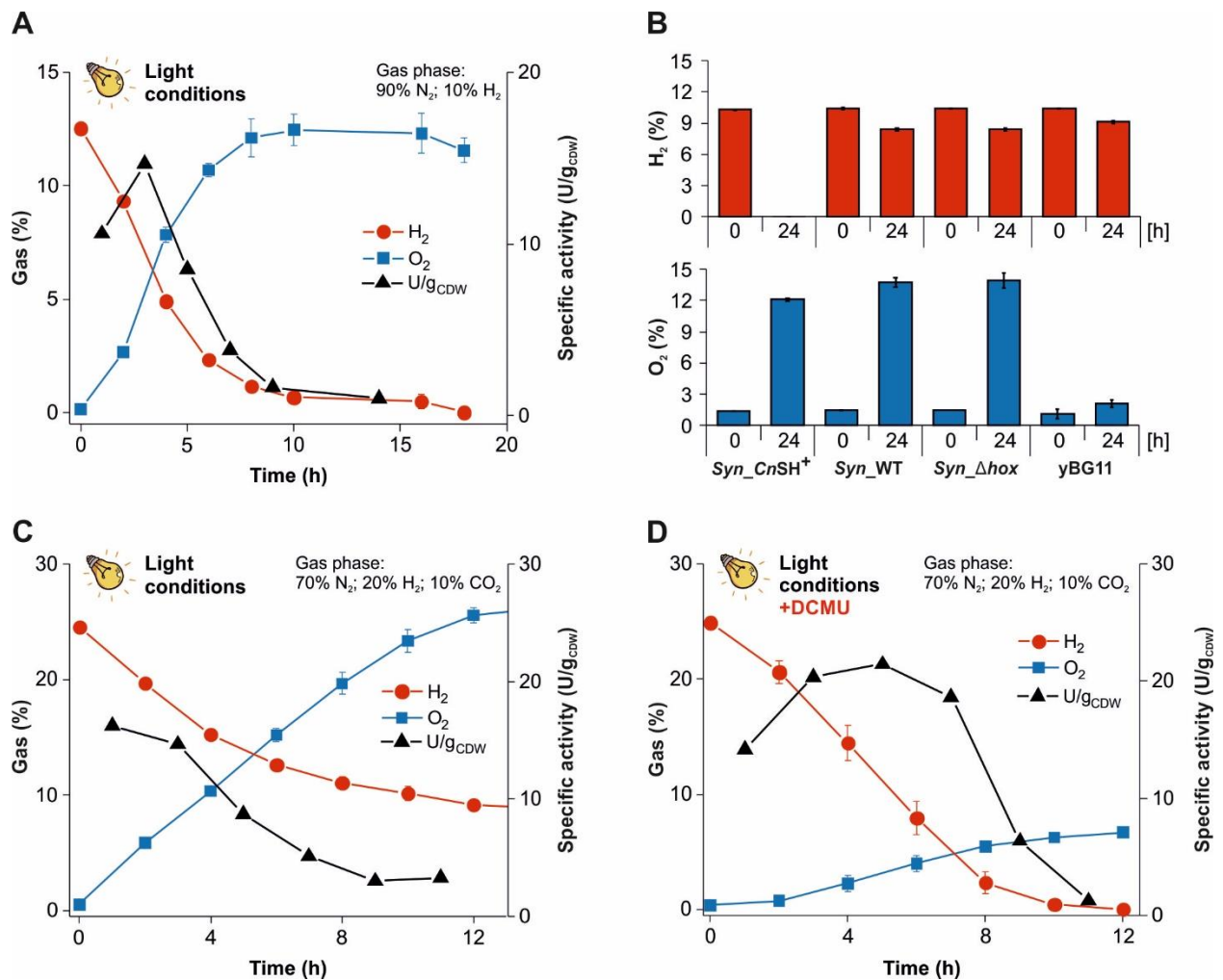


Figure 3.2. *CnSH* activity in photosynthetically active cells. *CnSH* activity was determined *in vivo* by monitoring H₂ consumption of sealed and illuminated cultures after aerobic precultivation in light. H₂ and O₂ concentrations were analyzed via gas chromatography (GC). **(A)** *Syn_CnSH*⁺ incubated in the presence of 90% N₂ and 10% H₂. Specific H₂ consumption rates given in U g_{CDW}⁻¹ were calculated based on concentration changes in respective time periods. **(B)** H₂ and O₂ concentrations for *Syn_CnSH*⁺, *Syn_WT*, *Syn_Δhox* strains and an abiotic control (yBG11) before and after incubation in light for 24 h. The conditions were the same as given for panel A. **(C, D)** H₂ and O₂ concentrations and specific H₂ consumption rates during illuminated incubation of *Syn_CnSH*⁺ with a gas phase initially composed of 20% H₂, 10% CO₂, and 70% N₂ in presence or absence of 3-(3,4-dichlorophenyl)-1,1-dimethylurea (DCMU) blocking electron flow from PSII. Data represent means ± standard deviations (n=3).

3.2.3. H₂-based cyanobacterial growth

The H₂ consumption experiments performed *in vitro* and *in vivo* clearly proved the functionality of the recombinant *CnSH* produced by *Synechocystis*. It however remained unclear, if and to what extent H₂ consumption and the accompanied generation of NADH is connected to cyanobacterial metabolism. Such an interconnection is a prerequisite to enable engineering of an efficient photobiocatalyst for H₂ production using, e.g. optimized *CnSH* variants in the future. We

hypothesized that *CnSH* catalyzed NADH formation can be coupled to CO₂ fixation as it is the case in *C. necator* [40], with the constraint that an electron transfer from NADH to NADP⁺ is necessary. We thus tested if H₂ oxidation by *CnSH* can support growth of *Synechocystis* in the presence of DCMU and thus substitute water oxidation at PS II and thus enable a lithoautotrophic lifestyle. Cultivation of *Syn_CnSH*⁺ in sealed vials containing 20% H₂, 10% CO₂, and 70% N₂ in the gas phase indeed enabled growth even when electron flow from PS II was blocked by DCMU (**Fig. 3.3A**). This, however, required illumination, indicating photolithoautotrophy, which still depends on light-driven electron flow through PS I. In contrast, *Syn_WT* and *Syn_Δhox* did not show any growth based on H₂ oxidation but showed comparable growth to *Syn_CnSH*⁺ under the same conditions without DCMU (control). The missing growth of *Syn_WT* in presence of DCMU can be attributed to inhibition of the native hydrogenase by low amounts of O₂ present in the sealed vials due to slow O₂ diffusion through the septa of the vials used (**Fig. 3.3C**). In presence of light and DCMU, all H₂ (20% v/v), provided daily via gas phase replacement, was completely consumed by *Syn_CnSH*⁺ within 24 h (**Fig. 3.3B**). H₂ concentration also slightly decreased in the headspace of dark incubated cultures of *Syn_CnSH*⁺, which did not enable significant growth, and of illuminated cultures without DCMU. *Syn_WT* and *Syn_Δhox* did not consume H₂ under any tested conditions. H₂ concentrations behaved similarly in the abiotic control (**Fig. 3.3B**) (minimal decrease due to H₂ diffusion through the septa). Under control conditions, all strains showed O₂ accumulation up to 15-18% (**Fig. 3.3C**). When DCMU was added, no O₂ formation was detectable except for a minimal O₂ increase due to slow diffusion through the septa, as this was also the case in the negative control. A slight O₂-level increase only was observed for *Syn_CnSH*⁺ and most likely resulted from increased air diffusion into the vial due to a decreasing pressure caused by vigorous gas consumption (complete and partial H₂ and CO₂ depletion, respectively; replacement by air results in 5-6% O₂ as found in this case). To test whether *Syn_CnSH*⁺ can grow as a true “Knallgas” bacterium, e.g., utilizing H₂ as electron donor and O₂ as acceptor, the 70% N₂ in the gas mixture was substituted with air (**Fig. 3.3A**). *Syn_CnSH*⁺ incubated with this gas mixture in presence of DCMU and light showed no significant growth and only minor H₂ consumption (**Fig. 3.3B**). Since O₂ tolerance of *CnSH* was verified *in vivo* we hypothesize that metabolic constraints not directly related to the hydrogenase limits its activity under these conditions.

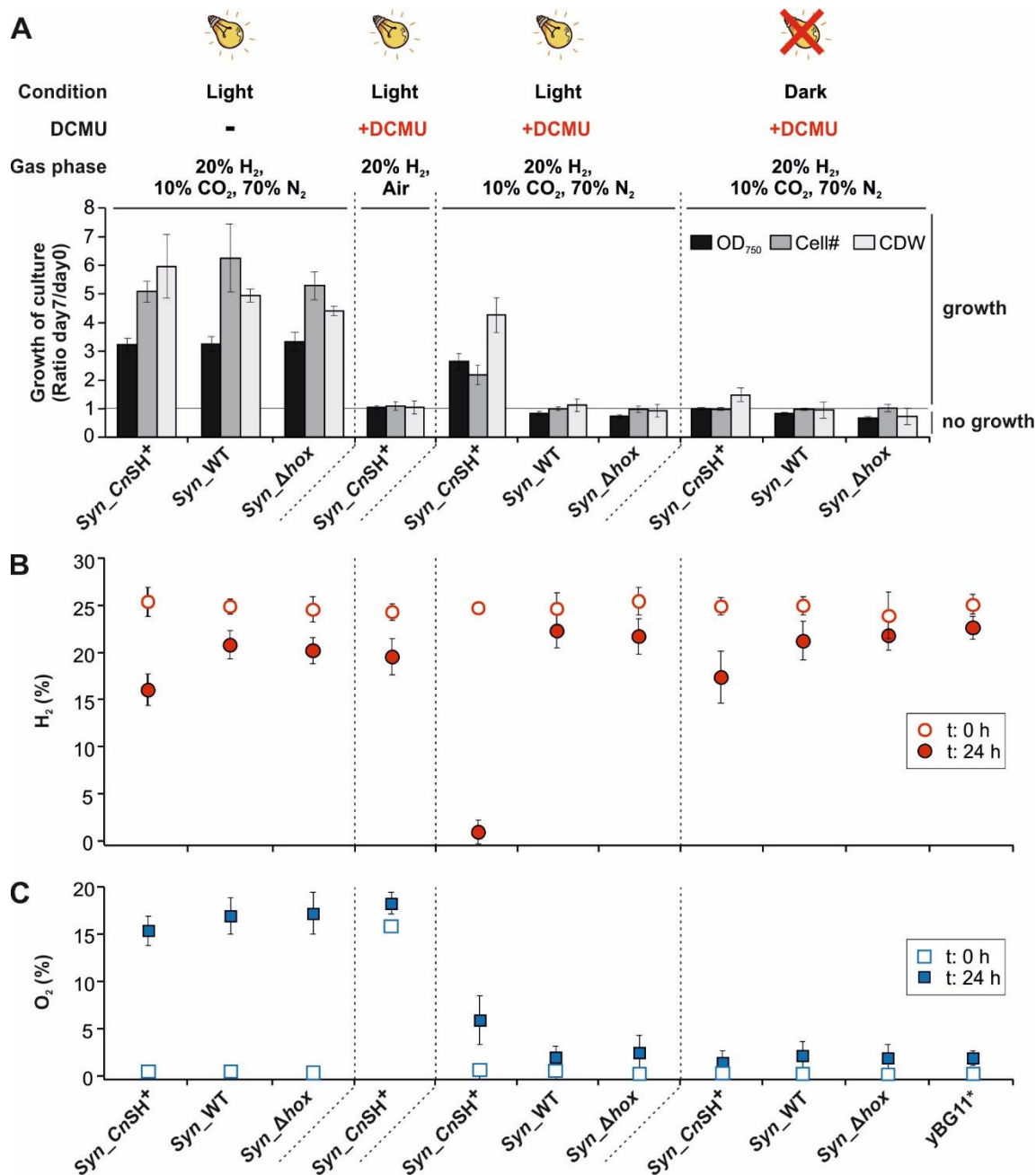


Figure 3.3. Photolithoautotrophic growth of *Syn_CnSH*⁺ based on H₂ instead of water oxidation. (A) Growth of *Synechocystis* strains is given as OD₇₅₀, cell number, and cell dry weight (CDW) increase within 7 days relative to initial values. Cultures were kept in sealed head space vials under different conditions, i.e., ± light, ± DCMU and different gas mixtures in the headspace (20% H₂, 10% CO₂, and 70% N₂ or air), which was exchanged daily. Panels (B) and (C) show H₂ and O₂ concentrations in the culture head space, respectively, before and after the 24 h incubations. Data represent mean values and standard deviation of four biological replicates each measured for 7 consecutive days. *A vial filled with the same volume of yBG11 medium was used as abiotic control for comparison.

Based on the CDW formed and considering a typical biomass composition of *Synechocystis*, photosynthetically grown *Syn_WT* cells used 70-73% of the carbon available for biomass

production, whereas H₂-fed *Syn_CnSH*⁺ in light + DCMU only used ~65%. Thus, at least 50% of the electrons derived from H₂ consumption were used for CO₂ fixation and at least 10% for nitrate assimilation [187]. The different solubility of H₂ (1.6 mg l⁻¹) compared to CO₂ (1688 mg l⁻¹) in the yBG11 medium may result in a limited supply of H₂, and could cause the slower growth based on H₂. The light dependency of H₂-based growth indicates that electron transfer from NADH to NADP⁺ mainly occurred via PS I. Potential electron routes in *Syn_CnSH*⁺ strain are given in **Fig. 3.4A**. Altogether, *CnSH* was obviously active for 7 days, supporting photolithoautotrophic growth of *Syn_CnSH*⁺ in the presence of DCMU, light, and low initial O₂ amounts (**Fig.3.4B**).

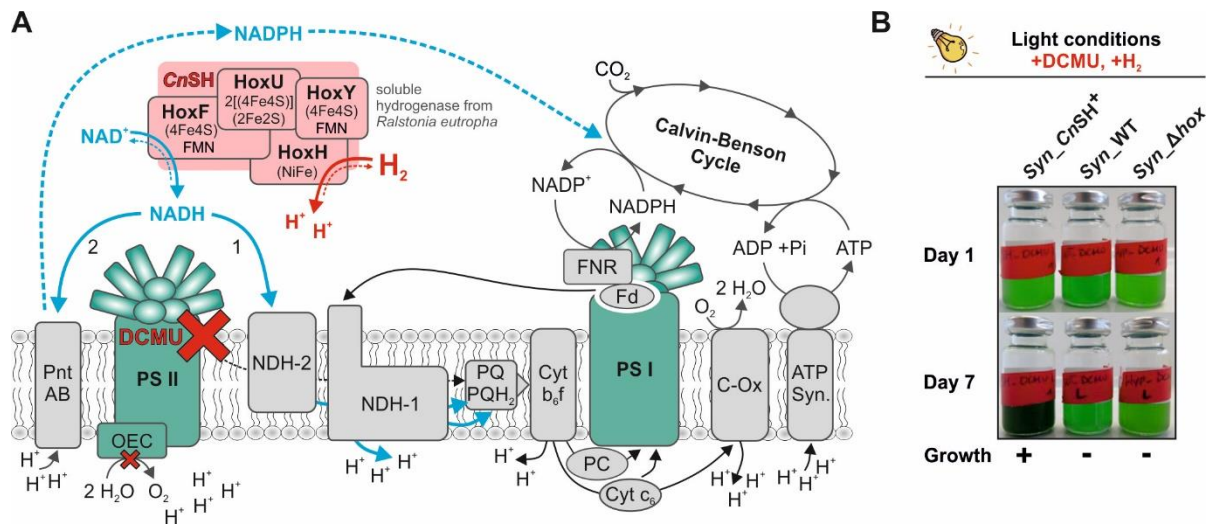


Figure 3.4. Model for electron transport routes enabling H₂-based growth of *Syn_CnSH*⁺. (A) The scheme shows the two main feasible routes for the transfer of reducing equivalents from H₂ via *CnSH* to the Calvin-Benson cycle (blue lines). Electrons from NADH may either be transferred directly to NADP⁺ via the transhydrogenase (PntAB) or enter the electron transport chain through NDH-2. In the latter case, electrons are channeled to and activated by PS I leading to NADPH formation via ferredoxin reductase (FNR) and thereby contribute to proton gradient and ATP formation. Addition of 3-(3,4-dichlorophenyl)-1,1-dimethylurea (DCMU) blocks electron transfer from the primary quinone electron acceptor Q_A to the secondary quinone electron acceptor Q_B on the reducing side of PS II and thus water oxidation at the O₂-evolving center (OEC). HoxFUYH designates the structural *CnSH* subunits present in *Syn_CnSH*⁺. PS II, photosystem II; NDH-2: type 2 NADH-dehydrogenase; NDH-1: NADPH-dehydrogenase (complex 1); PQ/PQH₂: plastoquinone/plastoquinol pool; Cyt b₆/f: cytochrome b₆/f complex; PC: plastocyanin; Cyt c₅₅₃: cytochrome c₅₅₃; PS I: photosystem I; C-Ox: cytochrome c oxidase; ATP syn.: ATP-synthase; Fd: ferredoxin. (B) Pictures of cultures incubated in presence of DCMU, 20% H₂ and light for 7 days (same conditions as described in legend of Fig. 3.3). Biomass formation (represented by dark green color) was only observed with *Syn_CnSH*⁺ and highlights the prominent growth of this strain as compared to *Syn_WT* and *Syn_Δhox*.

3.2.4. H₂ formation by *Syn_CnSH*⁺

Finally, we tested whether *Syn_CnSH*⁺ can produce H₂ *in vivo*. To drive *CnSH* catalyzed equilibrium reaction towards H₂ formation, a high intracellular NADH/NAD⁺ ratio and efficient

NADH supply are required. To this end, cells were supplied with 10 mM glucose. H₂ formation was monitored under light or dark and initially anoxic conditions. In the dark *Syn_CnSH*⁺ produced up to 0.4% fermentative H₂, corresponding to 177.6 μmol H₂ g_{CDW}⁻¹ within 24 h of incubation (**Fig. 3.5A**). No H₂ formation was detected any conditions in *Syn_CnSH*⁺ when glucose was omitted. *Syn_WT* showed a slightly higher H₂ formation activity within the first 5 h (12.7 as compared to 8.6 U g_{CDW}⁻¹), but showed a shorter production phase and thus less H₂ accumulation in 24 h. As expected, no H₂ formation was detectable with *Syn_Δhox*. *Syn_CnSH*⁺ also produced H₂ under illumination for up to 20 h (~11 μmol H₂ g_{CDW}⁻¹, **Fig. 3.5B**), whereas *Syn_WT* accumulated H₂ only within the first 2-5 h, probably due to emergence of low levels of O₂ (0.5 % after 5 h of incubation, see **Table S3.4**). It should be noted that H₂ formation by illuminated *Syn_CnSH*⁺ required, besides the presence of glucose, the omission of any other electron sink such as nitrate or carbonate/CO₂. O₂ levels generally remained low, as expected for glucose catabolizing cells in the absence of electron sinks other than the hydrogenase and respiratory systems. Albeit not offering a final solution for a sustainable H₂ production process based on oxygenic photosynthesis, our data lay the foundation for the utilization of O₂-tolerant, and hence permanently active hydrogenases in oxygenic phototrophs. Subsequent to this milestone, protein engineering will have to target *CnSH* itself, e.g. to shift its cofactor requirements towards NADPH or ferredoxin, to indeed utilize this enzyme for a continuous H₂ production based on photosynthetic water splitting.

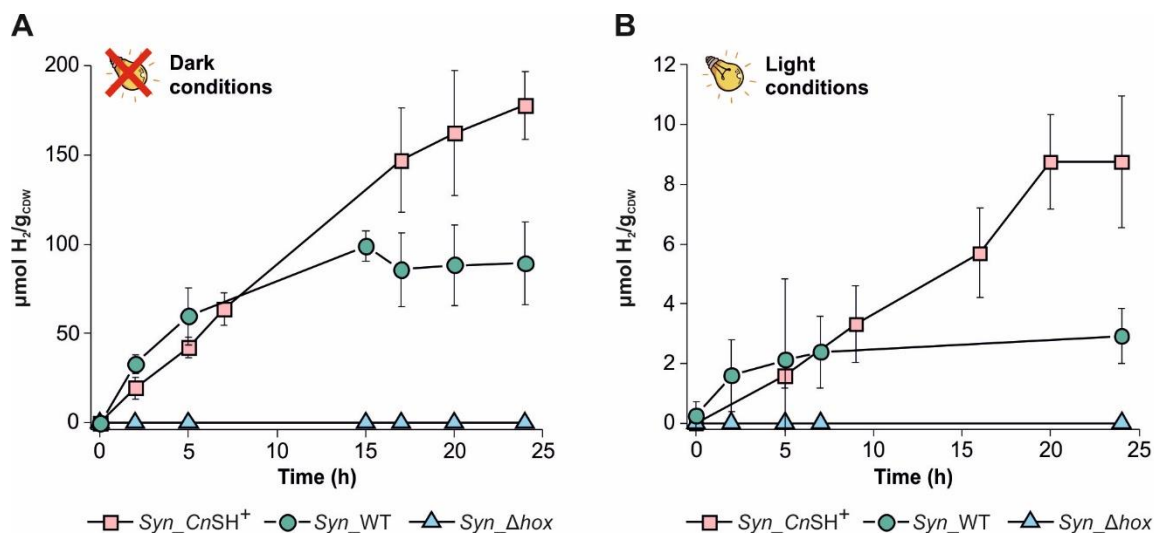


Figure 3.5. In vivo H₂ formation by *Syn_CnSH*⁺. (A) Fermentative H₂ formation by *Syn_CnSH*⁺, *Syn_WT*, and *Syn_Δhox* incubated anaerobically (N₂ saturated gas phase) under dark conditions with 10 mM glucose in K_{Pi} buffer. (B) H₂ formation by the same strains incubated for 24 h under illumination and initially anaerobic conditions with 10 mM glucose in K_{Pi} buffer. Data given represent means and standard deviations of biological replicates (n=3).

3.3. Discussion

Photosynthetic microorganisms such as cyanobacteria are in principle able to convert light energy into chemical energy in the form of H₂, but only for short time periods after a shift from dark to light conditions as all known cyanobacterial bidirectional [NiFe]-hydrogenases are O₂-sensitive [188][189]. O₂-evolution thus precludes sustained H₂ production via these enzymes during oxygenic photosynthesis and necessitates the introduction of an O₂ tolerant hydrogenase. Up to date, maturation and gene expression of O₂-tolerant hydrogenases has only been reported for *C. necator* hydrogenases in heterotrophic hosts [129][126][128]. In this study, we managed to functionally express all structural genes encoding the O₂-tolerant *CnSH* in *Synechocystis* and confirmed its activity when assembled in the cyanobacterial host. The O₂ tolerance of *CnSH* derived from *Synechocystis* was shown to be comparable to that derived from *C. necator* [99], or recombinant from *E. coli* [128]. Functional *CnSH* synthesis in *Synechocystis* was accomplished by co-expressing only the structural *hox* genes and *hoxW*, encoding a specific endopeptidase ensuring proper C-terminal processing of HoxH. This result is unique not only because it is the first successful transfer of an O₂-tolerant hydrogenase into a phototrophic strain so far, despite major efforts over the last decade years e.g. [185]. Also because heterologous expression of *CnSH* has only been reported in combination with the co-expression of all or part of the respective maturation genes [176]. Our results demonstrate that the maturation apparatus of *Synechocystis* is sufficient to mature *CnSH* *in vivo*. Fan et al. (2020) summarized the diverse hydrogenases introduced into various hosts, hypothesizing that a high similarity of homologous and heterologous hydrogenases increases the probability of success. However, the *Synechocystis* hydrogenase (*SynH₂ase*) and *CnSH* exhibit only ~50% similarity with respect to the amino acid sequence. Furthermore, Fan et al. (2020) proposed that a low homology among maturation proteins could cause a low activity of produced recombinant hydrogenases in the absence of their native maturases. Accordingly, the low amino acid similarity among the *C. necator* and *Synechocystis* Hyp proteins of 50-67% may be a reason for the rather low *CnSH* expression level and activity obtained in *Synechocystis* in the absence of the *C. necator* maturation apparatus. In accordance with previous studies on *CnSH*, HoxI was found not to be essential for *CnSH* functionality [88]. Most interestingly, our data show that hydrogenase maturation in *Synechocystis* to some extent is O₂-tolerant. *CnSH* was immediately active in *Synechocystis* in all experiments. This is in agreement with results of previous studies, showing that gene expression and maturation *SynH₂ase* does not depend on anoxia, but that the enzyme is constitutively expressed [75]. However, for *C. necator* under oxic conditions, HypX is known to be essential for the biosynthesis of CO and its insertion as a ligand into the Ni-Fe active site of *CnSH* (Burstel et al., 2016).

Therefore, it will be highly interesting to test if HypX can improve *CnSH* maturation in *Synechocystis* especially under oxygenic conditions. *CnSH* empowered *Syn_CnSH*⁺ to use H₂ as electron source, which in turn allowed autotrophic growth in the absence of water oxidation (**Fig. 3.3**). Recently, the native hydrogenase was shown to enhance growth of *Synechocystis* [190], which might be in contrast to our findings with *Syn_WT*. Yet, it can be explained by differences in the conditions applied. Besides the fact that PS II activity was blocked in our experimental setup, initial conditions were microaerobic (~1% O₂), whereas cultures of Sleutels *et al.* (2020) initially were anaerobic. Further, H₂ consumption was limited to low O₂ concentrations and virtually stopped at an O₂ level of ~2.3% (as can be calculated via redox balancing), due to the O₂ sensitivity of *SynH₂ase* under the experimental conditions used by Sleutels *et al.* (2020). Further, recombinant [FeFe]-hydrogenase has been shown to enable *Synechococcus elongatus*, upon PS II blockage, to grow solely on H₂, CO₂, and light [191]. As expected for [FeFe]-hydrogenases, this required strictly anaerobic conditions. In both referenced cases, growth on H₂ as electron donor depended on light. As NAD⁺ is the preferred electron-acceptor of *CnSH* [93], the cellular metabolism has to cope with NADH formation and balance the hydrogenase reaction with NADH reoxidation. Instead of enhanced respiration, which would be the most straightforward way of NADH reoxidation, but may be hampered at low O₂ levels, the cells managed to channel electrons towards the more rewarding CO₂ fixation (**Fig. 3.3**). Assuming that *CnSH* in *Syn_CnSH*⁺ is not affected by atmospheric O₂ levels (evidence shown in **Table S3.2**), the cells obviously even stalled NADH reoxidation in the presence of high O₂ levels. At the rather low H₂-mediated availability of reduction equivalents, this may be connected to a general down-regulation of electron transfer chains to avoid an ATP/NAD(P)H imbalance or wastage of reduction equivalents, which both can be considered a result of excessive respiration. For the channeling of electrons towards CO₂ fixation, electrons from NADH have to be transferred to NADP⁺, which can be accomplished by the transhydrogenase PntAB (**Fig. 3.4A**). Alternatively, electrons enter the photosynthetic or respiratory electron transport chain via the NADH:quinone oxidoreductase NDH-2, where they can be directed via PS I to NADP⁺ or are “lost” to respiration, respectively (see **Fig. 3.4**). Knowledge regarding function and regulation of these electron paths is still scarce [192][193][194][195]. However, H₂-uptake in cyanobacteria and algae is known to be light dependent [196][197], as it was the case for growth of *Syn_CnSH*⁺ with H₂ as sole electron donor (**Fig. 3.3**). Recently, it has been shown that electrons available from *SynH₂ase*-catalyzed H₂-oxidation all pass through PS I at higher light intensities [198]. For the growth of *Syn_CnSH*⁺ an electron transfer from NADH to NADP⁺ via NDH-2 and PS I would strictly depend on light, whereas the proton gradient necessary to drive PntAB can be established via respiration, the

pathway via NDH-2 running in parallel, or cyclic electron transfer [194][199][195]. Here, it will be interesting to investigate further the function and regulation of these electron paths, especially of the electron transport chains. Comparative H₂ production experiments revealed that *Syn_CnSH*⁺ produced more H₂ than *Syn_WT* under dark fermentative conditions as well as under illumination (**Fig. 3.5**). As expected H₂ evolution by *Syn_WT* under illumination ceased upon O₂ accumulation after about 2 h [75], whereas it continued with in *Syn_CnSH*⁺. This prolonged H₂ production can be attributed to the O₂-tolerance of *CnSH*. Besides glucose catabolism, also the light reaction might have fueled H₂ formation. As in recombinant *E. coli* [129], *CnSH* also enabled fermentative H₂ formation of *Syn_CnSH*⁺ in the dark, but astonishingly to a higher extent compared to *Syn_WT* (**Fig. 3.5A**). Possible explanations include differences in expression levels, enzyme regulation/activation and the nature of and kinetics/competition for the electron donor. The measured H₂ production rates for *Syn_WT* and *Syn_CnSH*⁺ are in good accordance to previous cyanobacteria based data reviewed by Krishnan et al (2018). Our results indicate that H₂ formation, with concurrent photosynthetic water splitting in *Syn_CnSH*⁺, depends on an elevated intracellular NADH/NAD⁺ ratio, achieved by glucose addition. It is clear that NADPH is more favorable than NADH as electron donor for H₂ formation in photosynthetically active cyanobacteria. In principle, the midpoint redox potential of -320 mV for the couples NADH/NAD⁺ or NADPH/NADP⁺ is, as also shown in this study, sufficient to drive H₂ evolution (H₂/H⁺: -413 mV) in *Synechocystis*. However, ferredoxin (-430 mV) would be a more a favorable electron donor. To realize sustained H₂ production with electrons supplied directly by the electron transport chain an O₂ tolerant hydrogenase accepting electrons from NADPH- or as final solution ferredoxin is needed. A NADPH-accepting O₂-tolerant *CnSH* has recently been engineered [200] and changing the nicotinamide cofactor specificity of oxidoreductases has been intensively investigated [201][202]. A ferredoxin dependence, which will allow direct utilization of electrons from the photosynthetic electron transport chain, may be engineered in analogy to the ferredoxin dependence of *SynH₂ase* [72]. As an alternative option, the *CnSH* hydrogenase module (HoxHY) may be fused to PS I as demonstrated recently for the native *SynH₂ase* hydrogenase module and a [FeFe] hydrogenase [74][183]. Such approaches, together with the elimination of competing pathways [171][172], augur well for an efficient and stable photosynthesis-driven H₂ production mediated by an O₂-tolerant hydrogenase. With the successful expression of the gene cluster of a fully functional O₂-tolerant hydrogenase in a cyanobacterium, our study provides a solid basis for these approaches and thus may significantly contribute to the sustainable production of green fuels in the future. An O₂-tolerant hydrogenase also paves the way to novel metabolic engineering concepts for cyanobacteria. In cells producing carbon skeletons by photosynthesis, externally

added H₂ could increase the intracellular NADH availability and thereby support biocatalytic production schemes with high demand for reduction equivalents and even O₂ as reactant [203][167] [137][190].

3.4. Conclusion

O₂-tolerant hydrogenases have a high potential for H₂ production via oxygenic photosynthesis. We demonstrate functional assembly of an O₂-tolerant hydrogenase derived from a *Knallgas*-bacterium in a model cyanobacterium. Its long-term activity in photosynthetically active cells continuously evolving O₂ is an important step in towards photosynthesis-driven H₂ production. Furthermore, growth of the generated strain with H₂ as the sole electron source, illustrates a high level of interconnection between the introduced hydrogenase and cyanobacterial redox metabolism. These achievements and finding lay the foundation for further engineering, e.g., of electron transfer to *CnSH* via NADPH or ferredoxin, to finally enable sustained photosynthesis-driven H₂ production.

Chapter 4

The activity of an O₂-tolerant hydrogenase recombinantly expressed in *Synechocystis* sp. PCC 6803 is controlled by fine-tuned gene expression in combination with sink and source availability.

Sara Lupacchini, Ron Stauder, Andreas Schmid, Bruno Bühler, Jörg Toepel

Author Contributions:

Sara Lupacchini (Conceptualization, investigation, writing, original draft preparation), Ron Stauder (investigation, writing), Bruno Bühler (Conceptualization, supervision, reviewing and editing), Andreas Schmid (reviewing and editing) Jörg Toepel (Conceptualization, investigation, writing, original draft preparation).

Submitted for publication in:

Plant Biotechnology Journal

The Supplementary Material can be found in the Appendix Section 4.

Abstract

Cyanobacteria bear the potential to function as photosynthetic cell factories. This promising approach depends on effective strain design, efficient and balanced enzyme synthesis, and appropriate reaction conditions. We established a modular cloning system based on CyanoGate to produce the multicomponent soluble O₂-tolerant hydrogenase of *Cupriavidus necator* (*CnSH*) in *Synechocystis* sp. PCC 6803. Functional gene expression was optimized by systematic selection and testing of suitable genetic elements. A genome-based expression system relied on the nickel inducible promoter and the strong synthetic RBS* turned out most suitable. Hydrogenase activity was limited by protein production efficiency but also by substrate and electron sink availability. The optimization of experimental conditions enabled a H₂ oxidation activity of up to 27 U g_{CDW}⁻¹. *In-vitro* hydrogenase activities in cell-free extracts of the investigated cyanobacterial strains reached up to 80 U g_{Prot}⁻¹, narrowing the gap to activities achieved with heterotopic expression hosts of the *CnSH* gene cassette. H₂ formation by *CnSH* was strictly dependent on an elevated cytosolic NADH pool and thus was restricted in *Synechocystis* to fermentative or mixotrophic conditions. For the latter, H₂ formation required the blockage of the electron transport chain. Two application scenarios can be sketched out for the strain developed: by combining the energy of sunlight and H₂, it can be applied for redox dependent biotransformation reactions, and it provides access to H₂ production from NADH fueled by organics. Enzyme engineering may open the door to H₂ formation with *CnSH* with direct utilization of electrons derived from photosynthetic water splitting.

4.1 Introduction

H₂ is a key element of future cyclic economies and it is of major interest within the field of renewable energy [204]. Despite the advantages of developing a decarbonized H₂-based economy and with H₂ featuring a high gravimetric energy content, 96% of H₂ production still relies on fossil resource usage. Therefore, in addition to technical issues regarding storage and H₂ conversion, the big challenge is to develop sustainable ways for H₂ production [205]. Nature comes in by showing diverse processes for microbial bio-H₂ production [174]. Many microorganisms can produce H₂ via dark and photo-fermentation and via interactions within microbial consortia [206]. Photoautotrophic organisms in principle are able to couple water-splitting photosynthesis with H₂ production [207][208]. In microalgae, H₂ formation relies on [FeFe] hydrogenases, which show high turnover rates of up to 10⁴ s⁻¹. They are however produced and active only under micro- or anaerobic conditions and are rapidly disintegrated in the presence of molecular oxygen. To circumvent hydrogenase inactivation by O₂, temporal separation of O₂ and H₂ formation or balancing photosynthetic activity with mitochondrial respiration constitute possible approaches, which involve efficiency losses. Alternatively, the development of O₂-tolerant [FeFe] hydrogenases is targeted [173][209]. Cyanobacteria are able to produce H₂ mainly via indirect biophotolysis of water, meaning they form H₂ via the action of O₂-sensitive nitrogenases or hydrogenases under O₂-depleted conditions, i.e., under dark fermentative conditions, at the onset of photosynthetic water oxidation or in heterocysts [210]. Both enzymes need a physical or temporal separation from photosynthetic water oxidation for stable H₂ evolution. In N₂-fixing cyanobacteria, H₂ is synthesized as byproduct of N₂ fixation in specialized cells called heterocysts maintaining low intracellular O₂ levels [211]. Nitrogenases have the advantage to be unidirectional in contrast to the generally bidirectional hydrogenases, but are usually coupled with an uptake [NiFe] hydrogenase, which utilizes the produced H₂ to save energy. The energy dependence of nitrogenases (4 ATP per H₂) constitutes a major downside constricting the H₂ conversion efficiency compared to hydrogenase-based indirect photolysis [209][212]. Cyanobacteria typically feature bidirectional [NiFe] hydrogenases, which are not disintegrated in the presence of O₂, but are reversibly inhibited. One of the best characterized cyanobacterial hydrogenases is the one of the unicellular model cyanobacterium *Synechocystis* sp. PCC 6803 (here after *Synechocystis*). This pentameric enzyme (composed of the hydrogenase module HoxYH and the diaphorase module HoxEFU) is expressed unconstrained by the presence of O₂ [75] and located at the thylakoid membrane by means of the HoxE subunit [213]. This position is favorable, as the diaphorase module HoxEFU can accept electrons from the photosynthetic electron transport chain via reduced flavodoxins and ferredoxins [72]. As natural function, the enzyme works as an

electron valve to bridge sudden switches from dark to light and compensate for transiently missing electron acceptors such as the Calvin-Bassham-Benson (CBB) cycle [214]. Recently, an involvement of this hydrogenase in electron balancing has been proposed, indicating a multi-functional role of this enzyme in cyanobacteria [215]. The main limiting factors for applying cyanobacterial hydrogenases for photo-H₂ production are its O₂-sensitivity, H₂ re-oxidation when C- and N-assimilatory pathways become available as native electron acceptors, and the competition with these for photosynthetically derived electrons [214]. During the past two decades, advances have been achieved to overcome these challenges. However, O₂-sensitivity still remains a main limitation. In this respect, functional heterologous expression of a [NiFe] hydrogenase tolerant up to 1-3% of O₂ has been achieved [216]. Promoting photosynthetic electron flow towards H₂ formation instead of nitrate, CO₂, and/or O₂ reduction recently has been targeted via metabolic engineering [75][217][218][219][191], and notably the direct coupling of H₂ production to the photosynthetic electron transport chain [183][74]. Recently, the hydrogenase module of *Synechocystis* was fused with photosystem I (PSI), which resulted in reduced competition with the downstream metabolic pathways and avoided H₂ uptake activity. Photo-H₂ production has been achieved with enzymatic O₂-removal, though O₂-sensitivity and electron transfer efficiency remain challenges to be addressed [76]. We recently reported the functional expression of the soluble O₂-tolerant [NiFe] hydrogenase from the Knallgas bacterium *Cupriavidus necator* (*CnSH*) in *Synechocystis* (*Syn_CnSH*⁺) [130]. Remarkably, this NAD(H)-dependent enzyme tolerates ambient O₂ levels [109][99]. In *Synechocystis*, *CnSH* was continuously active during oxygenic photosynthesis, oxidizing H₂ independently of the O₂ concentration. The results revealed a tight interconnection of the *CnSH* with *Synechocystis* metabolism. *Syn_CnSH*⁺ was able to use H₂-derived electrons to fix CO₂ and fuel growth even in the absence of water oxidation activity. Due to the strict dependency of *CnSH* on NADH as electron donor, H₂ formation was achieved only in the presence of glucose effecting an elevated cytosolic NADH/NAD⁺ ratio. For the application of *CnSH* for photo-H₂ production, it will be central to change its electron donor specificity or to couple the hydrogenase module directly to PSI. As another key issue for H₂ formation, in *Syn_CnSH*⁺ the specific enzyme activity reached was two orders of magnitude lower compared to that in its native host [130][93]. In heterologous systems, enzyme abundance and/or hydrogenase maturation may well limit the hydrogenase activity. Recent literature has emphasized the importance to choose suitable genetic regulatory elements, such as promoter, RBS, and terminator, when a controlled and stable recombinant multi-gene expression is aimed for [220][221][222]. For hydrogenase maturation, *Synechocystis* encodes 8 *hyp* genes (*hypA1*, *hypA2*, *hypB1*, *hypB2*, *hypC*, *hypD*, *hypE*, *hypF*), of which 6 are essential

[118]. This maturation machinery enabled functional *CnSH* assembly in *Synechocystis*. In *Syn_CnSH*⁺, the introduced *Cn_hox* operon is composed of *hoxFU**YHW*, encoding the *Cn* hydrogenase module HoxYH, the *Cn* diaphorase module HoxFU, and the specific endopeptidase HoxW necessary for processing HoxH [123]. Beside expression and maturation [176][120], factors relevant for intracellular hydrogenase activity include the availability of electron donors and acceptors. Especially, the H₂ oxidation activity of *CnSH* in *Synechocystis* relies on substrate (H₂) availability and electron acceptor (NAD⁺) recycling. In this study, we tackled the limited specific activity of heterologously expressed O₂-tolerant *CnSH* in *Synechocystis* [130]. We show that the expression of the *CnSH* multigene system in a controlled manner enables increased protein levels as well as *CnSH* activity. We also investigated the flow of H₂ derived electrons to unravel the potential of hydrogenases for biotechnological applications. Finally, we used the information regarding electron flow to produce H₂ with the *CnSH* in *Synechocystis*.

4.2 Results

4.2.1 Design of new expression systems for *CnSH* in *Synechocystis*

In order to generate a library of various genetic elements enabling combinations in vectors for chromosomal integration or plasmid-based expression, we developed a modified version of the CyanoGate system [153]. The complete cloning procedure is summarized in Chapter 2.6.2.2 and was based on the MoClo syntax. In *Syn_CnSH*⁺, the introduced *CnSH* genes were under the control of the light-inducible *psbA2* promoter without an additional terminator element after the STOP codon of the last gene (*hoxW*) (**Fig. 4.1A**). In recent studies, only poor *P_{psbA2}*-based recombinant expression has been reported, even though *P_{psbA2}* is considered one of the strongest promoters in *Synechocystis* [223][220]. Some alternative promoters of *Synechocystis* have been well characterized for biotechnological applications [220][221][224][225]. Among the inducible systems, the nickel inducible promoter *P_{nrsB}* showed low leakiness and strong induction [226][60]. The major drawbacks of using a metal inducible promoter include metal toxicity and active excretion [220]. The ribosome binding site (RBS) also plays a key role for the overall strength of protein synthesis. Previous studies investigated a broad range of RBSs in the cellular and genetic context [221][222]. We opted for the synthetic RBS*, which is widely used in *Synechocystis* for heterologous expression [60][227], providing high rates of translation. Further, the use of terminators can stabilize recombinant expression preventing interference with downstream genes, especially upon chromosomal integration [228][229]. We selected the *T_{psbC}* terminator enabling efficient Rho-independent termination, as shown in a study on a library of native *Synechocystis* terminators [221]. Besides changing the regulatory genetic elements, the *hoxI*

gene was included in a hexacistronic operon (*hoxFUYHWI*), as it is the case in the native *C. necator hox* sequence (Fig. 4.1B). Two constructs were generated for plasmid - and genome-based expression (Fig. 4.1C) and transformed into *Syn_Δhox* [76][130] via electroporation and natural transformation, respectively. Colony PCR confirmed the presence of the plasmid in *Syn_P_{nrsB}CnSHp* and chromosomal integration of the complete gene cassette in *Syn_P_{nrsB}CnSHg* (Fig. S4.1).

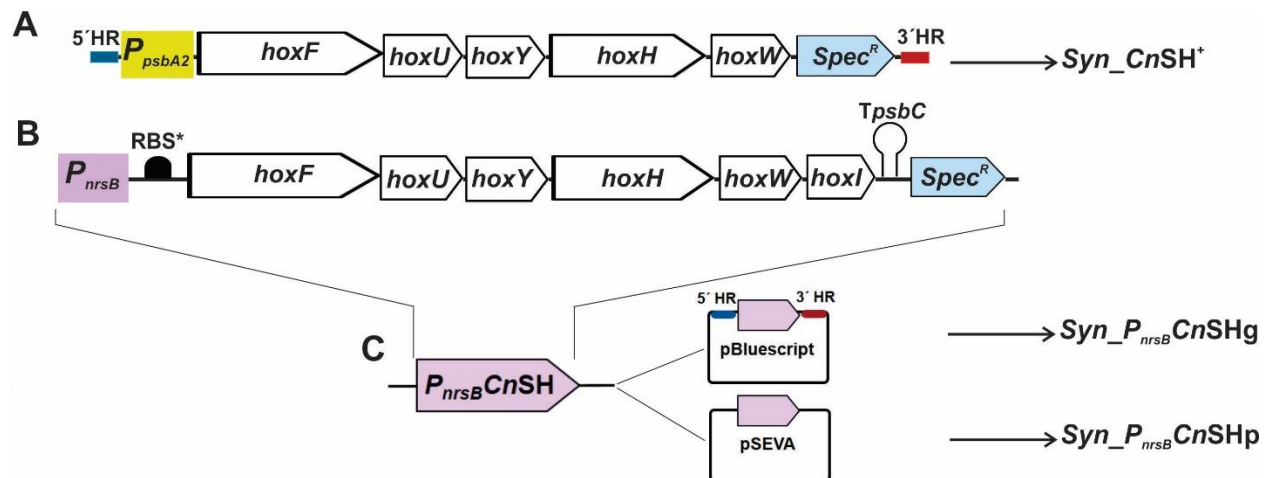


Figure 4.1. Comparison between *Syn_CnSH*⁺ and the newly designed nickel-inducible *CnSH* genetic setups in *Synechocystis*. (A) In *Syn_CnSH*⁺, the *CnSH* is encoded by a pentacistronic operon integrated in the genome under the control of the light inducible *psbA2* promoter. (B) In the newly designed *CnSH* expression system, the complete *CnSH* operon, including the *hoxI* gene, is enclosed by the nickel-inducible *nrsB* promoter, the synthetic RBS*, and the *psbC* terminator (*T_{psbC}*) from *Synechocystis*. (C) This system (*P_{nrsB}CnSH*) was assembled on the pBluescript II SK(+) vector for genome integration (*Syn_P_{nrsB}CnSHg*) and on the self-replicating pSEVA351 backbone (*Syn_P_{nrsB}CnSHp*). 5' and 3'HR: homologous regions; Spec^R: spectinomycin resistance.

4.2.2 Expression of *hox* genes from plasmid and genome with varying inducer concentration

In order to compare recombinant *CnSH* expression in *Syn_CnSH*⁺, *Syn_P_{nrsB}CnSHg*, and *Syn_P_{nrsB}CnSHp*, *CnSH* production and activity were systematically analyzed *in vitro* and *in vivo*. Cultures were supplemented with different NiSO₄ amounts to determine the optimal inducer concentration for *CnSH* production. First, synthesized *CnSH* levels were determined via Western blot analysis of soluble extracts derived from photosynthetically grown cells. For this purpose, we focused on [NiFe] harboring HoxH detected as a band at 55kDa (Fig. 4.2A).

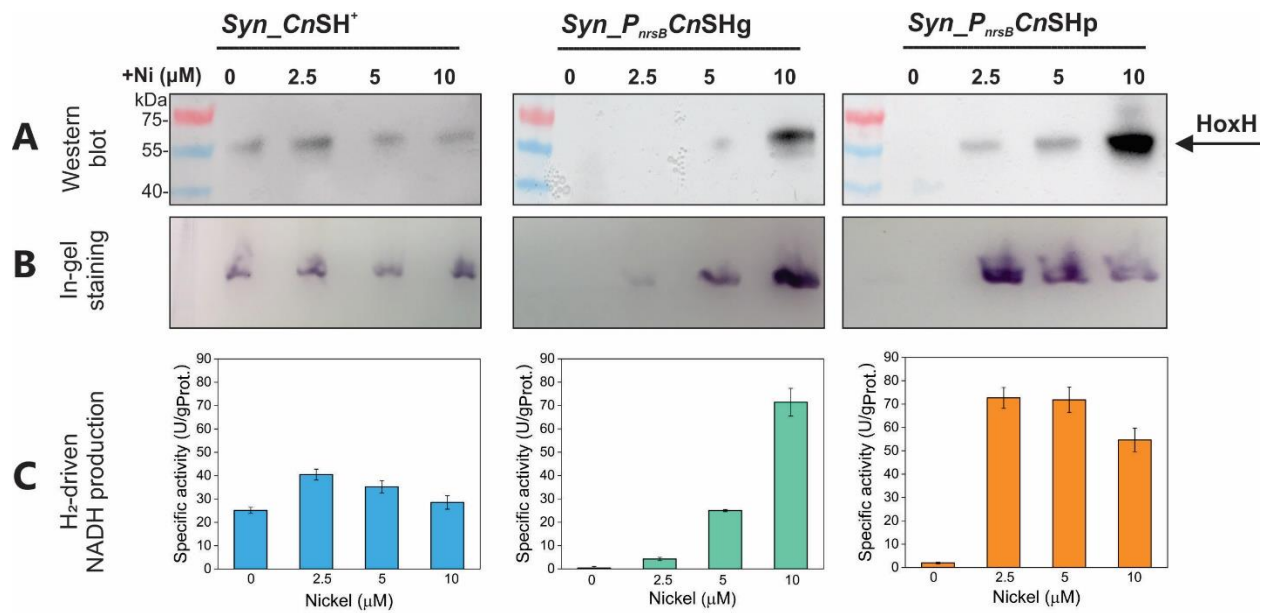


Figure 4.2. Expression levels and specific *CnSH* activities in cell extracts of the recombinant *Synechocystis* strains *Syn_CnSH⁺*, *Syn_P_{nrsB}CnSHg*, and *Syn_P_{nrsB}CnSHp* in response to different Ni²⁺ concentrations. All strains were grown photoautotrophically and treated with the given amounts of Ni²⁺. Cells were harvested 24 h after Ni²⁺ supplementation (A) HoxH (55kDa) detection via Western Blot analysis of soluble protein separated by SDS-PAGE. Standard SDS-PAGE with Coomassie-blue staining was conducted as loading control (Fig. S4.2) (B) In-gel activity staining to detect *CnSH* H₂-oxidising activity after native PAGE with soluble fractions. Activity staining relied on the coupling of *CnSH* H₂-based NADH formation to NADH-mediated reduction of NBT resulting in dark-colored bands. (C) Specific *CnSH* activity in soluble extracts quantified via NADH absorption in H₂ saturated buffer. Data represent means ± standard deviations (n = 3). As expected, no hydrogenase and respective activity were detected for the negative control *Syn_Δhox* (Fig. S4.3A-D).

As expected, HoxH abundance in *Syn_CnSH⁺* was not influenced by the applied Ni²⁺ concentration. By contrast, *Syn_P_{nrsB}CnSHg* and *Syn_P_{nrsB}CnSHp* showed increasing HoxH levels with increasing Ni²⁺ concentrations, reaching significantly higher HoxH levels than *Syn_CnSH⁺*. In agreement with literature data [226], plasmid-based expression led to a higher protein level than genome-based expression. In a second step, soluble cell extracts were analyzed via in-gel activity staining assays to estimate the abundance of functional *CnSH* complexes. While band intensities detected for *Syn_CnSH⁺* did not depend on the applied Ni²⁺ concentration, *Syn_P_{nrsB}CnSHg* extracts showed the strongest signal with 10 μM Ni²⁺, correlating with the highest HoxH abundance. Interestingly, plasmid-based expression resulted in an inverse correlation between HoxH level and in-gel activity, with the highest in-gel hydrogenase activity detected upon induction with 2.5 μM Ni²⁺ (Fig. 4.2B). Spectroscopic *in vitro* quantification of H₂-driven NADH production confirmed these results (Fig. 4.2C). *Syn_CnSH⁺* showed, with 40 U g_{Prot}⁻¹, a higher activity than previously determined [130], as a result of an optimized experimental

procedure (Chapter 2.8.1.2). With an activity around $70 \text{ U g}_{\text{Prot}}^{-1}$, optimally induced *Syn_P_{nrsB}CnSHp* and *Syn_P_{nrsB}CnSHg* extracts showed roughly a 1.8-fold higher activity than *Syn_CnSH⁺*.

4.2.3 Analysis of expression stability for plasmid- and genome-based systems

To evaluate *PnrsB*-based *CnSH* expression over time and respective differences for plasmid- and genome-based expression, we quantified HoxH, active *CnSH* levels, and specific H_2 oxidation activities within cells harvested 24, 48, and 72 h after induction with optimal Ni^{2+} concentrations. Western Blot analysis revealed decreased HoxH levels for the plasmid-based expression system, but an increase for *Syn_P_{nrsB}CnSHg* (Fig. 4.3A).

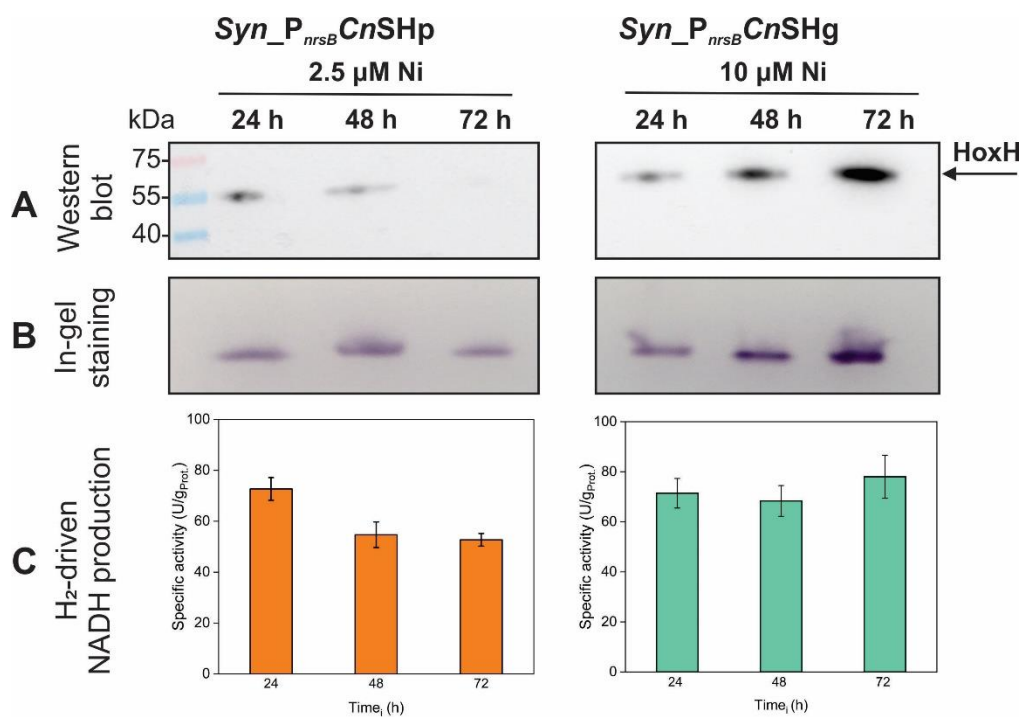


Figure 4.3. Time-dependent analysis of genome and plasmid-based *CnSH* gene expression after Ni^{2+} induction. *Syn_P_{nrsB}CnSHg* and *Syn_P_{nrsB}CnSHp* were compared regarding *CnSH* production and activity after 24, 48, and 72 h of induction via NiSO_4 addition. (A) Western Blot analysis for HoxH detection (55 kDa). Denaturing SDS-PAGE was run as loading control (Fig. S4.4). (B) In-gel staining assay to detect active *CnSH*. (C) Specific *CnSH* activity quantified by H_2 -derived NADH production. Data represent means \pm standard deviations (n = 3).

Additionally, *Syn_P_{nrsB}CnSHp* showed decreased active *CnSH* levels over time, as evidenced by in-gel activity staining and *in vitro* H_2 -based NADH formation activities, however, not as pronounced as visualized via Western blot analysis. *Syn_P_{nrsB}CnSHg* rather showed an increase indicating a more stable gene expression or higher protein stability enabling a maximum activity of roughly $80 \text{ U g}_{\text{Prot}}^{-1}$ detected 72 h after induction (Fig. 4.3B-C). As a possible reason, the

response of the Ni²⁺ efflux system of *Synechocystis* may lead to a decrease in intracellular metal concentration, especially affecting *Syn_P_{nrsB}CnSHp* with its lower Ni²⁺ concentration required for optimal induction. Further, plasmid-based expression may be affected by plasmid instability [230]. In conclusion, genome-based expression turned out to be the optimal choice, as it ensured high CnSH activity and expression stability.

4.2.4 Fate of H₂-derived electrons

Finally, CnSH activity was analyzed in living photosynthetically active cells. As discussed in our previous study [130], specific H₂ oxidation activities *in vivo* may be affected by the availability of electron source (H₂) and sinks (e.g. CO₂). Thus, the absence of CO₂ as sink for H₂-derived electrons may have limited H₂ oxidation activities, resulting in the observed decline in activity (**Fig. 4.4A, Fig. S4.5**). Indeed, CO₂ (10%) addition appeared to enhance and stabilize *in vivo* H₂ oxidation activities, especially in case of *Syn_P_{nrsB}CnSHg* and *Syn_P_{nrsB}CnSHp*, which retained 16-17 U g_{CDW}⁻¹ after 5 h (**Fig. 4.4B**). Nevertheless, these conditions resulted in pronounced O₂ evolution (up to 15%), a clear indication of boosted photosynthetic water oxidation, which along with H₂ oxidation, supplies additional electrons and may lead to a sink competition, i.e., CO₂ fixation via the CBB cycle. In order to avoid such competition, the cytochrome-b6f complex inhibitor dibromothymoquinone (DBMIB) was added to the cells to reduce the linear electrons flow. This led to initially low H₂ oxidation rates, which, after physiological adaptation, reached the same maximum as under standard condition and maintained it until the experiment was stopped after 6 h (**Fig. 4.4C**). This indicates a relief of the competition for CO₂ as electron sink and emphasizes that, *in vivo*, CnSH activity is subject to high levels of interaction with and dependency on cell physiology. In our previous study, we demonstrated that *Syn_CnSH*⁺ cells were able to grow on H₂ under illumination, when the PSII activity was inhibited by DCMU, basically relying on H₂ derived electrons for NADPH formation and on cyclic electron transport (CET) for ATP formation. We proposed 2 possible routes for electron transfer from NADH to NADP⁺: 1) via transhydrogenases (PntAB) or 2) via channeling into the ETC by the NDH-2 complex. Applying DBMIB in the presence of CO₂, H₂, and light, H₂-derived electrons can only be transferred to the CBB cycle via PntAB. Thus, high *in vivo* CnSH activities observed in the presence of DBMIB indicate that PntAB efficiently converts H₂-derived NADH to NADPH.

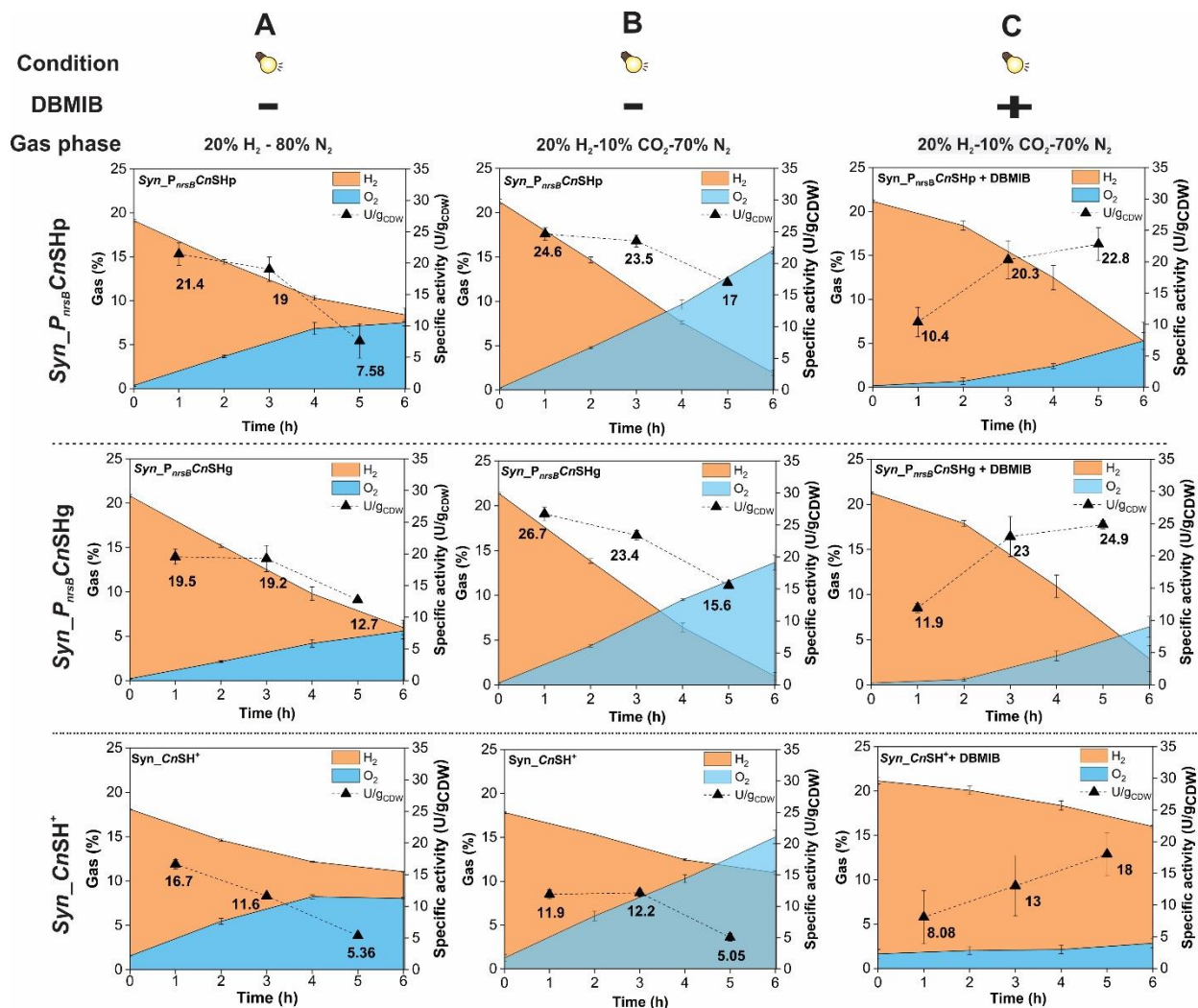


Figure 4.4. Physiological study of photosynthetically active cells containing CnSH. *Syn_CnSH⁺*, *Syn_P_{nrsB}CnSHg*, and *Syn_P_{nrsB}CnSHp* cells were incubated in sealed vials under illumination, 24 h after the addition of the optimal Ni²⁺ concentration for each strain (2.5 μM for *Syn_CnSH⁺* and *Syn_P_{nrsB}CnSHp* and 10 μM for *Syn_P_{nrsB}CnSHg*). In the experiments shown in column (A), the gas phase contained 20% H₂ and 80% N₂, whereas it contained 20% H₂, 10% CO₂ and 70% N₂ for columns (B) and (C). Experiments shown in column C were supplied with 20 μM of Dibromothymoquinone (DBMIB). Cells were incubated for 6 h in light, and the gas phase was analyzed via GC every 2 h to monitor H₂ and O₂ concentrations. *Syn_Δhox* and yBG11 medium were used as negative controls (Fig. S4.6). Data represent means ± standard deviations (n = 3).

4.2.5 *In vivo* fermentative H₂ production

H₂ production *in vivo* with CnSH in *Synechocystis* strictly depends on an elevated intracellular pool of NADH and elimination of major electron sinks, such as respiration. To evaluate the potential of the generated strains for H₂ formation, dark O₂-depleted and glucose-fueled fermentative conditions were applied. Whereas *Syn_CnSH⁺* and *Syn_P_{nrsB}CnSHp* produced 189-

200 $\mu\text{mol H}_2 \text{ g}_{\text{CDW}}^{-1}$ in 24 h, *Syn_P_{nrsB}CnSHg* doubled this amount to 384 $\mu\text{mol H}_2 \text{ g}_{\text{CDW}}^{-1}$, with a specific activity of 0.5 U $\text{g}_{\text{CDW}}^{-1}$ in the first 3 h (**Fig. 4.5A**). It is important to note that no substantial H_2 formation was detected under illumination even with glucose supplementation (data not shown). Thereby, the ETC, i.e., the NDH-2 complex, may outcompete *CnSH* as sink for fermentatively derived electrons. Indeed, DBMIB supply together with glucose in light enabled H_2 production by all strains with a maximum of 78 $\mu\text{mol H}_2 \text{ g}_{\text{CDW}}^{-1}$ produced in 24 h by *Syn_P_{nrsB}CnSHg*, which exhibited an initial activity of 0.15 U $\text{g}_{\text{CDW}}^{-1}$ (**Fig. 4.5B**). With DBMIB, blocking the ETC as well as respiration by means of *cyt_{b6}* inhibition, *CnSH*-catalyzed H_2 formation indeed was used to re-oxidize NADH as schematically depicted in **Fig. 4.5C**.

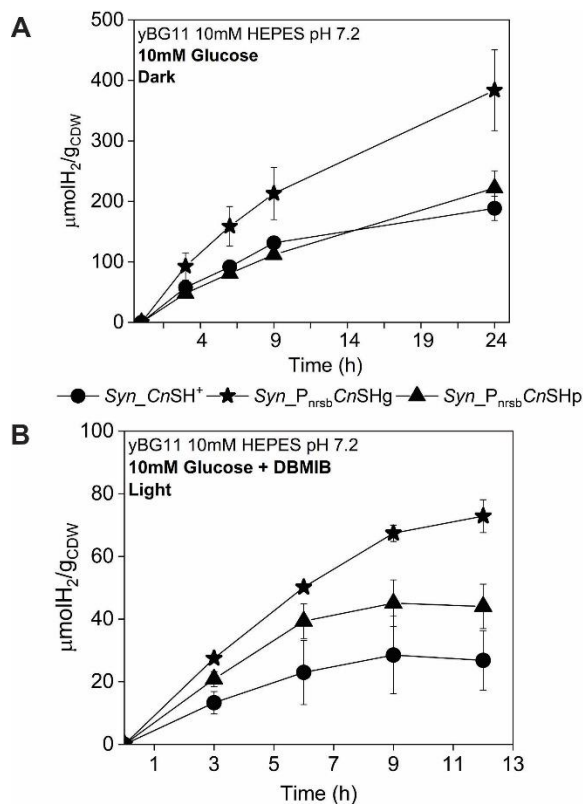
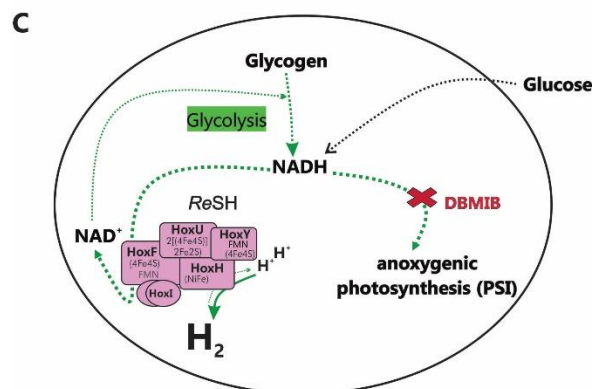


Figure 4.5. Fermentative H_2 production by recombinant *CnSH* in *Synechocystis* under anaerobic conditions. (A) Fermentative H_2 formation by *Syn_CnSH*⁺, *Syn_P_{nrsB}CnSHg*, and *Syn_P_{nrsB}CnSHg* upon anaerobic incubation in the dark with 10 mM glucose (N_2 saturated gas phase). **(B)** H_2 formation in light with 10 mM glucose and 20 μM DBMIB. Cultures were initially flushed with N_2 . Data represent means \pm standard deviations ($n = 3$). O_2 accumulation measured in parallel with H_2 formation is reported in **Table S4.1**. As expected, no H_2 production was detectable with *Syn_Δhox* (**Table S4.2**). **(C)** Simplified scheme of glycolysis derived-electrons fluxes under standard fermentative conditions with DBMIB blocking anoxygenic photosynthesis resulting in the redirection of electrons toward H_2 production.



4.3 Discussion

We recently described the first heterologous expression of a gene cassette of an oxygen-tolerant hydrogenase in a photoautotrophic organism. Specifically, we replaced the native H₂ase of *Synechocystis* with the soluble, O₂-tolerant [NiFe] hydrogenase from *C. necator* (*CnSH*). We could confirm O₂ tolerance and demonstrated the ability of the cells to use H₂-derived electrons for growth. Despite this success, the specific *CnSH* activity measured in cell-free extract of *C. necator* H16 and recombinant *E. coli* or *P. putida* was 4-200 times higher than that obtained with *Syn_CnSH*⁺ cell-free extract, as summarized in **Table 4.1** [93][128][137]. After technical and handling improvement in this study, an activity of 40 U g_{Prot}⁻¹ was reached with *Syn_CnSH*⁺.

Table 4.1. Specific H₂-oxidation activities of *CnSH* in soluble fractions of different host strains.

Strain		U g _{Prot} ⁻¹	Reference
<i>C. necator</i> H16	¹ CFE	800 – 8,000	Schneider and Schlegel, 1976 Schiffels <i>et al.</i> , 2013
<i>E. coli</i>	CFE	1,200	Schiffels <i>et al.</i> , 2013
<i>P. putida</i>	² PC	150	Lonsdale <i>et al.</i> , 2015
<i>Syn_CnSH</i> ⁺	CFE	18 –	Lupacchini <i>et al.</i> , 2021
		40	this work
<i>Syn_P_{nrsB}CnSHg</i>	CFE	80	This work

¹CFE: cell-free extract; ²Permeabilized cells

In the present study, we investigate whether the low *CnSH* activity detected in *Syn_CnSH*⁺ was caused by poor gene expression and/or physiological limitations. In this context, it is relevant to mention that a strong and stable recombinant gene expression in cyanobacteria still remains a challenge [64]. For this purpose, we developed a modular cloning system, similar to the recently reported CyanoGate [153]. By taking inspiration from the golden gate cloning strategy adapted for cyanobacteria, we designed a modified MoClo version to improve cloning efficiencies and fast screening of genetic elements. Previous studies indicated that expression levels are typically limited by slow transcription and translation, which are fundamentally controlled by the promoter and RBS elements, respectively [231]. Indeed, it was possible to improve heterologous *CnSH* production by means of regulatory elements such as the *nrsb* promoter, the synthetic RBS*, and the *psbC* terminator, also shown to be effective for *Synechocystis* metabolic engineering [232]. As compared to *Syn_CnSH*⁺, overall higher hydrogenase abundances and specific activities were detected for cell extracts of both *Syn_P_{nrsB}CnSH* strains featuring genome- or plasmid-based *Hox* operon expression. The *Syn_P_{nrsB}CnSH* strains differed regarding optimal Ni²⁺ concentration in

terms of final enzyme activity and long-term expression stability. With 10 μM Ni^{2+} , *Syn*_{*P*_{*nrsB*}*CnSHg* exhibited a 2-fold higher activity in cell extracts than *Syn*_{*CnSH*}⁺. This activity remained stable for 72 h post induction. In contrast, *Syn*_{*P*_{*nrsB*}*CnSHp* reached this activity already with 2.5 μM Ni^{2+} , but showed an activity decrease after 24 h post induction, which may be caused by low protein stability or by counter effects of the Ni^{2+} efflux system in *Synechocystis*. Further, we found that sink (CO_2) availability is crucial for the stabilization of *Syn*_{*CnSH*}-catalyzed H_2 oxidation during phototrophic growth (**Fig. 4A-B**). Whereas sink addition did not have a positive effect on *Syn*_{*CnSH*}⁺ activity and its stability, *Syn*_{*P*_{*nrsB*}*CnSHg* and *Syn*_{*P*_{*nrsB*}*CnSHp* showed a 3-fold higher average activity compared to *Syn*_{*CnSH*}⁺ after 5 h of incubation. It can be postulated that genome-based expression systems have an advantage in terms of stability and can generally be considered more suitable for metabolic engineering.}}}}

4.3.1 Routes for H_2 derived electrons in *Synechocystis*

Previously, we proposed two possible routes in *Synechocystis* for the transfer of electrons into NADH derived from *CnSH*-catalyzed H_2 oxidation via NADPH to cyanobacterial metabolism. Growth on H_2 as sole electron source, when PSII was blocked with DCMU, indicated that electron transfer from NADH to NADP^+ occurred, either via the transhydrogenase PntAB or NDH-2 and the ETC, with the resulting NADPH fueling the CBB cycle [130]. When blocking the ETC with the cytochrome b6f inhibitor DBMIB [233][234], the hydrogenase activity was comparable to that obtained without DBMIB after an adaptation phase (**Fig. 4.4C**). This indicates that transhydrogenases are the main pathway for electron transfer from NADH to NADP^+ under the conditions applied and that the competition with photosynthetically derived electrons under standard cultivations affected *CnSH*-catalyzed H_2 oxidation *in vivo*. We presume, therefore, that PntAB activity and cellular maintenance were supported by the protons motive force generated via PSII and cytochrome bd ubiquinol oxidase (Cyd) (**Fig. 4.6**) [194][235][236][195].

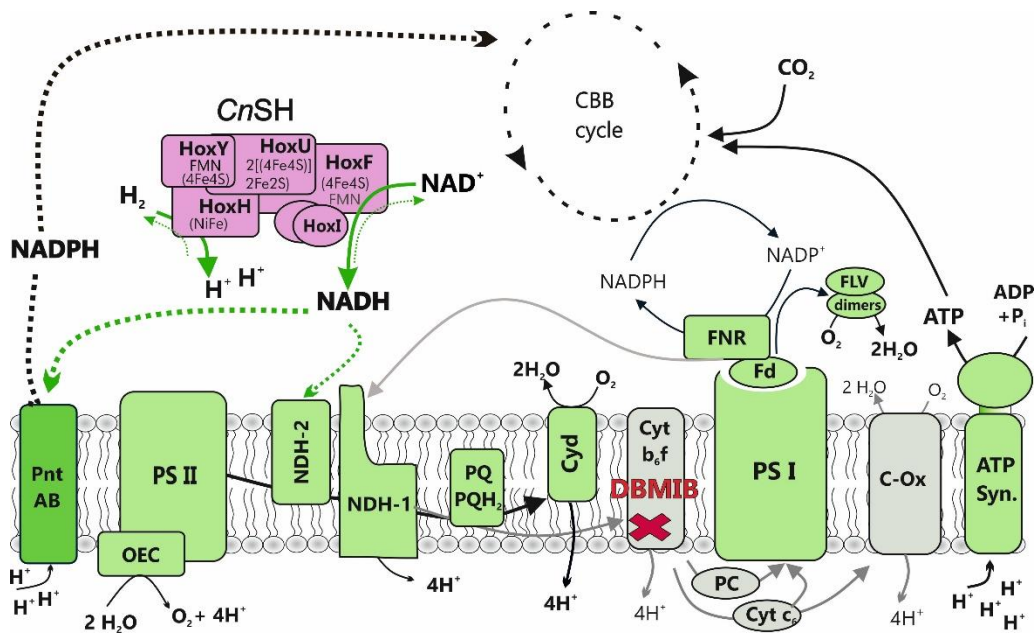


Figure 4.6. Schematic depiction of electron and proton routes in *Synechocystis* with an active *CnSH*. The scheme shows the transfer of reducing equivalents from H₂-derived NADH to the CBB cycle via NADPH. In the presence of 2,5-dibromo-6-isopropyl-3-methyl-1,4-benzoquinone (DBMIB), blocking electron transfer from ubiquinol (PQH₂) to the cytochrome b₆f complex (Cyt b₆f), the majority of electrons from NADH are transferred directly to NADP⁺ via the transhydrogenase PntAB (active fluxes and enzymes in green). Even though the electron transport chain (ETC) between PSII and PSI is blocked, reducing equivalents may enter the ETC through photosystem II (PSII) and type II NADH:quinone oxidoreductase (NDH-2) and be used by cytochrome bd ubiquinol oxidase (Cyd), to reduce O₂ to H₂O. The proton translocation in the lumen can be still established via PSII and Cyd. HoxHYUFI designate the *CnSH* subunits. PntAB, pyridine nucleotide transhydrogenase; PSII, photosystem II; (OEC), O₂-evolving center; PS I, photosystem I; NDH-1, NADPH-dehydrogenase (complex 1); PQ, plastoquinone; PC, plastocyanin; Cyt c₆: cytochrome c₆; C-Ox: cytochrome c oxidase; ATP syn.: ATP-synthase; Fd: ferredoxin; FNR: ferredoxin-NADP⁺ reductase.

Finally, we used the knowledge of these experiments to produce H₂. Besides dark fermentative H₂ production, all strains were able to form H₂ in light with glucose and DBMIB. The strict NAD(H)-dependency of the *CnSH* demands a reduced NAD(H) pool to enable H₂ production. NADH derived from glycolysis typically flows into the respiratory electron transport chain mainly via the NDH-2 complex [237]. Closing this electron path with DBMIB obviously led to H₂ formation to recycle NAD⁺ under illumination in yBG11 medium. Our results illustrate that the respiratory chain is the main competitor of *CnSH* for NADH under the conditions applied. Interestingly, under both conditions (dark fermentative and light + DBMIB), *Syn_P_{nrsB}CnSHg* produced up to 2 times more H₂ than *Syn_CnSH⁺*. This indicates again higher and more stable *CnSH* synthesis as a result of using the advanced expression system.

4.3.2 Future bottlenecks to be tackled

Overall, the prolonged activity in addition to higher amount of protein synthesized, raised the question if the presence of HoxI in *Syn_P_{nrsB}CnSHg* and *Syn_P_{nrsB}CnSHp* stabilized the enzyme complex and consequently influenced hydrogenase activity. The limited literature data didn't show a real influence in the H₂ driven NADH formation in *C. necator* [88]. The knowledge about this homodimeric subunit is poor and additional studies need to be performed to unravel the role of HoxI in its native host but also in *Synechocystis*. One possible issue in the functional recombinant expression of this multicomponent enzyme is its complex maturation. The *CnSH* maturation apparatus is encoded by the *hypABCDEFX* operon. At least the first 6 maturases are known to be essential for the proper assembly of the [NiFe] center in HoxH, while HypX has a crucial role for CO insertion under aerobic condition [119] [124]. Several studies reported the functional *CnSH* expression in various *E. coli* strains. Interestingly, they differed on whether or not it was necessary to co-express the specific *C. necator* maturation apparatus to achieve a functional recombinant enzyme. Despite the need for further research, key differences among these studies include the genetic background of the host strains, growth conditions applied, and the fine tuning between exogenous hydrogenase synthesis and maturation [128][129][126][127]. Surprisingly, the maturation apparatus of *Synechocystis* was sufficient to produce functional *CnSH* in *Synechocystis*, without hampering its O₂ tolerance and its H₂ oxidation activity. Nevertheless, the lack of *C. necator* maturases may be a reason for the lower specific *CnSH* activity established in *Synechocystis* compared to heterotrophic host strains (**Table 4.1**) [176]. The absence of its native maturases also may explain why *Syn_P_{nrsB}CnSHp* induced with 10 μM Ni²⁺ exhibited the highest protein abundance (based on Western blot analysis), but lowest specific activity within respective cell extracts (**Fig. 4.2**). This indicates the distinct presence of non-functional hydrogenase, in particular upon elevated plasmid-based gene expression relying on the higher gene copy number and strong induction. Thus, it will be interesting to introduce the maturation system of *C. necator* into *Synechocystis* and test its effect on *CnSH* expression level and activity.

4.4 Conclusion

The expression of the *Cn_hox* operon was optimized by adopting an efficient cloning strategy. This enabled a significant increase in *CnSH* expression levels and specific activities in *Synechocystis*, with genome-based expression relied on a Ni²⁺-inducible promoter and the synthetic RBS* enabling the highest activity and stability *in vitro* and *in vivo*. Even though the electron sink availability during phototrophic growth limited long term *CnSH*-based H₂ oxidation activity, hydrogenase activities in *Syn_P_{nrsB}CnSHp* and *Syn_P_{nrsB}CnSHg* were stabilized up to

several hours, strongly enhanced compared to *Syn_CnSH*⁺. We further found that, transhydrogenases also play a major role for the electron transfer from H₂-derived NADH to NADP⁺, finally enabling autotrophic growth with H₂ as sole electron donor. H₂ production with *CnSH* in *Synechocystis* depends on a strongly reduced NAD(H) pool and is limited by competing NADH-dependent pathways. However, with *CnSH* in *Synechocystis*, higher H₂ production was obtained compared to the WT strain with the native hydrogenase [130] under dark fermentative conditions, indicating a high protein abundance. Future studies are needed to investigate, whether insufficient maturation of *CnSH* limits its performance in *Synechocystis* and, for H₂ formation via direct biophotolysis, to engineer the cofactor dependency of this enzyme, with NADPH or reduced ferredoxins as promising electron donors.

Chapter 5

Co-expression of auxiliary and structural *Cupriavidus necator* genes enhances and stabilizes O₂-tolerant hydrogenase activity in *Synechocystis*

Sara Lupacchini, Ron Stauder, Franz Opel, Stephan Klähn, Bruno Bühler, Jörg Toepel

Author Contributions:

Sara Lupacchini (conceptualization, investigation, writing, original draft preparation), Ron Stauder (investigation, reviewing), Franz Opel (reviewing), Stephan Klähn (conceptualization, reviewing and editing) Bruno Bühler (conceptualization, supervision, reviewing and editing), Jörg Toepel (conceptualization, investigation, writing, original draft preparation).

This chapter is in preparation for submission as research article.

The Supplementary Material can be found in the Appendix Section 5.

Abstract

Oxygen-tolerant [NiFe] hydrogenases have the potential to be applied as biotechnological tools in phototrophic organisms due to their ability to cope with aerobic conditions. This makes them suitable for either generating photosynthetic H₂ or for fueling (O₂-dependent) redox reactions with reduction equivalents. We have previously introduced the soluble O₂-tolerant hydrogenase from *Cupriavidus necator* (HoxFUYHI = CnSH) into *Synechocystis* sp. PCC 6803 and improved its heterologous expression system. However, high enzyme levels did not fully translate into activities. In this study, we aimed at optimizing post-translational CnSH processing by co-expression of *hyp* genes encoding maturation factors of *C. necator*. For this purpose, we designed different expression systems to modulate *hyp* and *hox* operon expression. We additionally investigated the function of HypX, a maturase without a homolog in *Synechosystis*, which is involved in [NiFe] center maturation under aerobic conditions. Our results clearly show that a fine balance between heterologous hydrogenase and maturase synthesis is needed to ensure high specific activity over an extended time period and avoid extensive metabolic burden. Further, we optimized reaction conditions to maintain high and stable H₂ oxidation activity in photosynthetically active cells. The rates obtained are comparable with those achieved for other redox enzymes introduced into photosynthetic organisms.

5.1. Introduction

In nature, redox reactions play crucial roles in various biological routes, including photosynthesis and respiration, the two central processes fueling life on earth. Metal ion cofactors such as Fe-S clusters thereby constitute key elements in respective electron transfer processes. One of the most ancient group of complex Fe-S enzymes are the majority of hydrogenases [238], which play a key role in the hydrogen metabolism of archaea, bacteria, and lower eukarya [239]. Three classes of hydrogenase are defined according to the metal ions in their active site: [NiFe]-, [FeFe]-, and Fe-hydrogenases, while the latter represent Fe-S cluster-free enzymes [85] [80]. [NiFe] and [FeFe] hydrogenases catalyze the reversible transfer of electrons among H₂ and redox cofactors, primarily to fuel the cellular metabolism with H₂-derived reduction equivalents. On the other hand, H₂ evolution is used to dispose excess electrons [86]. In their reduced state, transition metals constitute targets for O₂-mediated oxidation, which leads to irreversible or reversible enzyme inactivation as it is the case for [FeFe]- or [NiFe]-hydrogenases, respectively. However, several [NiFe] hydrogenases are considered to be O₂-tolerant, enabling H₂ cycling under aerobic conditions [99] [106]. Even though [FeFe] and [NiFe] hydrogenases constitute phylogenetically distinct enzyme classes, they share some common features: 1) a chain of Fe-S clusters enabling electron transfer between the buried active site and the protein surface [131], 2) CO- and CN-ligands complexing the low-spin Fe center, and 3) the requirement of multiple accessory proteins for the assembly of the 2 metal ions with their ligands and their integration into the apo-protein [240][82]. Contrary to Fe-only hydrogenases, which are assembled under completely anaerobic conditions involving only 3 maturases, [NiFe] hydrogenase assembly, which in some cases even occurs under aerobic conditions, requires at least 6 auxiliary proteins [176][81]. [NiFe] hydrogenases, with their potential for applications under aerobic conditions, are heterodimeric with at least one large subunit (about 60 kDa) hosting the bimetallic active center and one small subunit (about 30 kDa) harboring an electron relay containing 1 to 3 Fe-S clusters. The nickel is coordinated with 4 cysteine-derived thiolates, of which 2 also coordinate to the iron atom, which further features a CO and 2 CN ligands [241]. Six maturases (termed HypABCDEF) are necessary for the formation of the [[NiFe](CN)₂(CO)] cofactor and its post-translational incorporation into the apo-protein. Auxiliary proteins generally play crucial roles in transition metals, avoiding undirected withdrawal by metal-binding complexes in the cell. Further, heavy metals together with CO- and CN-ligands are potentially toxic for microorganisms necessitating the action of shuttle and chaperone systems inside the cells [240]. The current model of intracellular [NiFe] cluster assembly includes the biogenesis of CO- and CN-ligands, {Fe(CO)(CN)₂} complex formation, and Ni²⁺ insertion as consecutive steps. The 2 CN-ligands are synthesized from carbamoyl phosphate

(an intermediate of the urea cycle) by HypF and HypE. Detailed knowledge on CO biosynthesis is restricted to aerobic conditions, under which the additional maturase HypX synthesizes CO from Formyl-THF via a formyl-CoA intermediate [120][119]. Subsequently, the HypCD complex acts as a scaffold for Fe(CO)(CN)₂ assembly and its integration into the apo-form of the large subunit. Then, the chaperons HypA and HypB coordinate Ni²⁺ insertion, and, eventually, the large subunit undergoes HoxW-catalyzed endoproteolytic cleavage releasing a C-terminal extension at HoxH and thereby inducing protein folding and the final assembly with the small subunit [114] [242][124]. Soluble O₂-tolerant [NiFe] hydrogenases are attractive in two ways: 1) for H₂ production fueled by the photosynthetic light reaction [185] and 2) for H₂-driven cofactor regeneration under oxic conditions as required, e.g., for oxygenases [243]. These purposes demand efficient expression strategies enabling high level synthesis of highly active enzymes in target hosts. High specificity of maturation systems for corresponding hydrogenases limits the host choice to closely related organisms, carrying hydrogenases of the same type. Thus, recombinant expression typically results in low specific activities, if the maturation system is not expressed together with the structural genes [176]. *Cupriavidus necator* (hereafter *C. necator*) features several O₂-tolerant [NiFe] hydrogenases, which have successfully been expressed in heterotrophic and more recently also phototrophic organisms [126][127][128][129][130]. Interestingly, introduction of the *C. necator* maturation apparatus was not in all cases necessary to achieve functional expression. Key differences among these studies include the genetic background of the host strains, growth conditions applied, and the fine-tuning of recombinant expression of multi-gene operons (Chapter 4). We recently reported the functional production of the soluble O₂-tolerant *C. necator* hydrogenase (*CnSH*) in the model cyanobacterium *Synechocystis* sp. PCC 6803 (hereafter *Synechocystis*), in which the native hydrogenase was knocked out (*Syn_CnSH*⁺). No *CnSH* maturation genes were co-expressed except for *hoxW* encoding an endopeptidase specific for HoxH. Obviously, hydrogenase maturation factors of *Synechocystis* to some extent can take over the role of *C. necator* maturases and process HoxH under aerobic condition [243]. This is in agreement with previous studies, showing that gene expression and maturation of the native *Synechocystis* hydrogenase (*SynSH*) does not depend on anoxia [75]. However, the specific *CnSH* activity in cell-free extract of *Syn_CnSH*⁺ was 4-200 times lower than those reported for *C. necator* and recombinant *E. coli* or *P. putida* (with *C. necator* genes encoding auxiliary proteins co-expressed). As hydrogenase activity in *Syn_CnSH*⁺ was limited by low enzyme abundance, *Cn_hox* operon expression was optimized via Golden Gate-type cloning, which resulted in *Syn_P_{nrsB}CnSH* strains relying on a Ni²⁺-inducible promoter and a strong synthetic RBS*. This enabled higher and more stable hydrogenase activities *in vitro*

(80 U g_{Prot}⁻¹) and *in vivo* (27 U g_{CDW}⁻¹). However, obtained activity increases did not correlate with the clearly more prominent increase in expression levels indicating that a large hydrogenase fraction was not active in the recombinant host (Chapter 4). We hypothesize that this discrepancy can be alleviated by co-expression of *C. necator* maturase genes in *Synechocystis*. The presence of the additional maturase HypX in *C. necator*, involved in CO biosynthesis under aerobic conditions, constitutes a main difference among *Synechocystis* and *C. necator* maturation systems [120]. In this study, we investigated if the specific activity of CnSH in *Syn_P_{nrsB}CnSH* strain can be enhanced by co-expressing the complete gene set for *C. necator* auxiliary proteins or just *hypX* alone.

5.2. Results and Discussion

5.2.1. Strain development and transcript analysis of *Cn_hyp* genes

To assess the influence of the Hyp proteins from *C. necator* on functional CnSH production in *Synechocystis*, we transformed *Syn_P_{nrsB}CnSHg*, carrying the CnSH genes on its genome, with a replicative plasmid carrying the corresponding accessory genes *hypABFCDEFX*. We made use of the synthetic construct from Opel *et al.*, 2023, in which each gene represents a separate translational unit with the synthetic ribosomal binding site, RBS* [227], placed upstream of every gene for efficient translation initiation. Furthermore, coding sequences were codon-usage optimized for translation in *Synechocystis*, and a Strep-tag sequence was fused to the last gene of the *hyp* operon, *hypX*, to facilitate protein detection [244]. The amplified *hyp* operon was implemented in the MoClo library (Chapter 4) to be further combined with different regulatory elements and generate diverse expression systems. We selected three different promoters: the L-rhamnose-inducible promoter *P_{rhaBAD}* from *E. coli* [224], the Ni²⁺-dependent *P_{nrsB}*, and the strong photosystem II promoter *P_{psbA2}* from *Synechocystis* [220][186]. Utilization of the Ni²⁺-inducible system for both *hox* and *hyp* genes aimed at similar expression strengths and induction times, but prevents separate regulation of the two operons, whereas induction via rhamnose allows separately tunable expression and *P_{psbA2}*, constitutive light-regulated expression. Each operon was combined with a transcriptional terminator at the 3' end. For the rhamnose inducible system, the regulatory *rhaS* cassette was placed after the terminator [224]. The constructs were assembled on the pSEVA351 vector, suitable for replication in *Synechocystis* [154]. The resulting plasmids *pP_{nrsB}CnHyp*, *pP_{rhaBAD}CnHyp*, and *pP_{psbA2}CnHyp* were used to transform *Syn_P_{nrsB}CnSHg* (**Fig. 5.1A**). Plasmid presence was verified in all obtained clones (**Fig. 5.1B**).

levels, qRT-PCR was performed. In the presence of the entire *hyp* operon, we targeted the first *hypA* and the last *hypX* gene (data not shown for *hypX*) in order to assess differences in transcript abundance as a result of the distance from the promoter (**Fig. 5.1CD**). Induction with Ni²⁺ and rhamnose significantly enhanced *hypA* transcript levels 24 h after induction compared to non-induced strains (**Fig. 5.1C**). Whereas a 14-18-fold increase in *hypA* transcript levels was reached with both 0.1 mM and 2 mM of rhamnose, Ni²⁺-induction effected a 6-fold increase (**Fig. 5.1D**). *Syn_P_{nrsB}CnSHg* + *pP_{psbA2}CnHyp* reveals lower transcript levels than the other two strains and no significant changes in the relative transcript levels after 24 h. By contrast, *hypX* transcript levels did not change or even decreased upon induction irrespective of the expression systems used. This result may reflect a negative correlation between transcription efficiency and distance to the promoter and may be due to low RNA stability. Therefore, to assess if *hypX* was at least transcribed we performed reverse transcriptase (RT)-PCR. The reversely transcribed complementary DNA (cDNA) was detected for every strain containing *Cn_hyp* operon, even without gene induction (**Fig.S5.1**). From *hypA* transcript analysis, we can observe background expression for both inducible systems, even prior inducers addition. The leaky activity of *P_{rhaBAD}*, as previously suggested, may be due to the strong promoter *Pj119* driving *rhaS* expression. The level of RhaS determines *rhaBAD* promoter activity [245]. As *Cn_HypX* doesn't have a homolog in *Synechocystis*, we aimed to assess, if its role as CoA-dependent formyl-tetrahydrofolate (THF) decarboxylase can support the maturation of the NiFe(CN)₂CO cofactor during aerobic growth [120] (oxygenic photosynthesis), a condition in which the CO availability becomes limiting [246]. Recombinant expression of *Cn_hypX* has been reported to support *CnSH* maturation in *E. coli* under aerobic conditions [128]. Thus, *Syn_P_{nrsB}CnSHg* was transformed with replicative plasmids carrying *hypX* only under the control of *P_{nrsB}* or *P_{rhaBAD}*, resulting in strains carrying *pP_{nrsB}CnHypX* or *pP_{rhaBAD}CnHypX* (**Fig. S5.2A**). Transcription of *hypX* was confirmed via qRT-PCR for both constructs (**Fig. S5.2B**). However, the protein again could not be detected via Western Blot targeting the C-terminally fused StrepTag (data not shown).

5.2.2. Impact of the *Cn_hyp* operon expression on growth and on the specific *Syn_CnSH* activity

In *Synechocystis* containing both the *hox* and *hyp* operons of *C. necator*, 13 recombinant genes are potentially expressed, whereby the synthesis/degradation of encoded proteins may present a high metabolic burden for the cells and consequently influence their growth behavior [247]. Thus, we analyzed whether heterologous *hox* and *hyp* expression affected phototrophic *Synechocystis* growth (**Fig. 5.2AB**). Overall, *Syn_P_{nrsB}CnSHg* grew faster than plasmid-containing strains, also in the absence of Ni²⁺ (complete overview of strains grown without and with *hox* and *hyp* induction

are given in **Fig. S5.3**). Besides a minor effect on growth observed for $pP_{psbA2}CnHyp$ (**Fig. 5.2A**), the double induction of *hox* (Ni^{2+}) and *hyp* (2mM Rha) operon in *Syn_P_{nrsB}CnSHg* carrying $pP_{rhaBAD}CnHyp$ led to 20% reduced cell density (**Fig. 5.2B**). This growth phenotype suggests that the *hyp* operon expression together with the *hox* genes force the cells to allocate a significant amount of resources to maturase and hydrogenase synthesis [247]. Further, we investigated if recombinant *hyp* gene expression increased active *CnSH* formation in *Synechocystis*, using the soluble protein extracts to determine specific H_2 ase activities *in vitro* via H_2 -driven NADH formation (**Fig. 5.2C**).

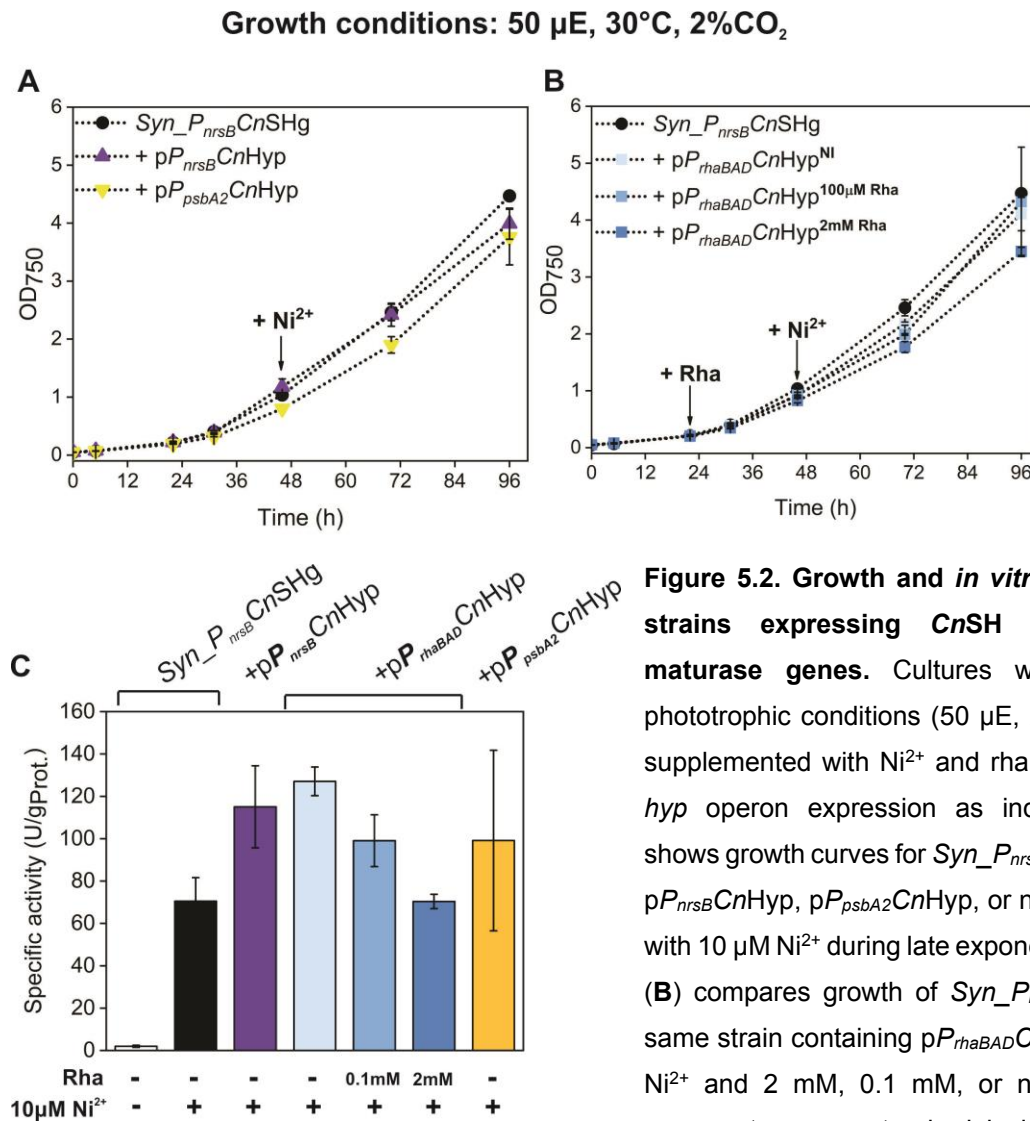


Figure 5.2. Growth and *in vitro* H₂ oxidation by strains expressing *CnSH* and *C. necator* maturase genes. Cultures were grown under phototrophic conditions (50 μ E, 2% CO₂) and were supplemented with Ni^{2+} and rhamnose for *hox* and *hyp* operon expression as indicated. Panel (A) shows growth curves for *Syn_P_{nrsB}CnSHg* containing $pP_{nrsB}CnHyp$, $pP_{psbA2}CnHyp$, or no plasmid provided with 10 μ M Ni^{2+} during late exponential growth. Panel (B) compares growth of *Syn_P_{nrsB}CnSHg* with the same strain containing $pP_{rhaBAD}CnHyp$ provided with Ni^{2+} and 2 mM, 0.1 mM, or no rhamnose. Data represent means \pm standard deviations ($n = 2$). Panel (C) shows specific *CnSH* activities of soluble protein extracts of each strain harvested after the 96 h growth histories shown in panels A and B. Given are mean values and standard deviations ($n=3$).

To this end, photoautotrophically grown *Syn_P_{nrsB}CnSHg* cells containing *pP_{nrsB}CnHyp*, *pP_{rhaBAD}CnHyp*, *pP_{psbA2}CnHyp*, or no plasmid were treated as shown in **Fig. 5.2AB**. Depending on the regulatory system and induction strength used for expression, *hyp* gene expression indeed resulted in higher *CnSH* activity. Specifically, this was the case for strains carrying *pP_{nrsB}CnHyp* and *pP_{rhaBAD}CnHyp* during non-induced (leaky) *hyp* operon expression and at low level of induction with rhamnose (0.1 mM). The latter case resulted in a 60% increase in *CnSH* activity, whereas this positive effect was abolished applying 2 mM rhamnose. The strain carrying *pP_{psbA2}CnHyp* showed a highly variable *CnSH* activity, indicating a growth phase dependent gene expression. Overall, we can conclude that expression of the entire *C. necator* maturase operon promotes functional *CnSH* synthesis in *Synechocystis*. Interestingly, continuous expression or strong induction of the *hyp* operon in combination with the *hox* operon, i.e., in strains containing *pP_{psbA2}CnHyp* or *pP_{rhaBAD}CnHyp* induced with 2 mM rhamnose, respectively, slightly affected growth and resulted in a weak or no positive effect on *CnSH* activities. Co-expression of *hypX* with the *hox* operon during oxygenic photosynthesis in *Synechocystis* didn't result in higher *CnSH* activity neither *in vitro* nor *in vivo* (**Fig. S5.2CD**).

5.2.3 *In vivo* H₂ consumption

As a next step, we set out to evaluate, if the higher *in vitro* activities obtained upon *C. necator hox* and *hyp* gene co-expression reflects in higher H₂ oxidation activities *in vivo*. Previously, we showed that *CnSH* is able to sustain autotrophic *Synechocystis* growth via NADH supplied by *CnSH*-mediated H₂ oxidation [130]. Specific *CnSH* activity and stability *in vivo* relied mainly on three factors: firstly, the amount of functional *CnSH* complexes and the availability of substrate (H₂) and electron sinks able to recycle NAD⁺. In order to characterize the *CnSH* activity *in vivo* and compare it to the active protein level in the cells, a specific setup was established to avoid H₂ and sink limitation. Initially, 5 mL cell culture was transferred into sealed 10 mL vials, followed by flushing with a defined gas mixture (20% H₂, 10% CO₂, 70% N₂) and incubation under light for 6 h. With this setup, *Syn_P_{nrsB}CnSHg* showed an initial activity of 28 U g_{CDW}⁻¹ followed by a rapid decrease to 15 U g_{CDW}⁻¹ between 4 and 6 h, which was mainly due to H₂ and CO₂ depletion (**Fig. 5.3A**). The latter (depletion of 10% CO₂) was estimated based on formed O₂ (according to the redox balance, 1.2 moles O₂ formation can be expected for the fixation of 1 mole CO₂ also considering the demand for NO₃ reduction), as O₂ had accumulated to 9% after 4 h and H₂ had been consumed as well, generating additional reducing power. This indicated that a highly reduced NAD(H) pool constrained *CnSH* activity.

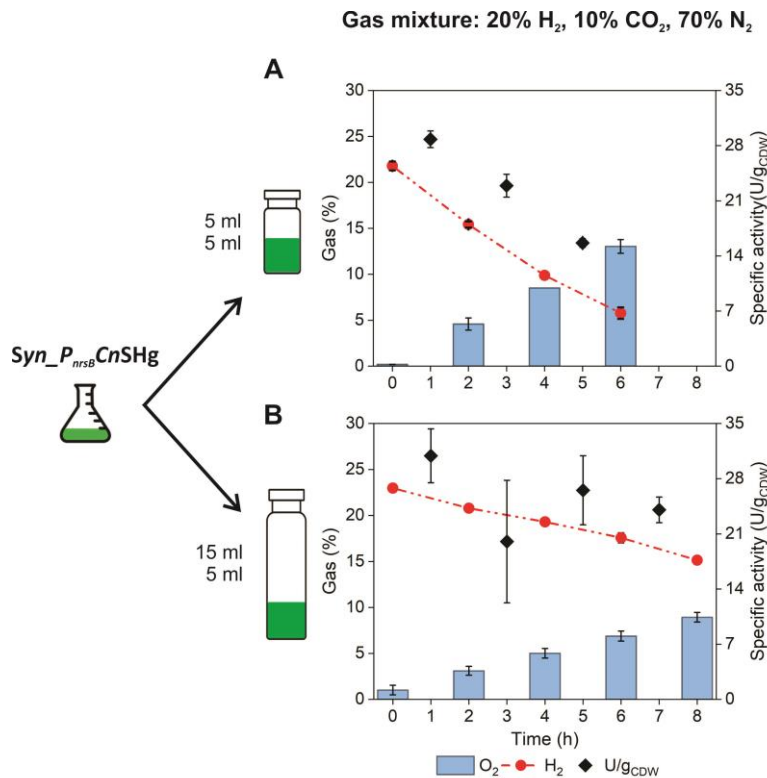


Figure 5.3. *In vivo* H₂ consumption by *Syn_P_{nrsB}CnSHg*. Five ml cell culture were transferred into (A) 10 ml or (B) 20 ml gas-tight vials, which were flushed with a gas mixture composed of 20% H₂, 10% CO₂, and 70% N₂ and incubated under illumination. Gas concentrations were measured via GC and activities were calculated from H₂ consumption as described in Chapter 2.8.2.1. Mean values and standard deviations (n=3) are given.

Hence, we tested 20 mL glass vials containing 5 mL cell culture and 15 mL gas phase, which increased the gas reservoir and also the interfacial area enabling enhanced mass transfer. With this setup not being constrained by H₂ and CO₂ availability, indeed higher maximal (32 U g_{CDW}⁻¹) and average (25 U g_{CDW}⁻¹ for 8 h) activities were obtained for H₂ oxidation by *Syn_P_{nrsB}CnSHg* (Fig. 5.3B). Considering that different studies reported a growth-dependence of product yields with transgenic cyanobacteria during batch cultivation [248], we performed a comparative analysis on changes in H₂ oxidation activities of cells induced in the late exponential and linear growth phases. Induction in the late linear phase resulted in a higher H₂ oxidation activity (Fig. S5.4), indicating some degree of growth phase dependency. Under optimized conditions, *Syn_P_{nrsB}CnSHg* containing *p_{nrsB}CnHyp*, *p_{rhaBAD}CnHyp* with no or low (0.1 mM rhamnose) induction, or *p_{psbA2}CnHyp* exhibited higher H₂ oxidation activities over a longer time period compared to *Syn_P_{nrsB}CnSHg* (Fig. 5.4). Remarkably, 46 U g_{CDW}⁻¹ were measured for *Syn_P_{nrsB}CnSHg* containing *p_{rhaBAD}CnHyp* induced with 0.1 mM rhamnose, which comes close to the activity determined *in vitro* assuming that 50% of the cell dry mass is protein (92 vs 98 U

$g_{\text{protein}^{-1}}$) [249]. Again, induction of *hyp* operon expression with 2 mM rhamnose resulted in a lower H_2 oxidation activity than without *hyp* genes from *C. necator*.

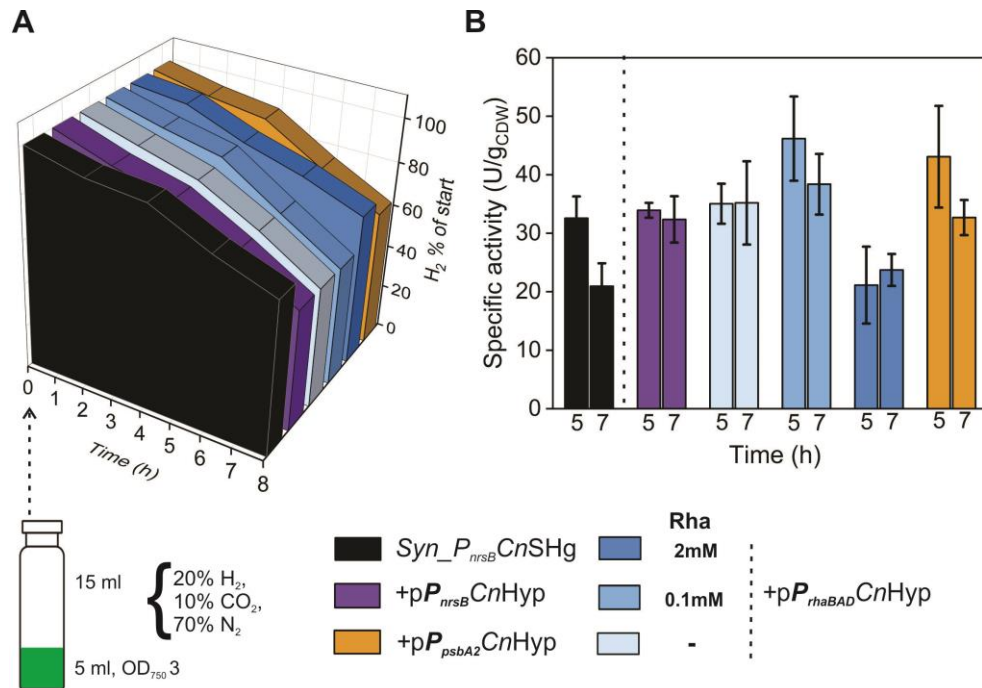


Figure 5.4. *In vivo* H_2 consumption by $Syn_P_{nrsB}\text{-}CnSHg$ co-expressing *C. necator* maturase genes. 24 h prior to the assay $10\mu\text{M Ni}^{2+}$ was supplemented to each strains. We used cell suspension with an OD₇₅₀ of 4-5, and diluted with fresh yBG11 medium to an optical density of 3. After an equilibration time of 4 h, we measured H_2 and O_2 concentrations (Fig. S5.5A) to determine H_2 ase activity over 4 h. The identical OD allowed us to directly calculate H_2 consumption activity out of the H_2 concentration. Five mL cell culture from each strain were transferred into 20 ml gas-tight vials, flushed with 20% H_2 , 10% CO_2 , and 70% N_2 , and incubated for 8 h under illumination. Panel (A) shows H_2 concentrations as percent fractions of the starting concentrations and panel (B) the specific H_2 oxidation activities for the time periods between 4-6 h and 6-8 h. Sterile yBG11 medium and uninduced $Syn_P_{nrsB}\text{-}CnSHg$ were used as negative controls (Fig. S5.5BC). Mean values and standard deviations ($n=3$) are given.

In conclusion, the beneficial effects of *C. necator* maturases on the Syn_CnSH activity also was found *in vivo*, with the same trend as observed *in vitro*, i.e., high level induction *C. necator hyp* gene expression rather had a negative effect on active $CnSH$ levels as well as cell physiology (see above). Thereby, the heterologous maturases may interfere with the endogenous $SynHyp$ proteins, which are known to be expressed constitutively [75]. This is in line with a recent study, showing that H_2 production in *E. coli* was completely repressed under conditions for high expression of $CnSH$ under the control of a strong promoter [127]. Further, *Synechocystis* does not contain a *hypX* gene. Thus, CO synthesis from the C1 metabolism by recombinant HypX may interfere with the cell physiology [120]. As an alternative to the expression of the entire *hyp* operon, introducing a subset of *C. necator* maturases may help to investigate, which auxiliary

proteins are most relevant for *CnSH* maturation and if recombinant and endogenous maturases interfere in *Synechocystis* [128] [126].

5.2.4 *In vivo* H₂ production

Finally, cells also were tested regarding fermentative H₂ production. All *Syn_P_{nrsB}CnSHg* strains containing *C. necator* maturases showed glucose-dependent H₂ production under illumination. Thereby, the cytochrome-b6f complex inhibitor dibromothymoquinone (DBMIB) was essential during incubation in light, in order to eliminate competition for the electrons by NAD(P)H dehydrogenase-like complex II proteins in the photosynthetic and respiratory electron transport chains [250] (Chapter 4.2.5). The strain containing *pP_{rhaBAD}CnHyp*, both without and with induction with 0.1 mM rhamnose, showed the highest initial activity (first 2 h, **Fig.5.5 insert**), twice as high as *Syn_P_{nrsB}CnSHg*, indicating once more the presence of a higher amount of active *CnSH* with the *C. necator* maturase genes co-expressed.

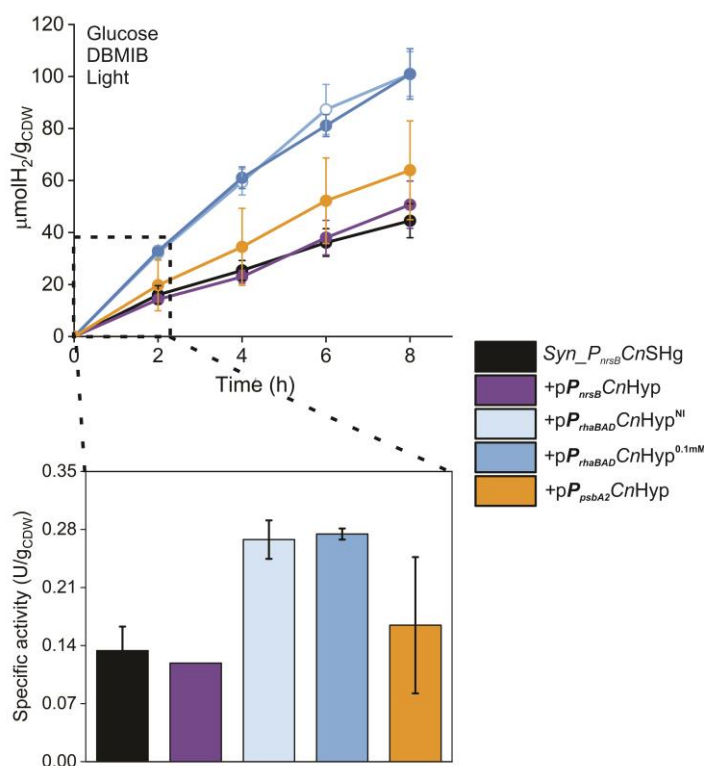


Figure 5.5. H₂ production under mixotrophic conditions. Time courses of H₂ production *in vivo* by *Syn_P_{nrsB}CnSHg* containing *pP_{nrsB}CnHyp*, *pP_{rhaBAD}CnHyp* (Not Induced; 0.1 mM rhamnose), *pP_{psbA2}CnHyp*, or no plasmid. Each of them was supplemented with 10 μM Ni²⁺ for *CnSH* expression. Five ml culture volume were transferred into gas-tight 10 mL vials containing 10 mM glucose and 20 μM DBMIB in yBG11 medium. Prior to incubation in light, the gas phase was saturated with N₂. The insert highlights initial activities (first 2 h). Mean values and standard deviations (n=3) are given.

Syn_P_{nrsB}CnSHg containing *pP_{psbA2}CnHyp* again exhibited a high variability, which indicates that expression from the *P_{psbA2}* promotor requires investigations regarding the influence of growth phases or the cellular redox status. The strain with *hox* and *hyp* operon expression under control of the Ni²⁺ showed the same H₂ production rate as *Syn_P_{nrsB}CnSHg*. Here, a high metabolic burden for protein production may hinder an efficient channeling of electrons towards the *CnSH*. However, the competition for the non-primary electron shuttle NADH obviously constitutes a main limitation of the NADH-dependent hydrogenases, when it comes to H₂ production in phototrophs. Such competition for electrons needs to be alleviated, e.g., via protein engineering towards the acceptance of ferredoxin or NADPH as electron donors.

5.3 Conclusion/ Outlook

Our study revealed that *C. necator* maturases can indeed foster active *CnSH* synthesis in *Synechocystis* sp. PCC 6803 and that a fine balance between hydrogenase and maturase gene expression is important to maximize functional *CnSH* levels in *Synechocystis*. However, elevated Hyp proteins production or activities appeared to negatively affect hydrogenase activity and cell growth, so that their expression had to be quantitatively and temporally controlled. With the fine balance of recombinant multigene expression, the presence of *CnSH*-dedicated auxiliary proteins enhanced its maturation efficiency in *Synechocystis* and, consequently, high and long-term stable *CnSH* activity was obtained *in vivo* in both H₂ consumption and production experiments. Further studies on partial expression of *C. necator* auxiliary proteins and knockouts of endogenous maturases will be useful to determine the most efficient combination of maturases and to optimize heterologous *CnSH* production in *Synechocystis*. Although the obtained *CnSH* activities in *Synechocystis* are still rather low compared to those achieved in *E. coli*, the 120 U g⁻¹_{prot.}, they are comparable with that obtained in *P. putida* (~160 U g⁻¹_{prot.}). Thus, the *CnSH* activity obtained augurs well for future applications for either photosynthesis-driven H₂ production (after changing the cofactor dependency) or for providing additional electrons for growth and biotransformation reactions. It has to be pointed out that the *Syn_CnSH* maximal activity *in vivo* is close to rates achieved in biocatalytic redox reactions implemented in *Synechocystis*. E.g., specific activities up to 40 and 60 U g_{CDW}⁻¹ have been achieved with cytochrome P450 monooxygenases and Bayer–Villiger monooxygenases (BVMOs), respectively, applied in *Synechocystis* on bioreactor scale [167][37]. Thereby, activities become limited by the constricted availability of reducing equivalents derived from photosynthetic water oxidation. Thus, such reactions can benefit from O₂-tolerant *CnSH* delivering a surplus of electrons via H₂ oxidation in addition to the O₂ and electrons supplied by photosynthetic water oxidation.

Chapter 6

Toward a synthetic hydrogen sensor in cyanobacteria: Functional production of an oxygen-tolerant regulatory hydrogenase in *Synechocystis* sp. PCC 6803

Franz Opel, Marvin Amadeus Itzenhäuser, Isabel Wehner, Sara Lupacchini, Lars Lauterbach, Oliver Lenz and Stephan Klähn

Author Contributions:

Stephan Klähn designed the study. Franz Opel, Marvin Amadeus Itzenhäuser and Isabel Wehner constructed the plasmids. Franz Opel and Isabel Wehner performed the gene expression and RH activity analyses in *Synechocystis*. Franz Opel performed the GFP reporter assays. Sara Lupacchini contributed to RH activity determination and experimental expertise for the in-gel assays. Lars Lauterbach and Oliver Lenz contributed methodology and know-how on O₂-tolerant hydrogenases. Franz Opel and Stephan Klähn wrote the manuscript with contributions from all co-authors. All authors contributed to the article and approved the submitted version.

Published in:

Frontiers in Microbiology, **2023**, 14:1122078. doi: 10.3389/fmicb.2023.1122078

The full publication incl. Supplementary Material can be found in the Appendix Section 6.

Abstract

Cyanobacteria have raised great interest in biotechnology, e.g., for the sustainable production of molecular hydrogen (H_2) using electrons from water oxidation. However, this is hampered by various constraints. For example, H_2 -producing enzymes compete with primary metabolism for electrons and are usually inhibited by molecular oxygen (O_2). In addition, there are a number of other constraints, some of which are unknown, requiring unbiased and systematic engineering approaches to improve the H_2 yield. Here, we introduced the regulatory [NiFe] hydrogenase (RH) of *Cupriavidus necator* (formerly *Ralstonia eutropha*) H16 into the cyanobacterial model strain *Synechocystis* sp. PCC 6803. In its natural host, the RH serves as a molecular H_2 sensor initiating a signal cascade to express hydrogenase-related genes when no additional energy source other than H_2 is available. Unlike most hydrogenases, the *C. necator* enzymes are O_2 -tolerant, allowing their efficient utilization in an oxygenic phototroph. Similar to *C. necator*, the RH produced in *Synechocystis* showed distinct H_2 oxidation activity, confirming that it can be properly matured and assembled under photoautotrophic, i.e., oxygen-evolving conditions. Although the functional H_2 -sensing cascade has not yet been established in *Synechocystis* yet, we utilized the associated two-component system consisting of a histidine kinase and a response regulator to drive and modulate the expression of a *superfolder gfp* gene in *Escherichia coli*. This demonstrates that all components of the H_2 -dependent signal cascade can be functionally implemented in heterologous hosts. Thus, this work provides the basis for the development of an intrinsic cyanobacterial H_2 biosensor that could be used to probe the effects of random mutagenesis and systematically identify promising genetic configurations to enable continuous and high-yield production of H_2 via oxygenic photosynthesis.

Chapter 7

General Discussion

7.1. The strategy: heterologous O₂-tolerant H₂ase in *Synechocystis*

Gas-processing metalloenzymes like H₂ases are nowadays a bioinspired fuel technology for a decarbonized economy. Despite their ability to catalyze redox reactions with a minimal overpotential, they typically suffer from O₂ sensitivity [251]. This shared feature set down to their origin in an anoxygenic era. Applications in oxygenic organisms are therefore challenging and in the last decade's most of the efforts were spent to engineered [NiFe] and [FeFe] H₂ases towards O₂ tolerance [173][252]. Particularly restricting is the O₂ sensitivity of [FeFe] H₂ases, which are irreversibly inhibited even by trace amount of O₂. Due to their higher H₂ production rates compared to [NiFe] H₂ases (*in vitro* close to one order of magnitude higher: [FeFe] ~10⁴ H₂/s; [NiFe] 1000–2000 H₂/s) [253][168], researchers tried intensively to discover or engineer O₂-tolerant [FeFe] H₂ases [210]. Recent findings include new aminoacidic residues involved in lowering O₂ sensitivity [254], and the characterization of a safety cap, which protects the enzyme against O₂, [255]. Lastly, moderate O₂-tolerant [FeFe] H₂ases were found, making them promising candidate for photobiological applications [256][257]. Contrariwise, [NiFe] H₂ases are reversibly inactivated by O₂, so strategies for increasing O₂ tolerance were targeting key aminoacids on the O₂ diffusion channel [258][178]. Recently, the [NiFe] H₂ase-1 from *E. coli* was encapsulated in a recombinant α -carboxysome shell from a chemoautotrophic organism, creating a unique nanoreactor where the catalyst showed increase O₂ tolerance and H₂ production was detected under anaerobic and aerobic conditions [259]. Since the carboxysome is a compartment present in cyanobacteria might be feasible to follow the same approach. A valid alternative strategy can be the substitution of the native cyanobacterial H₂ase with a recombinant O₂-tolerant [NiFe] H₂ase. In 2011, the first breakthrough was the heterologous expression of a moderately O₂-tolerant H₂ase (1-3% O₂) in *S. elongatus*. Although the [NiFe] H₂ase was incorporated together with the accessory proteins, H₂ production rates achieved were ten times lower than that obtained with the native H₂ase [216]. For practical applications, further improvements are required to increase O₂ tolerance, gene expression levels and to efficiently couple the H₂ase to the ETC. Our strategy was to heterologously express the soluble, bidirectional, NADH-dependent [NiFe], O₂-tolerant H₂ase from *C. necator* (*CnSH*) in *Synechocystis* for several reasons:

- 1) *Synechocystis* harbors a bidirectional [NiFe] H₂ase from the same group as the one from *C. necator*, and their structural and auxiliary proteins share a certain degree of similarity.
- 2) *Synechocystis* is a model cyanobacterium, on which most genetic tools have been developed and characterized [260].
- 3) *CnSH* is fully O₂-tolerant, meaning it shows unaltered activity up to 20% of O₂, which we expected to guarantee stability during oxygenic photosynthesis in *Synechocystis*.

- 4) *CnSH* was the first characterized enzyme of its group and already has been successfully overexpressed in heterotrophic hosts and shown to be active *in vivo* with as well as without the co-expression of the maturation system, depending on the genetic background of the host strains [176].
- 5) It has a cytoplasmatic location, which makes its characterization easier compared to *CnMBH*, which, in addition, is inhibited by H_2 [261].
- 6) Although the turnover frequency for H_2 production is roughly 1% of the faster [FeFe] H_2 ases, considering the most efficient connection of the ETC with PSI-fused H_2 ase (achieved so far), the main constraint will still be electron transport from PSI to the H_2 ase, as PSI delivers $47e^-/s$ (highest rate found for *Synechococcus* sp. 7002) [198], which is in the range of the maximal *CnSH* activity [71].

7.2. The O_2 tolerant *C. necator* SH in *Synechocystis*: unexpected results

The successful incorporation of a heterologous H_2 ases requires stable and controllable gene expression systems and possibly its specific maturation apparatus. In this study, we report the functional production of the O_2 -tolerant *CnSH* in *Synechocystis* only by expressing the four structural genes and the enzyme-specific endopeptidase HoxW (*hoxFU YHW*). The activity of *CnSH* in *Synechocystis* was confirmed *in vitro* and, for the first time to our knowledge, an active heterologous [NiFe] H_2 ase was characterized *in vivo* in cyanobacteria. A first striking finding was that *Synechocystis* maturation proteins are able to assemble *CnSH* under anaerobic and aerobic conditions. This is in agreement with the hypothesis that the native H_2 ase in *Synechocystis* is constitutively expressed, regardless of the presence of O_2 [75]. However, Stripp *et al.* investigated CO and CN^- biosynthesis and coordination with Fe by HypCD, hypothesizing that cofactor synthesis is inhibited by O_2 *in vivo*. In particular, their findings suggested that O_2 sensitivity occurs at an early stage of maturation prior to the incorporation of the cyanide ligand, while once Fe(II)–(CN) $_2$ CO is formed, HypCD is not affected by O_2 [262]. The data provided in this work suggest that cofactor maturation is not sensitive to O_2 , as *Syn_CnSH*⁺ was cultivated phototrophically and the enzyme was permanently active *in vitro* and *in vivo* during continuous O_2 evolution. Still under debate is the CO derivation and coordination to the Fe. CO biogenesis was unraveled in microbes harboring a *hypX* gene [263], of which the gene product acts on a N¹⁰-formyltetrahydrofolate (N¹⁰-formyl-THF) to release CO via a formyl-coenzyme A intermediate [119][120]. Although N¹⁰-formyl-THF is a metabolic intermediate common to all bacteria (it is the one-carbon donor in purine biosynthesis and the formylation of methionine required for translation initiation), a homolog of HypX is not present in *E. coli* or in any cyanobacterial proteome [242][130]. Under debate was the potential contribution of a heme oxygenases as a source of CO under aerobic conditions.

Forzi *et al.* ruled out this possibility by considering O₂-sensitivity of the [NiFe] H₂ase maturation process. In the light of our results, however, this hypothesis might be plausible (**Fig. 7.1**). *Synechocystis* possesses 2 heme oxygenase isoforms (HO1 and HO2), which catalyze the specific O₂-dependent cleavage of heme to produce biliverdin IXa (BV) and release Fe²⁺ and CO (the first reaction of the bilin pigment synthesis). [264].

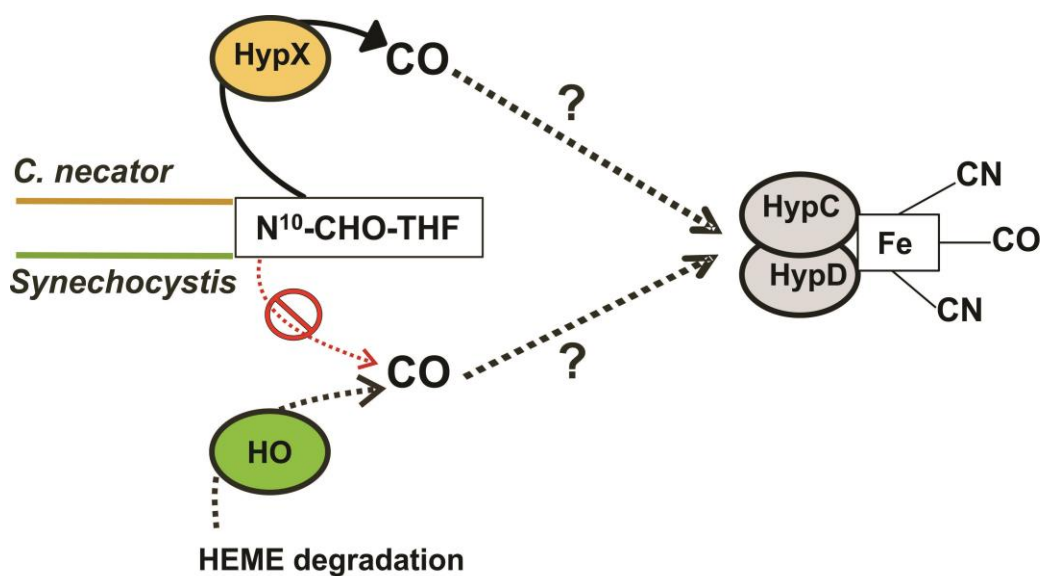


Figure 7.1. Metabolic origin of CO in *C. necator* and *Synechocystis* under aerobic conditions. In *C. necator*, metabolic CO derivation was elucidated, while it is still under debate in *Synechocystis* (and in *E. coli*), because *hypX* is not present and the route via heme degradation was discarded due to the O₂ dependent activity of HO oxygenase, which badly matches with the theory of an O₂-sensitive H₂ase maturation [242]. Still unclear is the mechanism of CO coordination with the Fe complex. HO: heme oxygenase, N¹⁰-formyl-THF: N¹⁰- formyltetrahydrofolate.

Together with the *C. necator* *hyp* operon, also the *hoxI* gene, encoding for an accessory, putatively NADPH binding subunit, was firstly excluded from the heterologous production of *CnSH* in *Synechocystis*, to avoid possible interference with NADPH metabolism. Although we didn't investigate its role in this thesis, the results showed that it was not required for functional *CnSH* assembly. When it was included in the *CnSH* operon, no evidence for meddling with *Synechocystis* metabolism was found. However, when it was included in the second generation strains, *hoxHYFUW* operon expression was differently regulated than in the first generation without *hoxI*. Therefore, the two strains with and without *hoxI* are not directly comparable. The construction of a *Syn_P_{nrsB}CnSHΔhoxI* is necessary to get a clear picture on the influence of *HoxI* on *CnSH* activity and stability in *Synechocystis*.

7.3. Enhancing recombinant CnSH activity via modular gene expression and functional bio-assembly

7.3.1. Balancing of heterologous gene expression in *Synechocystis*

As introduced previously, it is essential to rely on well characterized and predictable genetic regulatory elements for the successful introduction of multiple heterologous genes. The overall heterologous (multi)-gene expression level and protein synthesis are defined by transcription rates, translation rates, protein folding/maturation and protein degradation. It was observed that transcription generally has a predominant role over mRNA degradation when it comes to expression regulation in bacteria. So, the promoter activity primarily determines the mRNA level in the cell [265]. Transcription and translation in prokaryotes occur simultaneously. Therefore, mRNA abundance, secondary structures, and the affinity of ribosomes to ribosome binding sites (RBS) define the final translation efficiency. Depending on the genetic context, RBS binding affinity can vary widely. Furthermore, codon composition of foreign genes can affect expression, if it strays too far from the GC content of the host strain. In addition, it is crucial to balance the translation rate for synthetic constructs not to sequester an excessive amount of the translation machinery and thereby deteriorate cell maintenance and growth. Together with protein production, degradation processes supported by the cell's protein quality control then determines final protein levels [265][138]. The development of various synthetic constructs and recombinant strains in this study taught us the importance of fine tuning multigene expression. The transcriptional control of the first *C. necator* *hox* operon introduced in *Synechocystis* genome involved the native light-regulated *psbA2* promoter. Despite the successful expression of functional recombinant H₂ase in *Syn_CnSH*⁺, the specific enzyme activity determined in cell-free extracts was several times lower than the activities determined in the native and heterotrophic hosts (Chapter 3.2.1). These results pointed to poor gene expression and low protein abundance. Drawbacks of using native promoters like *psbA2* have been reported when applied for metabolic engineering purposes [223], since their activity heavily depend on light availability and growth status [266]. Therefore, we aimed for a well-controlled promoter with a wide dynamic range of induction. Among the native metal-inducible promoters, nickel-dependent *P_{nrsB}* has recently been characterized in *Synechocystis* as titratable and well-tight [220]. Together with *P_{nrsB}*, the hexacistronic operon (*hoxFUYHWI*) was completed with the strong synthetic RBS* and a native terminator (*T_{psbC}*) [227][221]. The final construct was assembled in an episomal plasmid or integrated in the chromosome, to compare plasmid- and genome-based expression (Chapter 4.2.1). The two resulting strains showed enhanced H₂ase synthesis and twice the specific H₂

oxidation activity *in vitro* (*Syn_CnSH*⁺: 18 - 40 U g⁻¹; *Syn_P_{nrsB}CnSH*: 80 U g⁻¹) and *in vivo* (*Syn_CnSH*⁺: ~12 U g_{CDW}⁻¹; *Syn_P_{nrsB}CnSH*: ~27 U g_{CDW}⁻¹). Additionally, high activities thereby could be preserved for 5 h (*Syn_CnSH*⁺: 5 U g_{CDW}⁻¹; *Syn_P_{nrsB}CnSH*: 17 U g_{CDW}⁻¹). Gene expression with RSF1010-based plasmids [267] is known to be superior over genome-based expression, especially regarding copy number per cell (~30 plasmids vs 2-20 chromosome copies in *Synechocystis*) [268] and increased transcription during stationary phases [265], but less stable [230]. Indeed, higher protein synthesis was achieved by plasmid-based expression, but only the genome-based strain maintained a stable H₂ase production over 3 days post-induction (Chapter 4.2.3). Moreover, the condition enabling the highest protein abundance did not result in the highest specific activity, revealing the presence of non-functional protein complexes or the occurrence of single subunits (Chapter 4.2.2). This outcome is in good accordance to literature data, as gene expression and/or enzyme maturation may well limit the H₂ase activity [176]. Therefore, we decided to complement the *Syn_P_{nrsB}CnSHg* with the entire maturation apparatus or only *hypX* from *C. necator*. This context demands a trade-off between heterologous gene expression and cell fitness without overloading the cell with recombinant proteins that interfere with metabolism (e.g., H₂ase, ATPase activity of HypEF). Ideally, titratable transcriptional regulation allows the uncoupling of H₂ase production from growth. Three different promoters (*psbA2*, *nrsb*, *rhas*) have been evaluated for the control of transcription of the *C. necator hyp* operon. Eventually, our study revealed that a fine balance between *C. necator* H₂ase and respective maturases abundance is important to maximize functional *CnSH* expression in *Synechocystis* (Chapter 5.2.2-3). Another critical point is the design of this polycistronic operon. Usually, multi-gene constructs that are placed under the control of the same promoter are characterized by similar transcript abundances, although this is not always the case [269][270]. Indeed, transcript analysis of the heterologous *hyp* genes revealed a reduced level with increased distance from the promoter. Alternatively, to ensure identical multigene expression, each gene can be equipped with a promoter and a terminator [128]. For further optimization and commercial feasibility, it will be necessary to screen alternative promoters involving non-toxic and cheap signaling compounds (or environmental / physical signals), as metals can interfere with cell homeostasis and be toxic at higher concentrations as it is the case for nickel [138].

7.3.2. Maturation of recombinant *C. necator* [NiFe] H₂ase in *Synechocystis*

Overall, heterologous H₂ase expression studies supported the hypothesis that the probability of obtaining a functional enzyme correlates with the abundance of homologous and heterologous Hyp proteins sharing a high degree of similarity [176]. By comparing protein sequences, we identified 50-67% sequence homology between *Synechocystis* and *C. necator* maturases [130].

Furthermore, the absence of a *hypX* gene homolog in *Synechocystis* could have represented a disadvantage for aerobic *CnSH* maturation. In studies conducted with heterotrophic hosts, co-presence of *C. necator* maturases led to higher recombinant enzyme activity. Therefore, we introduced either the complete set of accessory genes or only *hypX* into *Syn_P_{nrsB}CnSHg*. The best expression condition achieved for *C.necator hox* and *hyp* operons led to 60% higher activity and higher *in vivo* stability as compared to the introduction of the *hox* genes alone (Chapter 5.2.3). The rates obtained ($120 \text{ U g}^{-1} \text{ totprot.}$) are comparable to those achieved in *P. putida* ($\sim 160 \text{ U g}^{-1} \text{ totprot.}$) [137]. On the contrary, the introduction of *hypX* only into *Syn_P_{nrsB}CnSHg* did not influence the achieved H_2 ase activity, ruling out CO biogenesis as main limiting factor (Appendix). Further investigations, e.g., the separate expression of functional *CnHyp* complexes (HypCD, HypEF, HypAB) in *Synechocystis* may reveal, if the complementation of a specific maturase subset can optimize the heterologous production of *CnSH*. Intriguingly, different results have been observed, when *CnRH* was recombinantly expressed in *Synechocystis* (Chapter 6). A functional H_2 oxidizing *in vitro* activity of *CnRH* was detected only when the H_2 ase genes were co-expressed with the entire *hyp* operon. Although the protein was synthesized in any case, *Synechocystis* H_2 ase maturases were not sufficient to assemble an active regulatory H_2 ase. Differently from *CnSH* maturation, *CnRH* does not undergo a proteolytic cleavage as last step of biosynthesis, and the absence of HypF completely impaired active enzyme synthesis, whereas the individual knockout of each remaining Hyp proteins just decreased the RH activity [271]. Therefore, it might be interesting to investigate the complementation of *CnRH* with *Cn_hypF* in *Synechocystis*.

7.4. Physiological characterization of *CnSH* in *Synechocystis*

Within this study, H_2 oxidation activity of *CnSH* in photosynthetically active O_2 evolving cells was verified, up to O_2 levels of $\sim 15\%$. In addition, H_2 -derived NADH was found to be sufficient to support growth without PSII activity (in the presence of the photosynthesis inhibitor DCMU), only relying on cyclic electron transport (CET), whereas the *Synechocystis* WT could not grow under these conditions, probably due to the initially microaerobic gas phase (1-2% O_2). However, in an anaerobic environment, *SynH₂ase* enabled growth solely on H_2 , CO_2 , and light [190]. The same was found for a *Clostridial* [FeFe] H_2 ase recombinantly expressed in *S. elongatus* [191]. In contrast, we did not observe growth of *Syn_CnSH⁺* under light with DCMU, 20% H_2 , 10% CO_2 , and 15% initial O_2 . We hypothesize that, in this setting, NADH re-oxidation is hampered via the ETC to avoid ATP/ NAD(P)H imbalance or futile utilization of reducing equivalents by respiration. This initial physiological characterization revealed that *CnSH* provides an alternative electron transfer pathway including light-dependent activation of H_2 -derived electrons (Chapter 3.2.3). We further investigated the function and regulation of the two suggested electron paths, through which

the electrons are channeled for the transfer of electrons from H₂-derived NADH to NADP⁺. We employed a second ETC inhibitor, DBMIB, which blocks electrons at cytb₆f. Under these conditions, sustained H₂ oxidation via CnSH is only possible, if electron transfer from NADH to NADP⁺ occurs via transhydrogenases (PntABs). *Syn_P_{nrsB}CnSH* showed identical activities as under standard conditions, confirming the involvement of PntABs (Chapter 4.2.4). However, it still remains to be investigate, how NADH recycling via PntAB and the NDH-2 complex is regulated under standard conditions and if one prevails over the other. Overall the results obtained for *in vivo* H₂ consumption and H₂-base growth demonstrate the integration of CnSH in the cyanobacterial redox metabolism. In particular, H₂ase activity in the cell is mainly limited by the availability of source (H₂) and sink (e.g. CO₂) for NADH cycling. H₂-derived NADH competes with photosynthetically derived-NADPH, which is the primary electron donor of cell anabolism in *Synechocystis* [272]. This internal competition has a direct effect on *in vivo* H₂ase activity, which dropped under CO₂-limiting conditions. By supplying “unlimited” H₂ and CO₂ to the reaction mixture and implementing optimized expression of CnSH and maturase genes, a stable H₂ oxidation activity could be maintained *in vivo* for 8 h, with an average of 30 U g_{CDW}⁻¹ (Chapter 5.2.3). This rate is comparable with enzymes employed in whole-cell biocatalysis in cyanobacteria. Recombinant enzymes coupled directly with photosynthesis, as P450s, face competition for electrons with the different photosynthetic electron acceptors, with FNR as the most prominent one diverting 80% of reducing power to cellular metabolism [64]. Under NADPH-limiting conditions, O₂-tolerant H₂ases can reinforce electrons supply and provide the option to uncouple the electron supply to non-ATP-consuming reactions, such as oxyfunctionalization, from proton gradient generation [273]. H₂ oxidation thus may help to balance the ATP / NAD(P)H ratio, for sustained bioprocessing. This is especially beneficial for NADH-dependent biocatalytic reactions in cyanobacteria that are known to be limited by insufficient NADH concentration, reported to be ~6.5 times less than NADPH [274][202]. Recently, Sleutels *et al.* employed H₂ as additional energy source to the available light to achieve higher growth rates via a metabolic pathway named photoreduction. Because H₂ can be distributed evenly, this solution could circumvent light-limiting conditions in a bioreactor set up with high cell density and enabled the production of biomass to be utilized for other biotechnological processes [190].

7.5. H₂ formation in *Synechocystis* by the SH of *C. necator*

CnSH also enabled H₂ formation in *Synechocystis*, however, just under fermentative conditions upon glucose supplementation in the dark and to a minor extent in light. Under illumination, the prolonged H₂ formation activity exhibited by *Syn_CnSH*⁺ compared to the WT with only *SynH₂ase* is most likely enabled by its O₂-tolerance (Chapter 3.2.4). Enhanced CnSH gene expression in

Syn_P_{nrsB}CnSHg increased the amount of fermentative H₂ formed by a factor of two (*Syn_CnSH*⁺: ~ 190 μmol H₂ g_{CDW}⁻¹; *Syn_P_{nrsB}CnSHg*: 384 μmol H₂ g_{CDW}⁻¹) (Chapter 4.2.5). Further improvement in the rates were achieved, if the maturation machinery of *C. necator* was incorporated in *Syn_P_{nrsB}CnSHg*, confirming increased H₂ase activity (Chapter 5.2.4). However, H₂ production with concurrent photosynthetic water splitting in *Syn_CnSH*⁺ and *Syn_P_{nrsB}CnSH* relied on NADH supply achieved by glucose addition elevating the intracellular NADH/NAD⁺ ratio and was supported by the elimination of NADH sinks such as the ETC, which may outcompete the H₂ase regarding NADH [130]. Taking inspiration by the native *SynH*₂ase, engineering the O₂-tolerant *CnSH* to accept ferredoxin derived electrons (E°: - 440) could enable efficient and direct coupling of aerobic photosynthesis with photo-H₂ production [72]. An ultimate goal also may be the fusion of the *CnSH* H₂ase module (HoxHY) to PSI, as recently realized with the native *SynH*₂ase [74] and a [FeFe] H₂ase from *C. reinhardtii in vivo* [183]. In this regard, promising results have been achieved with the O₂-tolerant H₂ase module of *CnMBH* equipped with the PsaE subunit of PSI. The optimized hybrid complex built on a gold electrode reached H₂ production rates upon illumination comparable with those estimated via electrochemistry [182][275]. Alternatively, it might be attractive to compare the activity of closely related H₂ases from *C. necator* N9. When grown heterotrophically on gluconate under anaerobic condition, the SH from *C. necator* N9 enabled 15-35 times higher rates for H₂ evolution (73 μmol/h/g of protein) than *C. necator* H16 [23].

Chapter 8

Conclusions & Outlook

As extensively described in the introduction, the most efficient cyanobacterial application in biotechnology would be the production of high valuable chemicals or biofuels via the coupling of recombinant enzyme as close as possible to the photosynthetic electron transport chain. This will allow to retain a high energy conversion efficiency and minimize the loss during carbon metabolism. Therefore, the most teasing combination is to exploit electrons from water splitting and energy from sunlight, the most abundant and clean source of energy, to produce H₂ as energy carrier. However, a multidisciplinary approach, integrating catalyst, reaction, and process engineering is needed to make photobioprocesses economically feasible and competitive with modern H₂ production technologies. Thereby, catalyst engineering and characterization in terms of stability and product formation kinetics constitutes an important part. O₂ sensitivity of all enzymes of phototrophs involved in hydrogen metabolism, such as nitrogenases and [NiFe] and [FeFe] H₂ases can be considered a key drawback regarding instability impairing practical applications of these enzymes. This makes our study on the introduction of an O₂-tolerant hydrogenase into *Synechocystis* particularly relevant. A fully functional expression of the O₂-tolerant H₂ase of *C. necator* was achieved in the presence oxygenic photosynthesis. The bidirectional activity shown and investigated *in vivo* paves the way for both photo-H₂ production and H₂-supported photo-bioconversions. A prerequisite for establishing biophotolysis is an efficient coupling of the O₂-tolerant enzyme and the photosynthetic light reaction. Here, protein engineering approaches need to target *CnSH* variants accepting ferredoxin or its direct coupling to PSI. However, the native catalytic bias of O₂-tolerant *CnSH* toward H₂ oxidation makes it ideal for cofactor regeneration in whole-cell photobiocatalysis, in particular with oxyfunctionalization reactions. However, the functional production of an O₂-tolerant H₂ase in cyanobacteria will solve the O₂ issues to a certain extent. First of all, the continuous wastage of electrons to reduce O₂ to water will significantly hamper the energy conversion efficiency of H₂ production in the presence of O₂ [179]. For photosynthetically highly active cells, the O₂ partial pressure can reach 25%, impairing enzyme activity and cellular functions. Additionally, the formation of an explosive oxyhydrogen mixture has to be considered. Therefore, reaction engineering, e.g., the use of capillary biofilm reactor set ups in a segmented-flow operation may help to stabilize the catalyst over long time and ensure low growth rates reducing respective competition [276]. Further, the *in situ* removal of H₂ and O₂, e.g., via selective membranes, may play an important role. [67]. Including *Synechocystis* strain development, optimization in terms of heterologous multi-gene expression, post-translational modification /maturation, and physiological characterization *CnSH* carrying strains, this study represents the first step towards an O₂-tolerant H₂ metabolism in a phototrophic organism.

References

- [1] A.B., Hooper and A.A., DiSpirito, 2013. Chemolithotrophy, *Encycl. Biol. Chem. Second Ed.*,1:486–492.
- [2] C.F., Demoulin, Y.J., Lara, L., Cornet, C., François, D., Baurain, A., Wilmotte, E.J., Javaux, 2019. Cyanobacteria evolution: Insight from the fossil record, *Free Radic. Biol. Med.*,140:206–223.
- [3] R., Braakman and E., Smith, 2012. The emergence and early evolution of biological carbon-fixation, *PLoS Comput. Biol.*,8(4):e1002455.
- [4] M.C., Weiss, F.L., Sousa, N., Mrnjavac, S., Neukirchen, M., Roettger, S., Nelson-Sathi, W.F., Martin, 2016. The physiology and habitat of the last universal common ancestor, *Nat. Microbiol.*,1(9):16116.
- [5] T., Sumi and K., Harada, 2021. Kinetics of the ancestral carbon metabolism pathways in deep-branching bacteria and archaea, *Commun. Chem.*,4(1):1–9.
- [6] G., Fuchs, 2011. Alternative pathways of carbon dioxide fixation: Insights into the early evolution of life?, *Annu. Rev. Microbiol.*;65:631-58.
- [7] G., Wächtershäuser, 1988. Before enzymes and templates: theory of surface metabolism., *Microbiol. Rev.*, 52(4):452–484.
- [8] W., Martin, J., Baross, D., Kelley, and M.J., Russell, 2008. Hydrothermal vents and the origin of life, *Nat. Rev. Microbiol.*, 6(11):805–814.
- [9] K., Schuchmann and V., Müller, 2012. A bacterial electron-bifurcating hydrogenase, *J. Biol. Chem.*,287(37):31165–31171.
- [10] X., Feng, G.J., Schut, D.K., Haja, M.W.W., Adams, and H., Li, 2022. Structure and electron transfer pathways of an electron-bifurcating NiFe-hydrogenase, *Sci. Adv.*, 8(8):eabm7546.
- [11] V., Müller and J., Frerichs, 2013. Acetogenic Bacteria, *eLS*, John Wiley & Sons, Ltd, 1–9.
- [12] J., Asplund-Samuelsson and E.P., Hudson, 2021. Wide range of metabolic adaptations to the acquisition of the Calvin cycle revealed by comparison of microbial genomes, *PLoS Comput. Biol.*,17(2):1–26.
- [13] T.J., Erb and J., Zarzycki, 2018. A short history of RubisCO: the rise and fall (?) of Nature's predominant CO₂ fixing enzyme, *Curr. Opin. Biotechnol.*,49:100–107.
- [14] H., Ashida, Y., Saito, C., Kojima, K., Kobayashi, N., Ogasawara, and A., Yokota, 2003. A functional link between RuBisCO-like protein of *Bacillus* and photosynthetic RuBisCO, *Science*, 302(5643):286–290.
- [15] M.R., Badger and E.J., Bek, 2008. Multiple Rubisco forms in proteobacteria: Their functional significance in relation to CO₂ acquisition by the CBB cycle, *J. Exp. Bot.*,

- 59(7):1525–1541.
- [16] B., Kacar, V., Hanson-Smith, Z.R., Adam, and N., Boekelheide, 2017. Constraining the timing of the Great Oxidation Event within the Rubisco phylogenetic tree, *Geobiology*, 15(5):628–640.
- [17] C.F., Delwiche and J.D., Palmer, 1996. Rampant horizontal transfer and duplication of rubisco genes in eubacteria and plastids, *Mol. Biol. Evol.*, 13,(6):873–882.
- [18] M.F., Hohmann-Marriott and R.E., Blankenship, 2011. Evolution of photosynthesis, *Annu. Rev. Plant Biol.*, 62:515–548.
- [19] J.W., Schopf and B.M., Packer, 1987. Early Archean (3.3-Billion to 3.5-Billion-Year-Old) Microfossils from Warrawoona Group, Australia, *Science*, 237:70-3.
- [20] N., Noffke, D., Christian, D., Wacey, and R.M., Hazen, 2013. Microbially induced sedimentary structures recording an ancient ecosystem in the ca. 3.48 Billion-year-old dresser formation, pilbara, Western Australia, *Astrobiology*, 13(12):1103–1124.
- [21] M.M., Tice and D.R., Lowe, 2006. Hydrogen-based carbon fixation in the earliest known photosynthetic organisms, *Geology*, 34(1):37–40.
- [22] M.C., Schoelmerich and V., Müller, 2020. Energy-converting hydrogenases: the link between H₂ metabolism and energy conservation, *Cell. Mol. Life Sci.*, 77(8):1461–1481.
- [23] M., Kuhn, A., Steinbuchel, and H.G., Schlegel, 1984. Hydrogen evolution by strictly aerobic hydrogen bacteria under anaerobic conditions, *J. Bacteriol.*, 159(2):633–639.
- [24] T., Burgdorf, O., Lenz, T., Buhrke, E., Van Der Linden, A.K., Jones, S.P.J., Albracht, B., Friedrich, 2005. [NiFe]-hydrogenases of *Ralstonia eutropha* H16: Modular enzymes for oxygen-tolerant biological hydrogen oxidation, *J. Mol. Microbiol. Biotechnol.*, 10(2–4):181–196.
- [25] A.Y., Mulkidjanian, E.V. Koonin, K.S., Makarova, S.L., Mekhedov, A., Sorokin, Y.I., Wolf, A., Dufresne, F., Partensky, H., Burd, D., Kaznadzey, R., Haselkorn, M.Y., Galperin, 2006. The cyanobacterial genome core and the origin of photosynthesis, *Proc. Natl. Acad. Sci. U. S. A.*, 103(35):13126–13131.
- [26] W.F., Martin, D.A., Bryant, and J.T., Beatty, 2018. A physiological perspective on the origin and evolution of photosynthesis, *FEMS Microbiol. Rev.*, 42(2):205–231.
- [27] G.C., Dismukes, V.V., Klimov, S.V., Baranov, Y.N., Kozlov, J., DasGupta, and A., Tyryshkin, 2001. The origin of atmospheric oxygen on Earth: The innovation of oxygenic photosynthesis, *Proc. Natl. Acad. Sci. U. S. A.*, 98(5):2170–2175.
- [28] W.F., Martin, 2020. Older Than Genes: The Acetyl CoA Pathway and Origins, *Front.*

- Microbiol.*,11:817.
- [29] K., Gutekunst, 2018. Hypothesis on the Synchronistic Evolution of Autotrophy and Heterotrophy, *Trends Biochem. Sci.*,43(6):402–411.
- [30] B.C., Marreiros, A.P., Batista, A.M. S., Duarte, and M.M., Pereira, 2013. A missing link between complex i and group 4 membrane-bound [NiFe] hydrogenases, *Biochim. Biophys. Acta - Bioenerg.*,1827(2):198–209.
- [31] A.W., Rutherford and P., Faller, 2003. Photosystem II: Evolutionary perspectives, *Philos. Trans. R. Soc. B Biol. Sci.*,358(1429):245–253.
- [32] J.E., Johnson, S.M., Web, K., Thomas, S., Ono, J.L., Kirschvink, and W.W., Fischer, 2013. Manganese-oxidizing photosynthesis before the rise of cyanobacteria, *Proc. Natl. Acad. Sci. U. S. A.*,110(28):11238–11243.
- [33] R.M., Soo, J.,Hemp, D.H., Parks, W.W., Fischer, and P., Hugenholtz, 2017. On the origins of oxygenic photosynthesis and aerobic respiration in Cyanobacteria, *Science*, 355(6332):1436–1440.
- [34] J.F., Kasting, 1993. Earth's early atmosphere, *Science*,259(5097):920–926.
- [35] J., Olejarz, Y., Iwasa, A.H., Knoll, and M.A., Nowak, 2021.The Great Oxygenation Event as a consequence of ecological dynamics modulated by planetary change, *Nat. Commun.*,12(1):3985.
- [36] J.A., Raven, J., Beardall, and P., Sánchez-Baracaldo, 2017. The possible evolution and future of CO₂-concentrating mechanisms,*J. Exp. Bot.*,68(14):3701–3716.
- [37] J., Toepel, R., Karande, S., Klähn, and B., Bühler, 2023. Cyanobacteria as whole-cell factories: current status and future perspectives, *Curr. Opin. Biotechnol.*, 80:102892.
- [38] C., Brigham, 2019. Perspectives for the biotechnological production of biofuels from CO₂ and H₂ using *Ralstonia eutropha* and other 'Knallgas' bacteria, *Appl. Microbiol. Biotechnol.*,103(5):2113–2120.
- [39] M., Jahn, N., Crang, M., Janasch, A., Hober, B., Forsström, K., Kimler, A., Mattausch, Q., Chen, J., Asplund-Samuelsson, E.P., Hudson, 2021. Protein allocation and utilization in the versatile chemolithoautotroph *Cupriavidus necator*,*Elife*, 10:1–26.
- [40] R., Cramm, 2009. Genomic view of energy metabolism in *Ralstonia eutropha* H16, *J. Mol. Microbiol. Biotechnol.*,16(1–2):38–52.
- [41] J., Jablonsky, S., Papacek, and M., Hagemann, 2016. Different strategies of metabolic regulation in cyanobacteria: From transcriptional to biochemical control, *Sci. Rep.*, 6(August):1–11.

- [42] M., Janasch, J., Asplund-Samuelsson, R., Steuer, and E.P., Hudson, 2019. Kinetic modeling of the Calvin cycle identifies flux control and stable metabolomes in *Synechocystis* carbon fixation, *J. Exp. Bot.*,70(3):1017–1031.
- [43] L., You, B., Berla, L., He, H.B., Pakrasi, and Y.J., Tang, 2014. 13C-MFA delineates the photomixotrophic metabolism of *Synechocystis* sp. PCC 6803 under light- and carbon-sufficient conditions, *Biotechnol. J.*, 9(5):684–692.
- [44] D., Muth-Pawlak, S., Kreula, P.J., Gollan, T., Huokko, Y., Allahverdiyeva, and E.M., Aro, 2022. Patterning of the Autotrophic, Mixotrophic, and Heterotrophic Proteomes of Oxygen-Evolving Cyanobacterium *Synechocystis* sp. PCC 6803, *Front. Microbiol.*, 13(May):1–22.
- [45] E. Sporre, J., Karlsen, K., Schriever, J. Asplund Samuelsson, M., Janasch, D., Kotol, L. Strandsberg, L. Zeckey, I., Piazza, P., Syren, F., Edfors, E.P., Hudson, 2023. Metabolite interactions in the bacterial Calvin cycle and implications for flux regulation, *bioRxiv*, p. 2022.03.15.483797.
- [46] E.P., Hudson, 2023. The Calvin Benson cycle in bacteria: New insights from systems biology, *Semin. Cell Dev. Biol.*, Mar 29:S1084-9521(23)00070-8.
- [47] A.T., Wright, C., Ansong, N.C., Sadler, E.A. Hill, M.P. Lewis, E.M., Zink, R.D., Smith, A.S., Beliaev, A.E., Konopka., 2014. Protein redox dynamics during light-to-dark transitions in cyanobacteria and impacts due to nutrient limitation, *Front. Microbiol.*, 5(July):1–10.
- [48] M., Lindahl and F.J., Florencio, 2003. Thioredoxin-linked processes in cyanobacteria are as numerous as in chloroplasts, but targets are different, *Proc. Natl. Acad. Sci. U. S. A.*,100(26):16107–16112.
- [49] J.B., Waterbury, 2006. The Cyanobacteria—Isolation, Purification and Identification, in *The Prokaryotes*:1053–1073, Springer, New York, NY.
- [50] P.C., Hallenbeck, 2017. Modern Topics in the Phototrophic Prokaryotes: Metabolism, Bioenergetics, and Omics, *Mod. Top. Phototrophic Prokaryotes Metab. Bioenerg. Omi.*,1:1–350.
- [51] F., Gan and D.A., Bryant, 2015. Adaptive and acclimative responses of cyanobacteria to far-red light, *Environ. Microbiol.*,17(10):3450–3465.
- [52] L.A., Mills, A.J., McCormick, and D.J., Lea-Smith, 2020. Current knowledge and recent advances in understanding metabolism of the model cyanobacterium *Synechocystis* sp. PCC 6803, *Biosci. Rep.*,40(4):1–33.
- [53] N.J., Lang, 1968. The fine structure of blue-green algae, *Ann. rev. microbiol.*, 22:15–46.
- [54] R., Rippka, J., Deruelles, and J.B., Waterbury, 1979. Generic assignments, strain histories

- and properties of pure cultures of cyanobacteria, *J. Gen. Microbiol.*,111(1):1–61.
- [55] K.A., Palinska, Cyanobacteria, 2008. eLS pp. 1–11.
- [56] I., Berman-Frank, P., Lundgren, and P., Falkowski, 2003. Nitrogen fixation and photosynthetic oxygen evolution in cyanobacteria, *Res. Microbiol.*,154(3):157–164.
- [57] P., Aguiló-Nicolau, J., Galmés, G., Fais, S., Capó-Bauçà, G., Cao, and C., Iñiguez, 2023. Singular adaptations in the carbon assimilation mechanism of the polyextremophile cyanobacterium *Chroococcidiopsis thermalis*, *Photosynth. Res.*,156:231–245.
- [58] C.J., Howe, A.C., Barbrook, R.E.R., Nisbet, P.J., Lockhart, and A.W.D., Larkum, 2008. The origin of plastids, *Philos. Trans. R. Soc. B Biol. Sci.*,363(1504):2675–2685.
- [59] T., Kaneko, S., Sato, H., Kotani, A., Tanaka, E., Asamizu, Y., Nakamura, N., Miyajima, M., Hirosawa, M., Sugiura, S., Sasamoto, T., Kimura, T., Hosouchi, A., Matsuno, A., Muraki, N., Nakazaki, K., Naruo, S., Okumura, S., Shimpo, C., Takeuchi, T., Wada, A., Watanabe, M., Yamada, M., Yasuda, S., Tabata, 1996. Sequence analysis of the genome of the unicellular cyanobacterium *Synechocystis* sp. strain PCC6803. II. Sequence determination of the entire genome and assignment of potential protein-coding regions, *DNA Res.*, 3(3):109–136.
- [60] F., Opel, N.A., Siebert, S. Klatt, A.,Tüllinghoff, J.G., Hantke, J., Toepel, B., Bühler, D.J., Nürnberg, S., Klähn, 2021. Generation of Synthetic Shuttle Vectors Enabling Modular Genetic Engineering of Cyanobacteria, *ACS Synth. Biol.*, May 20;11(5):1758-1771.
- [61] L., Yao, K., Shabestary, S.M., Björk, J., Asplund-Samuelsson, H.N., Joensson, M., Jahn, E.P., Hudson, 2020. Pooled CRISPRi screening of the cyanobacterium *Synechocystis* sp PCC 6803 for enhanced industrial phenotypes, *Nat. Commun.*, Apr 3;11(1):1666.
- [62] Y., Yu, L., You, D., Liu, W., Hollinshead, Y.J., Tang, and F., Zhang, 2013. Development of *Synechocystis* sp. PCC 6803 as a phototrophic cell factory, *Mar. Drugs*, 11(8):2894–2916.
- [63] T., Wang, X., Wang, C., Hou, and J., Liu, 2020. Quaternary functionalized mesoporous adsorbents for ultra-high kinetics of CO₂ capture from air, *Sci. Rep.*,10(1) 21429.
- [64] J., Jodlbauer, T., Rohr, O., Spadiut, M.D., Mihovilovic, and F., Rudroff, 2021. Biocatalysis in Green and Blue: Cyanobacteria, *Trends Biotechnol.*, 39(9):875–889.
- [65] M., Hagemann, S., Song, E.M., Brouwer, 2021. Inorganic carbon assimilation in cyanobacteria: mechanisms, regulation, and engineering. In *Cyanobacteria Biotechnology*; John Wiley & Sons, Ltd; 123– 170.
- [66] H., Medipally, M.M., Nowaczyk, and M., Rögner, 2021. Parameters of photosynthesis relevant for a biotechnological application, in *Photosynthesis: Biotechnological*

- Applications with Microalgae*, edited by Matthias Rögner, Berlin, Boston: De Gruyter; 1-30.
- [67] K., Bühler, B., Bühler, S., Klähn, J.O., Krömer, C., Dusny, and A., Schmid, 2021. Biocatalytic production of white hydrogen from water using cyanobacteria,” *Photosynth. Biotechnol. Appl. with Microalgae*, edited by Matthias Rögner, Berlin, Boston: De Gruyter; 285–312.
- [68] C., Ding, K.L., Yang, and J., He, 2016. Biological and fermentative production of hydrogen, in *Handbook of Biofuels Production: Processes and Technologies: Second Edition*; 303–333.
- [69] IEA, 2021. The Role of Critical Minerals in Clean Energy Transitions – Analysis – IEA.
- [70] J.R., Benemann and J.C., Weissman, 1977. Biophotolysis: Problems and Prospects., *Microbial Energy Conversion*, 413–426.
- [71] S., Rexroth, K., Wiegand, and M., Rögner, 2015. Cyanobacterial design cell for the production of hydrogen from water, in *Biohydrogen*, edited by Matthias Rögner, Berlin, München, Boston: De Gruyter; 1–18.
- [72] K., Gutekunst, X., Chen, K., Schreiber, U., Kaspar, S., Makam, and J., Appel, 2014. The bidirectional NiFe-hydrogenase in *Synechocystis* sp. PCC 6803 Is reduced by flavodoxin and ferredoxin and is essential under mixotrophic, nitrate-limiting conditions, *J. Biol. Chem.*, 289(4):1930–1937.
- [73] P., Marco, T., Elman, and I., Yacoby, 2019. Binding of ferredoxin NADP+ oxidoreductase (FNR) to plant photosystem I, *Biochim. Biophys. Acta - Bioenerg.*, 1860(9):689–698.
- [74] J., Appel, V., Hueren, M., Boehm, and K., Gutekunst, 2020. Cyanobacterial *in vivo* solar hydrogen production using a photosystem I–hydrogenase (PsaD-HoxYH) fusion complex, *Nat. Energy*, 5(6):458–467,
- [75] F., Gutthann, M., Egert, A., Marques, and J., Appel, 2007. Inhibition of respiration and nitrate assimilation enhances photohydrogen evolution under low oxygen concentrations in *Synechocystis* sp. PCC 6803, *Biochim. Biophys. Acta - Bioenerg.*, 1767(2):161–169.
- [76] K.E., Redding, , J.,Appel, M., Boehm, W., Schuhmann, M.M., Nowaczyk, I., Yacoby, K., Gutekunst, 2022. Advances and challenges in photosynthetic hydrogen production, *Trends Biotechnol.*, Nov;40(11):1313-1325.
- [77] P.M., Vignais, B., Billoud, and J., Meyer, 2001. Classification and phylogeny of hydrogenases, *FEMS Microbiol. Rev.*, 25(4):455–501.
- [78] G.C., Hartmann, A.R., Klein, M., Linder, and R.K., Thauer, 1996. Purification, properties and primary structure of H₂-forming N₅,N₁₀-methylenetetrahydromethanopterin

- dehydrogenase from *Methanococcus thermolithotrophicus*, *Arch. Microbiol.*,165(3):187–193.
- [79] P.M., Vignais and B., Billoud, 2007. Occurrence, classification, and biological function of hydrogenases: An overview, *Chem. Rev.*,107(10):4206–4272.
- [80] P., Constant and P.C., Hallenbeck, 2019. Chapter 3 - Hydrogenase, in *Biomass, Biofuels, Biochemicals*, 49–78.
- [81] J.W., Peters, G.J., Schut, E.S., Boyd, D.W., Mulder, E.M, Shepard, J.B., Broderick, P.W., King, M.W., Adams, 2015. [FeFe]- and [NiFe]-hydrogenase diversity, mechanism, and maturation, *Biochim. Biophys. Acta - Mol. Cell Res.*,1853(6):1350–1369.
- [82] J.C., Fontecilla-camps, A., Volbeda, C., Cavazza, Y., Nicolet, and J., Fourier, 2007. Structure/Function Relationships of [NiFe] - and [FeFe] -Hydrogenases, *Chem. Rev.*, Oct;107(10):4273-303.
- [83] O., Lenz, L., Lauterbach, S., Frielingsdorf, and B., Friedrich, 2015. Oxygen-tolerant hydrogenases and their biotechnological potential, in *Biohydrogen*, edited by Matthias Rögner, Berlin, München, Boston: De Gruyter; 61–96.
- [84] A., Volbeda and J.C., Fontecilla-Camps, 2003.The active site and catalytic mechanism of NiFe hydrogenases, *J. Chem. Soc. Dalt. Trans.*, 3(21):4030–4038.
- [85] P.M., Vignais and A., Colbeau, 2004. Molecular biology of microbial hydrogenases, *Curr. Issues Mol. Biol.*,6(2):159–188.
- [86] M., Horch, L., Lauterbach, O., Lenz, P., Hildebrandt, and I., Zebger, 2012. NAD(H)-coupled hydrogen cycling - Structure-function relationships of bidirectional [NiFe] hydrogenases, *FEBS Lett.*, 586(5):545–556.
- [87] S.J., Pilkington, J.M., Skehel, J.E., Walker, and R.B., Gennis, 1991. Relationship between Mitochondrial NADH–Ubiquinone Reductase and a Bacterial NAD-Reducing Hydrogenase, *Biochemistry*, 30(8):2166–2175.
- [88] T. Burgdorf , E., van der Linden, M., Bernhard, Q., Yin, J., Back, A., Hartog, A., Muijsers, C.D., de Koster, S., Albracht, B., Friedrich, 2005. The Soluble NAD⁺-Reducing [NiFe]-Hydrogenase from *Ralstonia eutropha* H16 Consists of Six Subunits and Can Be Specifically Activated by NADPH, *J. Bacteriol.*,187(9):3122–3132.
- [89] O., Schmitz, G., Boison, H., Salzmann, H., Bothe, K., Schütz, S., Wang, T., Happe, 2002. HoxE - A subunit specific for the pentameric bidirectional hydrogenase complex (HoxEFUYH) of cyanobacteria, *Biochim. Biophys. Acta - Bioenerg.*,1554(1–2):66–74.
- [90] E., Aubert-Jousset, M., Cano, G., Guedeney, P., Richaud, and L., Cournac, 2011. Role of

- HoxE subunit in *Synechocystis* PCC6803 hydrogenase, *FEBS J.*, 278(21):4035–4043.
- [91] C.L., McIntosh, F., Germer, R., Schulz, J., Appel, and A.K., Jones, 2011. The [NiFe]-hydrogenase of the cyanobacterium *Synechocystis* sp. PCC 6803 works bidirectionally with a bias to H₂ production, *J. Am. Chem. Soc.*, 133(29):11308–11319.
- [92] K., Gutekunst and R., Schulz, 2018. CHAPTER 4: The Physiology of the Bidirectional NiFe-hydrogenase in Cyanobacteria and the Role of Hydrogen Throughout the Evolution of Life, in *Compr. Ser. Photochem. Photobiol. Sci.*, 16: 107–138.
- [93] K., Schneider and H.G., Schlegel, 1976. Purification and properties of soluble hydrogenase from *Alcaligenes Eutrophus* h 16, *Cell*, 452:66–80.
- [94] A., Tran-Betcke, U., Warnecke, C., Bocker, C., Zaborosch, and B., Friedrich, 1990. Cloning and nucleotide sequences of the genes for the subunits of NAD-reducing hydrogenase of *Alcaligenes eutrophus* H16, *J. Bacteriol.*, 172(6):2920–2929.
- [95] L., Lauterbach, H., Wang, M., Horch, L.B. Gee, Y., Yoda, Y., Tanaka, I., Zebger, O., Lenz, S. P. Cramer, 2015. Nuclear resonance vibrational spectroscopy reveals the FeS cluster composition and active site vibrational properties of an O₂-tolerant NAD⁺-reducing [NiFe] hydrogenase, *Chem. Sci.*, 6(2):1055–1060.
- [96] L., Lauterbach, J., Liu, M., Horch, P., Hummel, A., Schwarze, M., Haumann, K.A., Vincent, O., Lenz, I., Zebger, 2011. The hydrogenase subcomplex of the NAD⁺-reducing [NiFe] hydrogenase from *Ralstonia eutropha* - Insights into catalysis and redox interconversions, *Eur. J. Inorg. Chem.*, 7:1067–1079.
- [97] L., Lauterbach, Z., Idris, K.A., Vincent, and O., Lenz, 2011. Catalytic properties of the isolated diaphorase fragment of the NAD⁺-reducing [NiFe]-hydrogenase from *Ralstonia eutropha*, *PLoS One*, 6,(10):e25939.
- [98] E. Van Der Linden, B.W., Faber, B., Bleijlevens, T., Burgdorf, M., Bernhard, B., Friedrich, S.P.J., Albracht 2004. Selective release and function of one of the two FMN groups in the cytoplasmic NAD⁺-reducing [NiFe]-hydrogenase from *Ralstonia eutropha*, *Eur. J. Biochem.*, 271(4):801–808.
- [99] L., Lauterbach and O., Lenz, 2013. Catalytic production of hydrogen peroxide and water by oxygen-tolerant [NiFe]-hydrogenase during H₂ cycling in the presence of O₂, *J. Am. Chem. Soc.*, 135(47):17897–17905.
- [100] C.G., Friedrich, B., Friedrich, and B., Bowien, 1981. Formation of enzymes of autotrophic metabolism during heterotrophic growth of *Alcaligenes eutrophus*, *J. Gen. Microbiol.*, 122(1):69–78.

- [101] A., Erkens, K., Schneider, and A., Müller, 1996. The NAD-linked soluble hydrogenase from *Alcaligenes eutrophus* H16: Detection and characterization of EPR signals deriving from nickel and flavin, *J. Biol. Inorg. Chem.*,1(2):99–110.
- [102] M., Horch L., Lauterbach, M., Saggiu, P., Hildebrandt, F., Lenzian, R., Bittl, O., Lenz, I., Zebger, 2010. Probing the active site of an O₂-Tolerant NAD⁺-reducing [NiFe]-Hydrogenase from *Ralstonia eutropha* H16 by in situ EPR and FTIR spectroscopy, *Angew. Chemie - Int. Ed.*,49(43):8026–8029.
- [103] M. Saggiu, I., Zebger, M., Ludwig, O., Lenz, B., Friedrich, P., Hildebrandt, F., Lenzian, 2009. Spectroscopic insights into the oxygen-tolerant membrane-associated [NiFe] hydrogenase of *Ralstonia eutropha* H16, *J. Biol. Chem.*,284 (24):16264–16276.
- [104] T., Goris, A.F., Wait, M., Saggiu, J., Fritsch, N., Heidary, M., Stein, I., Zebger, F., Lenzian, F.A., Armstrong, B., Friedrich & O., Lenz 2011. A unique iron-sulfur cluster is crucial for oxygen tolerance of a [NiFe]-hydrogenase, *Nat. Chem. Biol.*,7(5):310–318.
- [105] J., Fritsch, P., Scheerer, S., Frielingsdorf, S., Kroschinsky, B., Friedrich, O., Lenz, C.M.T., Spahn, 2011. The crystal structure of an oxygen-tolerant hydrogenase uncovers a novel iron-sulphur centre, *Nature*, 479(7372):249–253.
- [106] J., Fritsch, O., Lenz, and B., Friedrich, 2013. Structure, function and biosynthesis of O₂-tolerant hydrogenases, *Nat. Rev. Microbiol.*,11(2):106–114.
- [107] K., Karstens, S., Wahlefeld, M., Horch, M., Grunzel, L., Lauterbach, F., Lenzian, I., Zebger, and O., Lenz, 2015. Impact of the iron-sulfur cluster proximal to the active site on the catalytic function of an O₂-tolerant NAD⁺-reducing [NiFe]-hydrogenase, *Biochemistry*,54(2):389–403.
- [108] M., Horch, L., Lauterbach, M.A., Mroginski, P., Hildebrandt, O., Lenz, and I., Zebger, 2015. Reversible active site sulfoxxygenation can explain the oxygen tolerance of a NAD⁺-reducing [NiFe] hydrogenase and its unusual infrared spectroscopic properties, *J. Am. Chem. Soc.*,137(7):2555–2564.
- [109] K., Schneider and H.G., Schlegel, 1981. Production of superoxide radicals by soluble hydrogenase from *Alcaligenes eutrophus* H16., *Biochem. J.*,193(1):99–107.
- [110] O., Lenz, M., Ludwig, T., Schubert, I., Bürstel, S., Ganskow, T., Goris, A., Schwarze, B.,Friedrich, 2010. H₂ conversion in the presence of O₂ as performed by the membrane-bound [NiFe]-Hydrogenase of *Ralstonia eutropha*, *Chem. Phys. Chem* ,11(6):1107–1119.
- [111] C., Schäfer, B., Friedrich, and O., Lenz, 2013. Novel, oxygen-insensitive group 5 [NiFe]-hydrogenase in *Ralstonia eutropha*, *Appl. Environ. Microbiol.*,79(17):5137–5145.

- [112] M., Bernhard, T., Buhrke, B., Bleijlevens, A.L., De Lacey, V.M., Fernandez, S.P., Albracht, B., Friedrich, 2001. The H₂ sensor of *Ralstonia eutropha*: Biochemical characteristics, spectroscopic properties, and its interaction with a histidine protein kinase," *J. Biol. Chem.*, 276(19):15592–15597.
- [113] T., Buhrke, O., Lenz, N., Krauss, and B., Friedrich, 2005. Oxygen tolerance of the H₂-sensing [NiFe] hydrogenase from *Ralstonia eutropha* H16 is based on limited access of oxygen to the active site, *J. Biol. Chem.*, 280(25):23791–23796.
- [114] A., Böck, P.W., King, M., Blokesch, and M.C., Posewitz, 2006. Maturation of Hydrogenases, *Advances in Microbial Physiology*, 51:1-71.
- [115] M.J., Lacasse and D.B., Zamble, 2016. [NiFe]-Hydrogenase Maturation, *Biochemistry*, 55(12):1689–1701.
- [116] E., Schwartz, A., Henne, R., Cramm, T., Eitinger, B., Friedrich, and G., Gottschalk, 2003. Complete nucleotide sequence of pHG1: A *Ralstonia eutropha* H16 megaplasmid encoding key enzymes of H₂-based lithoautotrophy and anaerobiosis, *J. Mol. Biol.*, 332(2):369–383.
- [117] P., Tamagnini, E., Leitão, P., Oliveira, D., Ferreira, F., Pinto, D.J., Harris, T., Heidorn, P., Lindblad, 2007. Cyanobacterial hydrogenases: Diversity, regulation and applications, *FEMS Microbiol. Rev.*, 31(6):692–720.
- [118] D., Hoffmann, K., Gutekunst, M., Klissenbauer, R., Schulz-Friedrich, and J., Appel, 2006. Mutagenesis of hydrogenase accessory genes of *Synechocystis* sp. PCC 6803: Additional homologues of hypA and hypB are not active in hydrogenase maturation, *FEBS J.*, 273(19):4516–4527.
- [119] I., Bürstel, E., Siebert, S., Frielingsdorf, I., Zebger, B., Friedrich, and O., Lenz, 2016. CO synthesized from the central one-carbon pool as source for the iron carbonyl in O₂-tolerant [NiFe]-hydrogenase, *Proc. Natl. Acad. Sci. U. S. A.*, 113(51):14722–14726.
- [120] A.C., Schulz, S., Frielingsdorf, P., Pommerening, L., Lauterbach, G., Bistoni, F., Neese, M., Oestreich, O., Lenz, 2020. Formyltetrahydrofolate Decarbonylase Synthesizes the Active Site CO Ligand of O₂-Tolerant [NiFe] Hydrogenase, *J. Am. Chem. Soc.*, 142(3):1457–1464.
- [121] S., Watanabe, D., Sasaki, T., Tominaga, and K., Miki, 2012. Structural basis of [NiFe] hydrogenase maturation by Hyp proteins, *Biol. Chem.*, 393(10):1089–1100.
- [122] R.D., Britt, G., Rao, and L., Tao, 2020. Bioassembly of complex iron–sulfur enzymes: hydrogenases and nitrogenases, *Nat. Rev. Chem.*, 4(10):542–549.
- [123] S., Thiemermann, J., Dervedde, M., Bernhard, W., Schroeder, C., Massanz, and B., Friedrich, 1996. Carboxyl-terminal processing of the cytoplasmic NAD-reducing

- hydrogenase of *Alcaligenes eutrophus* requires the *hoxW* gene product, *J. Bacteriol.*, 178(8):2368–2374.
- [124] Q., Fan, G., Caserta, C., Lorent, I., Zebger, P., Neubauer, O., Lenz and M., Gimpel, 2022. High-Yield Production of Catalytically Active Regulatory [NiFe]-Hydrogenase From *Cupriavidus necator* in *Escherichia coli*, *Front. Microbiol.*, 13:1–13.
- [125] M.A., Wells J., Mercer, R.A., Mott, A.G. Pereira-Medrano, A.M. Burja, H., Radianingtyas, P.C., Wright, 2011. Engineering a non-native hydrogen production pathway into *Escherichia coli* via a cyanobacterial [NiFe] hydrogenase, *Metab. Eng.*, 13(4):445–453.
- [126] C.M., Lamont and F., Sargent, 2017. Design and characterisation of synthetic operons for biohydrogen technology, *Arch. Microbiol.*, 199(3):495–503.
- [127] H., Teramoto, T., Shimizu, M., Suda, and M., 2022. Inui, Hydrogen production based on the heterologous expression of NAD⁺-reducing [NiFe]-hydrogenase from *Cupriavidus necator* in different genetic backgrounds of *Escherichia coli* strains, *Int. J. Hydrogen Energy*, 47(52):22010–22021.
- [128] J., Schiffels, O., Pinkenburg, M., Schelden, E.H.A.A., Aboulnaga, M.E.M., Baumann, and T., Selmer, 2013. An Innovative Cloning Platform Enables Large-Scale Production and Maturation of an Oxygen-Tolerant [NiFe]-Hydrogenase from *Cupriavidus necator* in *Escherichia coli*, *PLoS One*, 8,(7).
- [129] D., Ghosh, A., Bisailon, and P.C., Hallenbeck, 2013. Increasing the metabolic capacity of *Escherichia coli* for hydrogen production through heterologous expression of the *Ralstonia eutropha* SH operon, *Biotechnol. Biofuels*, 6(1):122.
- [130] S., Lupacchini, J., Appel, R., Stauder, P., Bolay, S., Klähn, E., Lettau, L. Adrian, L., Lauterbach, B., Bühler, A., Schmid, J., Toepel, 2021. Rewiring cyanobacterial photosynthesis by the implementation of an oxygen-tolerant hydrogenase, *Metab. Eng.*, 68:199–209.
- [131] J.A., Cracknell, K.A., Vincent, and F.A., Armstrong, 2008. Enzymes as working or inspirational electrocatalysts for fuel cells and electrolysis, *Chem. Rev.*, 108(7):2439–2461.
- [132] J., Ratzka, L., Lauterbach, O., Lenz, and M.B., Ansorge-Schumacher, 2011. Systematic evaluation of the dihydrogen-oxidising and NAD⁺-reducing soluble [NiFe]-hydrogenase from *Ralstonia eutropha* H16 as a cofactor regeneration catalyst, *Biocatal. Biotransformation*, 29(6):246–252.
- [133] L., Lauterbach, O., Lenz, and K.A., 2013. Vincent, H₂-driven cofactor regeneration with NAD(P)⁺-reducing hydrogenases, *FEBS J.*, 280(13):3058–3068.

- [134] H.A., Reeve, L., Lauterbach, P.A., Ash, O., Lenz, and K.A., Vincent, 2012. A modular system for regeneration of NAD cofactors using graphite particles modified with hydrogenase and diaphorase moieties, *Chem. Commun.*, 48(10):1589–1591.
- [135] L., Assil-Companiononi, S., Schmidt, P., Heidinger, H., Schwab, and R., Kourist, 2019. Hydrogen-Driven Cofactor Regeneration for Stereoselective Whole-Cell C=C Bond Reduction in *Cupriavidus necator*, *Chem. Sus. Chem*, 12(11):2361–2365.
- [136] L., Lauterbach and O., Lenz, 2019. How to make the reducing power of H₂ available for in vivo biosyntheses and biotransformations, *Curr. Opin. Chem. Biol.*, 49:91–96.
- [137] T.H., Lonsdale, L., Lauterbach, S., Honda Malca, B.M., Nestl, B., Hauer, and O., Lenz, 2015. H₂-driven biotransformation of n-octane to 1-octanol by a recombinant *Pseudomonas putida* strain co-synthesizing an O₂-tolerant hydrogenase and a P450 monooxygenase,” *Chem. Commun.*, 51(90):6173–16175.
- [138] A., Satta, L., Esquirol, and B.E., Ebert, 2023. Current Metabolic Engineering Strategies for Photosynthetic Bioproduction in Cyanobacteria, *Microorganisms*, 11(2):455.
- [139] D., Hanahan, 1983. Studies on transformation of *Escherichia coli* with plasmids, *J. Mol. Biol.*, 166(4):557–580.
- [140] R.Y., Stanier, R., Kunisawa, M., Mandel, and G., Cohen-Bazire, 1971. Purification and properties of unicellular blue-green algae (order Chroococcales)., *Bacteriol. Rev.*, 35(2):171–20.
- [141] E., Boutet, D., Lieberherr, M., Tognolli, M., Schneider, and A., Bairoch, 2007. UniProtKB/Swiss-Prot: The manually annotated section of the UniProt KnowledgeBase, *Methods Mol. Biol.*, 406:89–112.
- [142] M., Johnson, I., Zaretskaya, Y., Raytselis, Y., Merezhuk, S., McGinnis, and T.L., Madden, 2008. NCBI BLAST: a better web interface., *Nucleic Acids Res.*, 36(Web Server issue).
- [143] S., Shcolnick, Y., Shaked, and N., Keren, 2007. A role for mrgA, a DPS family protein, in the internal transport of Fe in the cyanobacterium *Synechocystis* sp. PCC6803, *Biochim. Biophys. Acta - Bioenerg.*, 1767(6):814–819.
- [144] O., Lenz, L., Lauterbach, and S., Frielingsdorf, 2018. O₂-tolerant [NiFe]-hydrogenases of *Ralstonia eutropha* H16: Physiology, molecular biology, purification, and biochemical analysis,” *Methods in Enzymology*, 613:117–151.
- [145] M., Ortega-Ramos, T., Jittawuttipoka, P., Saenkham, A., Czarnecka-Kwasiborski, H., Bottin, C., Cassier-Chauvat, F., Chauvat, 2014. Engineering *Synechocystis* PCC6803 for hydrogen production: Influence on the tolerance to oxidative and sugar stresses, *PLoS*

- One*, 9(2):1–13.
- [146] R.D., Gietz and R.H., Schiestl, 2007. Large-scale high-efficiency yeast transformation using the LiAc/SS carrier DNA/PEG method, *Nat. Protoc.*, 2(1):38–41.
- [147] G., Bertani, 2004. Lysogeny at Mid-Twentieth Century: P1, P2, and Other Experimental Systems, *J. Bacteriol.*, 186(3):595–600.
- [148] D.H., Juers, B.W., Matthews, and R.E., Huber, 2012. LacZ β -galactosidase: Structure and function of an enzyme of historical and molecular biological importance, *Protein Science*, 21(12):1792–1807.
- [149] K., Mullis, F., Faloona, S., Scharf, R., Saiki, G., Horn, and H., Erlich, 1986. Specific enzymatic amplification of DNA *in vitro*: The polymerase chain reaction, *Cold Spring Harb. Symp. Quant. Biol.*, 51(1):263–273.
- [150] P.Y., Lee, J., Costumbrado, C.Y., Hsu, and Y.H., Kim, 2012. Agarose gel electrophoresis for the separation of DNA fragments, *J. Vis. Exp.*, 62: e3923.
- [151] C., Engler, R., Kandzia, and S., Marillonnet, 2008. A one pot, one step, precision cloning method with high throughput capability,” *PLoS One*, 3(11): e3647.
- [152] S., Werner, C., Engler, E., Weber, R., Gruetzner, and S., Marillonnet, 2012. Fast track assembly of multigene constructs using golden gate cloning and the MoClo system, *Bioeng. Bugs*, 3(1):38–43.
- [153] R., Vasudevan, G.A.R., Gale, A.A. Schiavon, A., Puzorjov, J., Malin, M.D., Gillespie, K., Vavitsas, V., Zulkower, B., Wang, C.J., Howe, D.J., Lea-Smith, A.J., McCormick, 2019. Cyanogate: A modular cloning suite for engineering cyanobacteria based on the plant moclo syntax, 180(1):39-55.
- [154] E. Martínez-García, A., Goñi-Moreno, B., Bartley, J., McLaughlin, L., Sánchez-Sampedro, H., Pascual Del Pozo, C.P., Hernández, A.S. Marletta, D., De Lucrezia, G., Sánchez-Fernández, S., Fraile, V., de Lorenzo, 2020. SEVA 3.0: An update of the Standard European Vector Architecture for enabling portability of genetic constructs among diverse bacterial hosts, *Nucleic Acids Res.*, 48(D1):D1164–D1170.
- [155] W.J., Dower, J.F., Miller, and C.W., Ragsdale, 1988. High efficiency transformation of *E. coli* by high voltage electroporation, *Nucleic Acids Res.*, 16(13):6127–6145.
- [156] D.A., Julin, 2018. Blue/White Selection, *Molecular Life Sciences*, 72–73.
- [157] F. Brandenburg , E., Theodosiou, C., Bertelmann, M., Grund, S., Klähn, A., Schmid, J.O., Krömer, 2021. Trans-4-hydroxy-L-proline production by the cyanobacterium *Synechocystis* sp. PCC 6803, *Metab. Eng. Commun.*, 12:e00155.

- [158] F., Sanger, S., Nicklen, and A.R., Coulson, 1977. DNA sequencing with chain-terminating inhibitors., *Proc. Natl. Acad. Sci. U. S. A.*, 74(12):5463–5467.
- [159] S., Hein, I., Scholz, V., Björn, and W.R., Hess, 2013. Adaptation and modification of three CRISPR loci in two closely related cyanobacteria,” *RNA Biol.*,10(5):852–864.
- [160] C., Steglich, M.E., Futschik, D., Lindell, B., Voss, S.W., Chisholm, and W.,R. Hess, 2008. The challenge of regulation in a minimal photoautotroph: Non-coding RNAs in *Prochlorococcus*, *PLoS Genet.*,4(8):e1000173.
- [161] F., Pinto, C.C., Pacheco, D., Ferreira, P., Moradas-Ferreira, and P., Tamagnini, 2012. Selection of suitable reference genes for RT-qPCR analyses in cyanobacteria, *PLoS One*, 7(4):e34983.
- [162] K.J., Livak and T.D., Schmittgen, 2001. Analysis of relative gene expression data using real-time quantitative PCR and the 2- $\Delta\Delta$ CT method, *Methods*, 25(4):402–408.
- [163] M.M., Bradford, 1976. A rapid and sensitive method for the quantitation of microgram quantities of protein utilizing the principle of protein-dye binding, *Anal. Biochem.*, 72(1–2):248–254.
- [164] K., Seidel, J., Kühnert, and L., Adrian, 2018. The complexome of *Dehalococcoides mccartyi* reveals its organohalide respiration-complex is modular, *Front. Microbiol.*,9:1130.
- [165] U.K., Laemmli, 1970. Cleavage of structural proteins during the assembly of the head of bacteriophage T4, *Nature*, 227(5259):680–685.
- [166] H., Towbin, T., Staehelin, and J., Gordon, 1979. Electrophoretic transfer of proteins from polyacrylamide gels to nitrocellulose sheets: Procedure and some applications, *Proc. Natl. Acad. Sci. U. S. A.*, 76(9):4350–4354.
- [167] A., Hoschek, J., Toepel, A., Hochkeppel, R., Karande, B., Bühler, and A., Schmid, 2019. Light-Dependent and Aeration-Independent Gram-Scale Hydroxylation of Cyclohexane to Cyclohexanol by CYP450 Harboring *Synechocystis* sp. PCC 6803, *Biotechnol. J.*,14(8).
- [168] K., Gutekunst, D., Hoffmann, U., Westernströer, R., Schulz, D., Garbe-Schönberg, and J., Appel, 2018. In-vivo turnover frequency of the cyanobacterial NiFe-hydrogenase during photohydrogen production outperforms in-vitro systems, *Sci. Rep.*, 8,(1):1–10.
- [169] A., Krishnan, X., Qian, G., Ananyev, D., S., Lun, and G.C., Dismukes, 2018. Rewiring of cyanobacterial metabolism for hydrogen production: Synthetic biology approaches and challenges, *Adv. Exp. Med. Biol.*, 1080:171–213.
- [170] N., Khanna and P., Lindblad, 2015. Cyanobacterial hydrogenases and hydrogen metabolism revisited: Recent progress and future prospects, *Int. J. Mol. Sci.*, 16(5): 10537–

10561.

- [171] M.L., Ghirardi, 2015. Implementation of photobiological H₂ production: The O₂ sensitivity of hydrogenases, *Photosynth. Res.*, 125(3):383–393.
- [172] W., Khetkorn, R.P., Rastogi, A., Incharoensakdi, P., Lindblad, D., Madamwar, A., Pandey, C., Larroche, 2017. Microalgal hydrogen production – A review, *Bioresour. Technol.*, 243:1194–1206.
- [173] Y., Lu and J., Koo, 2019. O₂ sensitivity and H₂ production activity of hydrogenases—A review, *Biotechnol. and Bioeng.*, 116(11):3124–3135.
- [174] P.C., Hallenbeck, M., Abo-Hashesh, and D., Ghosh, 2012. Strategies for improving biological hydrogen production, *Bioresour. Technol.*, 110:1–9.
- [175] M., Rögner, 2013. Metabolic engineering of cyanobacteria for the production of hydrogen from water, *Biochem. Soc. Trans.*, 41(5):1254–1259.
- [176] Q., Fan, P., Neubauer, O., Lenz, and M., Gimpel, 2020. Heterologous hydrogenase overproduction systems for biotechnology—an overview, *Int. J. Mol. Sci.*, 21(16):1–25.
- [177] L., Avilan, B., Roumezi, V., Risoul, C.S., Bernard, A., Kpebe, M., Belhadjassine, M., Rousset, M., Brugna & A., Latifi, 2018. Phototrophic hydrogen production from a clostridial [FeFe] hydrogenase expressed in the heterocysts of the cyanobacterium Nostoc PCC 7120, *Appl. Microbiol. Biotechnol.*, 102(13):5775–5783.
- [178] M., Cano, A., Volbeda, G., Guedeney., E., Aubert-Jousset, P., Richaud, G., Peltier, L., Cournac, 2014. Improved oxygen tolerance of the *Synechocystis* sp. PCC 6803 bidirectional hydrogenase by site-directed mutagenesis of putative residues of the gas diffusion channel,” *Int. J. Hydrogen Energy*, 39(30):16872–16884.
- [179] J., Koo and J.R., Swartz, 2018. System analysis and improved [FeFe] hydrogenase O₂ tolerance suggest feasibility for photosynthetic H₂ production, *Metab. Eng.*, 49:21–27.
- [180] W., Song, J., Cheng, J., Zhao, C., Zhang, J., Zhou, and K., Cen, “Enhancing hydrogen production of *Enterobacter aerogenes* by heterologous expression of hydrogenase genes originated from *Synechocystis* sp.,” *Bioresour. Technol.*, vol. 216, pp. 976–980, 2016.
- [181] M., Ihara, Y., Kawano, M., Urano, and A., Okabe, 2013. Light Driven CO₂ Fixation by Using Cyanobacterial Photosystem I and NADPH-Dependent Formate Dehydrogenase, *PLoS One*, 8(8): e71581.
- [182] M., Ihara, H., Nishihara, K., Yoon, O., Lenz, B., Friedrich, H., Nakamoto, K., Kojima, D., Honma, T., Kamachi, I., Okura, 2006. Light-driven Hydrogen Production by a Hybrid Complex of a [NiFe]-Hydrogenase and the Cyanobacterial Photosystem I, *Photochem.*

Photobiol., 82(3):676.

- [183] A., Kanygin Y., Milrad, C., Thummala, K., Reifschneider, P., Baker, P., Marco, I., Yacoby, and K.E., Redding, 2020. Rewiring photosynthesis: A photosystem I-hydrogenase chimera that makes H₂: *In vivo*, *Energy Environ. Sci.*, 13(9):2903–2914.
- [184] C.E., Lubner P., Knörzer, P.J.N., Silva, K.A., Vincent, T., Happe, D.A., Bryant, J.H., Golbeck, 2010. Wiring an [FeFe]-hydrogenase with Photosystem i for light-induced hydrogen production, *Biochemistry*, 49(48):10264–10266.
- [185] A., Schwarze, M.J., Kopczak, M., Rogner, and O., Lenz, 2010. Requirements for construction of a functional hybrid complex of photosystem I and [NiFe]-hydrogenase, *Appl. Environ. Microbiol.*, 76(8):2641–2651.
- [186] P., Till, J., Toepel, B., Bühler, R.L., Mach, and A.R., Mach-Aigner, 2020. Regulatory systems for gene expression control in cyanobacteria, *Appl. Microbiol. Biotechnol.*, 104(5):1977–1991.
- [187] M., Grund, T., Jakob, C., Wilhelm, B., Bühler, and A., Schmid, 2019. Electron balancing under different sink conditions reveals positive effects on photon efficiency and metabolic activity of *Synechocystis* sp. PCC 6803, *Biotechnol. Biofuels*, 12:43.
- [188] M., Barz, C., Beimgraben, T., Staller, F., Germer, F., Opitz, C., Marquardt, C., Schwarz, K., Gutekunst, K.H., Vanselow, R., Schmitz, J., LaRoche, R., Schulz, J., Appel, 2010. Distribution analysis of hydrogenases in surface waters of marine and freshwater environments, *PLoS One*, 5(11):e13846.
- [189] V., Puggioni, S., Tempel, and A., Latifi, 2016. Distribution of hydrogenases in cyanobacteria: A phylum-wide genomic survey, *Front. Genet.*, 7:1–14.
- [190] T., Sleutels, R., Sebastião Bernardo, P., Kuntke, M., Janssen, C.J.N., Buisman, and H.V.M., Hamelers, 2020. Enhanced Phototrophic Biomass Productivity through Supply of Hydrogen Gas, *Environ. Sci. Technol. Lett.*, 7(11):861–865.
- [191] D.C., Ducat, G., Sachdeva, and P.A., Silver, 2011. Rewiring hydrogenase-dependent redox circuits in cyanobacteria, *Proc. Natl. Acad. Sci. U. S. A.*, 108(10):3941–3946.
- [192] T., Huokko, D., Muth-Pawlak, and E., M. Aro, 2019. Thylakoid localized type 2 NAD(P)H dehydrogenase NDBA optimizes light-activated heterotrophic growth of *Synechocystis* sp. PCC 6803, *Plant Cell Physiol.*, 60(6):1386–1399.
- [193] T., Huokko, D., Muth-Pawlak, N., Battchikova, Y., Allahverdiyeva, and E.M., Aro, 2017. Role of type 2 NAD(P)H dehydrogenase NdbC in redox regulation of carbon allocation in *synechocystis*, *Plant Physiol.*, 174(3):1863–1880.

- [194] J., Kämäräinen, T., Huokko, S., Kreula, P.R., Jones, E.M., Aro, and P., Kallio, 2017. Pyridine nucleotide transhydrogenase PntAB is essential for optimal growth and photosynthetic integrity under low-light mixotrophic conditions in *Synechocystis* sp. PCC 6803,” *New Phytol.*, 214(1):194–204.
- [195] G., Peltier, E.M., Aro, and T., Shikanai, 2016. NDH-1 and NDH-2 Plastoquinone Reductases in Oxygenic Photosynthesis, *Ann. Rev. Plant Biol.*, 67:55–80.
- [196] J., Appel and R., Schulz, 1998. Hydrogen metabolism in organisms with oxygenic photosynthesis: Hydrogenases as important regulatory devices for a proper redox poisoning?, *J. Photochem. and Photobiol. B: Biology*, 47(1):1–11.
- [197] A., Frenkel, H., Gaffron, and E.H., Battley, 1950. Photosynthesis and photoreduction by the blue green alga, *Synechococcus elongatus*, Näg.,” *Biol. Bull.*, 99(2):157–162.
- [198] M.L., Theune, S., Hildebrandt, A., Steffen-Heins, W., Bilger, K., Gutekunst, and J., Appel, 2021. *In-vivo* quantification of electron flow through photosystem I – Cyclic electron transport makes up about 35% in a cyanobacterium, *Biochim. Biophys. Acta - Bioenerg.*, 1862(3):148353.
- [199] J., Nogales, S., Gudmundsson, E.M., Knight, B.O., Palsson, and I., Thiele, 2012. Detailing the optimality of photosynthesis in cyanobacteria through systems biology analysis, *Proc. Natl. Acad. Sci. U. S. A.*, 109(7):2678–2683.
- [200] J., Preissler, H.A., Reeve, T., Zhu, J., Nicholson, K., Urata, L., Lauterbach, L.L., Wong, K.A., Vincent, Oliver Lenz 2020. Dihydrogen-Driven NADPH Recycling in Imine Reduction and P450-Catalyzed Oxidations Mediated by an Engineered O₂-Tolerant Hydrogenase, *Chem. Cat. Chem*, 12(19):4853–4861.
- [201] J.K.B., Cahn, C.A., Werlang, A., Baumschlager, S., Brinkmann-Chen, S.L., Mayo, and F. H., Arnold, 2017. A General Tool for Engineering the NAD/NADP Cofactor Preference of Oxidoreductases, *ACS Synth. Biol.*, 6(2):326–333.
- [202] J., Park and Y., Choi, , 2017. Cofactor engineering in cyanobacteria to overcome imbalance between NADPH and NADH: A mini review,,*Front. Chem. Sci. Eng.*, 11(1):66–71
- [203] A., Hoschek, A., Schmid, and B., Bühler, 2018. In Situ O₂ Generation for Biocatalytic Oxyfunctionalization Reactions, *Chem. Cat. Chem.*, 10(23):5366–5371
- [204] I. Staffell, D., Scamman, A., Velazquez Abad, P., Balcombe, P.E., Dodds, P.E., N. Shahd and K.R., Warda, 2019. The role of hydrogen and fuel cells in the global energy system, *Energy Environ. Sci.*, 12(2):463–491.
- [205] P.C., Hallenbeck, C.Z., Lazaro, and E., Sagir, 2018. CHAPTER 1: Photosynthesis and

- Hydrogen from Photosynthetic Microorganisms, *Compr. Ser. Photochem. Photobiol. Sci.*,16:3–30.
- [206] A., Trchounian, 2015. Mechanisms for hydrogen production by different bacteria during mixed-acid and photo-fermentation and perspectives of hydrogen production biotechnology, *Critical Rev. Biotechnol.*, 35(1):103–113.
- [207] D., Das and T.N., Veziroglu, 2008. Advances in biological hydrogen production processes, *Int. J. Hydrogen Energy*, 33(21):6046–6057.
- [208] K., Chandrasekhar, Y.J., Lee, and D.W., Lee, 2015. Biohydrogen production: Strategies to improve process efficiency through microbial routes, *Int. J. Mol. Sci.*,16(4):8266–8293.
- [209] M., Oey, A.L., Sawyer, I.L., Ross, and B., Hankamer, 2016. Challenges and opportunities for hydrogen production from microalgae, *Plant Biotechnol. J.*,14(7):1487–1499.
- [210] M.L., Ghirardi, A., Dubini, J., Yu, and P.C., Maness, 2009. Photobiological hydrogen-producing systems, *Chem. Soc. Rev.*, 38(1):52–61.
- [211] J.B., McKinlay and C.S., Harwood, 2010. Photobiological production of hydrogen gas as a biofuel, *Curr. Opin. Biotechnol.*, 21(3):244–251.
- [212] A.A., Esteves-Ferreira, J.H.F., Cavalcanti, M.G.M.V., Vaz, L.V., Alvarenga, A., Nunes-Nesi, and W.L., Araújo, 2017. Cyanobacterial nitrogenases: Phylogenetic diversity, regulation and functional predictions, *Genet. Mol. Biol.*, 40(1) 261–275.
- [213] N.J., Burroughs, M., Boehm, C., Eckert, G Mastroianni, E.M., Spence, J., Yu, P.J. Nixon, J.,Appel, C.W. Mullineaux, S.J., Bryan, 2014. Solar powered biohydrogen production requires specific localization of the hydrogenase, *Energy Environ. Sci.*, 7(11):3791–3800.
- [214] J., Appel, S., Phunpruch, K., Steinmüller, and R., Schulz, 2000. The bidirectional hydrogenase of *Synechocystis* sp. PCC 6803 works as an electron valve during photosynthesis, *Arch. Microbiol.*,173(5–6):333–338.
- [215] H., Burgstaller, Y., Wang, J., Caliebe, V., Hueren, J., Appel, M., Boehm, S., Leitzke, M., Theune, P.W. King, K. Gutekunst, 2022. *Synechocystis* sp. PCC 6803 Requires the Bidirectional Hydrogenase to Metabolize Glucose and Arginine Under Oxic Conditions, *Front. Microbiol.*,13:1–16.
- [216] P.D., Weyman, W.A., Vargas, Y., Tong, J., Yu, P., Maness, H.O., Smith, Q., Xu, 2011. Heterologous expression of alteromonas macleodii and thiocapsa roseopersicina [NiFe] hydrogenases in synechococcus elongatus, *PLoS One*, 6(5):e20126.
- [217] W., Baebprasert, S., Jantaro, W., Khetkorn, P., Lindblad, and A., Incharoensakdi, 2011. Increased H₂ production in the cyanobacterium *Synechocystis* sp. strain PCC 6803 by

- redirecting the electron supply via genetic engineering of the nitrate assimilation pathway, *Metab. Eng.*,13(5):610–616.
- [218] V., Nagy, A., Podmaniczki, A., Vidal-Meireles, R., Tengölics, L., Kovács, G., Rákhely, A., Scoma & S.Z., Tóth, 2018. Water-splitting-based, sustainable and efficient H₂ production in green algae as achieved by substrate limitation of the Calvin-Benson-Bassham cycle, *Biotechnol. Biofuels*,11(1):1–16.
- [219] D., Kannchen, J., Zabret, R., Oworah-Nkruma, N., Dyczmons-Nowaczyk, K., Wiegand, P., Löbber, A., Frank, M.M., Nowaczyk, S., Rexroth, M., Rögner, 2020. Remodeling of photosynthetic electron transport in *Synechocystis* sp. PCC 6803 for future hydrogen production from water, *Biochim. Biophys. Acta - Bioenerg.*,1861(8):148208.
- [220] E., Englund, F., Liang, and P., Lindberg, 2016. Evaluation of promoters and ribosome binding sites for biotechnological applications in the unicellular cyanobacterium *Synechocystis* sp. PCC 6803, *Sci. Rep.*, 6(36640).
- [221] D., Liu and H.B., Pakrasi, 2018. Exploring native genetic elements as plug-in tools for synthetic biology in the cyanobacterium *Synechocystis* sp. PCC 6803, *Microb. Cell Fact.*, 17(1):1–8.
- [222] K., Thiel, E., Mulaku, H., Dandapani, C., Nagy, E.M., Aro, and P., Kallio, 2018. Translation efficiency of heterologous proteins is significantly affected by the genetic context of RBS sequences in engineered cyanobacterium *Synechocystis* sp. PCC 6803, *Microb. Cell Fact.*,17(1):1–12.
- [223] K., Yoshikawa, T., Hirasawa, and H., Shimizu, 2015. Effect of malic enzyme on ethanol production by *Synechocystis* sp. PCC 6803, *J. Biosci. Bioeng.*,119(1):82–84.
- [224] A., Behle, P., Saake, A.T., Germann, D., Dienst, and I.M., Axmann, 2020. Comparative Dose-Response Analysis of Inducible Promoters in Cyanobacteria, *ACS Synth. Biol.*, vol. 9(4):843–855.
- [225] J., Zhou, H., Zhang, H., Meng, Y., Zhu, G., Bao, Y., Zhang, Y., Li, Y., Ma, 2014. Discovery of a super-strong promoter enables efficient production of heterologous proteins in cyanobacteria, *Sci. Rep.*,4:1–6.
- [226] A., Tüllinghoff, M.B., Uhl, F.E.H., Nintzel, A., Schmid, B., Bühler, and J., Toepel, 2022. Maximizing Photosynthesis-Driven Baeyer–Villiger Oxidation Efficiency in Recombinant *Synechocystis* sp. PCC6803, *Front. Catal.*, 1:780474.
- [227] T., Heidorn, D., Camsund, H., Huang, P., Lindberg, P., Oliveira, K., Stensjö, P., Lindblad 2011. Chapter Twenty-Four - Synthetic Biology in Cyanobacteria: Engineering and

- Analyzing Novel Functions, *Synthetic Biology, Part A*, 497:539–579.
- [228] C.L., Kelly, G.M., Taylor, A., Šatkutė, L., Dekker, and J.T., Heap, 2019. Transcriptional terminators allow leak-free chromosomal integration of genetic constructs in cyanobacteria, *Microorganisms*, 7(8).
- [229] G.A.R., Gale, B., Wang, and A.J., McCormick, 2021. Evaluation and Comparison of the Efficiency of Transcription Terminators in Different Cyanobacterial Species, *Front. Microbiol.*, 11: 624011.
- [230] M., Kadisch, C., Willrodt, M., Hillen, B., Bühler, and A., Schmid, 2017. Maximizing the stability of metabolic engineering-derived whole-cell biocatalysts, *Biotechnol. J.*, 12(8).
- [231] M., Eriksen, K., Sneppen, S., Pedersen, and N., Mitarai, 2017. Occlusion of the ribosome binding site connects the translational initiation frequency, mRNA stability and premature transcription termination, *Front. Microbiol.*, 8:362.
- [232] B., Wang, J., Wang, and D.R., Meldrum, 2012. Application of synthetic biology in cyanobacteria and algae, *Front. Microbiol.*, 3:344.
- [233] A.G., Roberts, M.K., Bowman, and D.M., Kramer, 2004. The inhibitor DBMIB provides insight into the functional architecture of the Qo site in the cytochrome b6f complex, *Biochemistry*, 43(24):7707–7716.
- [234] D., Fitzpatrick, E.M., Aro, and A., Tiwari A, 2020. A Commonly Used Photosynthetic Inhibitor Fails to Block Electron Flow to Photosystem I in Intact Systems, *Front. Plant Sci.*, 11(382):1–9.
- [235] A., Santana-Sanchez, D., Solymosi, H., Mustila, L., Bersanini, E.M., Aro, and Y., Allahverdiyeva, 2019. Flavodiiron proteins 1–to-4 function in versatile combinations in O₂ photoreduction in cyanobacteria, *Elife*, 8: e45766.
- [236] D.J., Lea-Smith, P., Bombelli, R., Vasudevan, and C.J., Howe, 2016. Photosynthetic, respiratory and extracellular electron transport pathways in cyanobacteria, *Biochim. Biophys. Acta - Bioenerg.*, 1857(3):247–255.
- [237] C.A., Howitt, P.K., Udall, and W.F.J., Vermaas, 1999. Type 2 NADH dehydrogenases in the cyanobacterium *Synechocystis* sp. Strain PCC 6803 are involved in regulation rather than respiration, *J. Bacteriol.*, 181(13):3994–4003.
- [238] J.D., Sutherland, 2017. Opinion: Studies on the origin of life-The end of the beginning, *Nat. Rev. Chem.*, 1:1–8.
- [239] J. Liu, , S., Chakraborty, P., Hosseinzadeh, Y., Yu, S., Tian, I., Petrik, A., Bhagi, Y., Lu, 2014. Metalloproteins containing cytochrome, iron-sulfur, or copper redox centers, *Chem.*

- Rev.*,114(8):4366–4369.
- [240] M., Blokesch, A., Paschos, E., Theodoratou, A., Bauer, M., Hube, S., Huth, A., Böck 2002. Metal insertion into NiFe-hydrogenases, *Biochem. Soc. Trans.*, 30(4):674–680.
- [241] G., Caserta, S., Hartmann, C., Van Stappen, C., Karafoulidi-Retsou, C., Lorent, S., Yelin, M., Keck, J., Schoknecht, I., Sergueev, Y., Yoda, P., Hildebrandt, C., Limberg, S., DeBeer, I., Zebger, S., Frielingsdorf & O., Lenz, 2022. Stepwise assembly of the active site of, *Nature Chem. Biol.*, 19:498-506.
- [242] L., Forzi and R.G., Sawers, 2007. Maturation of [NiFe]-hydrogenases in *Escherichia coli*, *BioMetals*, 20(3–4):565–578.
- [243] G. M. Rögner 2015. (ed): Biohydrogen. *Photosynth. Res.* 124, 337–339.
- [244] F., Opel, M. A., Itzenhäuser, I., Wehner, S., Lupacchini, L., Lauterbach, O., Lenz, S., Klähn, 2023. Toward a synthetic hydrogen sensor in cyanobacteria : Functional production of an oxygen-tolerant regulatory hydrogenase in *Synechocystis* sp . PCC 6803, 14:1122078.
- [245] D., Liu, V.M., Johnson, and H.B., Pakrasi, 2020. A Reversibly Induced CRISPRi System Targeting Photosystem II in the Cyanobacterium *Synechocystis* sp. PCC 6803, *ACS Synth. Biol.*, 9(6):1441–1449.
- [246] I., Bürstel, P., Hummel, E., Siebert, N., Wisitruangsakul, I., Zebger, B., Friedrich, O., Lenz, 2011. Probing the origin of the metabolic precursor of the CO ligand in the catalytic center of [NiFe] hydrogenase, *J. Biol. Chem.*, 286(52):44937–44944.
- [247] Z.X., Zhang, F., Nong, Y., Wang, C., Yan, Y., Gu, P., Song., X., Sun, 2022. Strategies for efficient production of recombinant proteins in *Escherichia coli*: alleviating the host burden and enhancing protein activity, *Microb. Cell Fact.*, 21(1):1–18.
- [248] R.M., Schuurmans, J.C.P., Matthijs, and K.J., Hellingwerf, 2017. Transition from exponential to linear photoautotrophic growth changes the physiology of *Synechocystis* sp. PCC 6803, *Photosynth. Res.*, 132(1): 69–82.
- [249] D., Herbert, 1976. Stoichiometric aspects of microbial growth., *Contin. Cult.*, 6:1–30.
- [250] J. W., Cooley and W.F.J., Vermaas, 2001. Succinate dehydrogenase and other respiratory pathways in thylakoid membranes of *Synechocystis* sp. strain PCC 6803: Capacity comparisons and physiological function, *J. Bacteriol.*, 183(14):4251–4258.
- [251] K.A., Vincent, A., Parkin, O., Lenz, S.P.J., Albracht, J.C., Fontecilla-Camps, R., Cammack, B., Friedrich, F.A., Armstrong, 2005. Electrochemical definitions of O₂ sensitivity and oxidative inactivation in hydrogenases, *J. Am. Chem. Soc.*, 127(51):18179–18189.
- [252] O., Lampret, C., Brocks, and M., Winkler, 2021. O₂ escape strategies for hydrogenases in

- application, *Photosynth. Biotechnol. Appl. Microalgae*, edited by Matthias Rögner, Berlin, Boston: De Gruyter, 93-128.
- [253] W., Lubitz, H., Ogata, O., Rüdiger, and E., Reijerse, 2014. Hydrogenases, *Chem. Rev.*, 114(8):4081–4148.
- [254] J., Koo, 2020. Enhanced aerobic H₂ production by engineering an [FeFe] hydrogenase from *Clostridium pasteurianum*, *Int. J. Hydrogen Energy*, 45(18):10673–10679.
- [255] M., Winkler, J., Duan, A., Rutz, C., Felbek, L., Scholtysek, O., Lampret, J. Jaenecke, U., Apfel, G., Gilardi, F., Valetti, V., Fourmond, E., Hofmann, C., Léger & T., Happe, 2021. A safety cap protects hydrogenase from oxygen attack, *Nat. Commun.*,12(1).
- [256] S., Morra, A., Giraudo, G., Di Nardo, P.W., King, G., Gilardi, and F., Valetti, 2012. Site Saturation Mutagenesis Demonstrates a Central Role for Cysteine 298 as Proton Donor to the Catalytic Site in CaHydA [FeFe]-Hydrogenase, *PLoS One*, 7(10).
- [257] G., Caserta, C., Papini, A., Adamska-Venkatesh, L., Pecqueur, C., Sommer, *et al.*, 2018. Engineering an [FeFe]-Hydrogenase: Do Accessory Clusters Influence O₂ Resistance and Catalytic Bias?, *J. Am. Chem. Soc.*,140(16):5516–5526.
- [258] P.P., Liebgott, A.L., Lacey, B., Burlat, L., Cournac, P., Richaud, M., Brugna, V.M. Fernandez, B., Guigliarelli, M., Rousset, C., Léger, S., Dementin, 2011. Original design of an oxygen-tolerant [NiFe] hydrogenase: Major effect of a valine-to-cysteine mutation near the active site, *J. Am. Chem. Soc.*,133(4):986–997.
- [259] Q., Jiang, T., Li, J., Yang, C.M., Aitchison, J., Huang, Y., Chen, F., Huang, Q., Wang, A. I. Cooper and L., Liu, 2023. Synthetic engineering of a new biocatalyst encapsulating [NiFe]-hydrogenases for enhanced hydrogen production, *J. Mater. Chem. B*, 11:2684-2692.
- [260] C., Leplat, R., Champeimont, P., Saenkham, C., Cassier-Chauvat, A., Jean-Christophe, and F., Chauvat, 2013. Genome-wide transcriptome analysis of hydrogen production in the cyanobacterium *Synechocystis*: Towards the identification of new players, *Int. J. Hydrogen Energy*, 38(4):1866–1872.
- [261] G., Goldet, A.F, Wait, J.A. Cracknell, K.A. Vincent, M. Ludwig, O. Lenz, B., Friedrich, F.A. Armstrong, 2008. Hydrogen production under aerobic conditions by membrane-bound hydrogenases from *Ralstonia* species, *J. Am. Chem. Soc.*, 130(33):11106–11113.
- [262] S.T., Stripp, U., Lindenstrauss, C., Granich, R., G., Sawers, and B., Soboh, 2014. The influence of oxygen on [NiFe]-hydrogenase cofactor biosynthesis and how ligation of carbon monoxide precedes cyanation, *PLoS One*,9(9):e107488.

- [263] T., Buhrke and B., Friedrich, 1998. hoxX (hypX) is a functional member of the *Alcaligenes eutrophus* hyp gene cluster, *Arch. Microbiol.*,170(6):460–463.
- [264] R., Aoki, T., Goto, and Y., Fujita, 2011. A heme oxygenase isoform is essential for aerobic growth in the cyanobacterium *Synechocystis* sp. PCC 6803: Modes of differential operation of two isoforms/enzymes to adapt to low oxygen environments in cyanobacteria, *Plant Cell Physiol.*, 52(10):1744–175.,
- [265] E.P., Hudson, 2021. Synthetic Biology in Cyanobacteria and Applications for Biotechnology, in *Cyanobacteria Biotechnology*,123–170.
- [266] G.C., Gordon and B.F., Pflieger, 2018. Regulatory tools for controlling gene expression in cyanobacteria, *Adv. Exp. Med. Biol.*,(1080):281–315.
- [267] P., Trieu-Cuot, C., Carlier, P., Martin, and P., Courvalin, 1987. Plasmid transfer by conjugation from *Escherichia coli* to Gram-positive bacteria, *FEMS Microbiol. Lett.*,48(1–2):289–294,
- [268] S. Watanabe, 2020. Cyanobacterial multi-copy chromosomes and their replication, *Biosci. Biotechnol. Biochem.*, 84(7):1309–1321.
- [269] L., Schäfer, K., Bühler, R., Karande, and B., Bühler, 2020. Rational Engineering of a Multi-Step Biocatalytic Cascade for the Conversion of Cyclohexane to Polycaprolactone Monomers in *Pseudomonas taiwanensis*, *Biotechnol. J.*, 15(11):e2000091.
- [270] J., Anfelt, D., Kaczmarzyk, K., Shabestary, B., Renberg, J., Rockberg, J., Nielsen, M., Uhlén & E.P., Hudson, 2015. Genetic and nutrient modulation of acetyl-CoA levels in *Synechocystis* for n-butanol production, *Microb. Cell. Fact.*,14, 167.
- [271] T., Buhrke, B., Bleijlevens, S.P.J., Albracht, and B., Friedrich, 2001. Involvement of hyp gene products in maturation of the H₂-sensing [NiFe] hydrogenase of *Ralstonia eutropha*, *J. Bacteriol.*,183(24):7087–7093.
- [272] H.C., Grimm, and R., Kourist, 2021. Cyanobacteria as catalysts for light-driven biotransformations, in *Photosynthesis: Biotechnological Applications with Microalgae*, 67–102.
- [273] S.B., Mellor, K., Vavitsas, A.Z., Nielsen, and P.E., Jensen, 2017. Photosynthetic fuel for heterologous enzymes: the role of electron carrier proteins, *Photosynth. Res.*, 134(3):329–342.
- [274] M., Tamoi, T., Miyazaki, T., Fukamizo, and S., Shigeoka, 2005. The Calvin cycle in cyanobacteria is regulated by CP12 via the NAD(H)/NADP(H) ratio under light/dark conditions, *Plant J.*, 42(4): 504–513.

- [275] H., Krassen, A., Schwarze, B., Friedrich, K., Ataka, O., Lenz, and J., Heberle, 2009. Photosynthetic hydrogen production by a hybrid complex of photosystem I and [NiFe]-hydrogenase, *ACS Nano*, 3(12):4055–4061.
- [276] C., David, K., Bühler, and A., Schmid, 2015. Stabilization of single species *Synechocystis* biofilms by cultivation under segmented flow, *J. Ind. Microbiol. Biotechnol.*, 42(7):1083–1089.
- [277] R.M.Q., Shanks, N.C., Caiazza, S.M., Hinsa, C.M., Toutain, and G.A., O'Toole, 2006. *Saccharomyces cerevisiae*-based molecular tool kit for manipulation of genes from gram-negative bacteria, *Appl. Environ. Microbiol.*, 72(7):5027–5036.
- [278] P., Prentki and H.M., Krisch, 1984. *In vitro* insertional mutagenesis with a selectable DNA fragment, *Gene*, 29(3):303–313.
- [279] B., Friedrich, E., Heine, A., Finck, and C.G., Friedrich, 1981. Nickel requirement for active hydrogenase formation in *Alcaligenes eutrophus*, *J. Bacteriol.*, 145(3):1144–1149.

Appendix

Supplementary Information to Chapter 2

Supplementary Tables

Table S2.1 Plasmids used and generated in this study

Plasmid	^a Characteristics		Ref.				
pMQ80	Expression vector for integration of <i>C. necator</i> <i>Hox</i> -operon; URA3, oriT, PoriV, rep, ColE1, aacC1, T1T2, yeast episomal plasmid replicon		[277]				
pGE3382	Carrying <i>C. necator</i> <i>hox</i> -operon HoxFUJHWI and <i>C. necator</i> <i>hyp</i> genes <i>hypB2F2D1E1X</i>		[139]				
pHP45Ω	Spectinomycin resistance cassette		[278]				
pAGS5	Hox1- <i>psbA2</i> -Hox2 construct		This study				
pAGS7	Hox1- <i>psbA2</i> -homSH1-homSH2-spec ^R -Hox2 construct		This study				
pAGS9	Hox1- <i>psbA2</i> -CnSH-spec ^R -Hox2 construct		This study				
pHySe_Hox_Hyp	pHySe_Hox backbone, <i>P_{nrsB}::hypA1B1F1CDEX</i> ^{codon, Strep}		[244]				
pSHDY_ <i>P_{rhaBAD}::mVenus_PJ23119-rhaS</i>	<i>P_{J23119}::rhaS, PrhaBAD</i>		[228] [244]				
Plasmid generated in this work and part of the Modular Cloning system							
Vector	Level	5' over hang	3' over hang	Backbone	Selection	Modified	Characteristics
pGGC 0	0	GATG	AAAG	pUC18	Amp ^R	yes	Level 0 empty entry vector based on pUC18 vector with additional integrated <i>Bpil/Bsal</i> restriction sites flanking LacZα
pGGC 8	0	GATG	AAAG	pGGC 0	Amp ^R	no	Level 0 <i>P_{nrsB}</i>
pGGC 9	0	GATG	AAAG	pGGC 0	Amp ^R	no	Level 0 <i>P_{rhaS}</i>
pGGC 10	0	GATG	AAAG	pGGC 0	Amp ^R	no	Level 0 <i>P_{psbA2}</i>
pGGC 11	0	GATG	AAAG	pGGC 0	Amp ^R	no	Level 0 Spec ^R
pGGC 12	0	GATG	AAAG	pGGC 0	Amp ^R	no	Level 0 T _{<i>psbC</i>}
pGGC 13	0	GATG	AAAG	pGGC 0	Amp ^R	no	Level 0 5' hom. region
pGGC 14	0	GATG	AAAG	pGGC 0	Amp ^R	no	Level 0 3' hom. region
pGGC 15	0	GATG	AAAG	pGGC 0	Amp ^R	no	Level 0 Cn <i>hox</i> operon
pGGC 39	0	GATG	AAAG	pGGC 0	Amp ^R	no	Level 0 pHG1_ <i>hypX</i>

pGGC 53	0	GATG	AAAG	pGGC 0	Amp ^R	no	Level 0 Kan ^R cassette
pGGC 57	0	GATG	AAAG	pGGC 0	Amp ^R	no	Level 0 <i>P</i> _{J23119} - <i>rhaS</i>
pGGC 115	0	GATC	AAAG	pGGC 0	Amp ^R	no	Level 0 <i>hyp</i> operon
pGGC 1	1	GCCA	GTTA	pUK21	Kan ^R	yes	Level 1 position 1 till 6 empty entry vector based on pUC19 vector with additional integrated <i>Bsal/Bpil</i> restriction sites flanking LacZα
pGGC 2	1	GTTA	CTAG	pUK21	Kan ^R	yes	
pGGC 3	1	CTAG	CAGA	pUK21	Kan ^R	yes	
pGGC 4	1	CAGA	TGTG	pUK21	Kan ^R	yes	
pGGC 5	1	TGTG	GAGC	pUK21	Kan ^R	yes	
pGGC 6	1	GAGC	AGGA	pUK21	Kan ^R	yes	
pGGC 16	1	GCCA	GTTA	pGGC 1	Kan ^R	no	Level 1 position 1 5' hom. region
pGGC 17	1	GTTA	CTAG	pGGC 2	Kan ^R	no	Level 1 position 2 <i>P</i> _{nrsB}
pGGC 18	1	GTTA	CTAG	pGGC 2	Kan ^R	no	Level 1 position 2 <i>P</i> _{rhaS}
pGGC 19	1	GTTA	CTAG	pGGC 2	Kan ^R	no	Level 1 position 2 <i>P</i> _{psbA2}
pGGC 20	1	CTAG	CAGA	pGGC 3	Kan ^R	no	Level 1 position 3 <i>Cnhox</i> operon
pGGC 21	1	CAGA	TGTG	pGGC 4	Kan ^R	no	Level 1 position 4 <i>T</i> _{psbC}
pGGC 22	1	TGTG	GAGC	pGGC 5	Kan ^R	no	Level 1 position 5 Spec ^R
pGGC 23	1	GAGC	AGGA	pGGC 6	Kan ^R	no	Level 1 position 6 3' hom. region
pGGC 40	1	GCCA	GTTA	pUK21	Kan ^R	yes	Endlinker level 1 spanning position 1 till 2 based on pUC19 vector with additional integrated <i>Bsal/Bpil</i> restriction sites flanking endlinker sequence TCGGTCACATGTGCATCCTCGATCTCA
pGGC 43	1	GAGC	CATC	pUK21	Kan ^R	yes	Endlinker level 1 spanning position 5 till 7 based on pUC19 vector with additional integrated <i>Bsal/Bpil</i> restriction sites flanking endlinker sequence TCGGTCACATGTGCATCCTCGATCTCA
pGGC 44	1	GAGC	CATC	pUK21	Kan ^R	yes	Endlinker level 1 spanning position 6 till 7 based on pUC19 vector with additional integrated <i>Bsal/Bpil</i> restriction sites flanking endlinker sequence

							TCGGTCACATGTGCATCCT CGATCTCA
pGGC 47	1	AGGA	CATC	pUK21	Kan ^R	yes	Endlinker level 1 spanning position 7 till 7 based on pUC19 vector with additional integrated <i>Bsal/Bpil</i> restriction sites flanking endlinker sequence TCGGTCACATGTGCATCCT CGATCTCA
pGGC 90	1	TGTG	GAGC	pGGC 5	Kan ^R	no	Level 1 Kan ^R cassette
pGGC 82	1	CTAG	CAGA	pGGC 3	Kan ^R	no	Level 1 position 3 <i>hypX</i>
pGGC 85	1	GAGC	AGGA	pGGC 6	Kan ^R	no	Level 1 position 6 <i>P_{J23119}-rhaS</i>
pGGC 86	1	TGTG	GAGC	pGGC 5	Kan ^R	no	Level 1 position 5 <i>P_{J23119}-rhaS</i>
pGGC 116	1	CTAG	CAGA	pGGC 3	Kan ^R	no	Level 1 position 3 <i>hyp</i> operon
pGGC 46	2	GCCA	CATC	pBlues cript II SK (+)	Amp ^R	yes	Level 2 empty entry vector based on pBluescript II SK (+) vector with additional integrated <i>Bsal</i> restriction sites flanking <i>LacZα</i>
pGGC 208	2	GCCA	CATC	pSEVA 351	Amp ^R	yes	Level 2 empty entry vector based on pSEVA 351 vector with additional integrated <i>LacZα</i> flanked by <i>Bsal</i> restriction sites
pGGC 209	2	GCCA	CATC	pGGC 208	Amp ^R	no	Level 2 pGGC208 with pGGC 40; 17; 20; 21; 22 and 44
pGGC 212	2	GCCA	CATC	pGGC 46	Amp ^R	no	Level 2 pGGC 46 with pGGC 16; 17; 20; 21; 22, 23 and 47
pGGC 243	2	GCCA	CATC	pGGC 208	Chl ^R	no	Level 2 pGGC208 with pGGC 40; 17; 82; 21; 90 and 44
pGGC 244	2	GCCA	CATC	pGGC 208	Chl ^R	no	Level 2 pGGC 208 with pGGC 40; 18; 82; 21; 85; 90 and 47
pGGC 271	2	GCCA	CATC	pGGC 208	Chl ^R	no	Level 2 pGGC208 with pGGC 40; 17; 116; 21 and 43
pGGC 272	2	GCCA	CATC	pGGC 208	Chl ^R	no	Level 2 pGGC 208 with pGGC 40; pGGC 18; 116; 21; 86 and 44
pGGC 273	2	GCCA	CATC	pGGC 208	Chl ^R	no	Level 2 pGGC 208 with pGGC 40; pGGC 19; 116; 21; 86 and 43

^aURA3, orotidine-5_-phosphate decarboxylase gene from *S. cerevisiae*; oriT, origin of conjugal transfer; PoriV-rep, pRO1600 broad-host-range replicon; ColE1, high-copy-number variants of the narrow-host-range ColE1 origin of replication; aacC1, gentamicin resistance determinant from Tn1696; T1T2, *E. coli* rrnB transcriptional terminators; Hox1 and Hox2, upstream (Hox1) and downstream (Hox2) fragments of the *hox* operon of *Synechocystis* sp. PCC 6803; psbA2, light inducible promoter; homSH1 and homSH2,

homologous fragments of the 5' end of *hoxF* (homSH1) and the 3' end of *hoxW* (homSH2); *spec*^R, spectinomycin resistance cassette.

Table S2.2. Sequences of primers used in this study. A. Primers used in Chapter 3. In case of the primers used to generate Northern blot probes by *in vitro* transcription, the added T7 promoter is underlined. **B.** Primers designed to generate MoClo vectors. **C.** Primers designed for cloning in Level 0. GGTCTC is the *BsaI* recognition site. The designed 4 bp overhangs used to enter level 0 are given in yellow and primer binding region in bold. **D.** Primers used for the colony PCR and qRT-PCR.

A) Primer name	Sequence 5' -> 3'	Description
5' Hox_for	CCAAAAAACGGGTATGGAGAAACAGT AGAGAGTTGCGATAAAAAGCGTCAGGT AGGTTTTTATCTGCCAGTGAAGCCCTT	Amplification of downstream homologous region located upstream of <i>ssr2227</i> for integration of <i>C. necator hox</i> -operon
5' Hox_rev	AATATCCACTGGAACGCTAAAGCCGCAA TCGATAAAAGATGATTGGGAGAGCCTA	
3' Hox_for	ATCGACAAATACATAAGGAATTTAAATC AACGGGCATCACCGAGGGCATATCT	Amplification of upstream homologous region located downstream of <i>fabF</i> for integration of <i>C. necator hox</i> -operon
3' Hox_rev	ATTTGCACGGCGTCACACTTTGCTATGC CATAGCATTTTTATCCATAAGATTAGCGT CCCCACGGCACTGGCACTCTT	
psbA2_for	TGGTTTAGGCTCTCCAATCATCTTTTAT CGATTGCGGCTTTAGCGTTCCAG	Amplification of <i>psbA2</i> promotor region from <i>Synechocystis</i> sp. PCC6803
psbA2_rev	TTCTCCTAGATATGCCCTCGGTGATGCC GGTTGATTTAAATTCCTTATGTATTTGTC GAT	
5' <i>C. necator</i> HoxF_for	TCAGTTCCAATCTGAACATCGACAAATA CATAAGGAATTTAACCAAATGGATAGT CGTATCACGACAATACTCGA	Amplification of upstream homologous region of <i>hoxF</i> located on pGE3382 plasmid
5' <i>C. necator</i> HoxF_rev	TCTCTTGCGGCTGATCAGGTCGGCATC CTCATTTAAATTCGGGTCTGGTTTCGCCG AA	
3' <i>C. necator</i> HoxW_for	GACTGGGATTTCGCTTCGGCGAAACCGA CCCGAATTTAAATGAGGATGCCGACCT GATCAGC	Amplification of downstream homologous region of <i>hoxW</i> located on pGE3382 plasmid
3' <i>C. necator</i> HoxW_rev	ACCCGAGAGCTTGGCACCCAGCCTGCG CGATCACGAGGTTTGACGCTCGGC	
Spec_cas_for	TCGATGCGGGCCGAGCGTCAAACCTCG TGATCGCGCAGGCTGGGTGC	Amplification of <i>aadA</i> located on pHP45Ω plasmid
Spec_cas_rev	GAGTTCTCCTAGATATGCCCTCGGTGAT GCCGTTGATTTGCCCTCGCTAGATTTT AATGCCGAT	
Col-PCR_for 34	CCCCAGAGCAAATTGACTTGATTCA	Amplification of <i>Synechocystis</i> sp. PCC 6803 <i>hox</i> region including <i>C. necator hox</i> -operon
Col-PCR_rev 31	GTTTTTATCTGCCAGTGAAGCCCTT	
hoxF-T7_fw	TAATACGACTCACTATAGGGTAGAACGA CGCCGT	Primers for the generation of a probe against <i>hoxF</i> (probe covers range from nt +58 to +178 of the <i>hoxF</i> open reading frame)
hoxF_rev	ATCGACATACTTTGGGATGTTC	
5sRNA_for	TAATACGACTCACTATAGGAGAAAGAGG AACTTGGCATCGGAC	Primers for probe against 5S rRNA
5sRNA_rev	GTCATGGAACCACTCCGATCCC	
B) Primer name	Sequence 5' -> 3'	Primer target
P_LacZ_for	AAAACGCGTGCGCAACGCAATTAATGT GAG	LacZ fragemt

P_LacZ_rev	AAACCATGGCTATGCGGCATCAGAGCA GA	
P_BB_pUC18_for	AAACCATGGGGTCTCTAAAGAAGTCTTC TTAAGCCAGCCCCGACA	Level 0 backbone with flanking <i>Bpil</i> and <i>Bsal</i> sites
P_BB_pUC18_rev	AAAACGCGTGGTCTCTCATCTAGTCTTC TCACTGCCCGCTTTCCA	
P_pUC18_Bsal_remove_for	AAAGGTCTCAGGCTCTCGCGGTATCATT G	Level 0 vector remove of internal <i>Bsal</i> site
P_pUC18_Bsal_remove_rev	AAAGGTCTCAAGCCACGCTCACCGGCT CCAG	
p_BB_pUK21_for Pos1	AAACCATGGGAAGACAAAAGGTTAAGA GACCGGCGGGTGTGGTGGTTA	Level 1 Position 1 backbone with flanking <i>Bsal</i> and <i>Bpil</i> sites
p_BB_pUK21_rev Pos1	AAAACGCGTGAAGACTTCATCTGGCTGA GACCATTGCGTTGCGCTCACTG	
p_BB_pUK21_for Pos2	AAACCATGGGAAGACTTAAAGAGGAGA AATACTAGTGAGACCGGCGGGTGTGGT GGTTA	Level 1 Position 2 backbone with flanking <i>Bsal</i> and <i>Bpil</i> sites
p_BB_pUK21_rev Pos2	AAAACGCGTGAAGACAACATCTAACTGA GACCATTGCGTTGCGCTCACTG	
p_BB_pUK21_for Pos3	AAACCATGGGAAGACAAAAGCAGAAG AGACCGGCGGGTGTGGTGGTTA	Level 1 Position 3 backbone with flanking <i>Bsal</i> and <i>Bpil</i> sites
p_BB_pUK21_rev Pos3	AAAACGCGTGAAGACAACATCTAGTGA GACCATTGCGTTGCGCTCACTG	
p_BB_pUK21_for Pos4	AAACCATGGGAAGACAAAAGTGTGAG AGACCGGCGGGTGTGGTGGTTA	Level 1 Position 4 backbone with flanking <i>Bsal</i> and <i>Bpil</i> sites
p_BB_pUK21_rev Pos4	AAAACGCGTGAAGACAACATCTCTGTGA GACCATTGCGTTGCGCTCACTG	
p_BB_pUK21_for Pos5	AAACCATGGGAAGACAAAAGGAGCAG AGACCGGCGGGTGTGGTGGTTA	Level 1 Position 5 backbone with flanking <i>Bsal</i> and <i>Bpil</i> sites
p_BB_pUK21_rev Pos5	AAAACGCGTGAAGACAACATCCACATGA GACCATTGCGTTGCGCTCACTG	
p_BB_pUK21_for Pos6	AAACCATGGGAAGACAAAAGAGGAAG AGACCGGCGGGTGTGGTGGTTA	Level 1 Position 6 backbone with flanking <i>Bsal</i> and <i>Bpil</i> sites
p_BB_pUK21_rev Pos6	AAAACGCGTGAAGACAACATCGCTCTG AGACCATTGCGTTGCGCTCACTG	
EL 1-->2_for	AAAGAAGACAGAATTGGTCTCAGCCATC GGTCACATGTGCATCCTCGATCTCAGTT ATGAGACCGTGTGGTGGTTACGCGCAG	Level 1 End-linkers with flanking <i>Bsal</i> sites
EL 6-->7_for	AAAGAAGACAGAATTGGTCTCAGAGCTC GGTCACATGTGCATCCTCGATCTCACAT CTGAGACCGTGTGGTGGTTACGCGCAG	
EL 7-->7_for	AAAGAAGACAGAATTGGTCTCAACGTTT GGTCACATGTGCATCCTCGATCTCACAT CTGAGACCGTGTGGTGGTTACGCGCAG	
EL_rev	AAAGAAGACATAATTGCGTTGCGCTCAC TG	
P_pBI_Bsal_re m_for	AAAGGTCTCAGTGGCTCTCGCGGTATC A	Level 2 integrative vector remove of internal <i>Bsal</i> site
P_pBI_Bsal_re m_rev	AAAGGTCTCACACGCTCACCGGCTCC AGA	
P_BB_pBI_for Pos 7	AAACCATGGGGTCTCTCATCGACGCGC CCTGTAGCG	Level 2 integrative backbone with flanking <i>Bsal</i> sites
P_BB_pBI_rev Pos 7	AAAACGCGTGGTCTCATGGCTCACTGC CCGCTTTCCAG	

p_BB_pSEVA35 1_for	AAACTCGAGGGTCTCTCATCGGGTCCC CAATAATTACG	Level 2 replicative backbone with flanking <i>Bsal</i> sites	
p_BB_pSEVA35 1_rev	AAAACGCGTGGTCTCATGGCGGCATCA AATAAACGAAAGG		
C) Primer name	Sequence 5' -> 3'	Primer target	
P_Hox-Gen_F1	AAAGGTCTCG GATG ATGGATAGTCGTA TCACGACAATACT	<i>C. necator</i> <i>hox</i> -operon out of pGE3382 plasmid	
P_Hox-Gen_R1	AAAGGTCTCGGTTTCAATCACTTGTTCG GGC		
P_Hox-Gen_F2	AAAGGTCTCGAAACCATCGTCGACTCC AG		
P_Hox-Gen_R2	AAAGGTCTCGGTTTCAACGTTGTTGAC GC		
P_Hox-Gen_F3	AAAGGTCTCGAAACCTTTGCCGCCGT		
P_Hox-Gen_R3	AAAGGTCTCTCGATACCCGCACCGTAC		
P_Hox-Gen_F4	AAAGGTCTCTATCGAAGGGCCTGAATG TCG		
P_Hox-Gen_R4	AAAGGTCTCCGATACCATCATGTCCAC CTCG		
P_Hox-Gen_F5	AAAGGTCTCGTATCGCGCTTTCCGTACC		
P_Hox-Gen_R5	AAAGGTCTCGTCCTCTCCTTCCAGCGC		
P_Hox-Gen_F6	AAAGGTCTCGAGGACAAATGAGAGCCC		
P_Hox-Gen_R6	AAAGGTCTCAACACGTTGCCCATCG		
P_Hox-Gen_F7	AAAGGTCTCCGTGTTGAGCTGAAAGA TTGTC		
P_Hox-Gen_R7	AAAGGTCTCCGATACCACCAGCGGCAT		
P_Hox-Gen_F8	AAAGGTCTCGTATCGGTCTTTGACGCG G		
P_Hox-Gen_R8	AAAGGTCTCG CTTT CTAACCCCGTCCC CTCC		
P_PnrsB_F	AAAGGTCTCG GATG TTCCACCAGCAAA ATTCGCA		<i>P_{nrsB}</i> promoter out of gDNA from <i>Synechocystis</i> sp. PCC6803
P_PnrsB_R	AAAGGTCTCG CTTT AATTGGGAATTTGT CCAAGATTTT		
P_TpsbC_F	AAAGGTCTCG GATG ATTGAGACTTTTCT GATTTTGCAAAGG	<i>T_{psbC}</i> terminator out of gDNA from <i>Synechocystis</i> sp. PCC6803	
P_TpsbC_R	AAAGGTCTCG CTTT AACACCAGCGGGG AAAGG		
P_spec_F1	AAAGGTCTCG GATG TCGCGCAGGCTGG G	Spectinomycin resistance cassette out of pHP45Ω plasmid	
P_spec_R1	AAAGGTCTCCGGAAGTCCTCGGCCG		
P_spec_F2	AAAGGTCTCCTTCCGATCTCCTGAAGC CAG		
P_spec_R2	AAAGGTCTCGGTTTCCACGCATCGTCA G		
P_spec_F3	AAAGGTCTCGAAACCGAAACCTTGCGC TC		
P_spec_R3	AAAGGTCTCG CTTT CTAGATTTTAATGC GGATGTTGCGA		
P_3'HomReg_F 1	AAAGGTCTCG GATG GCATCACCGAGGG CATATCTAG		3' flanking region out of gDNA from <i>Synechocystis</i> sp. PCC6803
P_3'HomReg_R 1	AAAGGTCTCGTTTCTGCCTCAGTTTTGG CT		

P_3'HomReg_F 2	AAAGGTCTCAGAAACCATAGTTTAAAG GGCTAGTTG	
P_3'HomReg_R 2	AAAGGTCTCGCTTTACGGCACTGGCA CTCT	
P_5' HomReg_F	AAAGGTCTCGGATGGTTTTATCTGCCA GTGAAGCCC	5' flanking region out of gDNA from <i>Synechocystis sp.</i> PCC6803
P_5' HomReg_R	AAAGGTCTCGCTTTGATAAAAGATGATT GGGG	
P_HypA1_F	AAAGGTCTCGGATGCACGAATTGTCCTT GGCC	<i>C. necator</i> codon optimised <i>hyp</i> - operon out of pHySe_Hox_Hyp
P_HypX_R	AAAGGTCTCGCTTTTATTTTTTCGAACTG CGGGTGGCT	
P_PrhaS_F	AAAGGTCTCGGATGCCACAATTCAGCAA ATT	<i>P_{J23119}::rhaS</i> , out of <i>P_{rhaBAD}</i> <i>pSHDY_P_{rhaBAD}::mVenus _PJ23119-</i> <i>rhaS</i>
P_PrhaS_R	AAAGGTCTCGCTTTTTCATTACGACCAG TCTA	
P_TrhaS_F	AAAGGTCTCGGATGTGACAGCTAGCT CAGT	<i>P_{J23119}::rhaS</i> , out of <i>P_{rhaBAD}</i> <i>pSHDY_P_{rhaBAD}::mVenus _PJ23119-</i> <i>rhaS</i>
P_TrhaS_R	AAAGGTCTCGCTTTTATAAACGCAGAAA GGCCA	
P_pGH1_hypX_ F1	AAAGGTCTCGGATGCGCATATTGCTCCT CACC	<i>C. necator hypX</i> out of the pGH1 mega plasmid
P_pGH1_hypX_ R1	AAAGGTCTCATCATCTTCCCAGTACCGG AACT	
P_pGH1_hypX_ F2	AAAGGTCTCGATGATTCCGGCGC	
P_pGH1_hypX_ StrpTag_R2	AAAGGTCTCGCTTTTATTTTTTCGAACTG CGGGTGGCTCCAAGCAGATCGTTTCCC CGC	
P_PsbA2_F	AAAGGTCTCGGATGTTCCAGTGGATAT TTGCTGG	<i>Syn6803 P_{psbA2}</i> out of gDNA
P_PsbA2_R	AAAGGTCTCGCTTTATGTATTTGTCGAT GTTCCAGATTGG	
D) Primer name	Sequence 5' -> 3'	Primer target
PCC6803- genome_F	CCTGGTTTAGGCTCTCCC	Targeting <i>Syn6803</i> genome region upstream of <i>CnHox</i> operon integration in <i>Syn_P_{nrsB}CnSHg</i>
<i>CnHox_HoxW_</i> R	CAAGGGTCACATAGGGAAACTC	Targeting <i>HoxW</i> from <i>CnHox</i> in <i>Syn_P_{nrsB}CnSHg</i>
pSEVA_F	CTAGCGCAGCGAATAGAC	Targeting pSEVA backbone upstream the <i>CnHox</i> operon in <i>Syn_P_{nrsB}CnSHp</i>
Term_R	AACACCAGCGGGGAAAGG	Targeting <i>T_{psbC}</i> terminator placed at the end of <i>CnHox</i> operon in <i>Syn_P_{nrsB}CnSHp</i>
P_HypA1_F	AAAGGTCTCGGATGCACGAATTGTCCTT GGCC	<i>hypA1</i> gene in the <i>hyp</i> operon
PS37_R	ATTGGCGTTCCAACATGG	<i>hypF1</i> gene in the <i>hyp</i> operon
#43_F	AAAGGTCTCGGATGTTCCACCAGCAAAA TTCGCA	<i>P_{nrsB}</i> in pGGC 243
# 38_R	AAAGGTCTCGCTTTAACACCAGCGGGG AAAGG	<i>T_{psbC}</i> in pGGC 243
# 62_F	AAAGGTCTCGGATGCCACAATTCAGCAA ATT	<i>P_{rhaBAD}</i> in pGGC 244

# 70_R	AAAGGTCTCGCTTTTATAAACGCAGAAA GGCCCA	<i>rhaS</i> cassette in pGGC 244
# 295_F	GCCTGGTGTTTGCAATGTAACG	<i>hypA1</i> gene in the <i>hyp</i> operon
# 296_R	CGGGACACCAGTGATCTTCC	
# 297_F	GCCACAGAAAAATACCGCCC	<i>mpB</i> housekeeping gene in <i>Syn6803</i> genome
# 298_R	CACCTTTGCACCCTTACCCT	
# 308_F	CATTCCGTGACCGAGGAGG	<i>hypX</i> gene in the <i>hyp</i> operon
# 309_R	GATCGCCGACAATGCCAG	
# 304_F	GGCCAGTATCGAGAGGAAG	<i>hypX</i> gene in the <i>hypX</i> operon from pGH1
# 305 R	GTGCCTGCAACTCTTGCC	

Table S2.3. PCR reaction set up and cycling program.

Reagent	stock conc.	working conc.	10 μ l	50 μ l
ddH ₂ O			to 10	to 50
buffer	5x	1x	2 μ l	10 μ l
dNTPs	10 mM	0.2 mM	0.2 μ l	1 μ l
Primer for	10 μ M	0.5 μ M	0.5 μ l	2.5 μ l
Primer rev	10 μ M	0.5 μ M	0.5 μ l	2.5 μ l
template	X	0.02 ng/ μ l plasmid DNA 2 ng/ μ l genomic DNA	x	x
polymerase	2 U/ μ l	0.02 U/ μ l	0.1 μ l	0.5 μ l

Cycling program	Phusion	
Initial denaturation	98°C	30 sec
Denaturation	98°C	10 sec
Annealing	*Ta	30 sec
Extension	72°C	30 sec/kb
• 35 cycles		
Final Extension	72°C	10 min
Hold	20°C	

*Ta: annealing temperature was set according to the melting temperature of primers pairs.

Supplementary Information to Chapter 3

Supplementary Information Text

Supplementary Note 3.1 –Cells of *Syn_CnSH*⁺ show hydrogenase activity during oxygenic photosynthesis. The elevated activity detected *in vivo* compared to the crude extract suggests a higher stability and continuous protein production in the living cell. Previous studies about whole cell assays revealed a specific SH activity in *C. necator* of about 6.9 U mg protein⁻¹ [99][279] again indicating a low heterologous expression of *CnSH* in *Syn_CnSH*⁺. With a rough comparison between *CnSH* activities given in literature for whole cell assays, we estimated a 230 times lower enzyme activity in *Syn_CnSH*⁺ as compared to *C. necator*.

Supplementary Figures

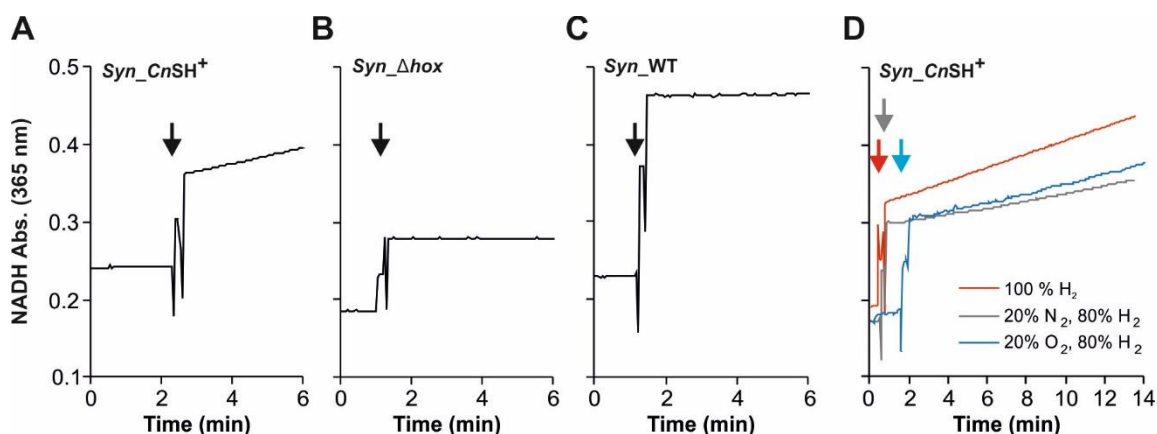


Figure S3.1. *In vitro* activity assay of *CnSH* in the soluble extract of *Synechocystis*. A-C: H₂-driven NAD⁺ reduction was recorded spectroscopically at a fixed wavelength (365nm) using cell extracts of *Syn_CnSH*⁺, *Syn_Δhox*, and *Syn_WT*. The black arrows indicate the addition of the soluble extract into the cuvette reflecting the starting point of the reaction. The assay was performed in Tris/HCl buffer (50 mM, pH 8.0) saturated with 100 % H₂. *Syn_Δhox* and *Syn_WT* cell extracts did not show any production of NADH under these standard conditions. (D) NADH production by *Syn_CnSH*⁺ crude extracts in Tris/HCl buffer (50 mM, pH 8.0) saturated with a gas mixture containing 80% H₂ combined with 20% of N₂ or O₂. The arrows indicate crude extract addition and refer to the graph of the same color. The large absorbance step observed in all the graphs is due to soluble extract addition. Absorbance data constitute representative examples. A detailed description of the assay conditions is given in **Table S3.1**.

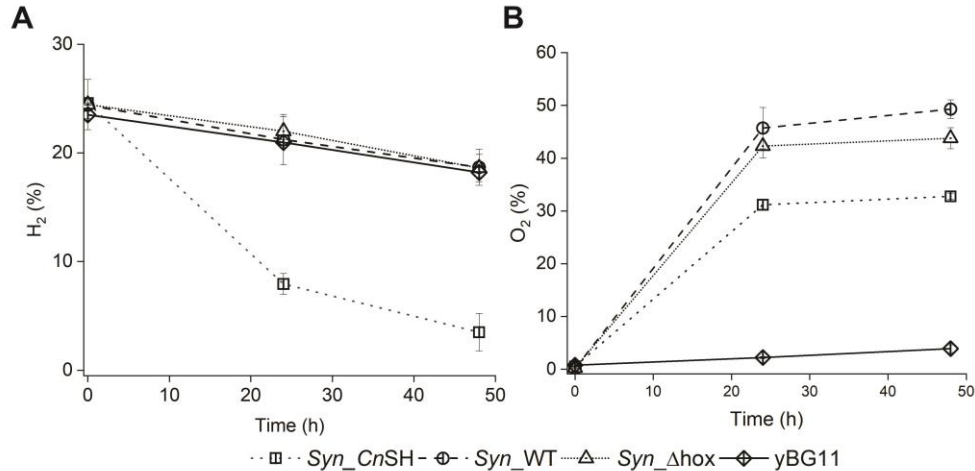


Figure S3.2. H₂ consumption activity of *Synechocystis* cultures incubated under defined conditions. Shown are H₂ and O₂ concentrations for *Syn_CnSH*, *Syn_WT*, *Syn_Δhox* cultures and an abiotic control (yBG11) incubated for 48 h under illumination with a defined gas mixture (20% H₂, 10% CO₂, 70% N₂) in the headspace. **(A)** *Syn_CnSH* completely consumed H₂ in 48 h. *Syn_WT*, *Syn_Δhox* strains, and the abiotic control (yBG11 media) showed only a small and similar decrease in H₂ concentration, most likely due to diffusional effects. **(B)** Rise of O₂ concentration is higher for *Syn_WT* and *Syn_Δhox* compared to *Syn_CnSH*⁺, while the small increase in O₂ concentration detected in the abiotic samples is due to diffusional effect. Data represent mean values and standard deviations (n=3).

Supplementary Tables

Table S3.1. *In vitro* activity assay of the CnSH in the soluble extract of *Synechocystis*. CnSH specific activity in the soluble extract of *Synechocystis* was determined for standard conditions (S.C.). Without supplying FMN and DTT to the reaction mixture, a lower activity was recorded, which is caused by the release of FMN, an essential cofactor of CnSH [98]. During consecutive measurements, we noticed a decrease of activity, likely due to the low protein stability when stored in a reduced state as postulated before [93]. The evaluation of the O₂ tolerance was performed by mixing buffers saturated with different gases (H₂, O₂ or N₂) in the desired ratio. Measurements were carried out as for the standard conditions^a. NAD⁺ reduction also was observed when extracts were incubated with 20% O₂, confirming O₂ tolerance under ambient condition. No activity was detected for *Syn_Δhox* and *Syn_WT*. Data represent mean values and standard deviations (n=2).

Strain	Reaction conditions	Specific activity (U/g _{prot})
<i>Syn_CnSH</i> ⁺	^a S.C. _f	17.9 ± 1.4
	^b no FMN no DTT	11.6 ± 2.6
	^c S.C. _s	7.4 ± 1.0
	^d 80% H ₂ ; 20% O ₂	5.1 ± 0.9
	^e 80% H ₂ ; 20% N ₂	3.6 ± 0.6
<i>Syn_WT</i>	S.C. _f	0.0 ± 0.0
<i>Syn_Δhox</i>	S.C. _f	0.0 ± 0.0

^a standard conditions (S.C.): H₂ saturated Tris/HCl (50 mM, pH 8.0) supplemented with FMN, DTT, and NAD⁺. Fresh soluble extract used. ^b H₂ saturated Tris/HCl (50 mM, pH 8.0) supplemented with only NAD⁺. Fresh soluble extract used. ^c H₂ saturated Tris HCl (50 mM, pH 8.0) supplemented with FMN, DTT, and NAD⁺. Soluble extract stored at 4°C for 3.5 h was used. ^d Tris HCl (50 mM, pH 8.0) supplemented with FMN, DTT, and NAD⁺. Soluble extract stored at 4°C for 3.5 h was used. 80/20 mixture of buffers saturated with H₂ and O₂. ^e Tris HCl (50 mM, pH 8.0) supplemented with FMN, DTT, and NAD⁺. Soluble extract stored at 4°C for 3.5 h was used. 80/20 mixture of buffers saturated with H₂ and N₂.

Table S3.2. Specific H₂ consumption activity of *Syn_CnSH*⁺ cultures incubated with different initial O₂ concentrations. *Syn_CnSH*⁺ cultures were incubated in sealed vials with three different gas mixtures with defined H₂, O₂, and N₂ concentrations, for 2 h under illumination. The H₂ concentration decrease was used to calculate the specific activity. Data represent mean values and standard deviations (n=3).

Gas mixture	U/g _{cdw}
20% H ₂ 20% O ₂ 60% N ₂	9.22± 0.50
20% H ₂ 10% O ₂ 70% N ₂	10.36± 0.98
20% H ₂ 5% O ₂ 75% N ₂	11.02± 0.30

Table S3.3. *In vivo* hydrogenase activity for *Synechocystis* cultures. Hydrogenase activity for each strain was measured with a Clark-type-electrode from Hansatech under strictly anaerobic conditions as described [75][170]. Cell cultures were grown photoautotrophically to an OD₇₅₀ of 3 and aliquots were mixed with 5 mM methylviologen and 10 mM sodium dithionite to directly record the hydrogenase activity *in vivo*. The data obtained for *Syn_CnSH*⁺ are comparable with those acquired with GC measurements. Data represent mean values and standard deviations (n=3).

Strain	U/g _{cdw}
<i>Syn_CnSH</i> ⁺	14.8± 3.7
<i>Syn_WT</i>	13.8± 1.3
<i>Syn_Δhox</i>	-0.03± 0.28

Table S3.4. H₂ production experiments in *Synechocystis* strains. O₂ concentrations monitored for 24 h for each tested *Synechocystis* strain during H₂ evolution under illumination (K_{P_H} + 10 mM glucose). The variability regarding the O₂ concentrations gives no clear trend. O₂ concentrations over 2 % are most likely due to diffusion through the vial septa rather than oxygenic photosynthesis.

μmol O ₂ / g _{CDW}									
Time (h)	Syn_CnSH			Syn_WT			Syn_Δhox		
0	84.7	104.9	305.7	91.4	432.9	102.6	106.5	56.4	48.5
2				94.6	224.6	80.3	620.2	109.3	153.4
5	622.1	531.9	515.2	186.4	224.6	153.4	791.9	104.2	77.5
7				219.4	664.7	188.4	1138.5	121.2	37.0
9	516.0	690.9	621.7						
16	352.2	184.1	991.0						
20	408.3	169.0	1178.3						
24	467.5	188.4	1173.1	284.2	1970.6	318.8	1594.5	331.1	114.9
Time (h)	O ₂ %								
0	0.2	0.3	0.8	0.2	1.1	0.3	0.3	0.1	0.1
2				0.2	0.6	0.2	1.6	0.3	0.4
5	1.6	1.3	1.3	0.5	0.6	0.4	2.0	0.3	0.2
7				0.6	1.7	0.5	2.9	0.3	0.1
9	1.3	1.7	1.6						
16	0.9	0.5	2.5						
20	1.0	0.4	3.0						
24	1.2	0.5	3.0	0.7	5.0	0.8	4.0	0.8	0.3

Supplementary information to Chapter 4

Supplementary Figures

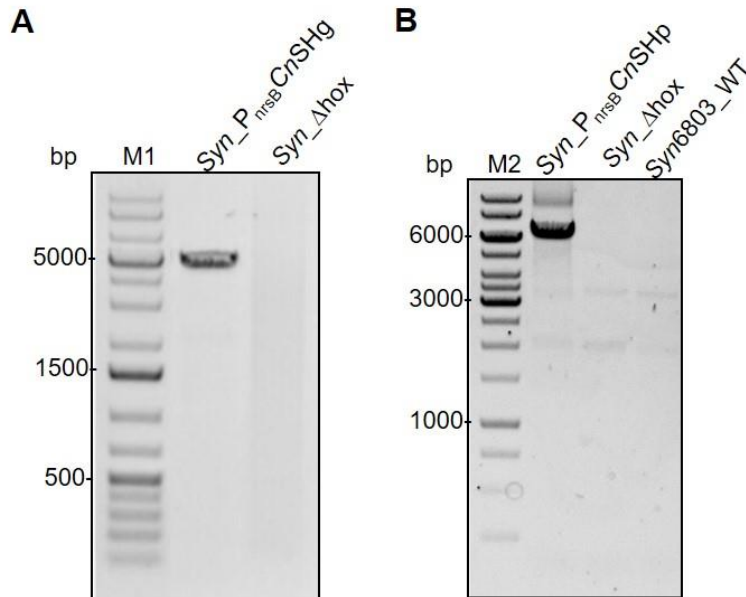


Figure S4.1. PCR to confirm the correct generation of *Syn_P_{nrsB}CnSHg* and *Syn_P_{nrsB}CnSHp* strains. *Hox* primers are given in **Table S2.2**. **(A)** The band at the expected product length of ~5200 bp indicates correct insertion of the *P_{nrsB}CnSH hox* operon in the *Synechocystis* genome (*Syn_P_{nrsB}CnSHg*). **(B)** The expected product size of ~6400 bp indicates the presence of the pGGC 209 plasmid carrying the *P_{nrsB}CnSH hox* operon (*Syn_P_{nrsB}CnSHp*). As negative control, the PCR also was performed using DNA from *Syn_Δhox* and *Synechocystis* WT. **M1**: GeneRuler 1 kb Plus DNA Ladder, 75-20,000 bp (Thermo Scientific™) **M2**: GeneRuler 1 kb DNA Ladder, 250-10,000 bp (Thermo Scientific™).

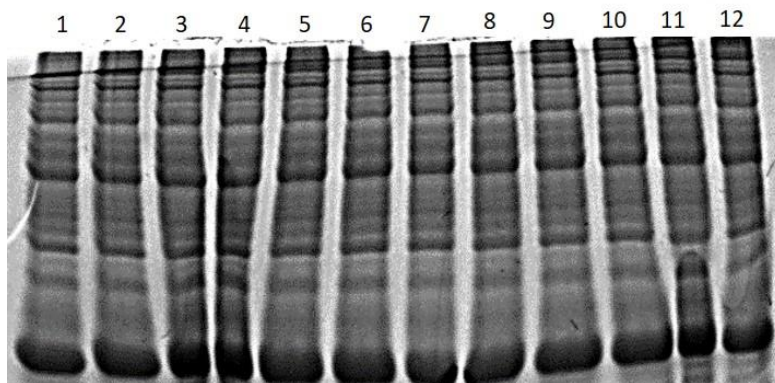


Figure S4.2. SDS-PAGE loading control for Western blot analysis. 1: *Syn_CnSH*⁺, 0 μM Ni²⁺; 2: *Syn_CnSH*⁺, 2.5 μM Ni²⁺; 3: *Syn_CnSH*⁺, 5 μM Ni²⁺; 4: *Syn_CnSH*⁺, 10 μM Ni²⁺; 5: *Syn_P_{nrsB}CnSHg*, 0 μM Ni²⁺; 6: *Syn_P_{nrsB}CnSHg*, 2.5 μM Ni²⁺; 7: *Syn_P_{nrsB}CnSHg*, 5 μM Ni²⁺; 8: *Syn_P_{nrsB}CnSHg*, 10 μM Ni²⁺; 9: *Syn_P_{nrsB}CnSHp*, 0 μM Ni²⁺; 10: *Syn_P_{nrsB}CnSHp*, 2.5 μM Ni²⁺; 11: *Syn_P_{nrsB}CnSHp*, 5 μM Ni²⁺; 12: *Syn_P_{nrsB}CnSHp*, 10 μM Ni²⁺.

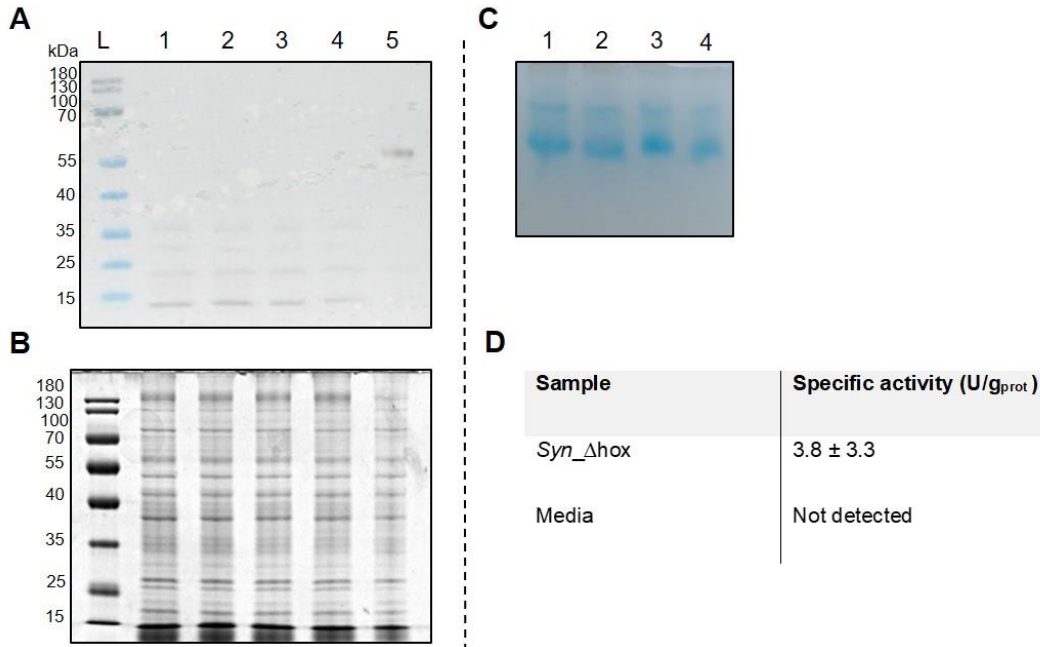


Figure S4.3. Soluble cell-free extract from *Syn_Δhox* used as negative control. (A) Western blot analysis for detection of Hox H and (B) denaturing SDS-PAGE analysis performed as loading control of the WB. L: Ladder; 1: *Syn_Δhox*, 0 μM Ni²⁺; 2: *Syn_Δhox*, 2.5 μM Ni²⁺; 3: *Syn_Δhox*, 5 μM Ni²⁺; 4: *Syn_Δhox*, 10 μM Ni²⁺; 5: *Syn_P_{nrsB}CnSHg*, 10 μM Ni²⁺). (C) In gel activity staining (1: *Syn_Δhox*, 0 μM Ni²⁺; 2: *Syn_Δhox*, 2.5 μM Ni²⁺; 3: *Syn_Δhox*, 5 μM Ni²⁺; 4: *Syn_Δhox*, 10 μM Ni²⁺). (D) *Syn_Δhox* and yBG11 medium used as negative control for H₂-driven NAD⁺ reduction.

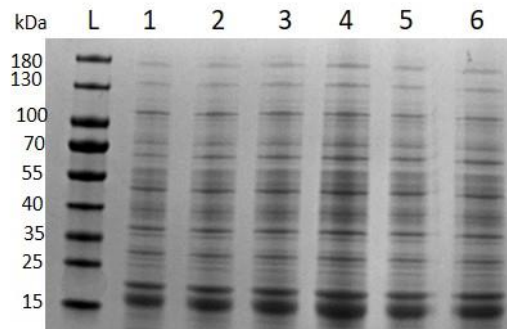


Figure S4.4. SDS-PAGE as loading control for Western Blot analysis. L: Ladder; 1: *Syn_P_{nrsB}CnSHp*, 24 h after induction; 2: *Syn_P_{nrsB}CnSHp*, 48 h after induction; 3: *Syn_P_{nrsB}CnSHp*, 72 h after induction; 4: *Syn_P_{nrsB}CnSHg*, 24 h after induction; 5: *Syn_P_{nrsB}CnSHg*, 48 h after induction; 6: *Syn_P_{nrsB}CnSHg*, 72 h after induction.

Gas phase: 20% H₂ - 80% N₂ 

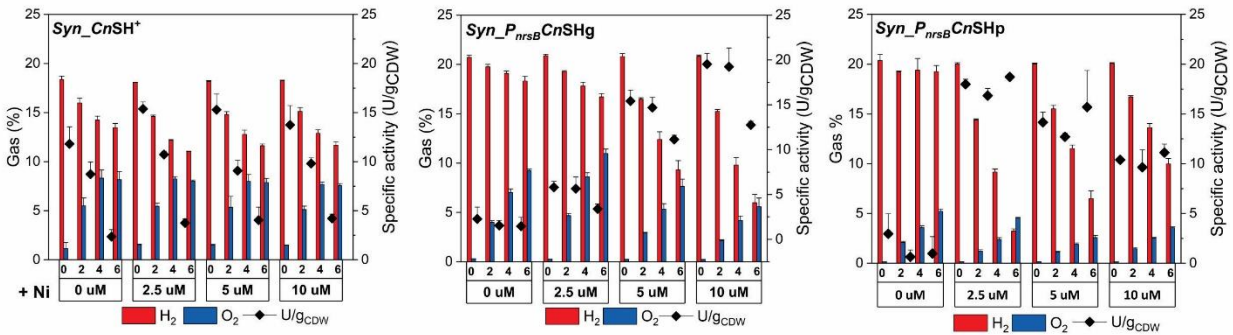


Figure S4.5: *In vivo* H₂ oxidation activities in light with different inducer (Ni²⁺) concentrations and their stability in time. *Syn_CnSH⁺*, *Syn_P_{nrsB}CnSHg*, and *Syn_P_{nrsB}CnSHp* cells were cultivated in yBG11 medium under continuous illumination. When applied, Ni²⁺ was supplemented to cell cultures 24 h before the whole-cell assay. Cultures with defined cell densities were incubated under continuous illumination in sealed glass vials with a headspace filled with 20% H₂ and 80% N₂. *In vivo* hydrogenase activity was determined in time dependent experiments (over 6 h). H₂ consumption activity of living *CnSH* expressing strains was analyzed in response to different inducer (Ni²⁺) concentrations. In accordance to the results obtained *in vitro* (Fig. 4.2C), *Syn_CnSH⁺* hydrogenase activity didn't show a direct correlation with the Ni²⁺ amount supplied. Nevertheless, a slightly higher activity was detected with 2.5 and 5 μM Ni²⁺ compared to without Ni²⁺ addition with a maximum specific activity (15 U g_{CDW}⁻¹). Ni²⁺ is required for active site maturation. Activity trends observed for *Syn_P_{nrsB}CnSHg* and *Syn_P_{nrsB}CnSHp* confirmed the results obtained with cell extracts: Induction with 10 μM Ni²⁺ resulted in the highest activity in *Syn_P_{nrsB}CnSHg*, while *Syn_P_{nrsB}CnSHp* showed maximal activity with 2.5 μM Ni²⁺. In both cases, a specific activity of 20 U g_{CDW}⁻¹ was reached, which in contrast to *Syn_CnSH⁺* was stable for at least 4 h. Conclusively, elevated levels of HoxH and larger abundance of active enzyme complexes together with the improved and stabilized activities obtained *in vitro* and *in vivo* indicate a substantially improved gene expression in terms of active protein level, which was achieved via the use of a well-controllable promoter and a strong ribosomal binding site.

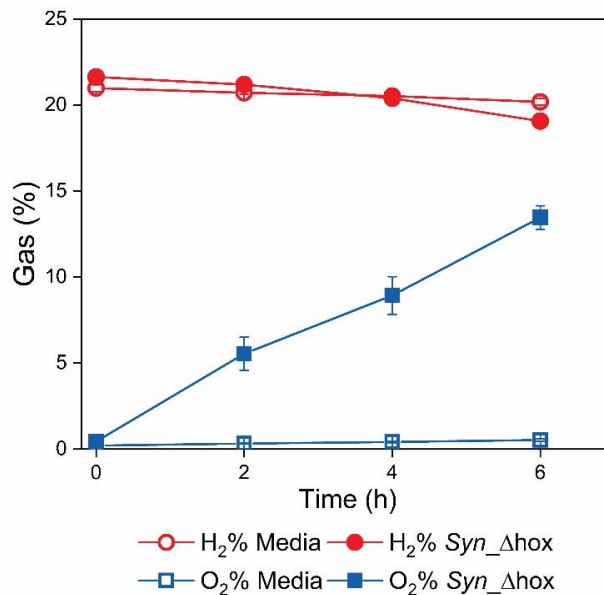


Figure S4.6. *Syn_Δhox* and yBG11 medium used as negative controls for *in vivo* H₂ consumption. H₂ and O₂ concentrations measured over 6 h.

Supplementary Tables

Table S4.1. O₂ concentrations during H₂ production by the different CnSH containing *Synechocystis* strains. (A) Dark condition; (B) illumination + DBMIB. The variability in the detected O₂ concentrations gives no clear trend. Low O₂ concentrations and slight increases can be attributed to remaining initial O₂ and diffusion through the vial septa, respectively.

A

H ₂ production (10mM Glucose_Dark)				
Strains	Time (h)	O ₂ %		
		1	2	3
<i>Syn_CnSH</i> ⁺	0	1.0	1.0	1.1
	3	0.9	0.9	1.0
	6	0.9	0.9	0.9
	9	0.9	1.0	1.0
	24	2.8	0.1	0.7
<i>Syn_P_{nrsB}CnSHp</i>	0	1.0	1.0	1.0
	3	0.6	0.9	0.9
	6	0.9	0.9	0.9
	9	0.2	0.6	0.9
	24	0.7	1.0	0.7
<i>Syn_P_{nrsB}CnSHg</i>	0	2.5	2.5	3.5
	3	3.4	2.4	1.9
	6	3.4	2.7	2.6
	9	3.4	2.9	2.9
	24	2.9	3.0	3.4

B

H ₂ production (10mM Glucose_DBMIB_Light)				
Strains	Time (h)	O ₂ %		
		1	2	3
<i>Syn_CnSH</i> ⁺	0	1.2	1.2	0.8
	3	1.2	1.2	1.2
	6	0.8	1.1	0.7
	9	1.2	1.2	0.7
	12	0.6	1.2	0.8
<i>Syn_P_{nrsB}CnSHp</i>	0	1.3	1.2	1.3
	3	1.2	0.8	1.2
	6	1.2	0.8	0.9
	9	1.2	1.1	1.2
	12	0.7	1.2	0.9
<i>Syn_P_{nrsB}CnSHg</i>	0	1.2	1.1	1.0
	3	1.1	1.1	1.1
	6	1.1	1.1	1.2
	9	1.2	1.2	0.8
	12	1.2	1.1	1.1

Table S4.2. H₂ and O₂ concentrations during control incubations of *Syn_Δhox*. As expected, no H₂ was detected under both conditions tested (A) 10 mM glucose, dark incubation; (B) 10 mM glucose, 20 μM DBMIB, light incubation). Low O₂ concentrations and slight increases can again be attributed to remaining initial O₂ and diffusion through the vial septa, respectively.

A

<i>Syn_Δhox</i> (10mM Glucose_Dark)						
Time (h)	H ₂ %			O ₂ %		
	0	0	0	0	1.2	1.2
3	0	0	0	1.1	1.1	1.1
6	0	0	0	1.1	1.1	1.1
9	0	0	0	1.1	1.1	1.1

B

<i>Syn_Δhox</i> (10mM Glucose_DBMIB_Light)						
Time (h)	H ₂ %			O ₂ %		
	0	0	0	0	1.2	1.2
3	0	0	0	1.3	1.3	1.3
6	0	0	0	1.9	1.8	1.8
9	0	0	0	2.9	2.7	2.7

Supplementary information to Chapter 5

Supplementary Figures

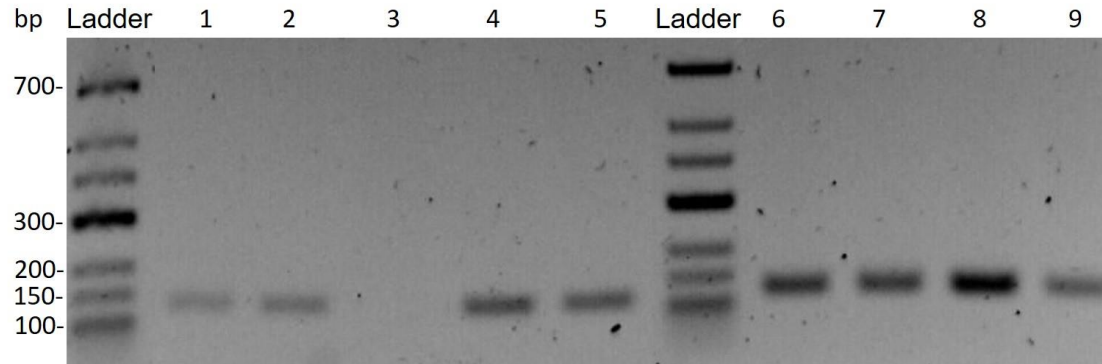


Figure S5.1: (RT)-PCR targeting *hypX*. The *hypX* mRNA is being transcribed for every strain analysed, before and 24 h after the induction, as shows the band visible at ~124 bp. The negative control (line 3), which is not harboring the *Cn_hyp* plasmid, does not show *hypX* transcription. Ladder: GeneRuler™ Low Range; **1:** +*pP_{nrsB}CnHypX* not induced; **2:** +*pP_{nrsB}CnHypX*: 10 μ M Ni²⁺; **3:** *Syn_P_{nrsB}CnSHg* only (negative control); **4:** +*pP_{rhaBAD}CnHyp* not induced; **5:** +*pP_{rhaBAD}CnHypX*^{0.1 mM Rha}; **6:** +*pP_{rhaBAD}CnHypX* not induced; **7:** +*pP_{rhaBAD}CnHyp*^{2mM Rha}; **8:** *pP_{psbA2}CnHyp*; ; **9:** *pP_{psbA2}CnHyp* (24 h later).

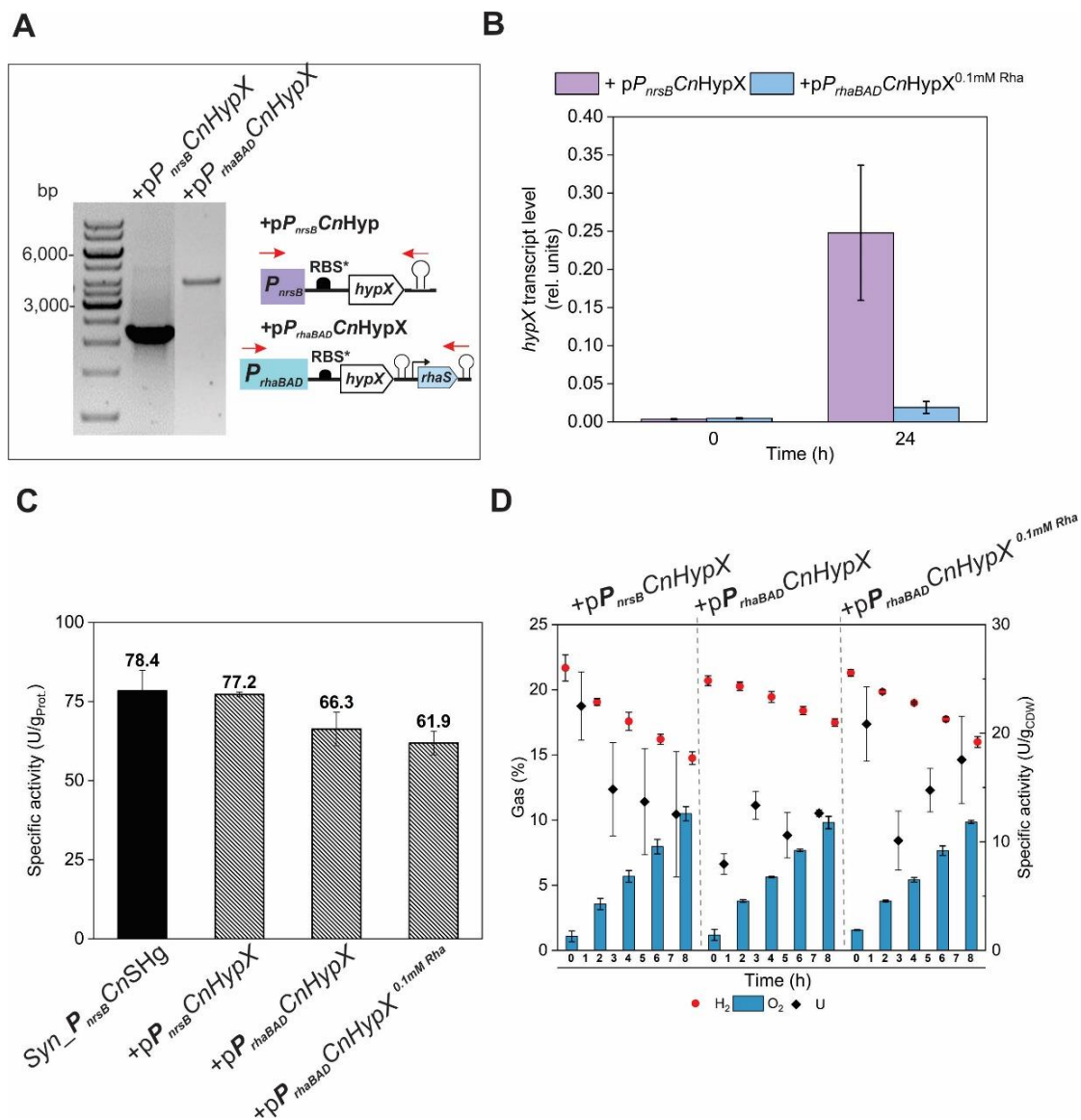


Figure S5.2. Characterization of +pP_{nrsB}CnHypX and +pP_{rhaBAD}CnHypX. (A) Genetic setup of HypX operons. Red arrows indicate the binding sites of primers used to verify the successful plasmids transformation in *Syn_P_{nrsB}CnSHg* via colony-PCR as shown by the agarose gel. The expected products size of ~2100 and ~4200 bp indicate the presence of the pGGC 243 and 244 plasmids in *Syn_P_{nrsB}CnSHg* respectively, giving +pP_{nrsB}CnHypX and +pP_{rhaBAD}CnHypX. (B) qRT-PCR expression of *hypX* was determined before (0 h) and 24 h after induction with nickel for +pP_{nrsB}CnHypX and rhamnose for +pP_{rhaBAD}CnHypX. Shown are the averages and standard deviations of biological duplicates. (C) *In vitro* specific H₂ase activity determined for the soluble protein extract of each strain. 10μM Ni²⁺ was supplemented 24 h before the assay to each strain. Shown are mean values and standard deviations (n=3). (D) 5 mL cell culture from each strain was transferred into 20 ml gas-tight vials and incubated for 8 h under illumination with 20% H₂, 10% CO₂, 70% N₂. 10μM Ni²⁺ was supplemented 24 h before the assay to each strain. *Syn_P_{nrsB}CnSHg* (positive control) is shown in Fig. 5.3A. Shown are mean values and standard deviations (n=3).

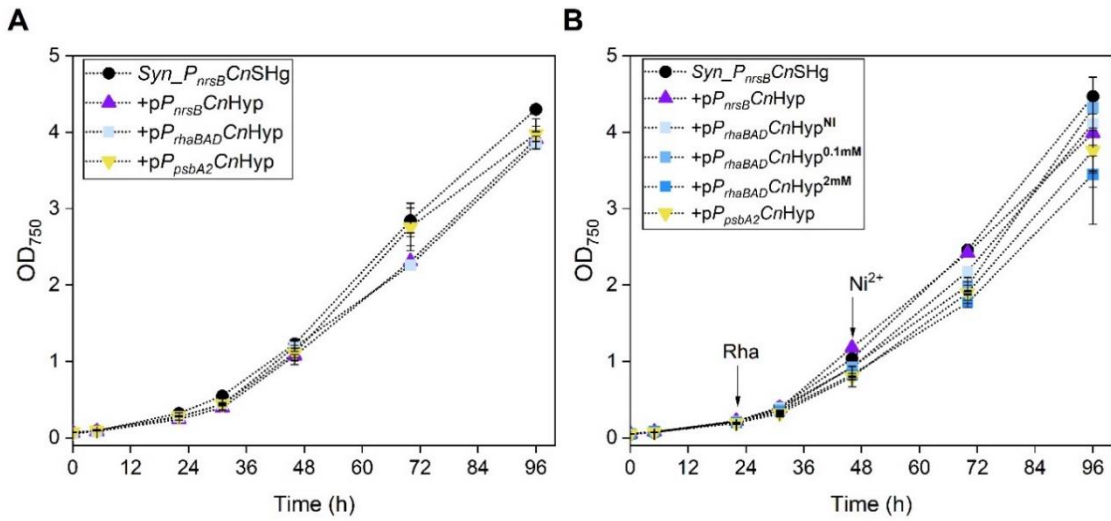


Figure S5.3. Growth curves. Not induced (A) and induced (B) strains expressing *C. necator* hydrogenase and maturases.

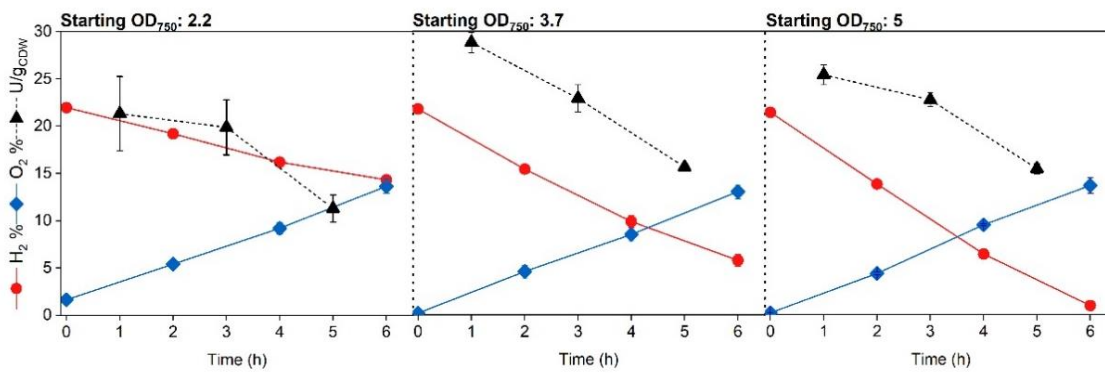


Figure S5.4. Optimum OD₇₅₀ for protein expression and activity *in vivo*. We investigated if *Cn_hox* induction at different OD might influence the H₂ oxidation activity *in vivo* for *Syn_P_{nrsB}CnSHg*. Phototrophically grown cells induced in the late log phase and in the linear phase were collected 24 h later and incubated in 10 mL gas-tight vials with 20% H₂, 10% CO₂, 70% N₂, for 8 h under illumination. The cultures induced in a late linear revealed a higher initial activity compared to cultures induced at OD₇₅₀ ~1.

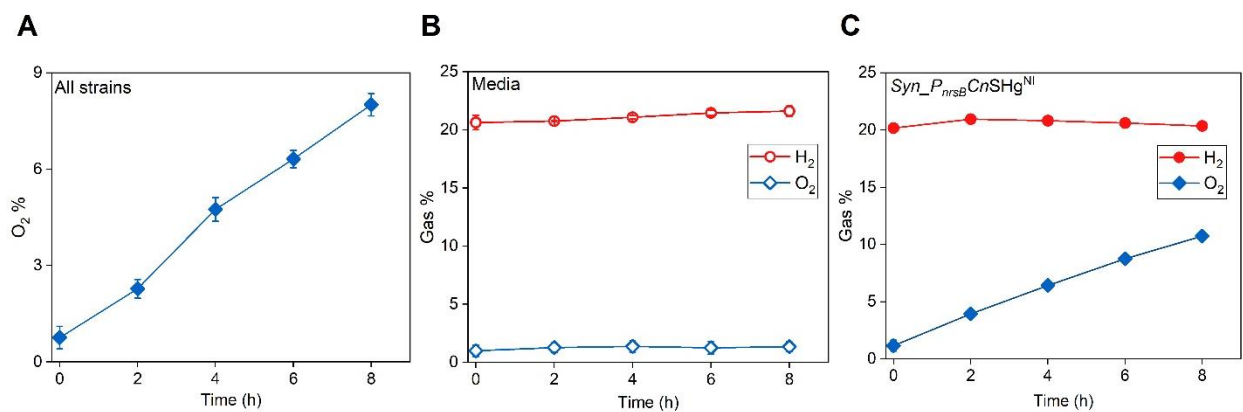


Figure S5.5. Gas concentrations measured in 20 mL vials during the 8 h of experiment. (A) The measurement represents the average concentration of the evolved O_2 in all strains characterized in Figure 5.4. **(B)** yBG11 medium and **(C)** $Syn_P_{nrsB}CnSHg^{NI}$ not induced were used as negative controls for *in vivo* H_2 consumption in 20 mL vials. Shown are mean values and standard deviations (n=3).

Supplementary information to Chapter 6



OPEN ACCESS

EDITED BY
Xuefeng Lu,
Qingdao Institute of Bioenergy and Bioprocess
Technology (CAS),
China

REVIEWED BY
Peter Lindblad,
Uppsala University,
Sweden
Annegret Wilde,
University of Freiburg,
Germany

*CORRESPONDENCE
Stephan Klähn
✉ stephan.klaehn@ufz.de

SPECIALTY SECTION
This article was submitted to
Microbiotechnology,
a section of the journal
Frontiers in Microbiology

RECEIVED 12 December 2022
ACCEPTED 22 February 2023
PUBLISHED 22 March 2023

CITATION
Opel F, Itzenhäuser MA, Wehner I, Lupacchini S,
Lauterbach L, Lenz O and Klähn S (2023)
Toward a synthetic hydrogen sensor in
cyanobacteria: Functional production of an
oxygen-tolerant regulatory hydrogenase in
Synechocystis sp. PCC 6803.
Front. Microbiol. 14:1122078.
doi: 10.3389/fmicb.2023.1122078

COPYRIGHT
© 2023 Opel, Itzenhäuser, Wehner, Lupacchini,
Lauterbach, Lenz and Klähn. This is an open-
access article distributed under the terms of
the [Creative Commons Attribution License
\(CC BY\)](https://creativecommons.org/licenses/by/4.0/). The use, distribution or reproduction
in other forums is permitted, provided the
original author(s) and the copyright owner(s)
are credited and that the original publication in
this journal is cited, in accordance with
accepted academic practice. No use,
distribution or reproduction is permitted which
does not comply with these terms.

Toward a synthetic hydrogen sensor in cyanobacteria: Functional production of an oxygen-tolerant regulatory hydrogenase in *Synechocystis* sp. PCC 6803

Franz Opel¹, Marvin Amadeus Itzenhäuser¹, Isabel Wehner¹, Sara Lupacchini¹, Lars Lauterbach², Oliver Lenz³ and Stephan Klähn^{1*}

¹Department of Solar Materials, Helmholtz Centre for Environmental Research – UFZ, Leipzig, Germany, ²Institute of Applied Microbiology (iAMB), RWTH Aachen University, Aachen, Germany, ³Institute of Chemistry, Technical University of Berlin, Berlin, Germany

Cyanobacteria have raised great interest in biotechnology, e.g., for the sustainable production of molecular hydrogen (H₂) using electrons from water oxidation. However, this is hampered by various constraints. For example, H₂-producing enzymes compete with primary metabolism for electrons and are usually inhibited by molecular oxygen (O₂). In addition, there are a number of other constraints, some of which are unknown, requiring unbiased screening and systematic engineering approaches to improve the H₂ yield. Here, we introduced the regulatory [NiFe]-hydrogenase (RH) of *Cupriavidus necator* (formerly *Ralstonia eutropha*) H16 into the cyanobacterial model strain *Synechocystis* sp. PCC 6803. In its natural host, the RH serves as a molecular H₂ sensor initiating a signal cascade to express hydrogenase-related genes when no additional energy source other than H₂ is available. Unlike most hydrogenases, the *C. necator* enzymes are O₂-tolerant, allowing their efficient utilization in an oxygenic phototroph. Similar to *C. necator*, the RH produced in *Synechocystis* showed distinct H₂ oxidation activity, confirming that it can be properly matured and assembled under photoautotrophic, i.e., oxygen-evolving conditions. Although the functional H₂-sensing cascade has not yet been established in *Synechocystis* yet, we utilized the associated two-component system consisting of a histidine kinase and a response regulator to drive and modulate the expression of a *superfolder gfp* gene in *Escherichia coli*. This demonstrates that all components of the H₂-dependent signal cascade can be functionally implemented in heterologous hosts. Thus, this work provides the basis for the development of an intrinsic H₂ biosensor within a cyanobacterial cell that could be used to probe the effects of random mutagenesis and systematically identify promising genetic configurations to enable continuous and high-yield production of H₂ via oxygenic photosynthesis.

KEYWORDS

sensing and signaling, biotechnological hydrogen, regulatory hydrogenase, biosensor, synthetic biology, cyanobacteria

1. Introduction

The anthropogenic emission of greenhouse gases like carbon dioxide (CO₂) derived from the usage of fossil resources is regarded as the major driver of climate change. To tackle this issue, new approaches need to be supplied toward a CO₂-neutral society and economy. Molecular hydrogen (H₂) is generally believed to be an ideal candidate as a future energy carrier due to its high energy density and greenhouse gas emission-free usage. Industrially, H₂ is, however, still mainly obtained *via* steam reforming of natural gases, therefore relying on fossil resources and leading to a considerable greenhouse gas footprint (Howarth and Jacobson, 2021).

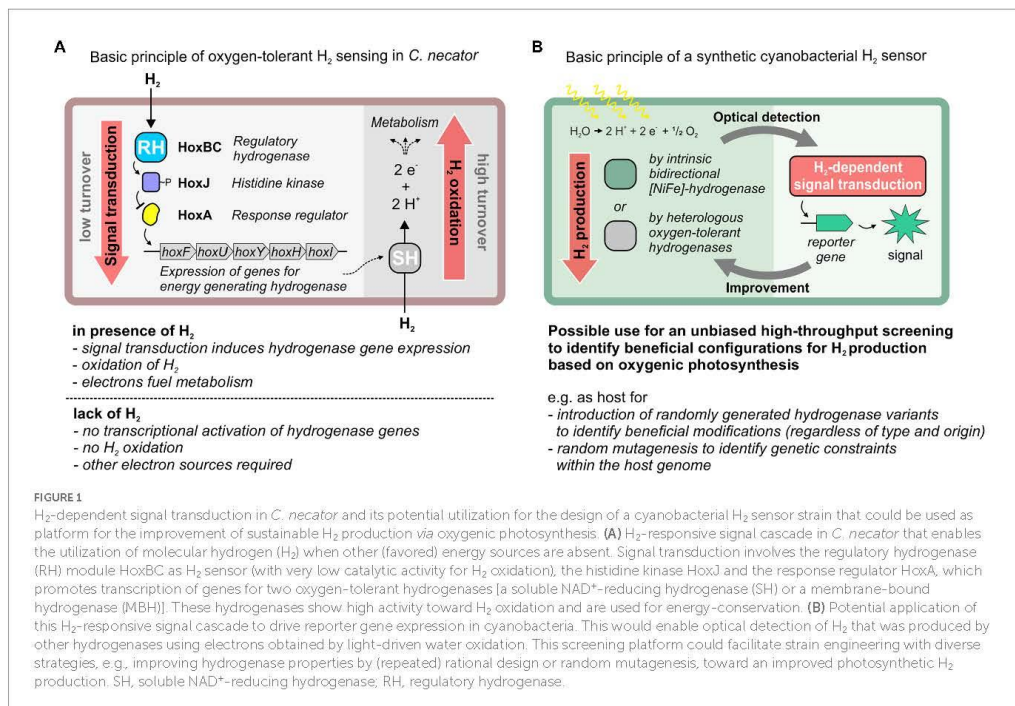
Biotechnological H₂ production using microorganisms as whole-cell biocatalysts offers the advantage of a sustainable process based on renewable resources. These biological H₂ formation routes encompass anaerobic fermentation using organic compounds as electron donors in, e.g., chemotrophic *Clostridium* and *Enterobacter* species or phototrophic sulfur and non-sulfur bacteria, as well as oxygenic photosynthesis using algae and cyanobacteria (Mahidhara et al., 2019). Approaches based on oxygenic photosynthesis appear most promising as they rely on electrons that have been obtained from light-dependent oxidation of water. Cyanobacteria are the only prokaryotes capable of this process. Great effort has been made to optimize H₂ production within cyanobacterial models such as the unicellular strain *Synechocystis* sp. PCC 6803 (hereafter referred to as *Synechocystis*). However, the breakthrough to enable continuous H₂ production in whole-cell cyanobacterial catalysts has not been achieved yet. Currently, it suffers from low yields and rates as well as the prototypical molecular oxygen (O₂) sensitivity of the enzymes involved in the formation of H₂, namely hydrogenases or nitrogenases. Hydrogenases are metalloenzymes that perform the reversible splitting of H₂ into protons and electrons. They are grouped based on the composition of their active site into nickel-iron [NiFe]-, iron-iron [FeFe]-, and iron [Fe]- or Hmd-hydrogenases (Lubitz et al., 2014). Previous studies tackled, for instance, the catalytic performance of H₂ production by introducing highly active, heterologous [FeFe]-hydrogenases into *Synechocystis* (Berto et al., 2011; Wegelius et al., 2018) or by fusing the endogenous [NiFe]-hydrogenase to photosystem I for a direct electron transfer from photosynthesis (Appel et al., 2020). The O₂ sensitivity has been addressed, for example, by introducing a heterologous O₂-tolerant [NiFe]-hydrogenase (Lupacchini et al., 2021). Another strategy enabling a continuous hydrogenase activity would be the spatial separation from O₂, e.g., through the encapsulation in synthetic microcompartments as demonstrated in *Escherichia coli* (hereafter referred to as *E. coli*) (Li et al., 2020). Moreover, metabolic engineering might target the redirecting of electron flows from competing pathways, like respiration and nitrate assimilation, to H₂ evolution (Baebprasert et al., 2011). Nevertheless, further research and alternative approaches are required to overcome the known as well as yet unknown limitations and to make photosynthesis-driven H₂ production amenable for biotechnological applications in the future (Bühler et al., 2021). In this regard, biosensors that respond to H₂ in an easily detectable way could help to enable, e.g., a systematic screening of mutant libraries and the selection of those that are beneficial for H₂ production.

Synthetic biosensors based on engineered bacterial cells, that respond to certain input stimuli with a desired output signal, can

be designed by harnessing natural signal transduction systems to drive the expression of a reporter gene (Zhang et al., 2015; Ni et al., 2021). Also cyanobacteria have already been used as hosts to implement such cascades, e.g., for the intracellular sensing of heavy metals (Lacey et al., 2019; Patyi et al., 2021), O₂ (Immethun et al., 2016), or toluene (Inaba et al., 2018). Natural H₂-responsive systems were described in *Bradyrhizobium japonicum* (*B. japonicum*) (Black et al., 1994; van Soom et al., 1997, 1999), *Rhodobacter capsulatus* (*R. capsulatus*) (Dischert et al., 1999; Elsen et al., 2003), and *Cupriavidus necator* (also known as *Ralstonia eutropha*) H16 (hereafter referred to as *C. necator*) (Lenz et al., 1997; Lenz and Friedrich, 1998). The purple non-sulfur bacterium *R. capsulatus* has already been engineered to follow H₂ production in co-cultivated green algae (Wecker et al., 2011). However, such a co-cultivation approach impedes the use as a tool for efficient mutant screening and is not feasible in the case of cyanobacteria as most bacterial strains do not grow in cyanobacterial growth media. In the long-term, a cyanobacterial biosensor strain that directly responds to intracellularly evolved H₂ appears promising to use it as platform for a systematic optimization of H₂ production within the same cell.

Cupriavidus necator has become the model organism for H₂ oxidation in presence of O₂. As a true “Knallgas” bacterium it can utilize H₂ as sole electron donor and O₂ as terminal electron acceptor. For this purpose, it uses O₂-tolerant [NiFe]-hydrogenases. *C. necator* contains even four [NiFe]-hydrogenases that are O₂-tolerant, among them the soluble NAD⁺-reducing (SH) and membrane-bound hydrogenase (MBH) as well as the regulatory hydrogenase (RH) (Lenz et al., 2015). The RH is a cytoplasmic enzyme and has a comparably simple structure composed of the two hydrogenase subunits, HoxB and HoxC (Pierik et al., 1998; Kleihues et al., 2000; Bernhard et al., 2001). The catalytic Ni-Fe center is coordinated by four cysteines to the protein matrix of the HoxC subunit (Winter et al., 2004). The active site iron carries three diatomic ligands, two cyanides (CN⁻) and one carbon monoxide (CO) (Pierik et al., 1998). Incorporation of the active site into the RH requires a set of seven auxiliary maturases, which are encoded by the *hypA1B1F1CDEX* genes (Buhrke et al., 2001; Bürstel et al., 2016). The RH serves as H₂ sensor in combination with a two-component regulatory system and transmits the H₂ input signal *via* the histidine kinase HoxJ to the response regulator HoxA, which functions as transcriptional activator for hydrogenase gene expression (Zimmer et al., 1995; Lenz et al., 1997; Schwartz et al., 1998; Figure 1A). Unlike canonical two-component systems, transcriptional activation is mediated by the unphosphorylated form of HoxA, and HoxJ phosphorylates/inactivates HoxA in the absence of H₂ (Lenz and Friedrich, 1998). Notably, the phosphorylating activity of HoxJ is knocked out in its parental strain *C. necator* H16. To restore the native activity of HoxJ, a specific amino acid exchange is required, resulting in a functional HoxJ(S422G), also referred to as HoxJ* (Lenz and Friedrich, 1998). HoxJ* and the RH form the ternary H₂-sensing complex (Buhrke et al., 2004). Production of active RH has already been established in *E. coli* (Lenz et al., 2007), very recently even under aerobic conditions (Fan et al., 2022).

In this study, we introduced the H₂-sensing module of the *C. necator* RH, i.e., HoxB and HoxC, into *Synechocystis*. For this purpose, synthetic operons for the structural and accessory genes were designed for expression in *Synechocystis*. Heterologously produced and catalytically active RH was extracted from photoautotrophically grown cells that continuously evolve O₂. Furthermore, as proof of



concept, we introduced functional HoxJ* and HoxA into *E. coli* to modulate the expression of a reporter gene fused to a HoxA-responsive heterologous promoter. Our study provides the basis for further engineering of a cyanobacterial H₂ biosensor strain that might enable a systematic screening of genetic setups and the selection of those beneficial for H₂ production by the host-specific or other introduced hydrogenases (Figure 1B).

2. Materials and methods

2.1. Strains and culture conditions

Escherichia coli strains DH5α or JM109 were grown at 37°C either on agar-solidified LB medium or in LB liquid medium supplemented with 5 g L⁻¹ NaCl under continuous shaking at 200 rpm. To select for the presence of certain plasmids the medium was supplemented with 100 μg mL⁻¹ ampicillin, 35 μg mL⁻¹ chloramphenicol, or 50 μg mL⁻¹ spectinomycin. *C. necator* (obtained from the German Collection of Microorganisms and Cell Cultures, DSMZ) was grown at 37°C in LB liquid medium supplemented with 2.5 g L⁻¹ NaCl under continuous shaking at 200 rpm. *Synechocystis* was cultivated in yBG11 (Scholnick et al., 2007) liquid medium under continuous shaking at 150 rpm, or BG11 (Stanier et al., 1979) solidified with 1.5% (w/v) Bacto agar (Becton Dickinson) and supplemented with 3 g L⁻¹ Na₂S₂O₃. The cyanobacterial growth media were buffered with 10–50 mM HEPES to pH 7.2. Photoautotrophic growth conditions were set to 30°C, ambient CO₂, constant light illumination with 50 μmol photons

m⁻² s⁻¹, and 75% (v/v) humidity. For the selection of mutants, the media were supplemented with 10 μg mL⁻¹ chloramphenicol, 20 μg mL⁻¹ spectinomycin, or 50 μg mL⁻¹ kanamycin. A non-motile, glucose tolerant strain of *Synechocystis*, originally received from Martin Hagemann (Rostock University, Germany), was used as the wild type (WT). The mutant *Synechocystis*(Δhox) that is devoid of the endogenous [NiFe]-hydrogenase was obtained from Kirsten Gutekunst (Kassel University, Germany). In particular, *hoxEFUYH* (*sil1220-sil1226*) have been replaced by a kanamycin resistance cassette (Appel et al., 2020).

2.2. Construction of plasmids and recombinant strains

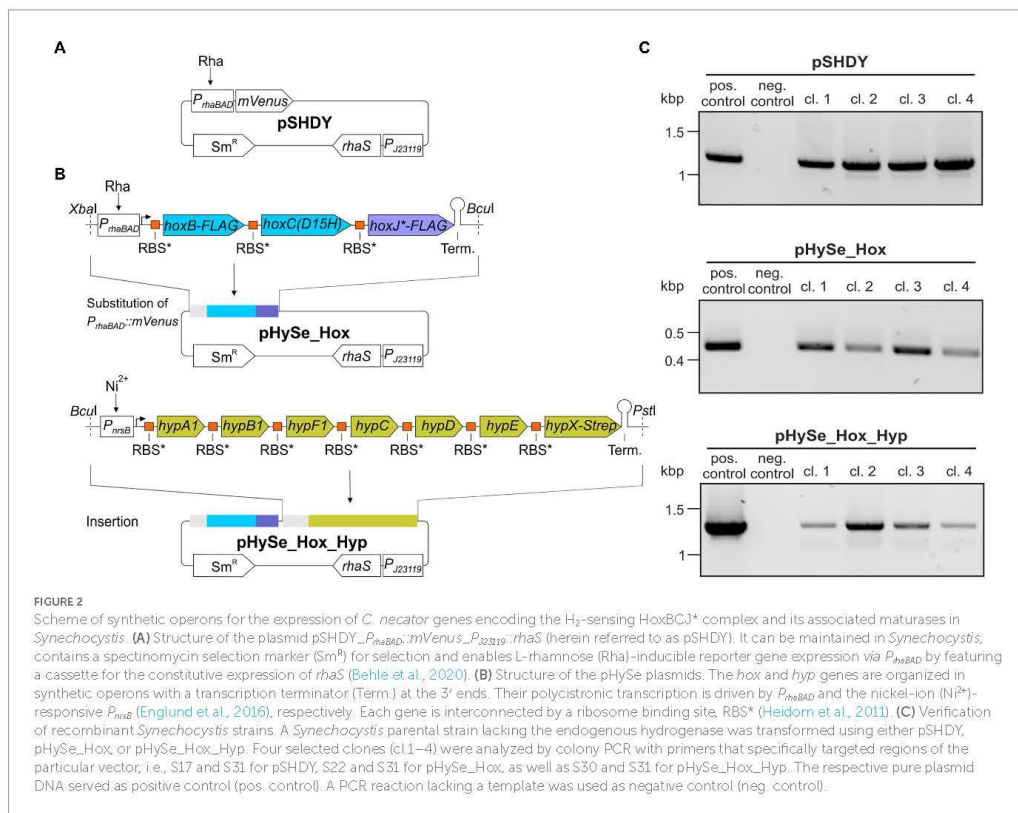
In silico work was performed using the software Geneious (Biomatters). Genetic constructs were generated through standard molecular cloning procedures and maintained on plasmids in *E. coli* DH5α. DNA processing and recombination were performed using FastDigest restriction endonucleases (Thermo Scientific), T4 DNA ligase (Thermo Scientific), and FastAP thermosensitive alkaline phosphatase (Thermo Scientific) following the manufacturer's instructions. The obtained constructs were verified by Sanger sequencing. Information about used oligonucleotides and plasmids is given in Supplementary Tables S1, S2.

The sequences for the design of synthetic operons encoding the H₂-sensing complex and the corresponding maturases were obtained from the megaplasmid pHG1 of *C. necator* (Schwartz

et al., 2003). The *hoxJ* sequence was modified to code for a variant exhibiting an amino acid substitution from serine to glycine at position 422, denoted as HoxJ* (Lenz and Friedrich, 1998). The *hoxC* sequence was altered to instead encode the variant HoxC(D15H) (Gebler et al., 2007). The gene sequences were codon-usage optimized for *Synechocystis* using the web-based tool JCat (Grote et al., 2005). The inducible promoters P_{rhaBAD} (Behle et al., 2020) and P_{rhaS} (Englund et al., 2016) were fused to the *hox* and *hyp* operons, respectively. The constructs were also equipped with unique restriction endonuclease sites flanking each operon, effective ribosome binding sites (RBS*, Heidorn et al., 2011) upstream of each ORF, as well as standardized transcription terminators (BioBrick Bba_B0015, Registry of Standard Biological Parts, 2003). Tag-encoding sequences were added to the 3' ends of the open reading frames of *hoxB* (3xFLAG-tag), *hoxJ** (3xFLAG-tag) and *hypX* (Strep-tag), respectively. The synthetic operons were chemically synthesized (Eurofins Genomics) and provided on plasmids, denoted as pHox2 and pHyp. For the maintenance in *Synechocystis*, the synthetic operons were transferred, either separately or combined, into the plasmid pSHDY_ $P_{rhaBAD}::mVenus_{P_{J23119}}::rhaS$ (Behle et al., 2020) via *XbaI/BclI* and *BclI/PstI* sites, respectively. Thereby, the $P_{rhaBAD}::mVenus$ cassette was replaced. The resulting plasmids were named pHySe_Hox and pHySe_Hox_Hyp

(Figure 2). The full sequences including annotations are provided in the Supplementary Data.

Plasmids of the pFO series and derivatives of pSB1A2_ P_{trc10} (Huang et al., 2010), all of which harbor various combinations of expression cassettes for the genes *hoxA*, *hoxJ** and *sfgfp*, were generated via the Gibson assembly procedure (Gibson et al., 2009). For this, respective sequences were amplified via PCR using primers with 5' extensions to create homologous overhangs for the desired assembly with other DNA fragments. The P_{SH} promoter, including the 5' untranslated upstream region of *hoxF* (Zimmer et al., 1995; Schwartz et al., 1998), was amplified from genomic DNA of *C. necator* using primer pair P17/P18. Together with the *sfgfp* reporter gene and a downstream BioBrick Bba_B0015 transcription terminator, which were generated through PCR with primers P16/Sam_102 from pSEVA351-*sfgfp* (Opel et al., 2022), it was used for the assembly of pFO6 utilizing *KpnI*-treated pSEVA351 (Martínez-García et al., 2020) as vector. The *hoxA* gene was amplified from gDNA of *C. necator* using P25 that additionally contained the ribosome binding site BioBrick Bba_B0034 (Registry of Standard Biological Parts, 2003) as 5' extension and P26 fusing a sequence encoding a hexahistidine-tag at the 3' end of the gene. The linear fragment was used for the assembly with *BclI*-cut pSB1A2, yielding pSB1A2_ P_{trc10} -*hoxA*. pSB1A2_ P_{trc10} -*hoxA*^{D55A} has a substitution at



the codon coding for the amino acid at position 55 of HoxA from 5'-GAT-3' (Asp) to 5'-GCC-3' (Ala). It was generated with the *DpnI*-digested product from an inverted PCR, taking pSB1A2-*P_{trcIO}*-*hoxA* as template and the primer pair P52/P53, as well as the homologous overhangs-supplying HoxA(D55A) double-stranded DNA fragment. The *P_{trcIO}*-*hoxA* and *P_{trcIO}*-*hoxA^{D55A}* constructs were PCR-amplified using primers P49 and P50 from either pSB1A2-*P_{trcIO}*-*hoxA* or pSB1A2-*P_{trcIO}*-*hoxA^{D55A}*, thereby fused to a 3' sequence encoding a Strep-tag II, instead of the His-tag, to be each inserted into *BcuI*-linearized pSEVA351, yielding pFO25 and pFO26, respectively. Analogously, these two synthetic gene constructs were inserted into *BcuI*-cut pFO6, which resulted in pFO27 and pFO28, respectively. To obtain pFO45 and pFO46, pHox2 was first subjected to an inverted PCR using P83 and P84, thereby deleting *hoxB^{FLAG}* and *hoxC^{D15H}* as well as the particular upstream situated RBS*. This was followed by AQUA cloning, creating pHox5 that encodes the *P_{hxBAD}::hoxF^{FLAG}* cassette. The latter was excised by restriction with *XbaI* and inserted into *XbaI*-linearized pFO27 and pFO28, yielding pFO45 and pFO46, respectively. Sequences of the pFO series are provided in the [Supplementary Data](#).

Synechocystis WT as well as *Synechocystis*(Δ *hox*) parental cells were made electro-competent and transformed *via* electroporation as described previously (Brandenburg et al., 2021). Plasmid-harboring strains were selected on BG11 agar plates containing appropriate antibiotics. Plasmid presence was verified by colony PCR using suitable primers and the GoTaq MasterMix (Promega) according to the manufacturer's instructions. Recombinant *E. coli* JM109 strains were generated by electroporation of electro-competent cells *via* standard procedures.

2.3. RNA isolation and transcript analyses

For the isolation of RNA, *Synechocystis* cells were grown until reaching an OD₇₅₀ ~0.8. The cultures were subsequently supplemented with final concentrations of 0.1% (w/v) L-rhamnose and 5 μ M NiSO₄. After 24 h, cells were harvested by rapid vacuum filtration applying sterilized polyether sulfone filters (pore size 0.8 μ m, PALL). RNA isolation was performed as described previously (Bolay et al., 2022). The RNA samples were treated with RNase-free DNase I (Thermo Scientific) according to the manufacturer's instructions. Afterwards, cDNA was generated by applying the high-capacity cDNA reverse transcription kit (Thermo Scientific) as given in the manufacturer's instructions. A total of ~0.4 ng cDNA were used as template for quantitative PCR. Amplification of specific regions within either the *rnpB* gene or *hypX* were performed using the GoTaq MasterMix (Promega) according to the manufacturer's instructions and primer pairs *rnpB*_{114F}/*rnpB*_{226R} and S30/P88, respectively ([Supplementary Table S1](#)).

2.4. Protein extraction and Western blots

Synechocystis cells were grown in presence of elevated CO₂ concentration of 2% (v/v) to an OD₇₅₀ of ~2. To induce expression of the *hox* and *hyp* genes the medium was supplemented with final

concentrations (f.c.) of 0.2% (w/v) L-rhamnose and 5 μ M NiSO₄. In addition, 17 μ M (f.c.) ferric ammonium citrate was added to foster hydrogenase maturation similar to previous reports (Lupacchini et al., 2021). Samples were collected by centrifugation after 24 and 48 h. Cells were resuspended in 750 μ L TBS lysis buffer (100 mM Tris, 150 mM NaCl, 1 mM PMSE, pH 7.5) and transferred to 2 mL Precellys tubes (Bertin), together with a mixture of glass beads (Sartorius) of 0.09–0.15, 0.17–0.18, and 0.5 mm diameter. Cell disruption was performed using a Precellys Evolution homogenizer (Bertin) equipped with a Cryolys cooling system (Bertin) for 4 \times 30 s at 10,000 rpm with 30 s interim breaks for cooling. The samples were subsequently separated in supernatant (soluble extract) and sediment (crude extract) by centrifugation and subjected to protein concentration determination using a Bradford dye reagent ready-to-use solution (Thermo Scientific) according to the manufacturer's instructions. Cell suspensions of recombinant *E. coli* JM109 strains were analogously treated to obtain soluble protein extracts. Those cells were beforehand cultivated as described for GFP fluorescence determination, but using 0.5% (w/v) D-glucose instead of glycerol. Protein separation was performed *via* SDS-PAGE using a total amount of 20 μ g protein for each sample. For immunodetection *via* Western blots the separated proteins were transferred to nitrocellulose membranes of 0.45 μ m pore size (GVS), followed by hybridization with either a Strep-Tactin horse radish peroxidase (HRP) (IBA Lifesciences GmbH) or a monoclonal ANTI-FLAG M2-Peroxidase conjugate (Sigma-Aldrich) according to the manufacturer's instructions. Chemiluminescence was detected by using the substrate solutions WesternSure PREMIUM Chemiluminescent (LI-COR) or WesterBright ECL (advansta) and the Fusion FX7 EDGE V0.7 imaging system (VILBER), following the manufacturer's instructions.

2.5. Hydrogenase activity assays

Pre-cultivation of *Synechocystis* was performed as described above and expression of heterologous genes was induced by 0.1% (w/v) L-rhamnose and/or 2.5 μ M NiSO₄. After 48 h, cells were harvested and disrupted analogously but using an alternative lysis buffer (5% (v/v) glycerol, 50 mM KPO₄, 1 mM PMSE, pH 8). A *Synechocystis* strain harboring the *hoxFUYHW* genes encoding the SH from *C. necator* (Lupacchini et al., 2021) served as control. Approximately 400 μ g of soluble proteins were separated *via* native PAGE and subjected to in-gel staining as previously described (Lupacchini et al., 2021) with few modifications. These concerned the supplementation of 90 μ M phenazine methosulfate, additionally to 800 μ M NAD⁺ and 60 μ M nitro blue tetrazolium (NBT) in an H₂-saturated activity buffer (50 mM Tris, pH 8). Furthermore, the incubation time was increased from ~0.5 h to ~2.5 h. Hydrogenase activity, i.e., the release of electrons from H₂ oxidation, is indicated *via* a step-wise reduction of the electron transfer mediators NAD⁺ and/or phenazine methosulfate and the colorimetric dye nitro blue tetrazolium, which finally results in a visible precipitation of formazan (Ponti et al., 1978). The gels were subsequently decolorized from the remaining loading dye in activity buffer overnight. Afterwards, presence of HoxB and HoxJ* proteins was confirmed by blotting the same polyacrylamide gel and hybridizing the membrane with antibodies against the attached 3xFLAG-tag as described above.

2.6. GFP fluorescence determination

Recombinant *Synechocystis* strains containing plasmids pFO25 (negative control), pFO6 ($P_{SH::sfgfp}$), pFO27 ($P_{SH::sfgfp} + P_{trcO::hoxA}$), or pFO28 ($P_{SH::sfgfp} + P_{trcO::hoxA}^{D55A}$) were analyzed *in vivo* regarding GFP fluorescence. The detection was performed as described previously (Opel et al., 2022). GFP fluorescence determination in *E. coli* JM109 was conducted for recombinant strains harboring the following plasmids: pSEVA351 (negative control), pFO27 ($P_{SH::sfgfp} + P_{trcO::hoxA}$), pFO45 ($P_{SH::sfgfp} + P_{trcO::hoxA} + P_{rhaBAD::hoxJ^*}$), and pFO46 ($P_{SH::sfgfp} + P_{trcO::hoxA}^{D55A} + P_{rhaBAD::hoxJ^*}$). Single colonies from selective LB agar plates were picked to inoculate liquid LB medium pre-cultures that were grown for ~18 h at 37°C. 1% (v/v) of these suspensions were taken to inoculate second pre-cultures using M9* medium, supplemented with 0.001% (w/v) thiamine, 2 mM MgSO₄, 0.4% (v/v) glycerol, US* trace elements solution, and buffered to pH 7.2. The M9* pre-cultures were incubated for ~24 h at 37°C. A volume of 100 µL of these cell suspensions were added to 10 mL M9* medium in baffled shake flasks, and the cells were further cultivated at 30°C instead, due to the temperature sensitivity of HoxA (Zimmer et al., 1995). These main cultures were supplemented with 10 µM IPTG and/or 0.2% L-rhamnose after 8 h, followed by another 16 h of cultivation. For GFP fluorescence determination, samples were diluted to an OD₆₀₀ of ~0.5 with TBS buffer (100 mM Tris, 150 mM NaCl, pH 7.5) in a final volume of 1,200 µL. Technical triplicates (each 200 µL) were transferred into an opaque black flat microtiter 96-well-plate (Nunc), followed by fluorescence measurements using an Infinite 200 PRO microplate reader (Tecan; gain: 123, integration time: 20 µs, excitation bandwidth: 9 nm, emission bandwidth: 20 nm, z-position: 2000 µm, 25 flashes) and excitation/emission wavelengths of 485 nm/520 nm, respectively. Furthermore, the same sample was used to measure the absorption at 600 nm in a transparent flat microtiter 96-well-plate (Nunc), also using the Infinite 200 PRO microplate reader (bandwidth: 9 nm, 25 flashes). The blank of the TBS buffer background was subtracted from the values detected for the cell suspensions. The fluorescence intensities were finally normalized by division of respective OD₆₀₀ values.

3. Results

3.1. Design of customized operons for the expression of a H₂-sensing complex in a cyanobacterial host

To functionally produce the RH of *C. necator* in *Synechocystis*, we rationally designed two operons *in silico* that were generated via chemical synthesis and inserted it into a vector that can be maintained in *Synechocystis* (Figures 2A,B). In case of the active site-containing HoxC subunit, we made use of the amino acid exchange variant HoxC(D15H), which, in contrast to the native protein, supports H₂-dependent growth of *C. necator* at an O₂ level of up to 10% (Gebler et al., 2007). The resulting gene cluster for the biosynthesis of the H₂-sensing complex comprised *hoxB*, *hoxC^{D15H}*, and *hoxJ^{*}*. For proper maturation of the catalytic [NiFe] center we also utilized the corresponding accessory genes *hypA1B1FCDEFX* (Buhrke et al., 2001; Bürstel et al., 2016). In *C. necator*, these genes are organized in

an operon structure with partially overlapping open reading frames (Schwartz et al., 2003). To ensure their correct expression in the cyanobacterial target organism, we altered the spatial organization by linking each *hox* and *hyp* gene by an artificial spacer region, resulting in separate translational units (Figure 2B). Furthermore, the synthetic ribosome binding site RBS* which functions in *Synechocystis* (Heidorn et al., 2011), was introduced upstream of every single gene to enable efficient translation initiation. For facile detection of the proteins, sequences encoding either a 3xFLAG-tag or a Strep-tag were fused to *hoxB*, *hoxJ^{*}*, and *hypX* (Figure 2B). The *hoxJ^{*}* and *hypX* genes were chosen because they are the dorsal genes of each particular operon. Detection of both proteins is considered representative of upstream gene expression.

All protein-coding sequences were codon-usage optimized for translation in *Synechocystis*. To drive the polycistronic transcription of *hox* and *hyp* gene clusters, we used the L-rhamnose-inducible promoter P_{rhaBAD} from *E. coli* (Behle et al., 2020) and the nickel ion (Ni²⁺)-dependent promoter P_{nrs} of *Synechocystis* (Englund et al., 2016), respectively. Thus, this setup permits a selective induction as well as a tight and tunable transcription of the synthetic gene constructs $P_{rhaBAD::hoxB}^{FLAG}C^{D15H}J^{*}FLAG$ (*hox* operon) and $P_{nrs::hypA1B}IF1CDEFX^{Strep}$ (*hyp* operon) in *Synechocystis*. Moreover, both operons were equipped with insulating transcription terminators at their 3' end.

The constructs were inserted into the replicative vector pSHDY- $P_{rhaBAD::mVenus}$ - P_{P23112} -*rhaS* (hereafter referred to as pSHDY), which encodes the heterologous transcriptional regulator RhaS that enables rhamnose-inducible gene expression in *Synechocystis* (Behle et al., 2020). The $P_{rhaBAD::mVenus}$ cassette present in this pSHDY construct (Figure 2A) was replaced with the synthetic *hox* operon resulting in the plasmid pHySe_Hox. Subsequently, the *hyp* operon was inserted downstream to obtain the plasmid pHySe_Hox_Hyp (Figure 2B). The resulting plasmids pHySe_Hox and pHySe_Hox_Hyp, as well as the precursor construct pSHDY, were used individually for the transformation of *Synechocystis*. For transformation, a strain devoid of the endogenous [NiFe]-hydrogenase, designated *Synechocystis*(Δ *hox*) (Appel et al., 2020), was used to prevent subsequent cross-reactions with the RH activity. Plasmid presence was verified in all obtained clones (Figure 2C).

3.2. The genes encoding the H₂-sensing complex are expressed in *Synechocystis*

C-terminal linkage with 3x-FLAG (HoxB & HoxJ^{*}) or Strep-tags (HypX), enabled protein detection by commercially available antibodies targeting the corresponding tag. The *Synechocystis* strain harboring pHySe_Hox_Hyp was grown in the presence of L-rhamnose and Ni²⁺ to trigger *hox* and *hyp* gene expression, respectively (see section "Materials and methods" for specific inducer concentrations). To confirm heterologous gene expression, we performed immunoblotting to detect HoxB and HoxJ^{*} using protein extracts of samples collected 24 and 48 h after induction. In addition to the crude extract, we also analyzed the soluble protein fraction obtained by centrifugation. In fact, distinct bands were detected, and their intensity increased according to the induction time. The bands represent HoxB-FLAG and HoxJ^{*}-FLAG, as no signal was detected in the same size

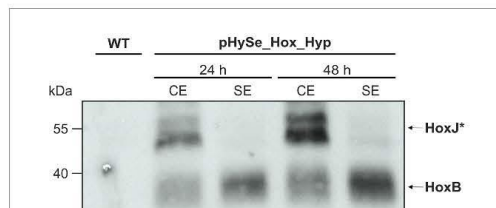


FIGURE 3
HoxJ* and HoxB from *C. necator* are synthesized in *Synechocystis*. Western blot for the detection of HoxJ*-FLAG and (~54kDa) HoxB-FLAG (~40kDa) fusion proteins. Samples were taken from *Synechocystis*(*ΔhoxJ*) that harbored the plasmid pHySe_Hox_Hyp, 24 and 48h after induction with 0.2% (w/v) L-rhamnose and 5μM NiSO₄. Protein extract of a *Synechocystis* wild type (WT) strain served as negative control. CE, crude extract; SE, soluble extract.

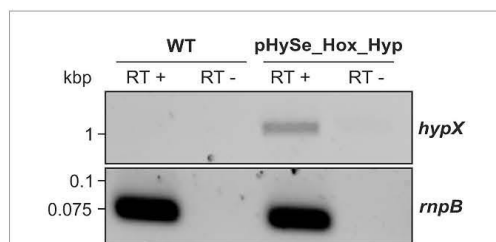


FIGURE 4
The polycistronic *hyp* mRNA is being transcribed in *Synechocystis*. PCR amplification of *hypX* or the housekeeping gene *rnpB* from cDNA that has been prepared from RNA isolates of *Synechocystis* wild type (control) or a strain harboring pHySe_Hox_Hyp. Samples in lanes denoted "RT +" were treated with reverse transcriptase beforehand, while those indicated "RT -" were not.

range in the *Synechocystis* wild-type strain (WT) (Figure 3). Consistent with the expected cytoplasmic localization of the RH, a strong signal for HoxB-FLAG was observed in the soluble extracts. However, the signal associated with HoxJ*-FLAG, which is also thought to be soluble, was predominantly present in the crude extract indicating partial protein misfolding or membrane association. Nevertheless, even though the signal was quite weak, a significant part was also found in the soluble fraction, in particular 48h after induction. Thus, both fusion proteins were specifically detected, confirming the expression of the corresponding genes.

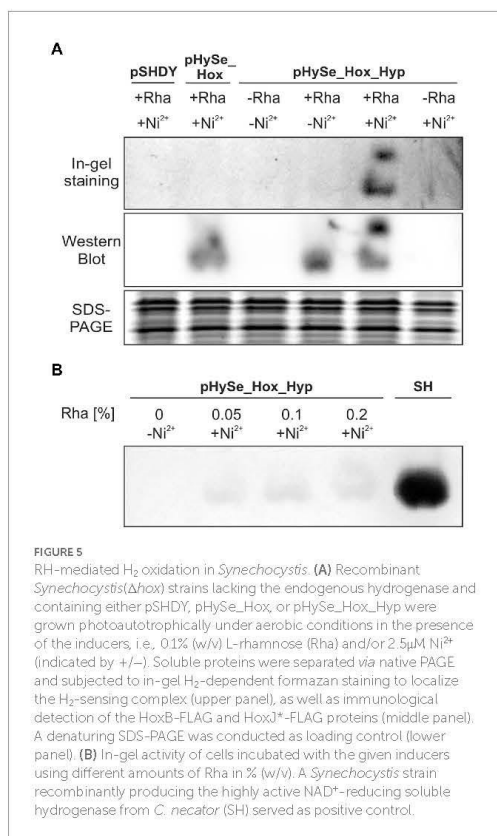
In case of HypX-Strep, however, no specific signal was observed in cells containing pHySe_Hox_Hyp (not shown), indicating either no translation or protein instability. To verify that the synthetic *hyp* operon is at least transcribed, we extracted total RNA from the same strain and performed classical reverse transcriptase (RT)-PCR targeting *hypX*. The reversely transcribed copy DNA (cDNA) for *hypX* was only detected in the *Synechocystis* strain containing pHySe_Hox_Hyp but not in the WT (Figure 4). That the band obtained is indeed a result of cDNA amplification of a *hypX* transcript was verified by a parallel RNA sample that was not treated with reverse transcriptase and consequently showed no bands for *hypX* and the housekeeping

gene *rnpB*. As *hypX* is situated at the 3' end of the synthetic gene cluster, we assume, that transcription of the upstream situated *hyp* genes also occurred. However, this analysis did not confirm the translation of the *hyp* gene transcripts. Nevertheless, sufficient synthesis of the maturation apparatus for the RH could be assumed, as indicated by the subsequent analysis (see below).

3.3. The H₂-sensing complex is active when matured in *Synechocystis* cells growing photoautotrophically

To investigate if the recombinant gene expression indeed results in the formation of active H₂-sensing RH, we analyzed the H₂ oxidation activity in soluble extracts of photoautotrophically grown cells of *Synechocystis* strains harboring the plasmids pSHDY, pHySe_Hox, and pHySe_Hox_Hyp. To this end, we used an in-gel activity assay under an H₂ atmosphere (Buhre et al., 2004), which has also been used recently to confirm the activity of hydrogenases in *Synechocystis* (Lupacchini et al., 2021). The recombinant strains were cultivated in the presence of different inducer combinations to achieve independent expression of the *hoxBCJ** genes (L-rhamnose) and the *hypA1B1FCDEX* operon (Ni²⁺). Soluble protein extracts were prepared and subjected to native polyacrylamide gel electrophoresis. Strikingly, in-gel H₂ oxidation activity was detected only for *Synechocystis*(pHySe_Hox_Hyp) induced with both L-rhamnose and Ni²⁺ (Figure 5A, In-gel staining panel). The resulting activity bands were located at the same positions as the bands in the immunoblot analysis (also based on the native gel), showing HoxB-FLAG in complex with HoxC as the hydrogenase core module, and potentially HoxJ*-FLAG (Figure 5A, Western Blot panel). As the production of both HoxB-FLAG and HoxJ*-FLAG has been confirmed by a previous Western blot (Figure 3), a separate detection of both proteins has not been performed in this case. No H₂ oxidation activity was detected in the corresponding native gel, when the Hyp proteins required to produce catalytically active RH were absent, either due to the lack of the *hyp* genes (in case of strain pHySe_Hox) or the inducer Ni²⁺ (in case of strain pHySe_Hox_Hyp) (Figure 5A). Thus, expression of both the *hox* and *hyp* gene clusters is required to obtain detectable H₂ oxidation activity for the H₂-sensing RH in *Synechocystis*. While most [NiFe]-hydrogenases are inactivated by traces of O₂ (Shafaat et al., 2013), the RH activity has shown to be O₂-tolerant (Ash et al., 2015). Remarkably, the RH activity was observed in extracts of O₂-evolving photoautotrophically grown *Synechocystis* cells, indicating that both the maturation process and the catalytic activity of the RH occurred in the presence of O₂.

The RH activity in *Synechocystis* is comparatively low, as demonstrated by the long incubation time of ~2.5h required to obtain detectable bands derived from H₂-dependent NBT reduction in the activity gel. A *Synechocystis* control strain containing the highly active SH from *C. necator* (Lupacchini et al., 2021) showed significantly stronger signal intensities after ~0.5h already. The low signal strength of the RH in *Synechocystis* could not be increased by enhanced L-rhamnose levels, suggesting a saturation at 0.05% (w/v) rhamnose and consequently no limitation of the RH structural proteins (Figure 5B). Altogether, these results demonstrate for the first time the functional production of a recombinant regulatory hydrogenase with low H₂ turnover activity in a cyanobacterium.



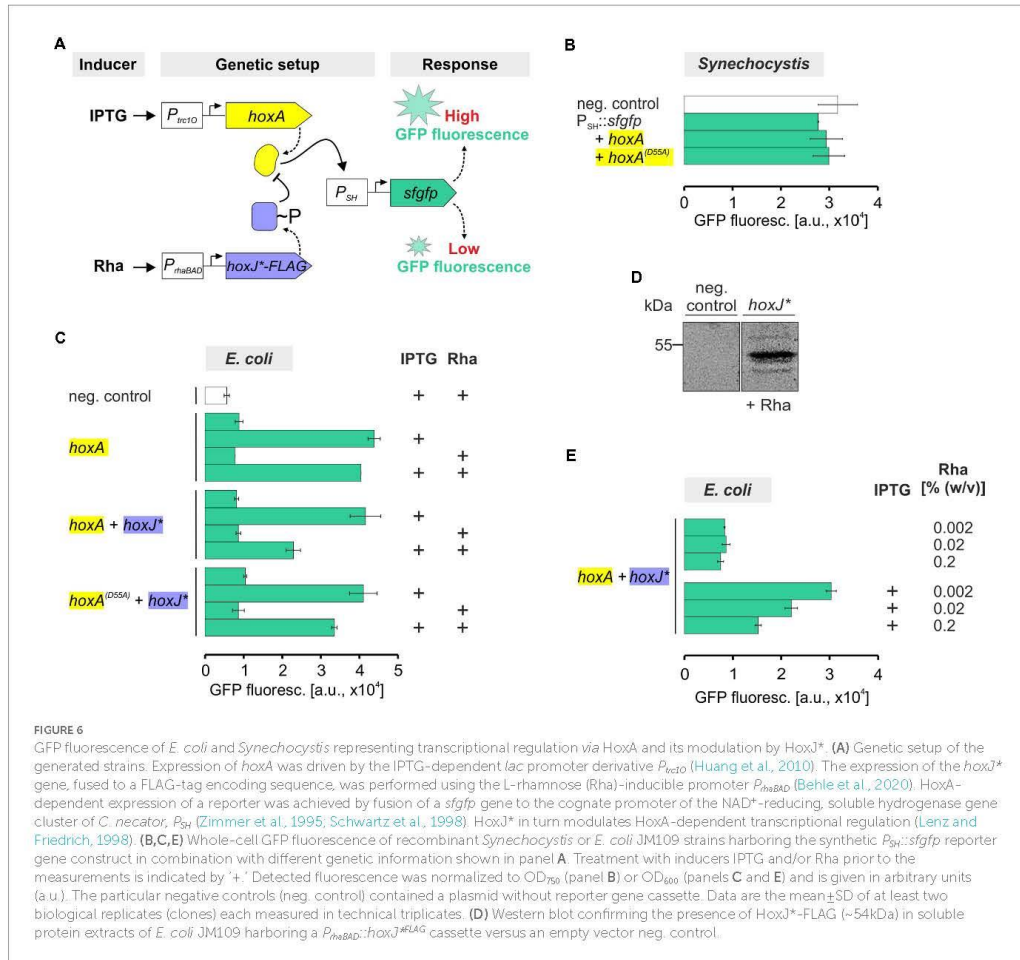
3.4. Transcriptional regulation and its modulation by the associated two-component system in a heterologous host

The final goal is to couple the functional RH with the associated kinase HoxJ* and the cognate response regulator HoxA to establish an H₂-sensing signal transduction cascade in *Synechocystis*. In *C. necator*, HoxA positively controls the transcription of the genes encoding the SH and the MBH through binding to the promoters P_{SH} and P_{MBH} , respectively (Zimmer et al., 1995; Schwartz et al., 1998). The HoxA activity is modulated by HoxJ*-mediated phosphorylation, with transcriptional activation by HoxA in its non-phosphorylated state (Lenz and Friedrich, 1998). To drive HoxA-mediated gene expression in *Synechocystis*, the *hoxA* gene was set under control of the IPTG-inducible P_{trc10} promoter, which has been shown to provide sufficient constitutive expression due to the lack of the *lac* repressor LacI in the cyanobacterial host (Huang et al., 2010). Furthermore, a *sfGFP* reporter gene encoding the superfolder green fluorescent protein (Pédrelacq et al., 2006) (hereafter referred to as GFP) was fused to the HoxA-dependent promoter P_{SH} (Figure 6A). The

synthetic gene constructs $P_{SH}::sfGFP$ and $P_{trc10}::hoxA$ were introduced into *Synechocystis* WT, either separately or combined on a replicative plasmid. However, no significant GFP fluorescence beyond background activity was detected in any strain carrying the reporter gene construct alone or in combination with $P_{trc10}::hoxA$ (Figure 6B). An inactivation of HoxA by unspecific phosphorylation could be excluded because the GFP fluorescence was similar in a reporter strain containing the phosphorylation-insensitive variant HoxA(D55A) instead of HoxA. This variant cannot be phosphorylated at the crucial aspartate at position 55 and has been shown to be always active (Lenz and Friedrich, 1998). Although several attempts have been made to improve *hoxA* expression, e.g., by using different promoters as well as codon-usage optimized gene variants, HoxA-dependent *sfGFP* expression has not yet been achieved in *Synechocystis* (not shown).

However, to validate the general functionality of our genetic constructs and to establish HoxA and HoxJ*-dependent gene expression in a heterologous system, we introduced the same replicative plasmids harboring $P_{trc10}::hoxA$ and $P_{SH}::sfGFP$ into *E. coli* JM109. As this host contains LacI, *hoxA* expression is IPTG-inducible. Indeed, a ~5-fold higher GFP fluorescence was detected in cells grown in presence of IPTG compared to cells grown in absence of IPTG (Figure 6C). Under non-induced conditions, the GFP fluorescence was similar to the background autofluorescence of control cells harboring the empty vectors. Thus, in contrast to *Synechocystis*, the expected activity of HoxA to promote reporter gene expression via the P_{SH} promoter was confirmed in *E. coli*.

Moreover, another synthetic gene construct encoding HoxJ* was included in the study to demonstrate the modulation of HoxA activity. HoxJ*-mediated phosphorylation of HoxA is expected to inactivate the response regulator (Lenz and Friedrich, 1998; Buhrke et al., 2004). A gene encoding HoxJ* carrying a C-terminal FLAG-tag (HoxJ*^{FLAG}) was set under control of the L-rhamnose-inducible promoter P_{rhaBAD} , and the resulting plasmid was introduced into the strain already harboring the $P_{trc10}::hoxA$ construct. In general, this promoter could also be used in *Synechocystis* (Behle et al., 2020). Again, IPTG-induced *hoxA* gene expression resulted in GFP fluorescence. Remarkably, a significant decrease in GFP fluorescence was observed in cells that were grown in presence of both IPTG and L-rhamnose (Figure 6C). This correlates well with the exclusive detection of HoxJ* in protein extracts of cells grown in presence of L-rhamnose and carrying the respective gene construct (Figure 6D). The GFP level decreased to 50% compared to values obtained with strains either lacking the *hoxJ** gene or that do not sufficiently express *hoxJ** due to the absence of L-rhamnose. HoxA(D55A), which cannot be inactivated by HoxJ* through phosphorylation (Lenz and Friedrich, 1998), was again included as a control. As expected, a higher reporter signal was obtained with the corresponding strain in the presence of both IPTG and L-rhamnose than with the strain expressing wild-type *hoxA* as well as *hoxJ** (Figure 6C). This result also suggests that the response regulator in *E. coli* JM109 is not inactivated by unspecific phosphorylation. Thus, for HoxA, an effective ~30% reduction in reporter signal strength was achieved by HoxJ* compared to HoxA(D55A), demonstrating the desired modulation. Moreover, the HoxJ*-mediated decrease of HoxA-dependent GFP fluorescence was further tunable by different amounts of L-rhamnose (Figure 6E).



4. Discussion

H₂-based signal transduction cascades are considered being widespread, as the corresponding genes have been detected in many available genomes and metagenomes (Greening et al., 2016). Nevertheless, the biochemical and molecular mechanisms of H₂ sensing have been studied in only a few representative bacteria to date. Ever since, these systems have been engineered and coupled with reporters. For example, *C. necator* has been engineered regarding a HoxBCJA-dependent expression of *lacZ* encoding β -galactosidase as reporter (Lenz and Friedrich, 1998). In principle, such recombinant strains could be utilized for the detection of H₂ synthesized by other microbes, e.g., by co-cultivation or agar overlay assays on petridish basis (Wecker and Ghirardi, 2014). Similar to *C. necator*, the H₂-sensing system of *R. capsulatus* consists of four proteins: HupUV which form the H₂-sensing hydrogenase, the histidine kinase HupT,

and the transcriptional regulator HupR that finally activates expression of an energy-generating uptake hydrogenase (Dischert et al., 1999; Elsen et al., 2003). This system has also been developed into a biosensor to screen large libraries of H₂-producing nitrogenase variants in *R. capsulatus* directly (Barahona et al., 2016). Moreover, the corresponding strain has also been used as whole-cell biosensor to track H₂ production in co-cultivated green algae (Wecker et al., 2011). However, in the case of cyanobacteria, such a co-cultivation approach is not feasible since most bacterial strains do not grow in cyanobacterial growth media lacking an organic carbon source.

In order to monitor H₂ evolution within cyanobacterial cells, however, a signal transduction cascade must be transferred to the corresponding strain. This would allow *in vivo* screening of H₂ evolution and the optimization of strains carrying, e.g., alternative hydrogenases (Figure 1). For example, Wecker et al. used engineered *R. capsulatus* strains that monitor H₂ by reporter fluorescence to track

the activity of a recombinant H₂-evolving hydrogenase from *Clostridium acetobutylicum*. Only low H₂ production has been detected, but the system potentially enables further screening and hydrogenase evolution approaches (Wecker et al., 2017). We successfully implemented two parts of the four-part H₂-responsive signal transduction cascade from *C. necator* in the cyanobacterium *Synechocystis*. This is considered as a first step toward a synthetic cyanobacterial H₂ biosensor that could be used analogously to previous reports (Wecker et al., 2017). A potential application would be, for instance, to optimize the H₂ evolution activities of heterologously produced O₂-tolerant, energy-converting hydrogenases, one of which was successfully implemented in *Synechocystis* recently (Lupacchini et al., 2021).

According to the current model, H₂-sensing requires continuous H₂ activation, i.e., H₂ binding, H₂ cleavage, as well as the corresponding proton and electron transfer (Lenz et al., 2015). Protein-protein complex formation with HoxJ* is of course also required (Buhrke et al., 2004; Löscher et al., 2010). Thus, continuous H₂ oxidation is a prerequisite for H₂-sensing. While the H₂ oxidation activity of RH itself has been shown to be O₂ insensitive (Buhrke et al., 2005), the signal transduction process is sensitive to high O₂ levels. In this study, we therefore used a variant of the RH large subunit with an amino acid exchange near the active site, HoxC(D15H) (Gebler et al., 2007). The turnover rate of the native RH is almost two orders of magnitude lower than that of energy-conserving standard [NiFe]-hydrogenases (Bernhard et al., 2001). The H₂ oxidation activity of the HoxBC(D15H) variant is indeed another two orders of magnitude lower, which explains the weak signals observed in the in-gel activity assay (Figure 5). However, it mediated native-like H₂ signal transduction *in vivo* and supported H₂-dependent growth of *C. necator* even at 10% O₂, where signal transduction by the native RH was shown to be impaired (Gebler et al., 2007). The active-site containing HoxC subunit of RH also lacks a C-terminal extension that is typical for standard [NiFe]-hydrogenases and is proteolytically cleaved after insertion of the catalytic center (Kleihues et al., 2000). The comparatively simple structure, the lack of need for proteolytic quality control, the low H₂ consumption, and of course the O₂-tolerant H₂-sensing ability make the RH an ideal candidate for a synthetic cyanobacterial H₂ biosensor.

Here, we demonstrated that the recombinant RH in *Synechocystis* is synthesized in a catalytically active form, as evidenced by the H₂ oxidation activity detected in protein extracts. Moreover, the cell extracts were obtained from photoautotrophically grown, O₂-evolving cells. This shows that both the biocatalyst RH and its maturation machinery function properly under aerobic conditions in *Synechocystis*. In addition to the structural *hox* genes, the co-expression of the accessory *hypA1B1F1CDEX* genes of *C. necator* was required to achieve active RH. *Synechocystis* contains six endogenous Hyp proteins, likewise denoted HypA-E, that are responsible for the maturation of the bidirectional [NiFe]-hydrogenase of this organism (Hoffmann et al., 2006). However, *Synechocystis* lacks a homolog of the *C. necator* HypX. Based on our results, we cannot conclude whether all Hyp components or rather a reduced set from *C. necator* are necessary to achieve H₂ oxidation activity of the RH in *Synechocystis*. The *Synechocystis* Hyp proteins may at least partially compensate for the maturation of O₂-tolerant [NiFe]-hydrogenases from *C. necator* in the absence of the

corresponding heterologous assembly apparatus. Notably, the NAD⁺-reducing [NiFe]-hydrogenase from *C. necator* was functionally produced in *Synechocystis*, without co-expression of the associated *hyp* genes (Lupacchini et al., 2021). However, it has been suggested that the *C. necator* Hyp proteins may be required for full SH activity as they have an amino acid sequence identity with the *Synechocystis* homologs of only 50–67%. Furthermore, HypX is required for aerobic maturation of the [NiFe]-hydrogenases of *C. necator* (Bürstel et al., 2016; Schulz et al., 2020).

The transfer of signal-responsive components into heterologous hosts usually includes a promoter and the associated transcriptional regulator (Fernandez-López et al., 2015; Sonntag et al., 2020; Ni et al., 2021). Our objective was to transfer the H₂-sensing module (HoxBC) and the associated two-component regulatory system (HoxJ* and HoxA) to a cyanobacterial species to establish an H₂-dependent transcriptional response. This has not yet been achieved in *Synechocystis*, presumably due to the absence of the minor sigma factor σ^{54} in cyanobacteria (Riaz-Bradley, 2019), which is required for the transcriptional activation of *P_{SH}* and *P_{MBSH}* in *C. necator* (Zimmer et al., 1995; Schwartz et al., 1998). In addition, the DNA-bending integration host factor (IHF) may participate in hydrogenase promoter activation in *C. necator* (Zimmer et al., 1995; Schwartz et al., 1998). Accordingly, the introduction of this heterologous sigma factor or promoter engineering in *Synechocystis* should be pursued, which was beyond the scope of this study. However, as a proof of principle, we introduced HoxA and HoxJ* into *E. coli* to demonstrate the transcriptional regulation of a *sfGFP* reporter gene fused to *P_{SH}*. Specific HoxA-dependent GFP fluorescence was detected, likely related to the presence of σ^{54} in *E. coli* (Jones et al., 1994). Our data are consistent with previous findings on functional, HoxA-controlled expression of a reporter gene fused to *P_{SH}* in *E. coli* (Schwartz et al., 1998). Moreover, as expected, the kinase activity of HoxJ* clearly modulated the HoxA-dependent GFP fluorescence in *E. coli*, leading to a decreased reporter signal. Overall, we now have all genetic elements in hand to eventually assemble a functional H₂ biosensor with optical readout in a cyanobacterium. This could ultimately be used to monitor cyanobacterial H₂ production, e.g., to enable evolutionary or high-throughput screening approaches to improve hydrogenase properties as well as to circumvent existing constraints.

Data availability statement

The original contributions presented in the study are included in the article/Supplementary material, further inquiries can be directed to the corresponding author.

Author contributions

SK designed the study. FO, MAI, and IW constructed the plasmids. FO and IW performed the gene expression and RH activity analyses in *Synechocystis*. FO performed the GFP reporter assays. SL contributed to RH activity determination and experimental expertise for the in-gel assays. LL and OL contributed methodology and know-how on O₂-tolerant hydrogenases. FO and SK wrote the

manuscript with contributions from all co-authors. All authors contributed to the article and approved the submitted version.

Funding

This project was initiated by a grant of the Max-Buchner Foundation to SK (MBFSt-Kennziffer: 3714). We acknowledge the use of the facilities of the Centre for Biocatalysis (MiKat) at the Helmholtz Centre for Environmental Research, which is supported by European Regional Development Funds (EFRE, Europe funds Saxony). We also acknowledge the use of the facilities of H2Saxony. This project (Nr. 100361842) is financed from funds of the European Regional Development Fund (EFRE) and co-financed by means of taxation based on the budget adopted by the representatives of the Landtag of Saxony.

Acknowledgments

The authors thank Jens Appel (University of Kassel, Germany) for the fruitful discussions at the beginning of the project.

References

- Appel, J., Hueren, V., Boehm, M., and Gutekunst, K. (2020). Cyanobacterial *in vivo* solar hydrogen production using a photosystem I-hydrogenase (PsaD-HoxYH) fusion complex. *Nat. Energy* 5, 458–467. doi: 10.1038/s41560-020-0609-6
- Ash, P. A., Liu, J., Coutard, N., Heidary, N., Horch, M., Gudim, I., et al. (2015). Electrochemical and infrared spectroscopic studies provide insight into reactions of the NiFe regulatory hydrogenase from *Ralstonia eutropha* with O₂ and CO. *J. Phys. Chem. B* 119, 13807–13815. doi: 10.1021/acs.jpcc.5b04164
- Baebprasert, W., Jantaro, S., Khetkorn, W., Lindblad, P., and Incharoensakdi, A. (2011). Increased H₂ production in the cyanobacterium *Synechocystis* sp. strain PCC 6803 by redirecting the electron supply via genetic engineering of the nitrate assimilation pathway. *Metab. Eng.* 13, 610–616. doi: 10.1016/j.ymben.2011.07.004
- Barahona, E., Jiménez-Vicente, E., and Rubio, L. M. (2016). Hydrogen overproducing nitrogenases obtained by random mutagenesis and high-throughput screening. *Sci. Rep.* 6, 38291. doi: 10.1038/srep38291
- Behle, A., Saake, P., Germann, A. T., Dienst, D., and Axmann, I. M. (2020). Comparative dose-response analysis of inducible promoters in cyanobacteria. *ACS Synth. Biol.* 9, 843–855. doi: 10.1021/acssynbio.9b00505
- Bernhard, M., Bührke, T., Blejlevens, B., de Lacey, A. L., Fernandez, V. M., Albracht, S. P., et al. (2001). The H₂ sensor of *Ralstonia eutropha*. Biochemical characteristics, spectroscopic properties, and its interaction with a histidine protein kinase. *J. Biol. Chem.* 276, 15592–15597. doi: 10.1074/jbc.M009802200
- Berto, P., D'Adamo, S., Bergantino, E., Vallesse, E., Giacometti, G. M., and Costantini, P. (2011). The cyanobacterium *Synechocystis* sp. PCC 6803 is able to express an active FeFe-hydrogenase without additional maturation proteins. *Biochem. Biophys. Res. Commun.* 405, 678–683. doi: 10.1016/j.bbrc.2011.01.095
- Black, L. K., Fu, C., and Maier, R. J. (1994). Sequences and characterization of *hupU* and *hupV* genes of *Bradyrhizobium japonicum* encoding a possible nickel-sensing complex involved in hydrogenase expression. *J. Bacteriol.* 176, 7102–7106. doi: 10.1128/jb.176.22.7102-7106.1994
- Bolay, P., Schlüter, S., Grimm, S., Riediger, M., Hess, W. R., and Klähn, S. (2022). The transcriptional regulator RbcR controls ribulose-1,5-bisphosphate carboxylase/oxygenase (RuBisCO) genes in the cyanobacterium *Synechocystis* sp. PCC 6803. *New Phytol.* 235, 432–445. doi: 10.1111/nph.18139
- Brandenburg, F., Theodosiou, E., Bertelmann, C., Grund, M., Klähn, S., Schmid, A., et al. (2021). Trans-4-hydroxy-L-proline production by the cyanobacterium *Synechocystis* sp. PCC 6803. *Metab. Eng. Commun.* 12, e00155. doi: 10.1016/j.mec.2020.e00155
- Bühler, K., Bühler, B., Klähn, S., Krömer, J. O., Dusny, C., and Schmid, A. (2021). "11 biocatalytic production of white hydrogen from water using cyanobacteria" in *Photosynthesis: Biotechnological applications with microalgae*. ed. M. Rögner (Berlin, Boston: DE GRUYTER), 279–306.
- Bührke, T., Blejlevens, B., Albracht, S. P., and Friedrich, B. (2001). Involvement of *hup* gene products in maturation of the H₂-sensing NiFe hydrogenase of *Ralstonia eutropha*. *J. Bacteriol.* 183, 7087–7093. doi: 10.1128/JB.183.24.7087-7093.2001
- Bührke, T., Lenz, O., Krauss, N., and Friedrich, B. (2005). Oxygen tolerance of the H₂-sensing NiFe hydrogenase from *Ralstonia eutropha* H16 is based on limited access of oxygen to the active site. *J. Biol. Chem.* 280, 23791–23796. doi: 10.1074/jbc.M503260200
- Bührke, T., Lenz, O., Porthun, A., and Friedrich, B. (2004). The H₂-sensing complex of *Ralstonia eutropha*: interaction between a regulatory NiFe hydrogenase and a histidine protein kinase. *Mol. Microbiol.* 51, 1677–1689. doi: 10.1111/j.1365-2958.2003.03933.x
- Bürstel, I., Siebert, E., Frielingsdorf, S., Zebger, I., Friedrich, B., and Lenz, O. (2016). CO synthesized from the central one-carbon pool as source for the iron carbonyl in O₂-tolerant NiFe-hydrogenase. *Proc. Natl. Acad. Sci. U. S. A.* 113, 14722–14726. doi: 10.1073/pnas.1614656113
- Dischert, W., Vignais, P. M., and Colbeau, A. (1999). The synthesis of *Rhodospirillum rubrum* HupSL hydrogenase is regulated by the two-component HupT/HupR system. *Mol. Microbiol.* 34, 995–1006. doi: 10.1046/j.1365-2958.1999.01660.x
- Elsen, S., Duché, O., and Colbeau, A. (2003). Interaction between the H₂ sensor HupUV and the histidine kinase HupT controls HupSL hydrogenase synthesis in *Rhodospirillum rubrum*. *J. Bacteriol.* 185, 7111–7119. doi: 10.1128/JB.185.24.7111-7119.2003
- Englund, E., Liang, F., and Lindberg, P. (2016). Evaluation of promoters and ribosome binding sites for biotechnological applications in the unicellular cyanobacterium *Synechocystis* sp. PCC 6803. *Sci. Rep.* 6, 36640. doi: 10.1038/srep36640
- Fan, Q., Caserta, G., Lorent, C., Zebger, I., Neubauer, P., Lenz, O., et al. (2022). High-yield production of catalytically active regulatory NiFe-hydrogenase from *Cupriavidus necator* in *Escherichia coli*. *Front. Microbiol.* 13, 894375. doi: 10.3389/fmicb.2022.894375
- Fernandez-López, R., Ruiz, R., La Cruz, F. D., and Moncalián, G. (2015). Transcription factor-based biosensors enlightened by the analyte. *Front. Microbiol.* 6, 648. doi: 10.3389/fmicb.2015.00648
- Geblert, A., Burgdorf, T., de Lacey, A. L., Rüdiger, O., Martínez-Arias, A., Lenz, O., et al. (2007). Impact of alterations near the NiFe active site on the function of the H₂ sensor from *Ralstonia eutropha*. *FEBS J.* 274, 74–85. doi: 10.1111/j.1742-4658.2006.05565.x
- Gibson, D. G., Young, L., Chuang, R.-Y., Venter, J. C., Hutchison, C. A., and Smith, H. O. (2009). Enzymatic assembly of DNA molecules up to several hundred kilobases. *Nat. Methods* 6, 343–345. doi: 10.1038/NMETH1318
- Greening, C., Biswas, A., Carere, C. R., Jackson, C. J., Taylor, M. C., Stott, M. B., et al. (2016). Genomic and metagenomic surveys of hydrogenase distribution indicate H₂ is a widely utilised energy source for microbial growth and survival. *ISME J.* 10, 761–777. doi: 10.1038/ismej.2015.153
- Grote, A., Hiller, K., Scheer, M., Munch, R., Nortemann, B., Hempel, D. C., et al. (2005). JCat: a novel tool to adapt codon usage of a target gene to its potential expression host. *Nucleic Acids Res.* 33, W526–W531. doi: 10.1093/nar/gki376
- Heidorn, T., Camsund, D., Huang, H.-H., Lindberg, P., Oliveira, P., Stensjö, K., et al. (2011). Synthetic biology in cyanobacteria engineering and analyzing novel functions. *Meth. Enzymol.* 497, 539–579. doi: 10.1016/B978-0-12-385075-1.00024-x

Conflict of interest

The authors declare that the research was conducted in the absence of any commercial or financial relationships that could be construed as a potential conflict of interest.

Publisher's note


All claims expressed in this article are solely those of the authors and do not necessarily represent those of their affiliated organizations, or those of the publisher, the editors and the reviewers. Any product that may be evaluated in this article, or claim that may be made by its manufacturer, is not guaranteed or endorsed by the publisher.

Supplementary material

The Supplementary material for this article can be found online at: <https://www.frontiersin.org/articles/10.3389/fmicb.2023.1122078/full#supplementary-material>

- Hoffmann, D., Gutekunst, K., Klissenbauer, M., Schulz-Friedrich, R., and Appel, J. (2006). Mutagenesis of hydrogenase accessory genes of *Synechocystis* sp. PCC 6803. Additional homologues of *hupA* and *hupB* are not active in hydrogenase maturation. *FEBS J.* 273, 4516–4527. doi: 10.1111/j.1742-4658.2006.05460.x
- Howarth, R. W., and Jacobson, M. Z. (2021). How green is blue hydrogen? *Energy Sci. Eng.* 9, 1676–1687. doi: 10.1002/ese3.956
- Huang, H.-H., Camsund, D., Lindblad, P., and Heidorn, T. (2010). Design and characterization of molecular tools for a synthetic biology approach towards developing cyanobacterial biotechnology. *Nucleic Acids Res.* 38, 2577–2593. doi: 10.1093/nar/gkq164
- Immethun, C. M., Ng, K. M., DeLorenzo, D. M., Waldron-Feinstein, B., Lee, Y.-C., and Moon, T. S. (2016). Oxygen-responsive genetic circuits constructed in *Synechocystis* sp. PCC 6803. *Biotechnol. Bioeng.* 113, 433–442. doi: 10.1002/bit.25722
- Inaba, Y., Morioka, R., Junaid, M., Shiraiwa, Y., and Suzuki, I. (2018). Development of engineered sensor perceiving gaseous toluene signal in the cyanobacterium *Synechocystis* sp. PCC 6803. *J. Appl. Phycol.* 30, 71–78. doi: 10.1007/s10811-017-1277-1
- Jones, D. H., Franklin, F. C., and Thomas, C. M. (1994). Molecular analysis of the operon which encodes the RNA polymerase sigma factor sigma 54 of *Escherichia coli*. *Microbiology* 140, 1035–1043. doi: 10.1099/13500872-140-5-1035
- Kleihues, L., Lenz, O., Bernhard, M., Buhrke, T., and Friedrich, B. (2000). The H₂ sensor of *Ralstonia eutropha* is a member of the subclass of regulatory NiFe hydrogenases. *J. Bacteriol.* 182, 2716–2724. doi: 10.1128/JB.182.10.2716-2724.2000
- Lacey, R. E., Ye, D., and Ruffing, A. M. (2019). Engineering and characterization of copper and gold sensors in *Escherichia coli* and *Synechococcus* sp. PCC 7002. *Appl. Microbiol. Biotechnol.* 103, 2797–2808. doi: 10.1007/s00253-018-9490-7
- Lenz, O., and Friedrich, B. (1998). A novel multicomponent regulatory system mediates H₂ sensing in *Alcaligenes eutrophus*. *Proc. Natl. Acad. Sci. U. S. A.* 95, 12474–12479. doi: 10.1073/pnas.95.21.12474
- Lenz, O., Lauterbach, L., Frielingsdorf, S., and Friedrich, B. (2015). “4 oxygen-tolerant hydrogenases and their biotechnological potential” in *Biohydrogen*. ed. M. Rögner (Berlin, München, Boston: DE GRUYTER), 61–69.
- Lenz, O., Strack, A., Tran-Betcke, A., and Friedrich, B. (1997). A hydrogen-sensing system in transcriptional regulation of hydrogenase gene expression in *Alcaligenes* species. *J. Bacteriol.* 179, 1655–1663. doi: 10.1128/jb.179.5.1655-1663.1997
- Lenz, O., Zebger, I., Hamann, J., Hildebrandt, P., and Friedrich, B. (2007). Carbamoylphosphate serves as the source of CN⁻, but not of the intrinsic CO in the active site of the regulatory NiFe-hydrogenase from *Ralstonia eutropha*. *FEBS Lett.* 581, 3322–3326. doi: 10.1016/j.febslet.2007.06.027
- Li, T., Jiang, Q., Huang, J., Aitchison, C. M., Huang, F., Yang, M., et al. (2020). Reprogramming bacterial protein organelles as a nanoreactor for hydrogen production. *Nat. Commun.* 11:5448. doi: 10.1038/s41467-020-19280-0
- Löscher, S., Gebler, A., Stein, M., Sanganas, O., Buhrke, T., Zebger, I., et al. (2010). Protein-protein complex formation affects the Ni-Fe and Fe-S centers in the H₂-sensing regulatory hydrogenase from *Ralstonia eutropha* H16. *ChemPhysChem* 11, 1297–1306. doi: 10.1002/cphc.200901007
- Lubitz, W., Ogata, H., Rüdiger, O., and Reijerse, E. (2014). Hydrogenases. *Chem. Rev.* 114, 4081–4148. doi: 10.1021/cr4005814
- Lupacchini, S., Appel, J., Stauder, R., Bolay, P., Klähn, S., Lettau, E., et al. (2021). Rewiring cyanobacterial photosynthesis by the implementation of an oxygen-tolerant hydrogenase. *Metab. Eng.* 68, 199–209. doi: 10.1016/j.ymben.2021.10.006
- Mahidhara, G., Burrow, H., Sasikala, C., and Ramana, C. V. (2019). Biological hydrogen production: molecular and electrolytic perspectives. *World J. Microbiol. Biotechnol.* 35:116. doi: 10.1007/s11274-019-2692-z
- Martínez-García, E., Goñi-Moreno, A., Bartley, B., McLaughlin, J., Sánchez-Sampedro, L., Pascual del Pozo, H., et al. (2020). SEVA 3.0: an update of the standard European vector architecture for enabling portability of genetic constructs among diverse bacterial hosts. *Nucleic Acids Res.* 48, D1164–D1170. doi: 10.1093/nar/gkz1024
- Ni, C., Dinh, C. V., and Prather, K. L. J. (2021). Dynamic control of metabolism. *Annu. Rev. Chem. Biomol. Eng.* 12, 519–541. doi: 10.1146/annurev-chembioeng-091720-125738
- Opel, F., Siebert, N. A., Klatt, S., Tillinghoff, A., Hantke, J. G., Toepel, J., et al. (2022). Generation of synthetic shuttle vectors enabling modular genetic engineering of cyanobacteria. *ACS Synth. Biol.* 11, 1758–1771. doi: 10.1021/acssynbio.1c06605
- Paty, G., Hódi, B., Solymosi, D., Vass, I., and Kós, P. B. (2021). Increased sensitivity of heavy metal bioreporters in transporter deficient *Synechocystis* PCC 6803 mutants. *PLoS One* 16:e0261135. doi: 10.1371/journal.pone.0261135
- Pédélecq, J.-D., Cabantous, S., Tran, T., Terwilliger, T. C., and Waldo, G. S. (2006). Engineering and characterization of a superfolder green fluorescent protein. *Nat. Biotechnol.* 24, 79–88. doi: 10.1038/nbt1172
- Pterik, A. J., Schmelz, M., Lenz, O., Friedrich, B., and Albracht, S. P. (1998). Characterization of the active site of a hydrogen sensor from *Alcaligenes eutrophus*. *FEBS Lett.* 438, 231–235. doi: 10.1016/S0014-5793(98)01306-4
- Ponti, V., Dianzani, M. U., Cheeseman, K., and Slater, T. F. (1978). Studies on the reduction of nitroblue tetrazolium chloride mediated through the action of NADH and phenazine methosulphate. *Chem. Biol. Interact.* 23, 281–291. doi: 10.1016/0009-2797(78)90090-x
- Registry of Standard Biological Parts (2003). Available at: <http://parts.igem.org> (Accessed October 2022).
- Riaz-Bradley, A. (2019). Transcription in cyanobacteria: a distinctive machinery and putative mechanisms. *Biochem. Soc. Trans.* 47, 679–689. doi: 10.1042/BST20180508
- Schulz, A.-C., Frielingsdorf, S., Pommerening, P., Lauterbach, L., Bistoni, G., Neese, F., et al. (2020). Formyltetrahydrofolate Decarboxylase synthesizes the active site CO ligand of O₂-tolerant NiFe hydrogenase. *J. Am. Chem. Soc.* 142, 1457–1464. doi: 10.1021/jacs.9b11506
- Schwartz, E., Gerischer, U., and Friedrich, B. (1998). Transcriptional regulation of *Alcaligenes eutrophus* hydrogenase genes. *J. Bacteriol.* 180, 3197–3204. doi: 10.1128/JB.180.12.3197-3204.1998
- Schwartz, E., Henne, A., Cramm, R., Eitinger, T., Friedrich, B., and Gottschalk, G. (2003). Complete nucleotide sequence of pHG1: a *Ralstonia eutropha* H16 megaplasmid encoding key enzymes of H₂-based Lithoautotrophy and Anaerobiosis. *J. Mol. Biol.* 332, 369–383. doi: 10.1016/S0022-2836(03)00894-5
- Shafaa, H. S., Rüdiger, O., Ogata, H., and Lubitz, W. (2013). NiFe hydrogenases: a common active site for hydrogen metabolism under diverse conditions. *Biochim. Biophys. Acta* 1827, 986–1002. doi: 10.1016/j.bbabbio.2013.01.015
- Scholnick, S., Shaked, Y., and Keren, N. (2007). A role for mrgA, a DPS family protein, in the internal transport of Fe in the cyanobacterium *Synechocystis* sp. PCC 6803. *Biochim. Biophys. Acta* 1767, 814–819. doi: 10.1016/j.bbabbio.2006.11.015
- Sonntag, C. K., Flachbart, L. K., Maass, C., Vogt, M., and Marienhagen, J. (2020). A unified design allows fine-tuning of biosensor parameters and application across bacterial species. *Metab. Eng. Commun.* 11:e00150. doi: 10.1016/j.mec.2020.e00150
- Stanier, R. Y., Dernelles, J., Rippka, R., Herdman, M., and Waterbury, J. B. (1979). Generic assignments, strain histories and properties of pure cultures of cyanobacteria. *Microbiology* 111, 1–61. doi: 10.1099/00221287-111-1-1
- van Soom, C., de Wilde, P., and Vanderleyden, J. (1997). HoxA is a transcriptional regulator for expression of the *hup* structural genes in free-living *Bradyrhizobium japonicum*. *Mol. Microbiol.* 23, 967–977. doi: 10.1046/j.1365-2958.1997.2781648.x
- van Soom, C., Lerouge, I., Vanderleyden, J., Ruiz-Argüeso, T., and Palacios, J. M. (1999). Identification and characterization of *hupT*, a gene involved in negative regulation of hydrogen oxidation in *Bradyrhizobium japonicum*. *J. Bacteriol.* 181, 5085–5089. doi: 10.1128/JB.181.16.5085-5089.1999
- Wecker, M. S. A., Beaton, S. E., Chado, R. A., and Ghirardi, M. L. (2017). Development of a *Rhodospirillum rubrum* self-reporting model system for optimizing light-dependent, FeFe-hydrogenase-driven H₂ production. *Biotechnol. Bioeng.* 114, 291–297. doi: 10.1002/bit.26076
- Wecker, M. S. A., and Ghirardi, M. L. (2014). High-throughput biosensor discriminates between different algal H₂-photoproducing strains. *Biotechnol. Bioeng.* 111, 1332–1340. doi: 10.1002/bit.25206
- Wecker, M. S., Meuser, J. E., Posewitz, M. C., and Ghirardi, M. L. (2011). Design of a new biosensor for algal H₂ production based on the H₂-sensing system of *Rhodospirillum rubrum*. *Int. J. Hydrog. Energy* 36, 11229–11237. doi: 10.1016/j.ijhydene.2011.05.121
- Wegelius, A., Khanna, N., Esmieu, C., Barone, G. D., Pinto, E., Tamagnini, P., et al. (2018). Generation of a functional, semisynthetic FeFe-hydrogenase in a photosynthetic microorganism. *Energy Environ. Sci.* 11, 3163–3167. doi: 10.1039/c8ee01975d
- Winter, G., Buhrke, T., Jones, A. K., and Friedrich, B. (2004). The role of the active site-coordinating cysteine residues in the maturation of the H₂-sensing NiFe hydrogenase from *Ralstonia eutropha* H16. *Arch. Microbiol.* 182, 138–146. doi: 10.1007/s00203-004-0680-6
- Zhang, J., Jensen, M. K., and Keasling, J. D. (2015). Development of biosensors and their application in metabolic engineering. *Curr. Opin. Chem. Biol.* 28, 1–8. doi: 10.1016/j.cop.2015.05.013
- Zimmer, D., Schwartz, E., Tran-Betcke, A., Gewinner, P., and Friedrich, B. (1995). Temperature tolerance of hydrogenase expression in *Alcaligenes eutrophus* is conferred by a single amino acid exchange in the transcriptional activator HoxA. *J. Bacteriol.* 177, 2373–2380. doi: 10.1128/jb.177.9.2373-2380.1995

Curriculum Vitae

Name Sara Lupacchini
Born 
Nationality Italian
Academic Degree Master of Science (Cellular and Molecular Biology)

Education

- 2018-2023 **PhD studies** at MLU Halle-Wittenberg & in the group Applied Biocatalysis in the Department of Solar Materials, Helmholtz-Centre for Environmental Research - UFZ, Leipzig, Germany
- 2015-2018 **Master studies** in Cellular and Molecular Biology, Master Thesis: “Structural and functional studies on variants of cytochrome P450 BM3 for biocatalytic applications” at University of Turin
- 2012-2015 **Bachelor studies** in Biological Sciences, Master Thesis: “Bifidobacteria from *S. oedipus*: characterization and study of the acidity resistance” at University of Bologna
- 2006-2011 **Linguistic high school**, Liceo Linguistico “Francesco Stelluti”, Fabriano (AN), Italy

Publications

Journal Publications

Lupacchini, S., Appel, J., Stauder, R., Bolay, P., Klähn, S., Lettau, E., Adrian, L., Lauterbach, L., Bühler, B., Schmid, A., Toepel, J., (2021): Rewiring cyanobacterial photosynthesis by the implementation of an oxygen-tolerant hydrogenase. *Metab. Eng.* 68, 199 – 209

Opel, F., Itzenhäuser, M.A., Wehner, I., **Lupacchini, S.**, Lauterbach, L., Lenz, O., Klähn, S., (2022): Towards a synthetic hydrogen sensor in cyanobacteria: Functional production of an oxygen-tolerant regulatory hydrogenase in *Synechocystis* sp. PCC 6803. *Front. Microbiol. – Microbiotechnology*.

Journal Paper in Review

Lupacchini, S., Stauder, R., Schmid, A., Bühler, B., Toepel, J., The activity of an O₂-tolerant hydrogenase recombinantly expressed in *Synechocystis* sp. PCC 6803 depends on gene expression and source/sink availability.

Journal Paper in preparation

Lupacchini, S., Stauder, R., Opel, F., Klähn, S., Bühler, B., Toepel, J. Co-expression of auxiliary and structural *Cupriavidus necator* genes enhances and stabilizes O₂-tolerant hydrogenase activity in *Synechocystis*. *In preparation for submission*

Presentation

“Functional oxygen-tolerant *Ralstonia* hydrogenase in *Synechocystis* - challenges and possible solutions”, 14th Workshop on Cyanobacteria, 16.-19.06.2022, Michigan State University, East Lansing, MI, USA

Poster

Lupacchini, S.; Stauder, R.; Bolay, P.; Adrian, L.; Appel J.; Lauterbach, L.; Lettau E.; Bühler, B.; Schmid, A.; Toepel, J. Design and development of hydrogen producing cyanobacterial strains, 6th Joint Conference of the DGHM VAAM, 8.-11.03.2020, Leipzig, Germany

Declaration of authorship

I, Sara Lupacchini, herewith declare that the presented thesis is entirely my work except where otherwise stated. The thesis has not been submitted either partially or wholly to another examination body for the attainment of a doctoral degree, and no academic degree has ever been withdrawn. Besides this, I declare that the thesis has been prepared according to the Rules of Good Scientific Practice of the German Research Foundation.

Leipzig, July 2023